

Unlocking the Potential of Dynamic Susceptibility Contrast Magnetic Resonance Perfusion for Non-Invasive Pre-Operative Diagnosis of Brain Tumors

Albert Pons-Escoda

ADVERTIMENT. La consulta d'aquesta tesi queda condicionada a l'acceptació de les següents condicions d'ús: La difusió d'aquesta tesi per mitjà del servei TDX (**www.tdx.cat**) i a través del Dipòsit Digital de la UB (**diposit.ub.edu**) ha estat autoritzada pels titulars dels drets de propietat intel·lectual únicament per a usos privats emmarcats en activitats d'investigació i docència. No s'autoritza la seva reproducció amb finalitats de lucre ni la seva difusió i posada a disposició des d'un lloc aliè al servei TDX ni al Dipòsit Digital de la UB. No s'autoritza la presentació del seu contingut en una finestra o marc aliè a TDX o al Dipòsit Digital de la UB (framing). Aquesta reserva de drets afecta tant al resum de presentació de la tesi com als seus continguts. En la utilització o cita de parts de la tesi és obligat indicar el nom de la persona autora.

ADVERTENCIA. La consulta de esta tesis queda condicionada a la aceptación de las siguientes condiciones de uso: La difusión de esta tesis por medio del servicio TDR (www.tdx.cat) y a través del Repositorio Digital de la UB (diposit.ub.edu) ha sido autorizada por los titulares de los derechos de propiedad intelectual únicamente para usos privados enmarcados en actividades de investigación y docencia. No se autoriza su reproducción con finalidades de lucro ni su difusión y puesta a disposición desde un sitio ajeno al servicio TDR o al Repositorio Digital de la UB. No se autoriza la presentación de su contenido en una ventana o marco ajeno a TDR o al Repositorio Digital de la UB (framing). Esta reserva de derechos afecta tanto al resumen de presentación de la tesis como a sus contenidos. En la utilización o cita de partes de la tesis es obligado indicar el nombre de la persona autora.

WARNING. On having consulted this thesis you're accepting the following use conditions: Spreading this thesis by the TDX (**www.tdx.cat**) service and by the UB Digital Repository (**diposit.ub.edu**) has been authorized by the titular of the intellectual property rights only for private uses placed in investigation and teaching activities. Reproduction with lucrative aims is not authorized nor its spreading and availability from a site foreign to the TDX service or to the UB Digital Repository. Introducing its content in a window or frame foreign to the TDX service or to the UB Digital Repository is not authorized (framing). Those rights affect to the presentation summary of the thesis as well as to its contents. In the using or citation of parts of the thesis it's obliged to indicate the name of the author.

Unlocking the Potential of Dynamic Susceptibility Contrast Magnetic Resonance Perfusion for Non-Invasive Pre-Operative Diagnosis of Brain Tumors

Doctoral thesis dissertation presented by

Albert Pons-Escoda

Radiology Department, Hospital Universitari de Bellvitge, L'Hospitalet de Llobregat, Barcelona, Spain. Neuro-Oncology Unit, Institut d'Investigació Biomedica de Bellvitge-IDIBELL, L'Hospitalet de Llobregat, Barcelona, Spain

to apply for the degree of doctor at the University of Barcelona

January 2025

Directed by:

Laura Oleaga Zufiria

School of Medicine and Health Sciences, Universitat de Barcelona-UB, Barcelona, Spain. Radiology Department, Hospital Clinic de Barcelona, Barcelona, Spain

Carles Majos Torro

Radiology Department, Hospital Universitari de Bellvitge, L'Hospitalet de Llobregat, Barcelona, Spain. Neuro-Oncology Unit, Institut d'Investigació Biomedica de Bellvitge-IDIBELL, L'Hospitalet de Llobregat, Barcelona, Spain

Doctoral Program in Medicine & Translational Research
School of Medicine & Health Sciences
University of Barcelona







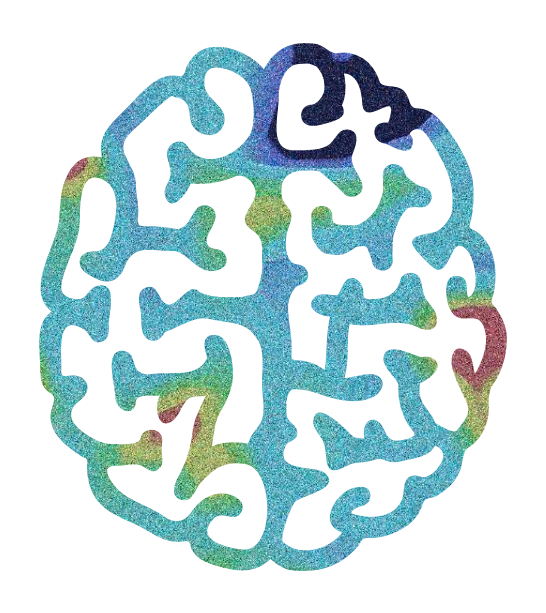


Doctoral Thesis. January 2025

Images and texts: Albert Pons-Escoda

Layout and illustration: NorArte Visual Science

Printing: Lankopi S.A.L.



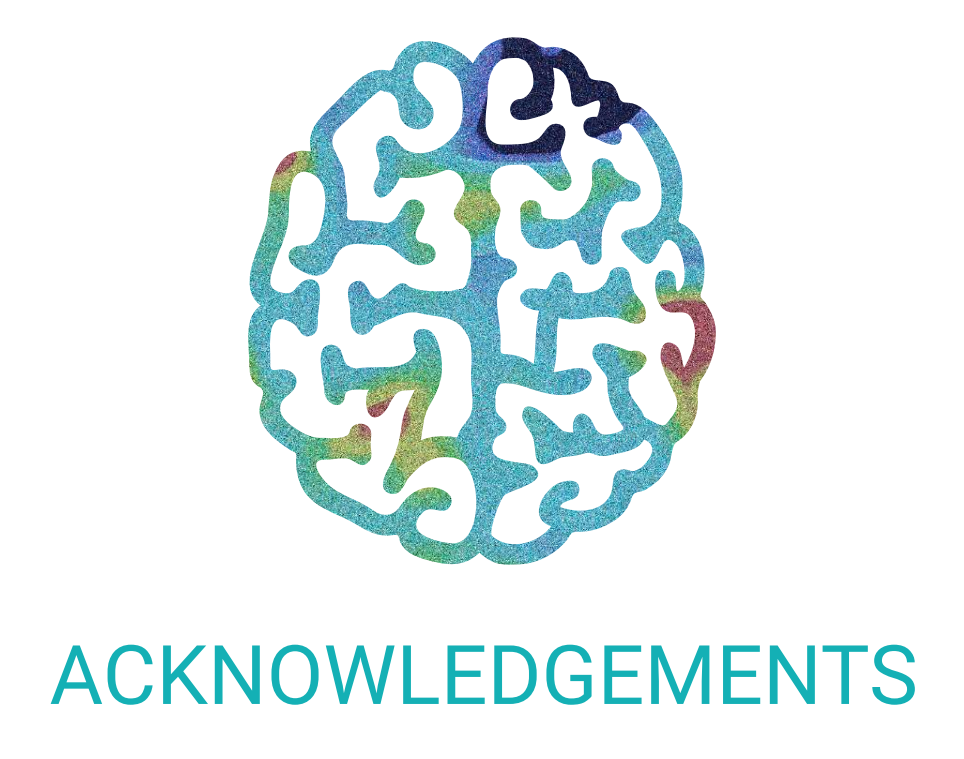
Unlocking the Potential of Dynamic Susceptibility Contrast Magnetic Resonance Perfusion for Non-Invasive Pre-Operative Diagnosis of Brain Tumors

Doctoral thesis dissertation presented by Albert Pons-Escoda

to apply for the degree of doctor at the University of Barcelona

January 2025

Doctoral Program in Medicine & Translational Research
School of Medicine & Health Sciences
University of Barcelona



ACKNOWLEDGMENTS

Els agraïments els faré en català, perquè és la llengua amb la qual penso i sento.

A tots els meus companys de l'Hospital Universitari de Bellvitge i de l'Institut de Diagnòstic per la Imatge; a la Unitat de Neuro-Oncologia; i a tots els pacients amb tumors cerebrals i les seves famílies.

Als meus directors de tesi, la Dra. Laura Oleaga i el Dr. Carles Majós, per la seva tutela dedicada.

A la Dra. Marion Smits, "Thank you Marion", i a tots els companys del Neuro-Oncologic Imaging Group de l'Erasmus MC, a Rotterdam, per haber-me rebut i fet sentir com a casa.

Al Dr. Carles Majós, més enllà d'aquesta direcció, per ser un mentor des del meu primer dia com a neuroradiòleg, i per haver despertat en mi l'interès científic. Al Dr. Pablo Naval, per imprimir passió en aquesta línia de recerca en particular, i en la radiologia en general. Als dos per ajudar-me a veure aquest projecte amb més confiança i grandesa del que jo mateix he percebut en molts moments.

Al Dr. Richard Mast, per ser el meu tutor des del primer dia de residència. Al Dr. Artur Renú, per ser el meu germà des del primer dia de carrera. Als dos, per compartir amb mi la passió per la medicina, però també, fora de l'hospital, per l'esport i la muntanya.

A la Bea i al Bru, la meva família, la meva gran passió i el pilar fonamental sobre el que es sustenta tot. Gràcies per respectar-me, per recolzar-me i per "obligar-me" a mantenir un equilibri vital indispensable.

Als meus pares, Montse i Albert, per ser un model de la medicina més humana, centrada en tenir cura del pacient en totes les seves dimensions. A la meva germana Mireia, per ser l'exemple viu que res és fàcil, però que si volem, podem. I finalment perquè, sense la insistència, però sobretot el suport de tots tres, segurament mai hauria fet aquesta tesi.

A tots els meus amics, primer de Valls i després de Barcelona, pel seu suport incondicional. Per entendre, i fins i tot a vegades sense entendre'ls, recolzar tots els meus projectes, tant personals com professionals.

I finalment a tots els que em puc oblidar i/ o, fins i tot sense saber-ho, formeu part d'una manera o altra, d'aquesta tesi.

A tots, gràcies.



FUNDING, AWARDS AND RECOGNITION

FUNDING

This thesis has received financial support from:

- The Instituto de Salud Carlos III (Proyectos de Investigación en Salud, PI20/00360).
- The 2023 Mobility Grant of the Spanish Society of Neuroradiology.
- The 2021 I Convocatòria d'ajuts per a la realització de tesis doctorals of the Institut de Diagnòstic per la Imatge.

Additionally, the author acknowledges that university fees were covered by the Radiology Department of Hospital Universitari de Bellvitge through the Bellvitge Biomedical Research Institute (IDIBELL).

The author of this thesis would also like to thank the CERCA Programme and the Generalitat de Catalunya for their institutional support.

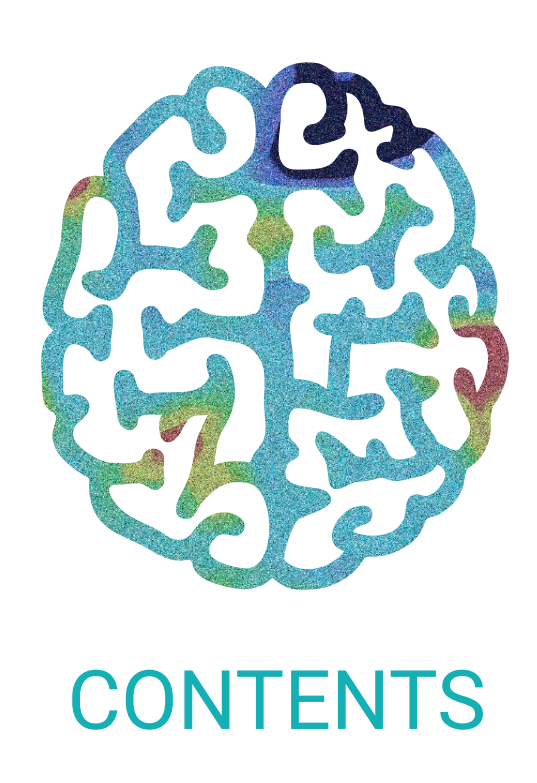
AWARDS AND RECOGNITION

This thesis has also been supported by two financial awards granted for its works:

- The European Society of NeuroRadiology Scientific Award in 2024.
- The Yearly Research Award from the Spanish Society of Neuroradiology in 2021.

Additionally, the studies included in this thesis have received recognition without financial support:

- The Best International Publication of the Spanish Society of Medical Radiology 2023.
- The accessit to the Best International Publication of the Spanish Society of Medical Radiology 2022.
- The Best Scientific Research Communication of the Spanish Society of Neuroradiology 2023.



CONTENTS

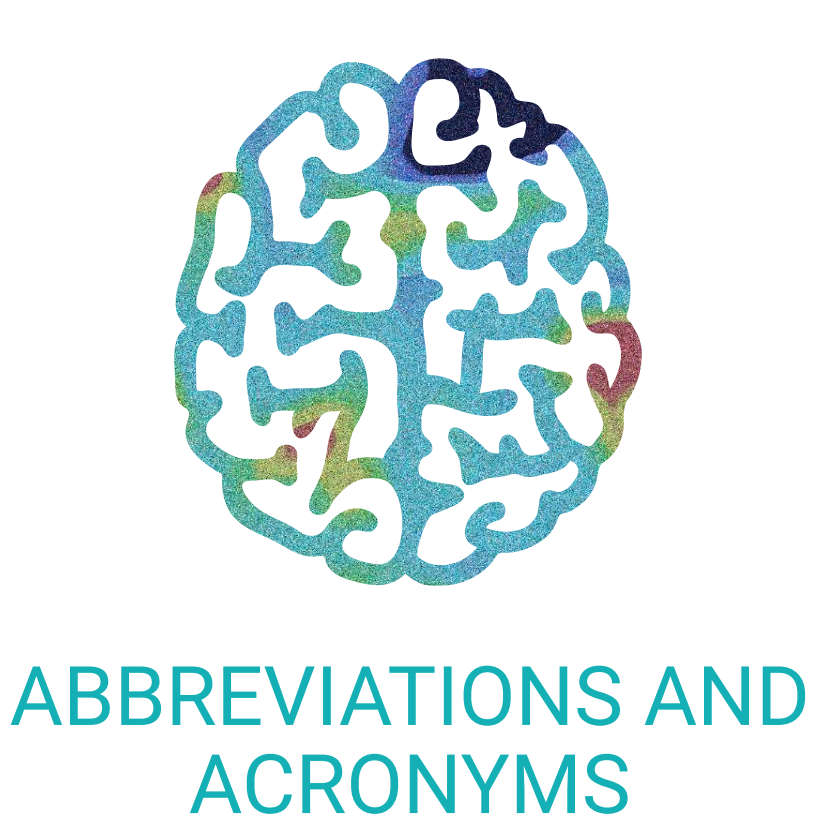
ACK	NOWLEDGMENTS		V
FUN	DING, AWARDS AND RECOGNITION		IX
CON	ITENTS		XII
ABB	REVIATIONS AND ACRONYMS		XIX
LIST	OF ARTICLES)	XXIII
THE	SIS SUMMARY)	XXIX
0.1.	ENGLISH		XXIX
0.2.	CATALAN	X	XXIV
0.3.	SPANISH		XL
1.	INTRODUCTION		3
1.1.	DSC-PWI: the Basis		3
1.2.	Clinical Use, Interests and Applications of DSC-PWI		6
1.3.	Brief Insights from Morphological MRI		12

1.4.	The	e Current Limitations of the DSC-PWI Sequence	13
1.5.	DS	C-PWI Data Selection/ Extraction Methods	16
1.6.	Мо	re Than Just CBV in DSC-PWI Sequences: PSR (and the Leakage Effects) and	
	Pea	ak Height	17
1.7.	Un	supervised Analysis of the Whole Time-intensity-curves	21
1.8.	MR	R Technique: Pulse-sequence Parameters Considerations	24
1.9.	Sui	mmarizing Rationales and Proposed Approaches	27
1.10	. Inti	roduction Appendix - Review Articles	29
1.10	.1.	Dynamic-Susceptibility-Contrast Perfusion-Weighted-Imaging (DSC-PWI) in Brain	
		Tumors: a Brief Up-To-Date Overview for Clinical Neuroradiologists	31
1.10	.2.	Imaging of Lymphomas Involving the CNS: An Update-Review of the Full Spec-	
		trum of Disease with an Emphasis on the World Health Organization Classifica-	
		tions of CNS Tumors 2021 and Hematolymphoid Tumors 2022	37
1.10	.3.	Presurgical Diagnosis of Diffuse Gliomas in Adults: Post-WHO 2021 Practical	
		Perspectives from Radiologists in Neuro-Oncology units	47
2.	НҮ	POTHESIS	67
3.	ОВ	SJECTIVES	71
4.	MA	ATERIAL, METHODS AND RESULTS	75
4.1.	Pre	esurgical Identification of Primary Central Nervous System Lymphoma with Nor-	
	ma	lized Time-Intensity Curve: A Pilot Study of a New Method to Analyze DSC-PWI	79
4.2.	Dif	fuse Large B-Cell Epstein-Barr Virus-Positive Primary CNS Lymphoma in Non-	
	AID	OS Patients: High Diagnostic Accuracy of DSC Perfusion Metrics	89

4.3.	Voxel-Level Analysis of Normalized DSC-PWI Time-Intensity Curves: A Potential
	Generalizable Approach and Its Proof of Concept in Discriminating Glioblastoma
	and Metastasis
4.4.	An Accessible Deep Learning Tool for Voxel-Wise Classification of Brain Malignan-
	cies from Perfusion MRI
4.5.	MR Dynamic-Susceptibility-Contrast Perfusion Metrics in the Presurgical Discrim-
	ination of Adult Solitary Intra-Axial Cerebellar Tumors
4.6.	Differentiating IDH-Mutant Astrocytomas and 1p19q-Codeleted Oligodendrogliomas
	Using DSC-PWI: High Performance through Cerebral Blood Volume and Percentage
	of Signal Recovery Percentiles
4.7.	DSC-PWI Presurgical Differentiation of Grade 4 Astrocytoma and Glioblastoma in
	Young Adults: rCBV Percentile Analysis across Enhancing and Non-Enhancing Re-
	gions
5.	DISCUSSION 163
5.1.	DSC-PWI Curves Normalization Method and Its Application for Pre-Surgical Identi-
	fication of CNS Lymphoma
5.2.	The Challenging Differentiation of Glioblastoma and Solitary Brain Metastasis 168
5.3.	A fully Automatic Tool for Main Brain Malignancies Pre-surgical Differentiation in
	Adults
5.4.	Intraaxial Cerebellar Tumors in Adults: Rarer, Yet Also Important
5.5.	Opening the Door to the Perfugenomics of Adult Diffuse Gliomas According to the
	last 2021 World Health Organization Classification of CNS Tumors

CONTENTS

5.6.	Specific Brain Tumor DSC-PWI Signatures and Hypothetical Pathophysiological	
	Correlates	175
5.7.	Strengths and Limitations	181
5.8.	Future Perspectives and Directions	182
6.	CONCLUSIONS	189
7.	REFERENCES	193



ABBREVIATIONS AND ACRONYMS

BBB Blood-Brain Barrier

CBV Cerebral Blood Volume

CE-T1 Contrast Enhanced T1

DLBC Diffuse Large B-Cell

DSC-PWI Dynamic Susceptibility Contrast Perfusion Weighted Imaging

EES Extravascular-Extracellular Space

FA Flip Angle

GBCA Gadolinium-Based Contrast Agent

IDH Isocitrate Dehydrogenase

MGMT O6-Methylguanine-DNA Methyltransferase

MRI Magnetic Resonance Imaging

NAWM Normal-Appearing White Matter

PACS Picture Archiving and Communication System

PCNSL Primary Central Nervous System Lymphoma

PH Peak Height

PSR Percentage of Signal Recovery

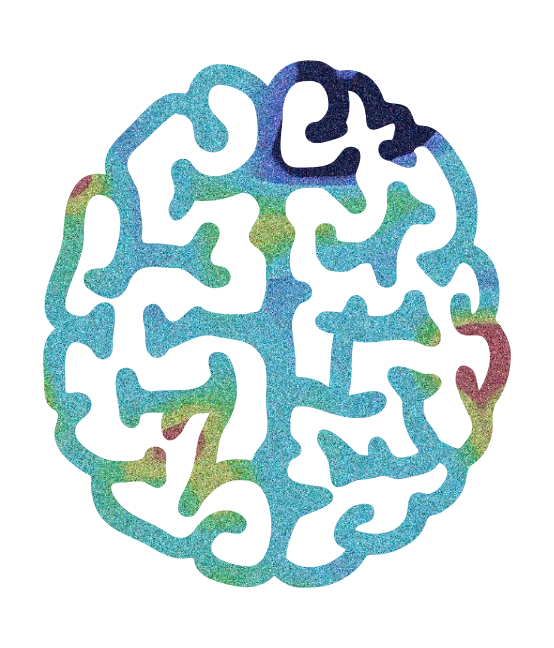
ROI Region of Interest

TE Echo Time

TIC Time-Intensity Curve

TR Repetition Time

VOI Volume of Interest



LIST OF ARTICLES IN THE THESIS

LIST OF ARTICLES IN THE THESIS

Thesis in compendium of publications format.

The thesis consists of 5 objectives and 7 original research articles.

Pons-Escoda A, Garcia-Ruiz A, Naval-Baudin P, Cos M, Vidal N, Plans G, Bruna J, Perez-Lopez R, Majos C. Presurgical Identification of Primary Central Nervous System Lymphoma with Normalized Time-Intensity Curve: A Pilot Study of a New Method to Analyze DSC-PWI. AJNR Am J Neuroradiol. 2020 Oct;41(10):1816-1824. doi: 10.3174/ajnr.A6761. Epub 2020 Sep 17. PMID: 32943424; PMCID: PMC7661072.

Journal Citation Report (JCR) Impact Factor: 3.825

Scimago Journal Rank (SJR) Quartile: **Q1** in Radiology Nuclear Medicine and Imaging

2. Pons-Escoda A, García-Ruíz A, Naval-Baudin P, Grussu F, Viveros M, Vidal N, Bruna J, Plans G, Cos M, Perez-Lopez R, Majós C. Diffuse Large B-Cell Epstein-Barr Virus-Positive Primary CNS Lymphoma in Non-AIDS Patients: High Diagnostic Accuracy of DSC Perfusion Metrics. AJNR Am J Neuroradiol. 2022 Nov;43(11):1567-1574. doi: 10.3174/ajnr.A7668. Epub 2022 Oct 6. PMID: 36202547; PMCID: PMC9731258.

Journal Citation Report (JCR) Impact Factor: 3.500

Scimago Journal Rank (SJR) Quartile: **Q1** in Radiology Nuclear Medicine and Imaging

3. Pons-Escoda A, Garcia-Ruiz A, Naval-Baudin P, Grussu F, Fernandez JJS, Simo AC, Sarro NV, Fernandez-Coello A, Bruna J, Cos M, Perez-Lopez R, Majos C. Voxel-level analysis of normalized DSC-PWI time-intensity curves: a potential generalizable approach and its proof of concept in discriminating glioblastoma and metastasis. Eur Radiol. 2022 Jun;32(6):3705-3715. doi: 10.1007/s00330-021-08498-1. Epub 2022 Feb 1. PMID: 35103827.

Journal Citation Report (JCR) Impact Factor: 5.900

Scimago Journal Rank (SJR) Quartile: **Q1** in Radiology Nuclear Medicine and Imaging

4. Garcia-Ruiz A, Pons-Escoda A (co-first author), Grussu F, Naval-Baudin P, Monreal-Aguero C, Hermann G, Karunamuni R, Ligero M, Lopez-Rueda A, Oleaga L, Berbís MÁ, Cabrera-Zubizarreta A, Martin-Noguerol T, Luna A, Seibert TM, Majos C, Perez-Lopez R. An accessible deep learning tool for voxel-wise classification of brain malignancies from perfusion MRI. Cell Rep Med. 2024 Mar 19;5(3):101464. doi: 10.1016/j.xcrm.2024.101464. Epub 2024 Mar 11. PMID: 38471504; PMCID: PMC10983037.

Journal Citation Report (JCR) Impact Factor: 11.700

Scimago Journal Rank (SJR) Quartile: **Q1** in Biochemistry, Genetics and Molecular Biology

5. Pons-Escoda A, Garcia-Ruiz A, Garcia-Hidalgo C, Gil-Solsona R, Naval-Baudin P, Martin-Noguerol T, Fernandez-Coello A, Flores-Casaperalta S, Fernandez-Viñas M, Gago-Ferrero P, Oleaga L, Perez-Lopez R, Majos C. MR dynamic-susceptibility-contrast perfusion metrics in the presurgical discrimination of adult solitary

intra-axial cerebellar tumors. Eur Radiol. 2023 Dec;33(12):9120-9129. doi: 10.1007/s00330-023-09892-7. Epub 2023 Jul 13. PMID: 37439938.

Journal Citation Report (JCR) Impact Factor: 4.700

Scimago Journal Rank (SJR) Quartile: **Q1** in Radiology Nuclear Medicine and Imaging

6. Pons-Escoda A, Garcia-Ruiz A, Naval-Baudin P, Martinez-Zalacain I, Castell J, Camins A, Vidal N, Bruna J, Cos M, Perez-Lopez R, Oleaga L, Warnert E, Smits M, Majos C. Differentiating IDH-mutant astrocytomas and 1p19q-codeleted oligodendrogliomas using DSC-PWI: high performance through cerebral blood volume and percentage of signal recovery percentiles. Eur Radiol. 2024 Aug;34(8):5320-5330. doi: 10.1007/s00330-024-10611-z. Epub 2024 Jan 29. PMID: 38282078; PMCID: PMC11255054.

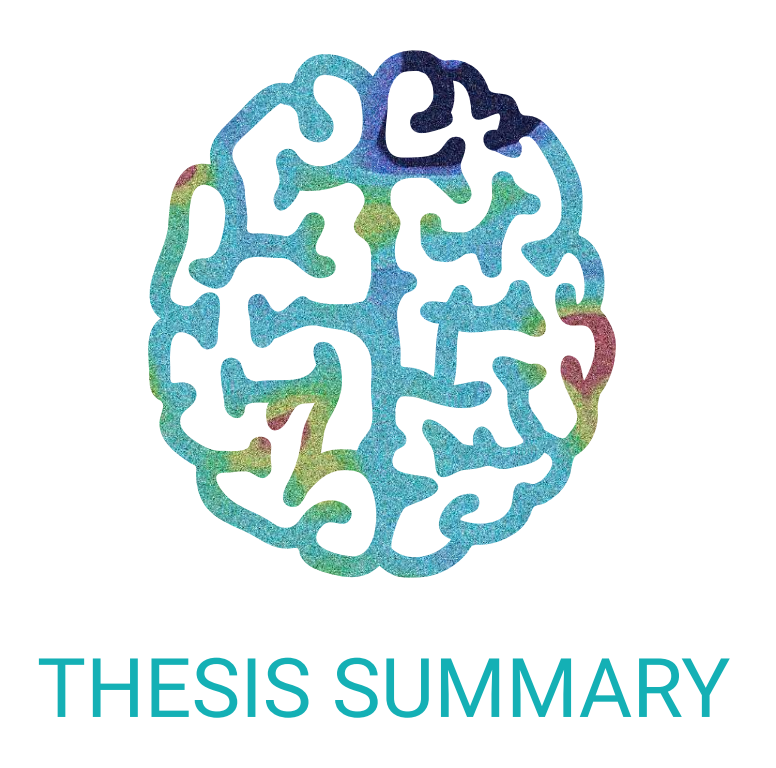
Journal Citation Report (JCR) Impact Factor: 4.700

Scimago Journal Rank (SJR) Quartile: **Q1** in Radiology Nuclear Medicine and Imaging

7. Pons-Escoda A, Naval-Baudin P, Viveros M, Flores-Casaperalta S, Martinez-Zalacaín I, Plans G, Vidal N, Cos M, Majos C. DSC-PWI presurgical differentiation of grade 4 astrocytoma and glioblastoma in young adults: rCBV percentile analysis across enhancing and non-enhancing regions. Neuroradiology. 2024 Aug;66(8):1267-1277. doi: 10.1007/s00234-024-03385-0. Epub 2024 Jun 5. PMID: 38834877; PMCID: PMC11246293.

Journal Citation Report (JCR) Impact Factor: 2.4

Scimago Journal Rank (SJR) Quartile: **Q1** in Radiology Nuclear Medicine and Imaging



THESIS SUMMARY

0.1. ENGLISH

Title

Unlocking the Potential of Dynamic Susceptibility Contrast Perfusion Magnetic Resonance Imaging for Non-Invasive Pre-Surgical Diagnosis of Brain Tumors

Introduction

Dynamic Susceptibility Contrast Perfusion Magnetic Resonance Imaging (DSC-PWI) is a non-invasive imaging technique that evaluates the vascular and microvascular environments of central nervous system tissues. This technique uses the dynamic passage of a gadolinium-based contrast bolus to generate time-intensity curves that provide various metrics. The most commonly used metric in neuro-oncology is cerebral blood volume (CBV). DSC-PWI complements morphological MRI and provides advanced semi-quantitative information that has proven useful in the non-invasive pre-surgical differential diagnosis of brain tumors.

Clinical evaluations are often visual or semi-quantitative and mainly rely on CBV. Visual assessments using color-coded maps can be insufficient in high-complexity scenarios and, in some cases, even misleading. Standard semi-quantitative analyses in routine clinical practice involve the manual selection of a region of interest (e.g., the tumor) and a reference for normalization, usually on a single axial slice. This approach can exclude large portions of the tumor from evaluation, is highly operator-dependent, and has low

reproducibility. Additionally, focusing solely on CBV oversimplifies the information available in the time-intensity curves, which constitute the raw data of the sequence and allow for deriving more metrics beyond CBV.

Therefore, there is an unmet need in this field: on the one hand, to automate the selection of regions of interest, including the entire tumor heterogeneity, as well as the references for normalization, to make interpretations more robust and reproducible. On the other hand, to integrate multiple metrics, such as Percentage of Signal Recovery (PSR) or Peak Height (PH), beyond the isolated assessment of CBV, to extract richer and more multi-dimensional information. An interesting alternative for this latter point is to analyze the time-intensity curves as a unit of analysis in an unsupervised manner (without the need to extract predefined metrics such as CBV, PSR, or PH), an approach we have termed DSC-PWI curvology. With these approaches, the sequence would not only provide information about overall vascularity, as CBV does, but also data on blood-brain barrier integrity, vascular dynamics, and aspects of cytoarchitecture and vasculoarchitecture.

Hypothesis

Multiparametric and/or curvological evaluation of DSC-PWI provides enhanced diagnostic capability surpassing the information offered by CBV alone.

The application of three-dimensional segmentation methods, semi-automatic analyses, and voxel-level approaches reduces operator-dependence and incorporates tumor heterogeneity, improving the performance of conventional approaches based on a single metric and a single value from a manual and two-dimensional region of interest.

Objectives

The objectives of this thesis are:

- To improve the pre-surgical diagnostic precision and analysis robustness of DSC-PWI in the evaluation of brain tumors through a semi-automatic, volumetric, curvological, and multiparametric approach.
- To differentiate types and subtypes of brain tumors in adults in a non-invasive, pre-surgical manner using these advanced DSC-PWI analysis methods.
- To develop practical and clinically applicable classifiers that are explainable and based on a solid pathophysiological foundation.

Methods

Seven original studies were conducted with retrospective cohorts, both single-center and multi-center. All studies followed a common methodology for data extraction, based on:

- Volumetric segmentations of tumors and normal white matter reference regions for normalization in morphological MRI sequences.
- Co-registration of segmentations to DSC-PWI.
- And data extraction (voxel-by-voxel time-intensity curves, CBV, PSR, and/or PH)
 from the entire tumor volume.

Thus, the common unit of analysis was constituted by the multiple metrics or timeintensity curves in each voxel within the tumor, which were analyzed using different data analysis methods and applied to various clinically relevant tumor differentiations, impacting patient management.

Results

In this thesis, an innovative method for normalizing DSC-PWI time-intensity curves was developed, enabling robust point-by-point statistical comparisons. This method achieved diagnostic accuracies ranging from 71% to 96% for pairwise differentiation of cerebral lymphoma from glioblastomas, metastases, and meningiomas, and was also successfully applied to immunodeficiency-associated cerebral lymphomas, with accuracies between 82% and 93%.

This approach was also adapted to address the differentiation between glioblastoma and solitary brain metastasis using voxel-by-voxel percentile analysis to better capture the heterogeneity of these tumors. This yielded a diagnostic accuracy of 81%.

Additionally, an automated deep learning-based tool (DISCERN) was developed, integrating normalized curves and voxel-by-voxel analyses for the three-class, single-step classification of glioblastoma, metastases, and lymphoma. This tool achieved accuracies of 80% to 95% in training and test datasets and 75% to 80% in multi-center validation cohorts, demonstrating robustness and generalizability. For intra-axial cerebellar tumors, different metrics (CBV, PSR, PH, and normalized curves) were combined with machine learning methods, achieving an accuracy of 85% in differentiating metastases, meduloblastomas, hemangioblastomas, and pilocytic astrocytomas.

Finally, a multiparametric analysis (CBV and PSR) based on voxel percentiles was applied to capture tumor heterogeneity in molecular subtypes of adult diffuse gliomas. This allowed differentiation between IDH-mutant astrocytomas and IDH-mutant oligodendrogliomas with 1p19q codeletion (grades 2-3) with an area under the ROC curve of 0.87, and between grade 4 IDH-mutant astrocytomas and IDH-wildtype glioblastomas with an area under the ROC curve of 0.81.

In all studies, the innovative methodologies employed demonstrated superiority over standard metrics and analyses based on a single metric and a single value.

Conclusions

- Our innovative methodologies significantly increased the diagnostic precision of DSC-PWI, enabling a more reliable and detailed understanding of the vascular and microvascular characteristics of brain tumors.
- Their application facilitates the non-invasive, pre-surgical differentiation of various clinically relevant tumors, such as lymphomas, glioblastomas, metastases, cerebellar tumors, and molecular subtypes of adult diffuse gliomas.
- 3. These results can be transferred to daily clinical practice through robust and comprehensible classifiers that integrate the potential of advanced data analysis, classical statistics, and a solid pathophysiological basis.

0.2. CATALAN

Títol

Desbloquejant el Potencial de la Ressonància Magnètica de Perfusió per Susceptibilitat Dinàmica de Contrast en el Diagnòstic Prequirúrgic No Invasiu de Tumors Cerebrals

Introducció

La Ressonància Magnètica (RM) de Perfusió per Susceptibilitat Dinàmica de Contrast (DSC-PWI) és una tècnica d'imatge no invasiva que permet avaluar els entorns vasculars i microvasculars dels teixits del sistema nerviós central. Aquesta tècnica utilitza el pas dinàmic d'un bolus de contrast basat en gadolini per generar corbes temps-intensitat que proporcionen diverses mètriques. La mètrica més utilitzada en neuro-oncologia és el volum sanguini cerebral (CBV). La DSC-PWI complementa la RM morfològica i aporta informació semiquantitativa avançada que ha demostrat utilitat en el diagnòstic diferencial prequirúrgic i no invasiu dels tumors cerebrals.

Les avaluacions clíniques solen ser visuals o semiquantitatives i es basen principalment en el CBV. Les avaluacions visuals mitjançant mapes codificats per colors poden ser insuficients en escenaris d'alta complexitat i, en alguns casos, fins i tot enganyoses. Les anàlisis semiquantitatives més estàndards en la pràctica clínica habitual impliquen la selecció manual d'una regió d'interès (p. ex., el tumor) i una referència per a la normalització, generalment en un únic tall axial. Aquest enfocament, d'una banda, pot deixar fora de l'avaluació una gran part del tumor i, de l'altra, fa que aquestes anàlisis siguin altament dependents de l'operador i presentin una baixa reproductibilitat. A més, limitar-

se exclusivament al CBV simplifica en excés la informació disponible en les corbes temps-intensitat, que constitueixen la dada crua de la seqüència i permeten derivar més mètriques, més enllà del CBV.

Per tant, hi ha una necessitat no resolta en aquest camp: d'una banda, automatitzar la selecció de les regions d'interès, incloent-hi tota la heterogeneïtat tumoral, així com de les referències per a la normalització, per tal de fer les interpretacions més robustes i reproduïbles. De l'altra, integrar múltiples mètriques, com el Percentatge de Recuperació de Senyal (PSR) o l'Alçada del Pic (PH), més enllà de la valoració aïllada del CBV, per extreure una informació més rica i multidimensional. Una alternativa interessant per aquest darrer punt és analitzar les corbes temps-intensitat tractant-les com una unitat d'anàlisi de manera no supervisada (sense necessitat d'extreure mètriques predeterminades com el CBV, el PSR o el PH), en un enfocament que els autors hem denominat corbologia de DSC-PWI. Amb aquestes aproximacions, la seqüència no només proporcionaria informació sobre la vascularitat global, com fa el CBV, sinó que també aportaria dades sobre la integritat de la barrera hematoencefàlica, les dinàmiques vasculars i aspectes de citoarquitectura i vasculoarquitectura.

Hipòtesi

L'avaluació multiparamètrica i/o corbològica de la DSC-PWI proporciona capacitat diagnòstica millorada superant la informació oferta pel CBV en solitari.

L'aplicació de mètodes de segmentació tridimensional, anàlisi semiautomàtics i a nivell del vòxel redueixen la operador- dependència i incorporen la heterogeneïtat tumoral mi-

llorant el rendiment dels enfocaments convencionals basats en una única mètrica i un únic valor d'una regió d'interès manual i bidimensional.

Objectius

Els objectius d'aquesta tesi són:

- Millorar la precisió diagnòstica prequirúrgica i la robustesa d'anàlisi de la DSC-PWI en l'avaluació de tumors cerebrals mitjançant un enfocament semi-automàtic, volumètric, corbològic i multiparamètric.
- 2. Diferenciar tipus i subtipus de tumors cerebrals en adults de manera prequirúrgica i no invasiva emprant aquests mètodes avançats d'anàlisi de DSC-PWI.
- Desenvolupar eines classificadores pràctiques i aplicables a la pràctica clínica, que siguin explicables i fonamentades en una base fisiopatològica sòlida.

Mètodes

S'han realitzat set treballs originals amb cohorts retrospectives, tant unicèntriques com multicèntriques.

En tots els estudis s'ha seguit una metodologia comuna per a l'extracció de dades, basada en:

- Segmentacions volumètriques dels tumors, i de les referències de substància blanca normal per a la normalització, en seqüències morfològiques de RM.
- Coregistre de les segmentacions a la DSC-PWI.

 Y extracció de les dades (corbes temps-intensitat, CBV, PSR i/o PH) vòxel a vòxel de tot el volum tumoral.

Per tant, la unitat comuna d'anàlisi ha estat constituïda per les múltiples mètriques o les corbes temps-intensitat en cada vòxel dins del tumor, les quals s'han analitzat utilitzant diferents mètodes d'anàlisi de dades i s'han aplicat a diverses diferenciacions tumorals d'interès clínic, amb un impacte en el maneig del pacient.

Resultats

En aquesta tesi, s'ha desenvolupat un mètode innovador de normalització de corbes temps-intensitat de DSC-PWI, que permet comparacions estadístiques robustes punt-per-punt. Aquest mètode ha aconseguit precisions diagnòstiques d'entre el 71 % i el 96 % per diferenciar per parelles el limfoma cerebral de glioblastomes, metàstasis i meningiomes, i s'ha aplicat també amb èxit a limfomes cerebrals associats a la immunodeficiència, amb precisions del 82 % al 93 %.

També s'ha adaptat aquest enfocament per abordar la diferenciació entre glioblastoma i metàstasi cerebral solitària, amb una anàlisi basada en percentils vòxel-a-vòxel per capturar millor l'heterogeneïtat d'aquests tumors. Això ha permès aconseguir una precisió diagnòstica del 81 %.

A més, s'ha desenvolupat una eina automàtica basada en aprenentatge profund (DIS-CERN), que integra corbes normalitzades i anàlisis vòxel-a-vòxel per a la classificació, a tres bandes i en un únic pas, de glioblastoma, metàstasis i limfoma. Aquesta eina ha aconseguit precisions d'entre el 80 % i el 95 % en conjunts d'entrenament i prova, i del

75 % al 80 % en cohorts de validació multicèntriques, demostrant robustesa i generalitzabilitat.

En el cas dels tumors cerebel·losos intraaxials, s'han combinat diferents mètriques (CBV, PSR, PH i corbes normalitzades) amb mètodes d'aprenentatge automàtic, aconseguint una precisió del 85 % per diferenciar metàstasis, medul·loblastomes, hemangioblastomes i astrocitomes pilocítics. Finalment, s'ha aplicat una anàlisi multiparamètrica (CBV i PSR) i basada en percentils dels vòxels per capturar l'heterogeneïtat tumoral en subtipus moleculars de gliomes difusos d'adults. Això ha permès diferenciar entre astrocitomes IDH-mutats i oligodendrogliomes IDH-mutats i amb codelecció 1p19q graus 2-3 amb un àrea sota la corba ROC de 0,87; i entre astrocitomes IDH-mutats grau 4 i glioblastomes IDH-wildtype amb un àrea sota la corba ROC de 0,81.

En tots els treballs, les metodologies innovadores emprades han demostrat superar les mètriques i anàlisis estàndard basades en una única mètrica i un únic valor.

Conclusions

- Les nostres metodologies innovadores han augmentat significativament la precisió diagnòstica de la DSC-PWI, permetent una comprensió més fiable i detallada de les característiques vasculars i microvasculars dels tumors cerebrals.
- 2. La seva aplicació facilita la diferenciació prequirúrgica i no invasiva de diversos tumors clínicament rellevants, com limfomes, glioblastomes, metàstasis, tumors cerebel·losos i subtipus moleculars de gliomes difusos en adults.
- 3. Aquests resultats es poden transferir a la pràctica clínica diària mitjançant classificadors robustos i comprensibles que integren el potencial de l'anàlisi de dades avançada, l'estadística clàssica i una base fisiopatològica sòlida.

0.3. SPANISH

Título

Desbloqueando el Potencial de la Resonancia Magnética de Perfusión por Susceptibilidad Dinámica de Contraste en el Diagnóstico Prequirúrgico No Invasivo de Tumores Cerebrales

Introducción

La Resonancia Magnética (RM) de Perfusión por Susceptibilidad Dinámica de Contraste (DSC-PWI) es una técnica de imagen no invasiva que evalúa los entornos vasculares y microvasculares de los tejidos del sistema nervioso central. Esta técnica utiliza el paso dinámico de un bolo de contraste basado en gadolinio para generar curvas tiempointensidad que proporcionan diversas métricas. La métrica más utilizada en neuro-oncología es el volumen sanguíneo cerebral (CBV). La DSC-PWI complementa la RM morfológica al aportar información semicuantitativa avanzada que ha demostrado utilidad en el diagnóstico diferencial prequirúrgico y no invasivo de los tumores cerebrales.

Las evaluaciones clínicas suelen ser visuales o semicuantitativas y se basan principalmente en el CBV. Las evaluaciones visuales mediante mapas codificados por colores
pueden ser insuficientes en escenarios de alta complejidad y, en algunos casos, incluso
engañosas. Los análisis semicuantitativos estándar en la práctica clínica habitual implican la selección manual de una región de interés (p. ej., el tumor) y una referencia
para la normalización, generalmente en un único corte axial. Este enfoque, por un lado,
puede dejar fuera de la evaluación una gran parte del tumor y, por otro, hace que estos

análisis sean altamente dependientes del operador y presenten baja reproducibilidad. Además, limitarse exclusivamente al CBV simplifica en exceso la información disponible en las curvas tiempo-intensidad, que constituyen el dato bruto de la secuencia y permiten derivar métricas adicionales más allá del CBV.

Por lo tanto, existe una necesidad no resuelta en este campo: por un lado, automatizar la selección de las regiones de interés, incluyendo toda la heterogeneidad tumoral, así como de las referencias para la normalización, con el objetivo de hacer las interpretaciones más robustas y reproducibles. Por otro lado, integrar múltiples métricas, como el Porcentaje de Recuperación de Señal (PSR) o la Altura del Pico (PH), más allá de la valoración aislada del CBV, para extraer una información más rica y multidimensional. Una alternativa interesante para este último punto es analizar las curvas tiempo-intensidad tratándolas como una unidad de análisis de manera no supervisada (sin necesidad de extraer métricas predeterminadas como el CBV, el PSR o el PH), en un enfoque que los autores hemos denominado curvología de DSC-PWI. Con estos enfoques, la secuencia no solo proporcionaría información sobre la vascularidad global, como hace el CBV, sino que también aportaría datos sobre la integridad de la barrera hematoencefálica, las dinámicas vasculares y aspectos de citoarquitectura y vasculoarquitectura.

Hipótesis

La evaluación multiparamétrica y/o curvológica de la DSC-PWI proporciona una capacidad diagnóstica mejorada, superando la información ofrecida exclusivamente por el CBV.

La aplicación de métodos de segmentación tridimensional, análisis semiautomáticos y a nivel de vóxel reduce la dependencia del operador e incorpora la heterogeneidad tumoral, mejorando el rendimiento de los enfoques convencionales basados en una única métrica y un único valor de una región de interés manual y bidimensional.

Objetivos

Los objetivos de esta tesis son:

- Mejorar la precisión diagnóstica prequirúrgica y la robustez del análisis de la DSC-PWI en la evaluación de tumores cerebrales mediante un enfoque semiautomático, volumétrico, corbológico y multiparamétrico.
- Diferenciar tipos y subtipos de tumores cerebrales en adultos de manera prequirúrgica y no invasiva utilizando estos métodos avanzados de análisis de DSC-PWI.
- Desarrollar herramientas clasificadoras prácticas y aplicables a la práctica clínica, que sean explicables y estén fundamentadas en una sólida base fisiopatológica.

Métodos

Se han realizado siete trabajos originales con cohortes retrospectivas, tanto unicéntricas como multicéntricas.

En todos los estudios se ha seguido una metodología común para la extracción de datos, basada en:

- Segmentaciones volumétricas de los tumores y de las referencias de sustancia blanca normal para la normalización, en secuencias morfológicas de RM.
- Coregistro de las segmentaciones a la DSC-PWI.
- Extracción de los datos (curvas tiempo-intensidad, CBV, PSR y/o PH) vóxel a vóxel de todo el volumen tumoral.

Por lo tanto, la unidad común de análisis ha sido constituida por las múltiples métricas o las curvas tiempo-intensidad en cada vóxel dentro del tumor, las cuales se han analizado utilizando diferentes métodos de análisis de datos y se han aplicado a diversas diferenciaciones tumorales de interés clínico, con un impacto en el manejo del paciente.

Resultados

En esta tesis, se ha desarrollado un método innovador de normalización de curvas tiempointensidad de DSC-PWI, que permite comparaciones estadísticas robustas punto por
punto. Este método ha logrado precisiones diagnósticas del 71 % al 96 % para diferenciar por pares el linfoma cerebral de glioblastomas, metástasis y meningiomas, y también se ha aplicado con éxito a linfomas cerebrales asociados a la inmunodeficiencia,
con precisiones del 82 % al 93 %.

Asimismo, se ha adaptado este enfoque para abordar la diferenciación entre glioblastoma y metástasis cerebral solitaria, utilizando un análisis basado en percentiles vóxel a vóxel para capturar mejor la heterogeneidad de estos tumores. Esto permitió alcanzar una precisión diagnóstica del 81 %.

Además, se ha desarrollado una herramienta automática basada en aprendizaje profundo (DISCERN), que integra curvas normalizadas y análisis vóxel a vóxel para la clasificación, en tres categorías y en un único paso, de glioblastoma, metástasis y linfoma. Esta herramienta logró precisiones del 80 % al 95 % en conjuntos de entrenamiento y prueba, y del 75 % al 80 % en cohortes de validación multicéntricas, demostrando robustez y generalización.

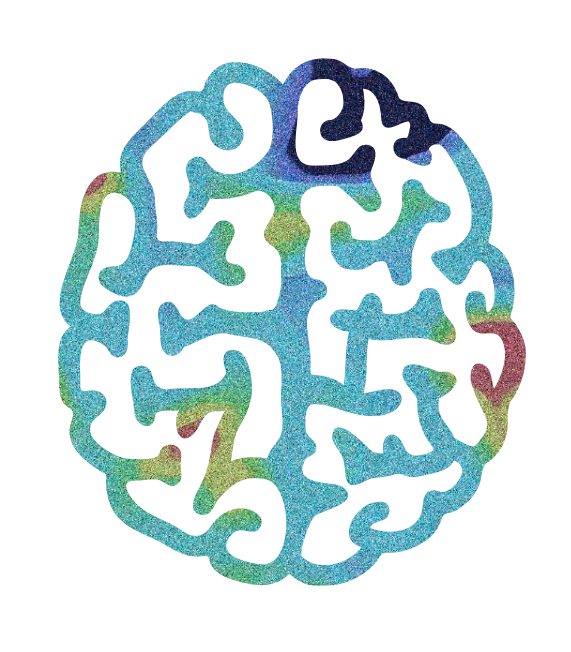
En el caso de los tumores cerebelosos intraaxiales, se combinaron diferentes métricas (CBV, PSR, PH y curvas normalizadas) con métodos de aprendizaje automático, logrando una precisión del 85 % para diferenciar metástasis, meduloblastomas, hemangioblastomas y astrocitomas pilocíticos.

Finalmente, se aplicó un análisis multiparamétrico (CBV y PSR) y basado en percentiles de los vóxeles para capturar la heterogeneidad tumoral en subtipos moleculares de gliomas difusos en adultos. Esto permitió diferenciar entre astrocitomas IDH-mutados y oligodendrogliomas IDH-mutados con codelección 1p19q grados 2-3 con un área bajo la curva ROC de 0,87; y entre astrocitomas IDH-mutados grado 4 y glioblastomas IDH-wildtype con un área bajo la curva ROC de 0,81.

En todos los trabajos, las metodologías innovadoras empleadas han demostrado superar las métricas y análisis estándar basados en una única métrica y un único valor.

Conclusiones

- Nuestras metodologías innovadoras han incrementado significativamente la precisión diagnóstica de la DSC-PWI, permitiendo una comprensión más fiable y detallada de las características vasculares y microvasculares de los tumores cerebrales.
- 2. Su aplicación facilita la diferenciación prequirúrgica y no invasiva de diversos tumores clínicamente relevantes, como linfomas, glioblastomas, metástasis, tumores cerebelosos y subtipos moleculares de gliomas difusos en adultos.
- 3. Estos resultados son transferibles a la práctica clínica diaria mediante clasificadores robustos y comprensibles que integran el potencial del análisis avanzado de datos, la estadística clásica y una base fisiopatológica sólida.



1. INTRODUCTION

1. INTRODUCTION

1.1. DSC-PWI: the Basis

Dynamic Susceptibility Contrast Perfusion Weighted Imaging (DSC-PWI) is a non-invasive magnetic resonance imaging (MRI) technique used for in vivo assessment of the vascular and microvascular environments in CNS tissues. It is widely utilized in clinical settings and is a standard component of consensus protocols for brain tumor imaging [1–4].

DSC-PWI involves a dynamic acquisition as the gadolinium-based contrast agent (GBCA) bolus transits the vasculature. In the realm of brain tumor imaging, gradient-echo-based sequences are preferred. The introduction of GBCA causes an initial decrease in the T2* signal intensity of the tissues, which subsequently recovers during the washout phase. This sequence generates time-intensity curves (TICs) as showed in *figure 1*, which yield various metrics. Among these metrics, cerebral blood volume (CBV) is most commonly used for brain tumor evaluations [1,2].

The CBV is determined by evaluating the area under the time-intensity curve. It is typically considered relative since the signal intensity is not quantified in absolute values but rather in terms of the change in intensity or, more preferably, the change in relaxation rate ($\triangle R2^*$) and its value is only relative to that of other regions of the brain [1,2].

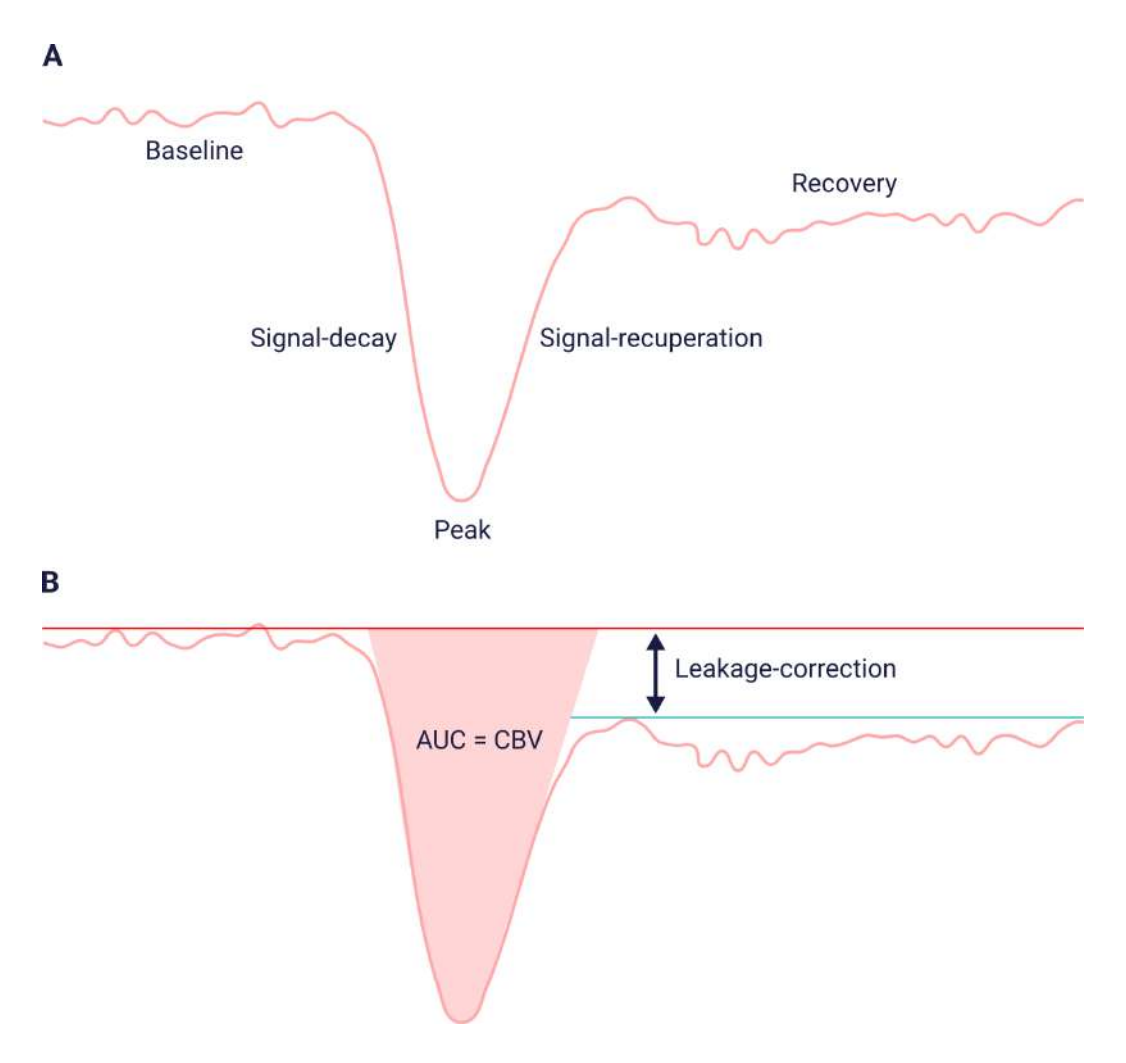


Figure 1 (*Original graphic created by the author, redesigned by Norarte Visual Science for this thesis*): **A.** Illustration of a time-intensity curve. The curve showcases the initial baseline, followed by signal decay attributed to the T2* reduction caused by the contrast agent. This leads to a maximum signal intensity drop, or peak, before transitioning to signal recovery during the contrast washout phase. Following the ascent of the curve is the post-contrast vascular transit recovery phase. **B.** Illustration of the CBV calculation process using the AUC method after leakage correction.

The transformation from signal intensity to $\Delta R2^*$ is considered relevant for calculating CBV because this metric directly depends on the concentration of the contrast agent within a specific region and establishes a linear relationship with this concentration. In contrast, T2* signal intensity has an exponential relationship with contrast concentration,

which makes it less suitable for quantitative calculations. For example, it may lead to signal saturation at high contrast concentrations, resulting in an underestimation of the actual contrast levels [5].

 Δ R2* is derived from the equation: Δ R2*(t)=-1/TE ln (S(t)/So). This transformation converts the nonlinear changes in signal intensity into a metric directly proportional to the contrast concentration in the tissue. It also mitigates some technical variabilities enabling more accurate CBV calculations. Ultimately, CBV is calculated by integrating the area under the time- Δ R2* curve during the contrast passage phase. Performing this integration directly using time-intensity data would theoretically be less reliable due to the nonlinear relationship and signal saturation at high contrast concentrations [5].

However, all these calculations assume that GBCA remains exclusively intravascular and that the time required for it to flow through the vessels is uniform and consistent. Under these assumptions, the recovery phase of the time-intensity curve would return identically to the baseline (i.e., the signal intensity in vessels within the tissue would begin at a baseline value x, experience a decay as the contrast enters, reach a peak, and then return entirely to the initial x value). However, this idealized scenario does not reflect the reality, particularly in brain tumors, where factors such as vascular heterogeneity, blood-brain barrier (BBB) disruption, and vascular tortuosity introduce complexities. These deviations from the assumed vascular dynamics lead to additional intra- and extra-vascular effects, commonly referred to as T1 and T2* (leakage) effects that affect the curve morphology [6,7]. Consequently, these phenomena can introduce inaccuracies, causing the area under the curve (AUC) to be either underestimated or overestimated, depending on the recovery phase of the curve, which may be influenced by T1 effects (recovery above

baseline, leading to underestimations) or T2* effects (recovery below baseline, leading to overestimations), particularly in tumor tissue. A more in-depth discussion on leakage effects is presented later in this introduction. At any rate, this emphasizes the importance of applying leakage correction methods to achieve accurate CBV calculations. The most widely adopted approach for this purpose is the Boxerman-Schmainda-Weisskoff (BSW) model [1,2]. *Figure 1*.

It is worth noting that modern commercial software packages typically include tools that streamline this entire process, automating steps such as the conversion from signal intensity to $\Delta R2^*$, as well as leakage correction.

Furthermore, for robust quantification, given its relative nature, the CBV of a specific region should be normalized, most commonly to the normal-appearing white matter (NAWM). This results in the frequently utilized metric of relative, corrected, and normalized CBV (nrCBVcorr), though it is often simply referred to as CBV or rCBV. This metric correlates with histological measures of tissue vascularization [1,2].

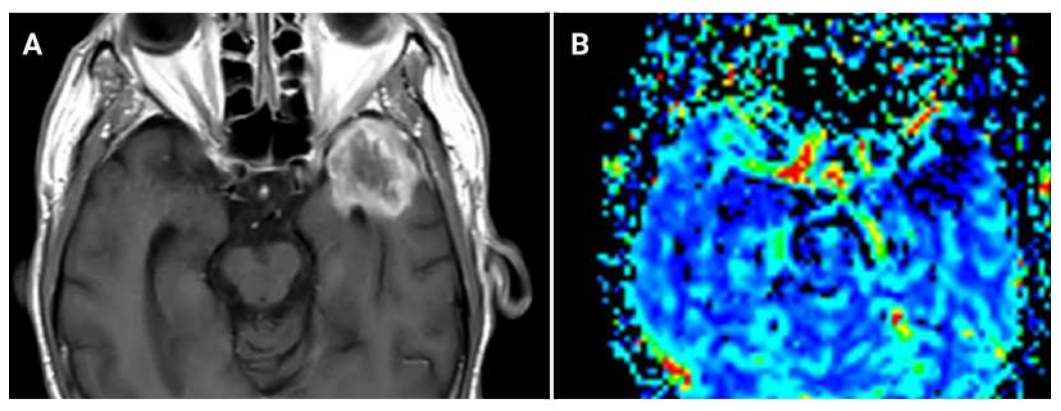
1.2. Clinical Use, Interests and Applications of DSC-PWI

DSC-PWI is an advanced additional sequence that complements morphological MRI. While morphological MRI is valuable, it has limitations and is highly dependent on the radiologist's experience. In this context, DSC-PWI provides advanced semi-quantitative information, offering added value to the evaluation provided by morphological imaging alone.

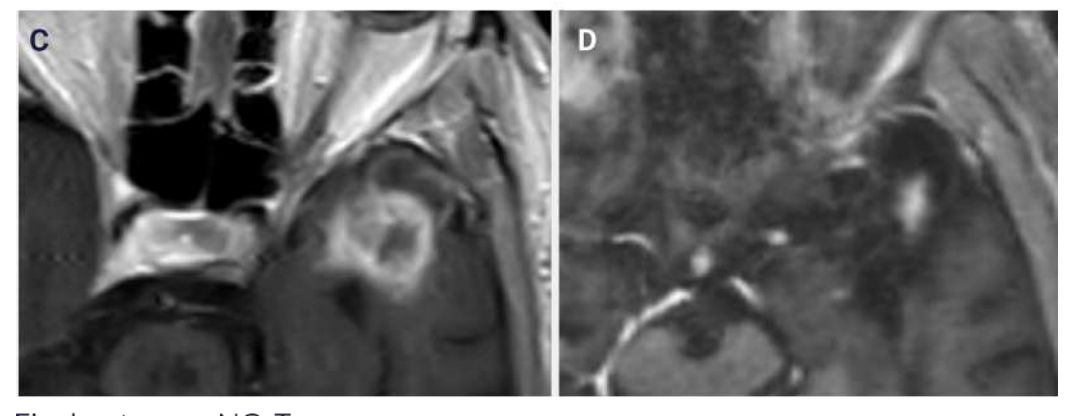
DSC-PWI has demonstrated significant efficacy in the scientific literature, and it is regarded as a valuable clinical tool by a majority of neuroradiologists across various scenarios such as:

- Differentiation of tumoral and non-tumoral entities [8]; (example in figure 2).
- Pre-surgical diagnosis of tumors with characteristic perfusion patterns such as lymphoma [9]; (example in figure 3).
- Differentiation of high-grade glioma and metastasis, considering the enhancing tumor and particularly the peri-enhancing area [10]; (example in *figure 3*).
- Histological grading [11,12] and prognostic stratification [11,13] of astrocytomas
 [14].
- Differentiation of tumor recurrence and post-treatment effects [15].

Diagnostic MR.



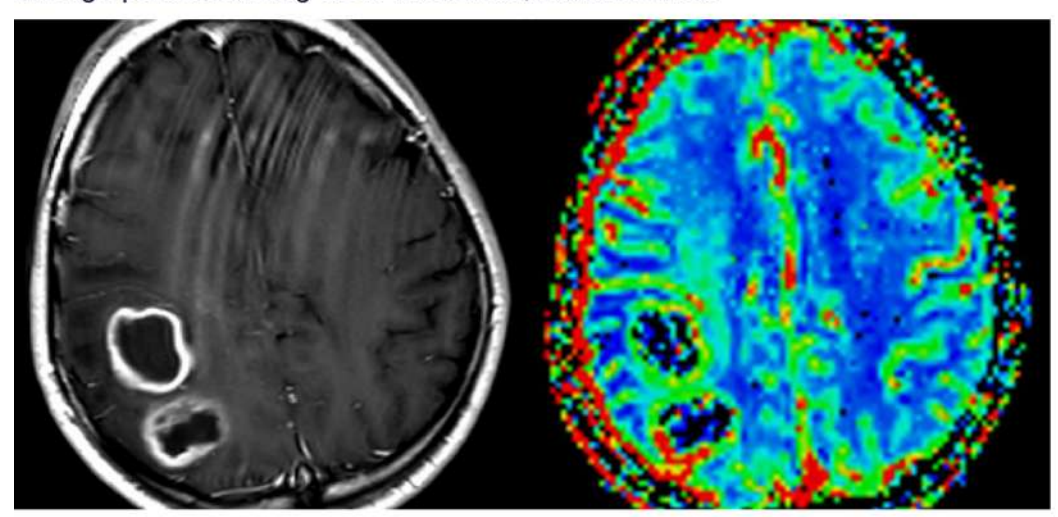
Follow-up MRs.



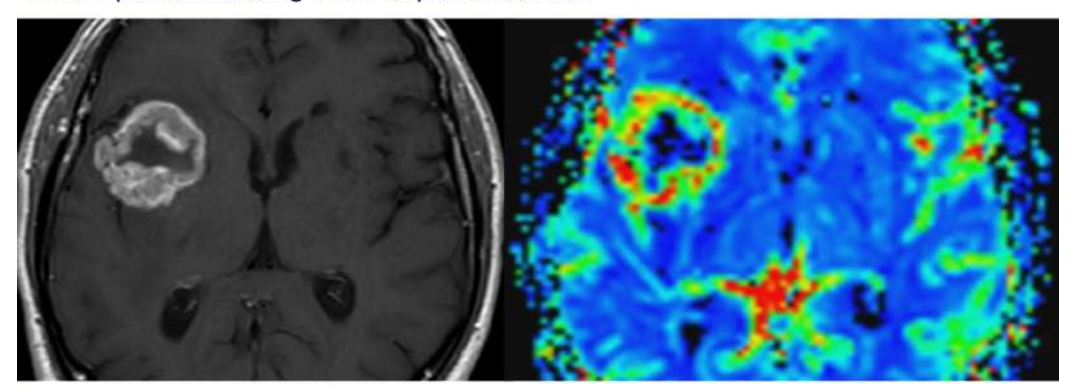
Final outcome: NO-Tumor

Figure 2 (*Created by the author for this thesis*): Example case illustrating a mass-like enhancing lesion with low CBV, raising suspicion of a non-tumoral entity. **A**. The CE-T1 sequence from the diagnostic MRI suggested a right temporal tumor. **B**. However, the low CBV observed on the CBV color map indicated the possibility of a non-tumoral lesion. **C**. CE-T1 in follow-up MR imaging at 1 month demonstrated a reduction in lesion size. **D**. The reduction continued at the 4-month follow-up, confirming the lesion was indeed not a tumor. Consequently, the patient was spared unnecessary aggressive neurosurgery.

A. High perienhancing CBV: infiltrative, multifocal Gb



B. Low perienhancing CBV: expansive, Met



C. Low to intermediate CBV: Lymphoma

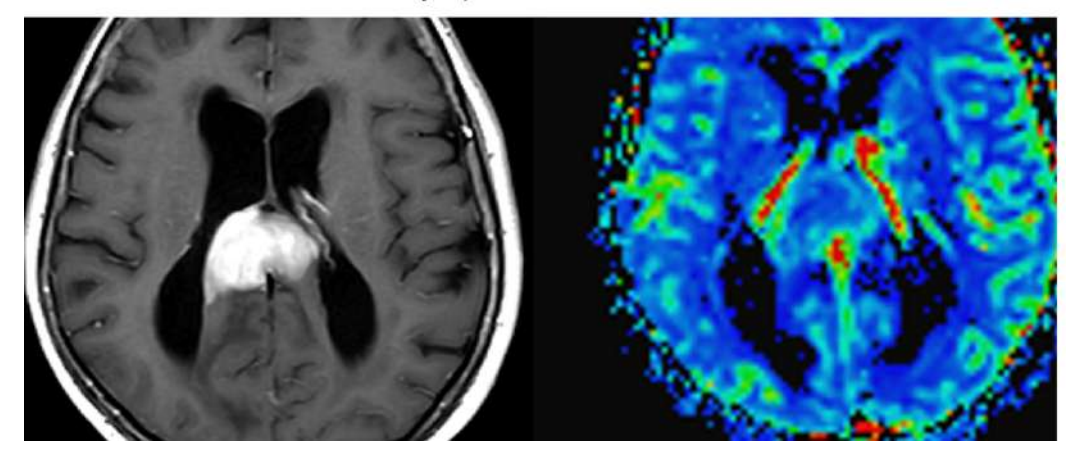


Figure 3 (*Created by the author for this thesis*): Three different example cases demonstrating how CBV contributed to the differential diagnosis of adult brain tumors, enabling reliable pre-surgical assessment. CE-T1 and CBV color maps provided for each case. **A**. High CBV observed around a right parietal bifocal enhancing necrotic tumor suggested an infiltrative neoplasm, consistent with Glioblastoma. **B**. In contrast, low CBV surrounding a necrotic enhancing tumor in the right insular and opercular regions pointed towards a solitary Metastasis. **C**. A homogeneously enhancing mass with low CBV in the splenium of the corpus callosum indicated the possibility of a Lymphoma.

9 |

The favored approach for clinical analysis and visualization involves creating CBV colorencoded maps. These maps facilitate the comparison of specific regions of interest (e.g., tumor regions) with other reference areas within the brain. For example, a red color usually signifies a structure with high vascularity and elevated CBV, while a blue color represents structures with low vascularity and diminished CBV.

All of these applications are of great clinical interest and utility for patient care. Firstly, the management and treatment of tumor and non-tumoral entities differ entirely [8]. Secondly, the pre-surgical identification of lymphoma is of utmost importance because corticosteroids should not be administered before a definitive diagnosis is made. In addition, lymphomas should be managed with a biopsy to prioritize chemo-radiotherapy, rather than direct maximal resection as is done in suspected glioblastomas [9,16–18]. Thirdly, when a metastasis is suspected, additional diagnostic studies may be conducted to identify a primary tumor and perform staging in non-oncologic patients or re-staging in known oncologic patients, to decide the best systemic or local treatment approach. In contrast, if glioblastoma is suspected, surgery may be performed without further diagnostic studies [10,17,18]. In summary, the maximal resection of a tumor pre-surgically miss-diagnosed as glioblastoma could represent a non-beneficial and morbid approach in case of lymphoma or metastasis.

Fourthly, the histological grading of astrocytomas can be biased in cases where only a biopsy is performed instead of a maximal resection. This bias can be reduced by DSC-PWI, which may suggest a higher histological grade than the actual biopsy result (known as biopsy bias). Additionally, non-invasive astrocytoma grading may be used to guide patient management, especially in cases where biopsy carries risks (e.g., brain

stem tumors) [11–13]. Finally, tumor recurrence typically necessitates modifications in oncospecific treatment, while post-treatment effects do not. Therefore, misdiagnosing these entities may result in discontinuing effective treatments or continuing ineffective ones that may cause complications.

Recent literature also enhances the role of DSC-PWI in gliomas' molecular characterization (e.g., IDH, MGMT, or 1p19q mutation status) [11,19]. Given the World Health Organization trends in considering biomolecular profiling the cornerstone of gliomas' classification, this potential application may continue to increase. At any rate, this may still be considered under research and has not widely reached the clinic in most neuroradiology departments.

Ultimately, the inclusion of DSC-PWI in the most recent consensus recommendations [2–4] for brain tumor imaging is an essential proof of its importance in current neuroradiology.

In this thesis, the use of DSC-PWI for the specific identification of various types of brain lymphomas will be examined, with an emphasis on their differential diagnosis from a wide spectrum of brain tumors. Additionally, the challenging differentiation between single metastases and glioblastoma will be addressed. The study will also focus on the detection of distinct imaging signatures of rarer adult cerebellar tumors—pilocytic astrocytoma, hemangioblastoma, medulloblastoma, and metastases—which are infrequent, remain underexplored and present unique management challenges. Furthermore, the molecular classification of adult-type diffuse gliomas will be explored. In particular, the differentiation between IDH-mutant astrocytomas and oligodendrogliomas, as well as

the distinction between IDH-mutant grade 4 astrocytomas and glioblastomas, will be analyzed. These topics will be expanded upon through the works presented in the subsequent sections of this thesis.

1.3. Brief Insights from Morphological MRI

As previously introduced, morphological MRI can be helpful but remains insufficient for optimal evaluations. However, some morphological features can provide valuable insights in different clinical scenarios.

For instance, regarding entities relevant to this thesis, lymphomas typically appear as homogeneously hyperdense lesions on CT, hypointense on T2-weighted MRI, exhibit diffusion restriction, and show homogeneous post-contrast enhancement [9,20]. However, in the context of immunodeficiency and Epstein-Barr virus positivity, lymphomas may present with extensive necrosis, mimicking other brain tumors such as glioblastomas or metastases [21]. Necrotic lesions with an infiltrative pattern and coexisting ill-defined enhancing and non-enhancing tumor regions suggest glioblastoma [14,22]. In contrast, expansile well-defined ring-enhancing lesions with an expansile nature are characteristic of metastases [23].

On the other hand, in adult cerebellar tumors, hemangioblastomas and pilocytic astrocytomas often present as cystic lesions with a solid mural nodule, whereas medulloblastomas are characterized by prominently restricted diffusion in their solid components [24].

Furthermore, molecularly defined adult-type diffuse gliomas also exhibit distinct morphologic characteristics: IDH-mutant astrocytomas are typically nodular, well-defined, and may show a T2-FLAIR mismatch sign; whereas oligodendrogliomas often display calcifications, heterogeneity, and ill-defined margins, with growth patterns that tend to follow the cortex [14,25,26]. Meanwhile, IDH-mutant grade 4 astrocytoma remains a relatively poorly understood entity. Differentiating its features from those of IDH-wildtype glioblastoma, particularly in young adults, is a challenging but still under-researched topic [14,27].

Although these summarized morphological imaging findings can be helpful, they are highly variable, not always present, sometimes overlap, and rare presentations of diseases exist. Additionally, their detection and characterization depend on the radiologist's experience and skills. This variability underscores the potential added value of advanced physiological and quantitative/semi-quantitative sequences such as DSC-PWI, as well as the importance of integrating this sequence into comprehensive evaluations, as recommended by the most recent consensus guidelines for brain tumor imaging [2–4].

1.4. The Current Limitations of the DSC-PWI Sequence

The CBV is widely accepted among clinicians due to its intuitive correlation with underlying pathophysiology and its straightforward visualization in color maps, typically integrated within PACS tools. However, several limitations should be acknowledged.

Relying solely on a dichotomous visual representation (the "hot-red" versus "cold-blue" approach) can be insufficient for addressing more complex cases. Moreover, an im-

portant caution to note in visual evaluations of color maps is that many color-encoding schemes are non-linear, which can artificially amplify very subtle differences in perfusion, potentially leading to misinterpretation [1].

For clarification, the difference between linear and nonlinear CBV maps lies in how the values are visually represented. Linear CBV maps display values proportionally to their actual magnitude. For instance, a CBV value that is twice as high will be represented by a color that is twice as intense on the scale. The advantage of this approach is that it preserves the true quantitative relationship between values. In contrast, nonlinear CBV maps apply a transformation, such as a logarithmic scale, which distorts the true proportionality of the values and can lead to less precise interpretations. Also, the common radiological practice of manual thresholding, in nonlinear color maps, may further exaggerate the contrast between structures, even though the actual underlying CBV values remain unchanged—another potential limitation that can lead to visual misinterpretation and is significantly mitigated with linear maps.

On the other hand, in standard clinical practice, for situations requiring quantification, the manual selection of regions of interest (ROIs) in tumor tissue and normal-appearing white matter (NAWM) references is highly operator-dependent, resulting in limited reproducibility and reduced inter-reader agreement. To address this, adopting more robust and reproducible data extraction methods—such as automated selection of the entire tumor volume of interest (VOI) or standardized/automated NAWM references—could significantly enhance global reliability, reproducibility, generalizability, and robustness [28–30]. *Figure 4*.

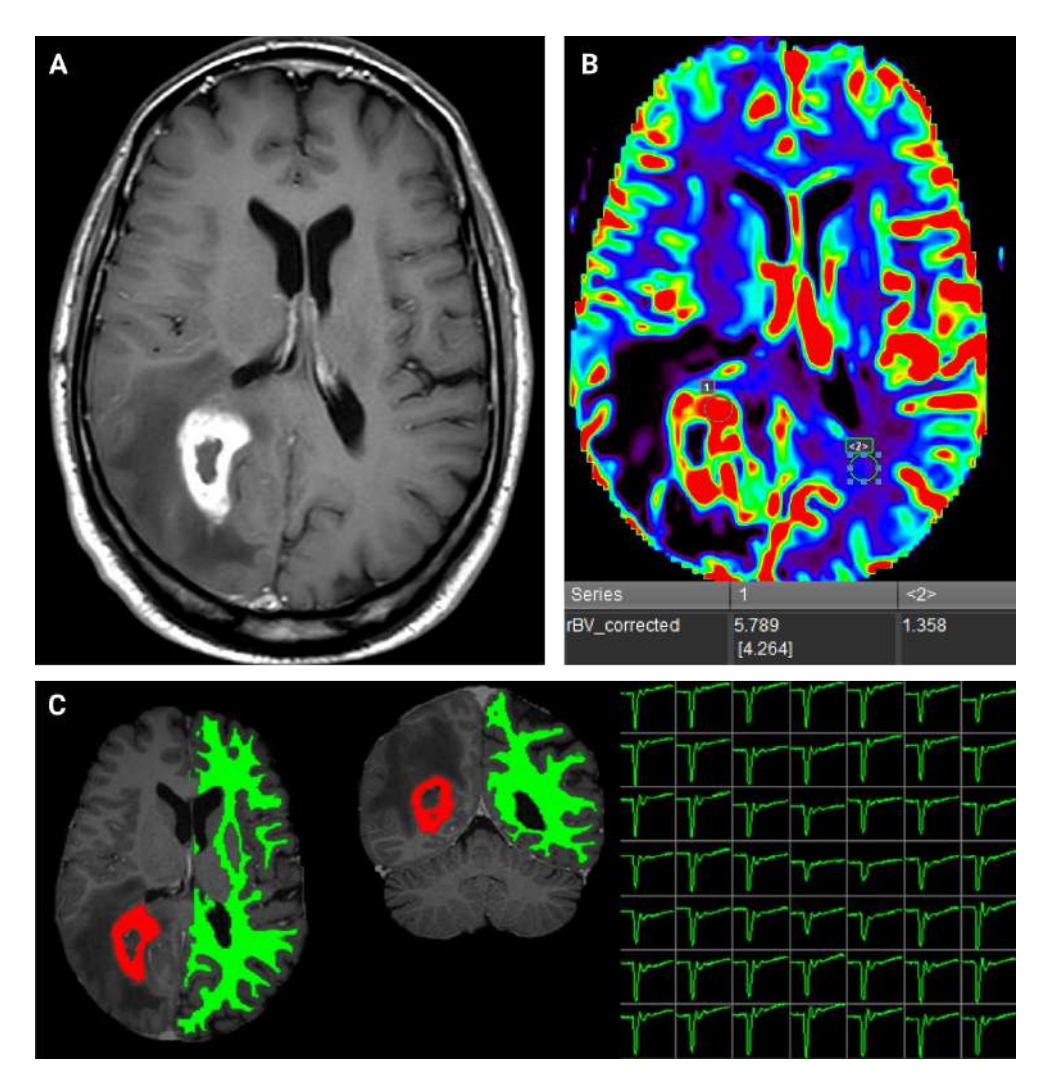


Figure 4 (*Created by the author for this thesis*): **A.** CE-T1 imaging demonstrates a necrotic tumor with peripheral enhancement located in the right parietal lobe. **B.** Representation of the current standard methods of quantification in clinical practice, focusing on manually depicted ROIs (Circle 1 and Circle 2). ROI 1 represents tumor tissue (note that the vast majority of the tumor is not included in the ROI). ROI 2 represents the NAWM reference. Note that these ROIs may differ in size, shape, and location, depending on the operator. The software provides a single quantifiable value corresponding to the normalized CBV of the tumor: 5.789 (tumor ROI) / 1.358 (NAWM ROI) = 4.264 (normalized corrected relative CBV). **C.** Representation of an alternative method using volumetric, full-tumor, and automatic NAWM selection for improved data extraction from the sequence. In contrast to the standard methodology, computations can be performed using 3D automatic segmentations of both the tumor (red) and NAWM (green). This approach allows raw-data extraction at the voxel level and extends beyond CBV, enabling the incorporation of additional metrics derived from the time-intensity curve in each voxel.

Furthermore, limiting evaluations to CBV alone oversimplifies the wealth of information available from the sequence. Incorporating complementary metrics alongside CBV offers an opportunity to enrich the depth and accuracy of sequence evaluations [1,31,32].

1.5. DSC-PWI Data Selection/ Extraction Methods

The literature presents various approaches to DSC-PWI analysis, encompassing a broad spectrum of complexity. Analyses range from determining average or extreme (maximum or minimum) values within manually delineated 2D axial ROIs to employing voxel-level histograms and percentiles derived from 3D volumetric segmentations [28,33].

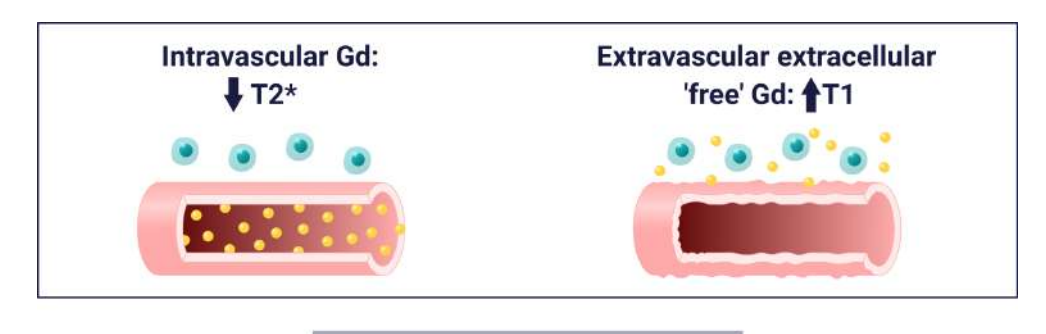
Assessing mean CBV values from manual axial ROIs or obtaining maximum CBV values, primarily through manual 'hot-spots', is not uncommon. While this relatively simplistic approach might suffice in situations where the anticipated differences between entities are pronounced or the tissues are histologically homogeneous, it may not be the most robust.

To achieve the best outcomes in challenging scenarios, it is essential to employ volumetric, voxel-level analysis that accounts for tissue heterogeneity and extracts critical information on a voxel-by-voxel basis. Additionally, NAWM references should be selected automatically to reduce operator dependency and enhance the robustness of normalized values. Indeed, such methods should be considered requisite for optimal evaluations [1,28,33]. *Figure 4*.

1.6. More Than Just CBV in DSC-PWI Sequences: PSR (and the Leakage Effects) and Peak Height

The main raw data of DSC-PWI are time-intensity curves. These curves convey much more information than just CBV. For instance, a metric that has gained traction in neuro-oncology radiology is the Percentage of Signal Recovery (PSR) [31,34–37].

It is currently well understood that the curve morphology is not solely determined by the intravascular transit of gadolinium. If the BBB is compromised, leakage can occur, which then modifies the recovery phase of the curves. This alteration is influenced by the disruption of the BBB and by the composition of the extravascular-extracellular space (EES) - including cells and molecules - that interacts with the leaked contrast. Moreover, even without BBB disruption, certain abnormal vascular structures can modify the typical contrast transit through vessels, further affecting curve morphology. These events lead to what are known as leakage effects, which can manifest as both T1-effects and T2*-effects [6,7]. Figure 5. For clarity through simplification: T1 effects result in an elevation of the recovery line, while T2* effects lead to its descent. These effects necessitate the correction for leakage when calculating CBV. If T1 effects dominate, the AUC and, consequently, the CBV could be underestimated. Conversely, if T2* effects are more prominent, there is a risk of overestimation.



PERMEABILITY

NO BBB DISRUPTION

VASCULARITY Normal vessels: No leakage effect: VASCULO-ARCHITECTURE Increased, big and tortuous vessels, 'retained' intravascular Gd: T2*- effect

BBB DISRUPTION

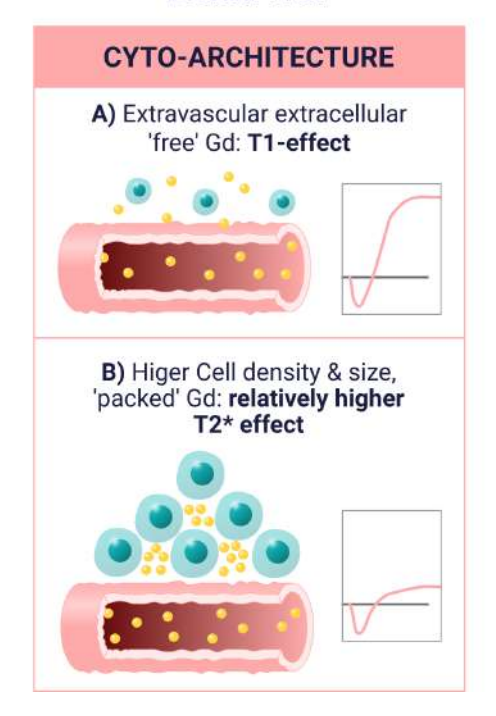


Figure 5 (Original graphic created by the author, redesigned by Norarte Visual Science for this thesis): This illustration depicts the physiopathological mechanisms underlying leakage effects and the interplay between extra- and intravascular phenomena, which depend on BBB integrity (permeability), EES composition (cyto-architecture), and vascular characteristics (vasculo-architecture). In summary: intravascular GBCA reduce the T2* signal, while gadolinium in the EES increases the T1 signal. When the BBB is intact, the contrast remains confined within the blood vessels. In normal tissue, this results in an ideal time-intensity curve that provides accurate information about total vascularity. In tissue without BBB disruption but with abnormal vascularity or microvascularity, dense capillaries may retain GBCA, leading to T2* effects that indirectly provide additional information about the vasculo-architecture. Lastly, in cases where the BBB is disrupted, GBCA leaks into the EES, producing T1 effects. These effects are further influenced by the interaction of GBCA molecules with each other and with cell membranes, offering additional insights into BBB permeability and integrity and also indirectly about the cyto-architecture. Note that in cases of BBB disruption, there may also be a contribution of vasculature architecture to the final leakage effects and curve morphology, which ultimately reflect the equilibrium between permeability, vascularity, vasculo-architecture, and cyto-architecture.

However, it is crucial not to disregard these leakage effects as irrelevant. In reality, they encapsulate a broad spectrum of underlying pathophysiological phenomena that can provide valuable insights into tumor tissue evaluation. In this context, the PSR serves as an indirect indicator of these effects, and its diagnostic value has been well-established, particularly when differentiating between tumor types that vary in permeability, cellularity, and vascularity. For instance, pronounced BBB disruption observed in Lymphomas can lead to a heightened PSR, primarily due to T1 effects [9,34,36]. Conversely, marked vascular tortuosity seen in hypervascular metastases or hemangioblastomas can result in a reduced PSR, stemming primarily from T2* effects [36,38].

These effects can be distinctly interpreted based on whether the tumor is associated with BBB disruption or integrity. In the presence of disruption: gadolinium that has diffusely leaked into the EES (i.e., in an environment with low cell volume and/or density) can lead to an increase in T1, manifesting as T1-effects and a consequent elevation in PSR. In contrast, concentrated leaked gadolinium in the EES (i.e., in an environment with high cell volume and/or density) results in the shortening of T2*, culminating in a decreased PSR. Thus, within the context of BBB disruption, PSR also offers insights into cellularity. In contrast, in tumors without BBB (such as metastases, meningiomas, and hemangioblastomas) or in cases without BBB disruption (like non-enhancing lower-grade gliomas), the PSR primarily serves as a vasculo-architectural marker. This is because both permeability and cellularity, phenomena that occur within EES, are excluded from consideration, as all the contrast remains intravascular in such cases. Hence, from this understanding, it is evident that both intra- and extravascular components play roles in determining leakage effects [6,7]. However, the entirety of this data is intricate to deci-

pher (disentangle) given multicausality deriving only in somewhat binary leakage effects [39,40]. I.e., PSR is only a reflection of the equilibrium between T1 and T2* effects, therefore, a high PSR may indicate significant BBB rupture but not necessarily the absence of vascular tortuosity, or vice versa: it simply represents an estimation of the proportion between these phenomena. *Figure 5*. From the author's perspective, an in-depth understanding of leakage effects is essential for clinical neuroradiologists using DSC-Perfusion. This understanding is crucial both for interpreting derived metrics and for maintaining a critical perspective when using a DSC sequence with specific pulse-sequence parameters.

Another fundamental metric derived from time-intensity curves, in addition to PSR, often incorporated in DSC-PWI evaluations in neuro-oncology, is peak height (PH). *Figure 6*. PH is characterized as a measure of the total capillary volume, distinguishing it from CBV, which quantifies the overall gross vascularization [38,41].

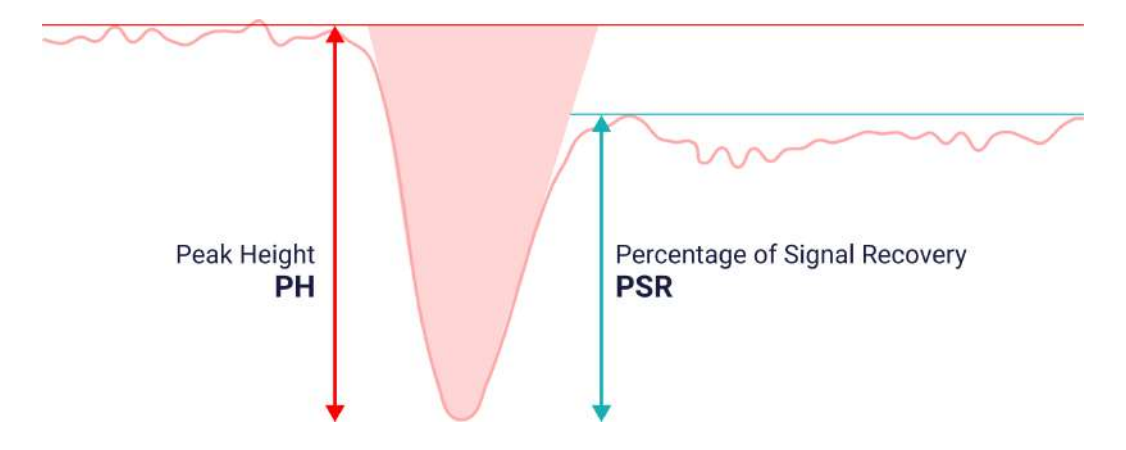


Figure 6 (Original graphic created by the author, redesigned by Norarte Visual Science for this thesis): Illustration of PSR and PH on a time-intensity curve.

Usually, authors using PSR and/or PH, compares the results with CBV, as if one must choose between the metrics. However, the information provided by each metric is different and they probably provide additive rather than exclusive information. In fact, including PSR and PH to single CBV evaluations (making combined use of all the information) could be a step toward richer data interpretation.

However, the time-intensity curves hold even more information. For instance, time parameters (time to peak, mean transit time), descending and ascending curves slopes, recovery at different time-points, etc. can offer also valuable and otherwise hidden and unknown information. At this regard, another approach to enhance the insights derived from DSC curves is a comprehensive analysis of the whole curves themselves, evaluated unsupervisedly (exploratory, without the input of prior knowledge or assumptions) point-by-point, without reliance on pre-selected specific metrics such as CBV, PSR or PH.

1.7. Unsupervised Analysis of the Whole Time-intensity-curves

As previously explained, DSC-PWI produces time-intensity curves by dynamically monitoring T2* signal intensity changes during contrast administration. Metrics such as CBV, PSR, and PH are derived from these TICs. Several methods, ranging from visual evaluation [42] to complex curve components analyses or deep-learning pattern recognition of the entire TICs has been suggested by some authors [43–45].

However, no prior studies have quantitatively assessed the entire TIC by viewing it as a continuum of points that together form the curve. Such an approach is more reproducible than visual evaluations and also more intuitive, contrasting with complex methods that often remain beyond the grasp of many clinicians. This challenge may arise from various technical and physiological factors that impede direct point-by-point comparisons, such as variations in the timing of dynamics between sequences or differing heart rates among patients. Therefore, for a point-by-point comparison to be feasible, the curves must be normalized both in time and, as somewhat commonly done with CBV, also in intensity. I.e., given that raw intensity is arbitrary and relative, its significance emerges only when compared to the intensity of reference normal white matter. Additionally, temporal aspects are crucial; for instance, the curve of a patient with a heart rate of 40 beats per minute might vary significantly from that of a patient with a heart rate of 90. Thus, the creation of normalized TICs would mitigate the effects of both physiological and certain technical factors. This includes considerations such as patient's cardiovascular constants and the dynamic timing of sequences. For normalization, both reference intensity and time values should be derived from the contralateral normal-appearing contralateral white matter (NAWM). To ensure reproducibility and robustness, the optimal parameters would be the maximal signal intensity drop and the time to peak minus the time to arrival (TTP-TTTA). The latter can be equivalently expressed as relative time to peak (rTTP). Figure 7.

Implementing this approach could offer several compelling advantages: 1) It may enable the possibility of performing a direct comparison of the entire TIC between tumor types on a point-by-point basis, not limited to concrete parameters such as CBV or PSR; and 2) it may enhance the construction of user-friendly classifiers based on quantitative and visual comparison of the curves of new unknown particular cases to a data set of

From non-comparable tumor curves of different patients and their respective NAWM curves,... Patient 1 Patient 2 NAWM curves ... tumor intensity is normalized to Peak Height (PH) and time is to rTTP (TTP-TTA) of the NAWM.

Finally obtaining directly and quantitatively comparable curves among different patients and exams.

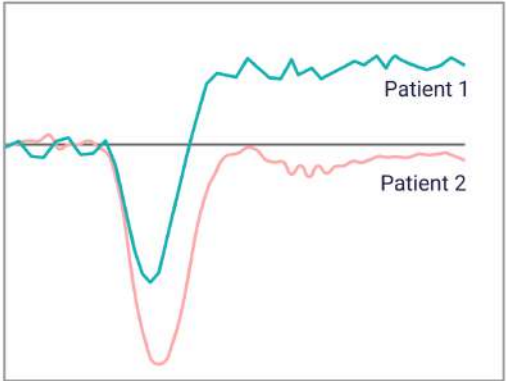


Figure 7 (*Original graphic created by the author, redesigned by Norarte Visual Science for this thesis*): Illustrative scheme emphasizing the necessity for TIC normalization to facilitate comparison. Tumor curves from two distinct patients and their corresponding NAWM curves are displayed. Direct comparison of the tumor curves is hindered due to variations in baseline, starting points, timings. The reference values, maximal signal intensity drop (PH) and time-to-peak minus time-to-arrival (rTTP) from the NAWM, are indicated. Resulting normalized curves are shown, being now comparable visually and quantitatively on a point-by-point basis.

different brain tumors. This alternative hypothetical methodology was named DSC-PWI Curvology by the author of this thesis.

For clarification, one might wonder whether curve morphology analysis, like CBV calculation, should be performed using time- Δ R2* curves. However, when analyzing DSC curve morphology (which applies not only to overall curvology but also to specific curvologic metrics such as PSR), it is important to note that this evaluation should be based on time-intensity curves rather than time- Δ R2* curves. Time- intensity curves preserve the raw data acquired by the scanner, capturing both T1 and T2* effects. While the conversion from signal to Δ R2* is crucial for accurate CBV calculation, it may oversimplify or obscure critical morphological features of the curve, such as recovery dynamics influenced by contrast leakage or vascular heterogeneity. For a comprehensive analysis of DSC curve morphology, the original time- intensity data offer a more complete representation of the complex interplay between physiological and technical factors.

Ultimately, by recognizing DSC as a complex, four-dimensional data matrix (dynamic sequence) that captures a broad spectrum of TIC point values, CBV, PSR, and PH values, we gain insight into its intricate nature and its place in the emerging realm of big data. This viewpoint situates the sequence squarely within the expanding domains of artificial intelligence, deep learning, machine learning, and radiomics.

1.8. MR Technique: Pulse-sequence Parameters Considerations

Historically, DSC-PWI quantitative results from single-site and localized studies have sometimes deteriorated or failed during external validation or clinical trials. Apart from

potential variances in metric calculations steps—ranging from normalization, relativization, and leakage correction to data selection—these discrepancies can be attributed to pulse-sequence parameters. Primary factors include the flip angle (FA), taking into account the common echo time (TE) and repetition time (TR) values of approximately 35 ms and 1500 ms, respectively, whether contrast preload (dose of contrast given before the main DSC acquisition) is used, and the interaction between these parameters [2].

Currently, it is widely recognized that an intermediate-FA (approximately 60°) with a fulldose preload, and a low-FA (approximately 30°) without a preload, are the preferred flip angles for accurate CBV measurements, minimizing leakage phenomena. Fractional dose preloads are not commonly recommended [2]. Firstly, it is important to emphasize that using a preload is not essential for acquiring accurate CBV measurements when low FAs are employed. Avoiding preload simplifies the technical process, reduces potential variables (such as preload dose and incubation time), and eliminates the need for a double dose of contrast when it is not warranted. Notably, the choice to use a preload and its associated dose significantly impacts the leakage effects (and consequently metrics such as PSR or curve morphology), which ideally should be evaluated in sequences without a preload [46]. I.e., administering a preload of contrast saturates the extravascular extracellular space (EES), thereby preventing contrast leakage. Consequently, this eliminates the ability to capture information regarding such phenomena. In fact, the two most recent consensus guidelines recommend using a 30°FA sequence without preload as the primary option, unless there are specific reasons to administer a double dose of contrast [3,4].

However, the debate remains open. The sequences recommended by the consensus are rooted in theoretical models, computer simulations, in vivo studies, and clinical data, all aimed at accurately capturing CBV values. This necessitates the reduction of leakage effects. However, while sequences optimized for CBV might provide accurate values, they could potentially compromise the performance of those metrics related to leakage effects. This is of note since for example PSR has already also been highlighted as a valuable diagnostic tool in certain neuroradiological challenges, such as distinguishing lymphomas or even identifying post-treatment effects [31,32,34,36,47,48]. Given these considerations, one must question: Are sequences optimized for CBV always the best choice for diagnostic accuracy across all clinical scenarios? This is likely open for debate.

The solution could involve tailoring data acquisition strategies based on the specific clinical context, or perhaps by merging different acquisition or post-processing methods to best capture all pertinent metrics. Future innovations may address these potential limitations, for instance, by developing DSC-PWI protocols that combine different pulse-sequence parameters to harness optimal information for every metric (e.g. dual-echo DSC-PWI) [37,39]. However, nowadays single pulse-sequence parameters acquisitions (standard DSC) dominate the clinic and are the one considered in this thesis mainly focused on direct clinical applicability. At any rate, regardless of the approach, the authors acknowledge standardization—from pulse-sequence parameters to post-processing and data generation—is crucial for achieving widespread generalizability and global applicability. All these more technical aspects will also be discussed in this thesis.

1.9. Summarizing Rationales and Proposed Approaches

Time-intensity curves offer a wealth of information not just about total gross vascularization (CBV), but also about the nature of vascularity and vasculoarchitecture (whether it is venous, arterial, capillary, or irregular and tortuous), permeability of the BBB, and cellularity. While some of this information may be somewhat grasped by including PSR and PH in the analysis, some information may still remain hidden. Undoubtedly, the full TIC provides a richer understanding than any single metric alone, leading to the emergence of DSC-PWI Curvology. Also, metrics such as CBV, PSR, TICs, and PH might be viewed as complementary rather than mutually exclusive. Thus, integrating them in a voxel-wise manner could herald the advent of a holistic Perfunomics.

The main goals of this thesis focus on addressing specific challenges associated with data selection, the process of extraction for analysis, and the exclusive reliance on CBV evaluation from DSC. To meet these objectives, the research introduced in this thesis proposes multiple methodologies. These methodologies predominantly hinge on the unsupervised (exploratory, without the input of prior knowledge or assumptions) selection of metrics (PSR, PH, CBV and TICs) derived from comprehensive tumor segmentations. This approach ensures an encompassing representation of all DSC-PWI information together with whole tumor heterogeneity, drawing a sharp contrast to the narrow but usual perspective offered by 2D manual ROIs and preselected values of only CBV. Also important, the automatic selection of NAWM references is a preferred method for improving reproducibility.

The innovation of this work is underscored by the introduction of unsupervised analysis of time-intensity curves on a point-by-point basis. Additionally, by amalgamating various metrics and optimally selecting their values without pre-determined criteria, we break new ground. The utilization of normalized curves, multi-metric considerations, and unsupervised value selection in a voxel-wise methodology is anticipated to significantly enhance diagnostic outcomes, setting it apart from traditional approaches that rely on single metrics with predetermined values.

Ultimately, we will leverage our methodologies on retrospective datasets, aiming to address salient clinical inquiries pertaining to the non-invasive pre-surgical diagnosis of brain tumors. While the author proudly recognizes that this entire research line extends beyond the pre-surgical diagnosis scope of the thesis, and its fields of application are vast (e.g., imaging follow-up of treated brain tumors), he wants to highlight that the non-invasive diagnostic field has a burgeoning clinical impact and continues to address a crucial unmet need. As personalized medicine advances, the capability to non-invasively identify specific entities directly influences patient management, surgical approaches, treatment strategies, and prognostic estimations. Ultimately, this profoundly affects the delivery of patient care in a tailored fashion.

Of note, two narrative reviews and one extensive scientific commentary published during the course of this thesis are included following this introduction (See section introduction appendix). These reviews explore the importance and state of the art of imaging-based pre-surgical diagnostic approaches for major adult brain tumors, such as lymphomas and gliomas, and provide a comprehensive, up-to-date critical overview of DSC-PWI sequences relevant to clinical neuroradiologists.

1.10. Introduction Appendix - Review Articles

This appendix comprises three articles, presented in their published form and organized in the following order:

- Pons-Escoda A, Smits M. Dynamic-susceptibility-contrast perfusion-weightedimaging (DSC-PWI) in brain tumors: a brief up-to-date overview for clinical neuroradiologists. Eur Radiol. 2023 Nov;33(11):8026-8030. doi: 10.1007/s00330-023-09729-3. Epub 2023 May 13. PMID: 37178200.
- 2. Pons-Escoda A, Naval-Baudin P, Velasco R, Vidal N, Majós C. Imaging of Lymphomas Involving the CNS: An Update-Review of the Full Spectrum of Disease with an Emphasis on the World Health Organization Classifications of CNS Tumors 2021 and Hematolymphoid Tumors 2022. AJNR Am J Neuroradiol. 2023 Apr;44(4):358-366. doi: 10.3174/ajnr.A7795. Epub 2023 Feb 23. PMID: 36822829; PMCID: PMC10084903.
- 3. Pons-Escoda A, Majos C, Smits M, Oleaga L. Presurgical diagnosis of diffuse gliomas in adults: Post-WHO 2021 practical perspectives from radiologists in neuro-oncology units. Radiologia (Engl Ed). 2024 May-Jun;66(3):260-277. doi: 10.1016/j.rxeng.2024.03.002. Epub 2024 Mar 23. PMID: 38908887.

COMMENTARY





Dynamic-susceptibility-contrast perfusion-weighted-imaging (DSC-PWI) in brain tumors: a brief up-to-date overview for clinical neuroradiologists

Albert Pons-Escoda^{1,2} • Marion Smits^{3,4,5}

Received: 14 March 2023 / Revised: 26 April 2023 / Accepted: 2 May 2023 / Published online: 13 May 2023 © The Author(s), under exclusive licence to European Society of Radiology 2023

Abbreviations

CBV Cerebral blood volume

DSC-PWI Dynamic-susceptibility-contrast

perfusion-weighted-imaging

GBCA Gadolinium-based contrast agent

IDH Isocitrate dehydrogenase

MGMT O(6)-Methylguanine-DNA methyltransferase

PSR Percentage of signal recovery

ROI Region of interest

Introduction

Dynamic-susceptibility-contrast perfusion-weighted-imaging (DSC-PWI) is an MRI technique that provides non-invasive in vivo assessment of microvascular environments. It consists of a dynamic acquisition during the vascular transit of a gadolinium-based contrast agent (GBCA) bolus. In the field of brain tumors, it is preferably gradient-echo based. The GBCA causes an initial reduction in T2* signal intensity of tissues and subsequent recovery during 'washout'. Time-intensity curves are generated from this process and render various metrics. The most used for brain tumors is cerebral blood volume (CBV) [1], but some others, such as

 ✓ Albert Pons-Escoda albert.pons@bellvitgehospital.cat

Medical Delta, Delft, The Netherlands



percentage of signal recovery (PSR), have gained interest in recent years [1, 2].

The basics

The CBV is calculated by assessing the area under the signal intensity curve and is usually relative, because the signal intensity is not measured in absolute values but as the change in intensity or, preferably, in relaxation rate ($\Delta R2^*$). Leakage correction methods should be applied (the most common being the BSM, Boxerman-Schmainda-Weisskoff) to avoid miscalculations due to leakage effects [1]. The leading current commercial software packages perform all these steps automatically. Finally, the CBV of a concrete region should also be normalized, the most accepted to the normal-appearing white matter. The result is the most frequently used parameter of relative, corrected, and normalized CBV (often terminologically [mis]-simplified as rCBV), which has been related to histological measures of tissue vascularization.

On the other hand, the PSR is measured relative to the time-intensity curve baseline. It quantifies the T1 (signal recovery above baseline) or T2 (signal recovery below baseline) leakages. These effects are explained by a complex combination of blood–brain barrier permeability, vascular volume fraction and vessel size, and tumor cell size and density [2].

In an oversimplified statement, higher CBV and lower PSR may be related to hypervascularization and angiogenesis, while lower CBV and higher PSR may correspond to a leaky blood–brain barrier.

Clinical applications

DSC-PWI has shown excellent results in scientific literature, and it is considered of actual clinical aid by most of the neuroradiologists in many scenarios:

Department of Radiology, Hospital Universitari de Bellvitge, Barcelona, Spain

Neurooncology Unit, Institut d'Investigacio Biomedica de Bellvitge - IDIBELL, Barcelona, Spain

Department of Radiology & Nuclear Medicine, Erasmus MC – University Medical Centre Rotterdam, Rotterdam, The Netherlands

Brain Tumour Centre, Erasmus MC Cancer Institute, Rotterdam, The Netherlands

- (a) differentiation of tumoral and non-tumoral entities [3];
- (b) presurgical diagnosis of tumors with characteristic perfusion patterns such as lymphoma [4, 5];
- (c) histological grading [6, 7] and prognostic stratification[6, 8] of astrocytomas;
- (d) differentiation of tumor-recurrence and post-treatment effects [9];
- (e) differentiation of high-grade glioma and metastasis, considering the enhancing tumor and particularly the peri-enhancing area [10, 11].

All of these applications are of great clinical interest and utility for patient care. Firstly, the management and treatment of tumor and non-tumoral entities differ entirely [3]. Secondly, the presurgical identification of lymphoma is of utmost importance because corticosteroids should not be administered before a definitive diagnosis is made. In addition, lymphomas should be managed with a biopsy to prioritize chemo-radiotherapy, rather than direct maximal resection as is done in suspected glioblastomas [4, 5]. Thirdly, the histological grading of astrocytomas can be biased in cases where only a biopsy is performed instead of a maximal resection. This bias can be reduced by DSC-PWI, which may suggest a higher histological grade than the actual biopsy result (known as 'biopsy bias'). Additionally, non-invasive astrocytoma grading may be used to guide patient management, especially in cases where biopsy carries risks (e.g., brain stem tumors) [6-8]. Fourthly, tumor recurrence typically necessitates modifications in oncospecific treatment, while post-treatment effects do not. Therefore, misdiagnosing these entities may result in discontinuing effective treatments or continuing ineffective ones that may cause complications [9]. Finally, concerning the differentiation of metastasis and glioblastoma, it is worth noting that histology is not always available. For instance, in known oncologic patients with imaging findings consistent with metastases, a biopsy of the brain lesion may not be performed, and the tumor may be treated based solely on its radiological features. On the other hand, when a metastasis is suspected in nononcologic patients, additional diagnostic studies may be conducted to identify a primary tumor. In contrast, if glioblastoma is suspected, surgery may be performed without further diagnostic studies [10, 11].

Recent literature also enhances the role of DSC-PWI in gliomas' molecular characterization (e.g., IDH, MGMT, or 1p19q mutation status) [6, 12]. Given the World Health Organization trends in considering biomolecular profiling the cornerstone of gliomas' classification, this potential application may continue to increase. At any rate, this may still be considered under research and has not widely reached the clinic in most neuroradiology departments.

Of note, the inclusion of DSC-PWI in the most recent consensus recommendations for brain tumor imaging [1, 13, 14] is an essential proof of its importance in current neuroradiology.

Clinical implementation issues

Data selection/extraction methods

The understandability of the pathophysiology behind CBV and PSR, the availability of friendly software for CBV calculation, and the simplicity of PSR have probably yielded their success among clinical users. However, PSR quantifications are (still) not included in the main commercial software packages and thus is generally still limited to visual inspection of time-intensity curves.

Different approaches with a wide range of complexity in DSC-PWI analysis are found in academic literature. The analysis can include from average or extreme (maximum or minimum) values of manually delineated 2D axial regions of interest (ROI) to voxel-level histograms and percentiles of 3D volumetric segmentations [10]. From a clinical perspective, the more complex and time-consuming the method, the fewer possibilities to be used in the overloaded daily practice. In the authors' experience, visual assessment of CBV color maps or, in particular situations, CBV values assessment of manual axial ROIs are the most frequent DSC-PWI evaluation performed by clinical neuroradiologists. An important word of warning here is that many color-encoding schemes are non-linear, and may artificially enhance small differences in perfusion. Only those more 'DSC-motivated' professionals may venture out and try volumetric segmentations, obtention of maximum CBV values (through manual 'hot-spots' or at best, automatically), and visual evaluations of PSR or time-intensity curve morphology. This quite 'simplistic' approach may be valid for situations where expected differences between entities are extreme or tissues are histologically homogenous. Nevertheless, volumetric voxel-level information that considers tissue heterogeneity and extracts the most relevant information is necessary to reach the best performances in the most challenging situations and, indeed, are the currently preferred methods on the academic side.

An obstacle that may hinder the clinical implementation of more complex approaches is the scarcity of commercial software packages that facilitate straightforward data extraction and user-friendly displays that ideally should be integrated into the PACS system; i.e., voxel-level volumetric information of different DSC-PWI metrics could be presented understandably through visually friendly histograms or percentile tables, facilitating the implementation of the latest research insights into daily practice.



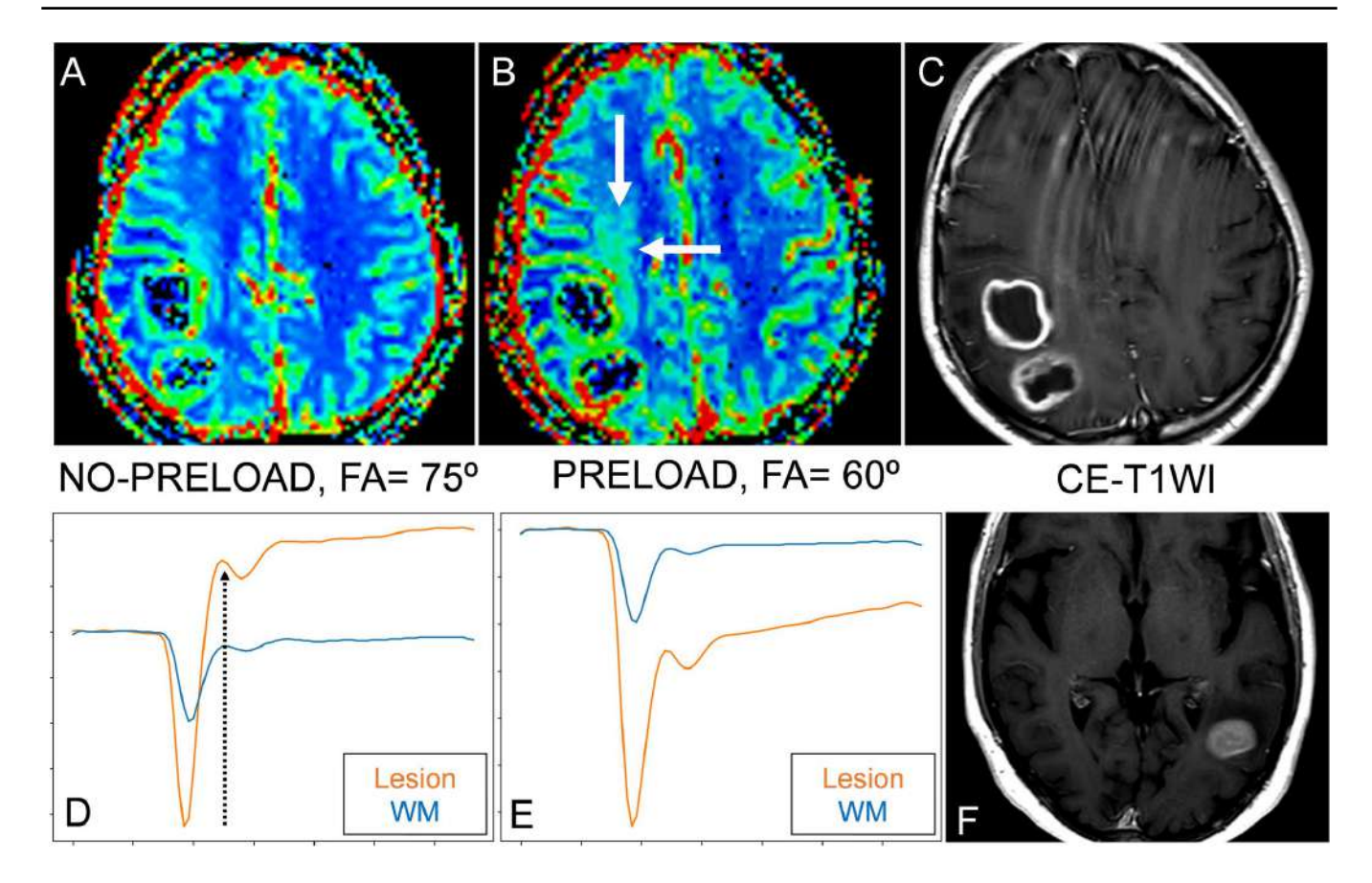


Fig. 1 Examples of the impact of DSC-PWI technique in clinical applications. Two different DSC-PWI sequences. First, FA=75° without preload (**A** and **D**), highly T1-weighted, theoretically favoring PSR performance. Second, FA=60° with preload (**B** and **E**), optimized for CBV calculations. Two different patients. First patient (**A**–**C**): Leakage-corrected rCBV color maps (**A** and **B**) of fronto-parietal ring enhancing lesions (**C**) that could be multifocal glioblastoma or metastasis. In **B** (preloaded, FA=60°), the CBV increase around the enhancing lesions (arrows) is visually much more pronounced than in **A**, which confirms

the infiltrative nature of the lesion and supports the diagnosis of glioblastoma. Second patient (**D** and **E**): Time-intensity-curves (**D** and **E**) of a posterior temporal homogeneously enhancing lesion (**F**) that could be a lymphoma. In **D** (non-preloaded, $FA=75^{\circ}$), the curve morphology with a high recuperation part above the baseline—high PSR- (dashed arrow) strongly suggests lymphoma, whereas the curve in **E** (preloaded, $FA=60^{\circ}$) would not provide such specific information. Case **A**–**C** was an IDH-wildtype glioblastoma and case **D**–**F** was a primary diffuse large B-cell lymphoma of the CNS, both histopathologically confirmed

Pulse-sequence parameters

Historically specific DSC-PWI quantitative results obtained in single-site and local studies tended to worsen, or even fail, when externally validated or clinically tested. Additional to possible differences in any of the steps of metrics calculation (from the normalization, relativization, and leakage correction to data selection), this is explained by pulse-sequence parameters: mainly flip angle (FA) (considering usual echo time (TE) and repetition time (TR) around 35 and 1500 ms), preload administration or not, and the interaction between both [1].

It is currently accepted that intermediate-FA ($\approx 60^{\circ}$) with full-dose preload and low-FA ($\approx 30^{\circ}$) without preload are the preferred flip angles to obtain accurate CBV measurements reducing leakage phenomena. Fractional dose preloads are not among the main recommendations [1, 13, 14]. First, the authors consider it necessary to point out that preload

is not mandatory to obtain accurate CBV measures if low FAs are used. Moreover, preload avoidance reduces technical complexity and potential confounders (preload dose and incubation time) while preventing a double dose of contrast administration when unnecessary. Also interestingly, preload usage and dose greatly influence the PSR, which should be optimally evaluated in non-preloaded sequences [15]. Indeed, the two most recent consensus recommend the 30°FA sequence without preload as the first option if there are no other reasons for double contrast dose [1, 13, 14].

However, the discussion may still arise. The consensus sequences are based on theory, computer simulations, in vivo studies, and clinical data to specifically obtain the most accurate CBV values, which requires minimization of leakage effects. Therefore, CBV-optimized sequences could limit the PSR performance, which has also been described as of diagnostic interest in some neuroradiologists' clinical challenges, such as lymphoma or even post-treatment effects



identification [16–19]. Under this specific consideration: are CBV-optimized sequences, always and without question, the most diagnostic accurate in all clinical scenarios? It is probably debatable, and could be addressed by tailoring the approach to acquiring data based on the clinical context, or by combining acquisitions or post-processing methods that optimally adapt to all relevant metrics. Surely further developments will overcome these potential limitations: e.g., by designing DSC-PWI protocols combining acquisitions with different pulse-sequence parameters, such as acquiring a non-preloaded sequence followed by a preloaded sequence, to extract optimal information for all metrics; or even by constructing correction methods that render comparable CBVs and PSRs regardless of pulse-sequences parameters. At any rate, standardization in all the several steps from pulse-sequences parameters to post-processing and data generation is mandatory towards the desired generalizability and global applicability.

Conclusions

Radiologists should be familiar with the DSC-PWI technique, post-processing details, and their impact on perfusion metrics calculation to evaluate imaging accordingly. E.g., the clinician probably should not expect such a prominent T1 leakage effect (or high PSR) in a lymphoma when using low FA or preloaded sequences; or such optimal CBV performances in assessing high-grade tumor recurrence vs. treatment effects or peri-enhancing area infiltration in glioblastoma when using an intermediate-high FA non-preloaded sequence, non-corrected values, or average values instead of specific percentile or extreme values (see examples in Fig. 1).

Consensus recommendations must be followed in support of generalizability, but research should go on to provide protocols that fit optimally in all clinical scenarios.

Commercial software packages must also converge in alignment with consensus recommendations and provide optimized tools to enable the clinical application of the most recent academic advances.

Recent advances have been magnificent and DSC-PWI could be considered unquestionably successful. Nevertheless, there may still be chances for improvement to ensure and maintain the maximal DSC-PWI's widespread success in the neuroradiological practice.

Funding The authors state that this work has not received any funding.

Declarations

Guarantor The scientific guarantor of this publication is Albert Pons-Escoda.

Conflict of interest Albert Pons-Escoda is a member of the *European Radiology* Editorial board and has therefore not taken part in the review or selection process of this article.

Marion Smits declares speaker fees (paid to institution) from GE Healthcare and AuntMinnie, and consultation fees (paid to institution) from Bracco.

Statistics and biometry No complex statistical methods were necessary for this paper.

Informed consent Written informed consent was obtained from all subjects (patients) in this study.

Ethical approval Institutional review board approval was not required for this editorial.

Study subjects or cohorts overlap N/A.

Methodology N/A.

References

- Boxerman JL, Quarles CC, Hu LS et al (2020) Consensus recommendations for a dynamic susceptibility contrast MRI protocol for use in high-grade gliomas. Neuro Oncol 22:1262–1275. https://doi.org/10.1093/neuonc/noaa141
- Lupo JM, Cha S, Chang SM, Nelson SJ (2005) Dynamic susceptibility-weighted perfusion imaging of high-grade gliomas: characterization of spatial heterogeneity. AJNR Am J Neuroradiol 26:1446–1454
- Sawlani V, Patel MD, Davies N et al (2020) Multiparametric MRI: practical approach and pictorial review of a useful tool in the evaluation of brain tumours and tumour-like lesions. Insights Imaging 11:84. https://doi.org/10.1186/s13244-020-00888-1
- Pons-Escoda A, Garcia-Ruiz A, Naval-Baudin P et al (2020) Presurgical identification of primary central nervous system lymphoma with normalized time-intensity curve: a pilot study of a new method to analyze DSC-PWI. AJNR Am J Neuroradiol 41:1816–1824. https://doi.org/10.3174/ajnr.A6761
- Pons-Escoda A, García-Ruíz A, Naval-Baudin P et al (2022) Diffuse large B-cell Epstein-Barr virus-positive primary CNS lymphoma in non-AIDS patients: high diagnostic accuracy of DSC perfusion metrics. AJNR Am J Neuroradiol 43:1567–1574. https://doi.org/10.3174/ajnr.A7668
- Hirschler L, Sollmann N, Schmitz-Abecassis B et al (2023) Advanced MR techniques for preoperative glioma characterization: Part 1. J Magn Reson Imaging. https://doi.org/10.1002/jmri. 28662
- Boxerman JL, Schmainda KM, Weisskoff RM (2006) Relative cerebral blood volume maps corrected for contrast agent extravasation significantly correlate with glioma tumor grade, whereas uncorrected maps do not. AJNR Am J Neuroradiol 27:859–867
- JabehdarMaralani P, Melhem ER, Wang S et al (2015) Association of dynamic susceptibility contrast enhanced MR Perfusion parameters with prognosis in elderly patients with glioblastomas. Eur Radiol 25:2738–2744. https://doi.org/10.1007/s00330-015-3640-4
- Fu R, Szidonya L, Barajas RFJ et al (2022) Diagnostic performance of DSC perfusion MRI to distinguish tumor progression and treatment-related changes: a systematic review and meta-analysis. Neurooncol Adv 4:27. https://doi.org/10.1093/noajnl/vdac027
- Pons-Escoda A, Garcia-Ruiz A, Naval-Baudin P et al (2022)
 Voxel-level analysis of normalized DSC-PWI time-intensity curves: a potential generalizable approach and its proof of concept



- in discriminating glioblastoma and metastasis. Eur Radiol. https://doi.org/10.1007/s00330-021-08498-1
- Cha S, Lupo JM, Chen MH et al (2007) Differentiation of glioblastoma multiforme and single brain metastasis by peak height and percentage of signal intensity recovery derived from dynamic susceptibility-weighted contrast-enhanced perfusion MR imaging. AJNR Am J Neuroradiol 28:1078–1084. https://doi.org/10.3174/ ajnr.A0484
- van Santwijk L, Kouwenberg V, Meijer F et al (2022) A systematic review and meta-analysis on the differentiation of glioma grade and mutational status by use of perfusion-based magnetic resonance imaging. Insights Imaging 13:102. https://doi.org/10.1186/ s13244-022-01230-7
- Kaufmann TJ, Smits M, Boxerman J et al (2020) Consensus recommendations for a standardized brain tumor imaging protocol for clinical trials in brain metastases. Neuro Oncol 22:757–772. https://doi.org/10.1093/neuonc/noaa030
- Barajas RF, Politi LS, Anzalone N et al (2021) Consensus recommendations for MRI and PET imaging of primary central nervous system lymphoma: guideline statement from the International Primary CNS Lymphoma Collaborative Group (IPCG). Neuro Oncol 23:1056–1071. https://doi.org/10.1093/neuonc/noab020
- 15. Bell LC, Hu LS, Stokes AM, McGee SC, Baxter LC, Quarles CC (2017) Characterizing the influence of preload dosing on percent signal recovery (PSR) and cerebral blood volume (CBV) measurements in a patient population with high-grade glioma using

- dynamic susceptibility contrast MRI. Tomography 3:89–95. https://doi.org/10.18383/j.tom.2017.00004
- Mangla R, Kolar B, Zhu T et al (2011) Percentage signal recovery derived from MR dynamic susceptibility contrast imaging is useful to differentiate common enhancing malignant lesions of the brain. AJNR Am J Neuroradiol 32:1004–1010. https://doi.org/10. 3174/ajnr.A2441
- Boxerman JL, Paulson ES, Prah MA, Schmainda KM (2013) The effect of pulse sequence parameters and contrast agent dose on percentage signal recovery in DSC-MRI: implications for clinical applications. AJNR Am J Neuroradiol 34:1364–1369. https://doi. org/10.3174/ajnr.A3477
- Cindil E, Sendur HN, Cerit MN et al (2021) Validation of combined use of DWI and percentage signal recovery-optimized protocol of DSC-MRI in differentiation of high-grade glioma, metastasis, and lymphoma. Neuroradiology 63:331–342. https://doi.org/10.1007/s00234-020-02522-9
- Barajas RF, Chang JS, Sneed PK et al (2009) Distinguishing recurrent intra-axial metastatic tumor from radiation necrosis following gamma knife radiosurgery using dynamic susceptibility-weighted contrast-enhanced perfusion MR imaging. AJNR Am J Neuroradiol 30:367–372. https://doi.org/10.3174/ ainr.A1362

Publisher's Note Springer Nature remains neutral with regard to jurisdictional claims in published maps and institutional affiliations.





This information is current as of January 9, 2025.

Imaging of Lymphomas Involving the CNS: An Update-Review of the Full Spectrum of Disease with an Emphasis on the World Health Organization Classifications of CNS Tumors 2021 and Hematolymphoid Tumors 2022

A. Pons-Escoda, P. Naval-Baudin, R. Velasco, N. Vidal and C. Majós

AJNR Am J Neuroradiol 2023, 44 (4) 358-366 doi: https://doi.org/10.3174/ajnr.A7795 http://www.ajnr.org/content/44/4/358

Imaging of Lymphomas Involving the CNS: An Update-Review of the Full Spectrum of Disease with an Emphasis on the World Health Organization Classifications of CNS Tumors 2021 and Hematolymphoid Tumors 2022

DA. Pons-Escoda, P. Naval-Baudin, R. Velasco, N. Vidal, and C. Majós

ABSTRACT

SUMMARY: Lymphomas of the CNS are the second most frequent primary brain malignancy in adults after gliomas. Presurgical suspicion of lymphoma greatly impacts patient management. The radiologic features of this tumor have been widely covered in the literature for decades, but under current classifications, mainly corresponding to the most common presentations of the most frequent type: primary diffuse large B-cell lymphoma of the CNS. Nevertheless, rarer presentations of this specific lymphoma and of other World Health Organization lymphoma subtypes with different imaging features are rarely treated. Moreover, important advances in imaging techniques, changing epidemiologic factors with relevant impact on these tumors (eg, immunodeficiency/dysregulation), and recent updates of the World Health Organization Classification of CNS Tumors 2021 and Hematolymphoid Tumors 2022 may have rendered some accepted concepts outdated. In this article, the authors aim to fulfill a critical need by providing a complete update-review, emphasizing the latest clinical-radiologic features of the full spectrum of lymphomas involving the CNS.

ABBREVIATIONS: ALK+/ALK- = anaplastic lymphoma kinase positive and negative; CLIPPERS = chronic lymphocytic inflammation with pontine perivascular enhancement responsive to steroids; DLBCL = diffuse large B-cell lymphoma; EBV = Epstein-Barr virus; MALT = mucosa-associated lymphoid tissue; NK = natural killer; PSR = percentage of signal recovery; WHO = World Health Organization

ymphomas of the CNS are the second most frequent primary brain malignancy in adults after gliomas, accounting for 7% of all malignant tumors. A presurgical suspicion of this tumor will greatly impact patient management. Corticoids should be avoided before a definitive diagnosis is made, and prompt biopsy is recommended to prioritize chemoradiotherapy instead of tumor resection, such as in the case of suspected glioblastoma. ^{2,3}

The radiologic features of these tumors have been widely covered in the literature in recent decades. Imaging characteristics of lymphomas may be considered typical, leading to a potential misunderstanding of this tumor as a straightforward presurgical suspicion. Nevertheless, this is often far from the reality in daily practice. In fact, the typical appearance of lymphomas is currently almost exclusively related to the most common presentations of

the most frequent type: primary diffuse large B-cell lymphoma (DLBCL) of the CNS, negative for Epstein-Barr virus (EBV). If rarer presentations of this specific lymphoma or other specific subtypes with different characteristic imaging features are considered, the complexity increases, and it becomes a great mimicker with a challenging differential diagnosis. Also, important advances in imaging techniques, dynamic changes in epidemiologic factors with relevant impact on these tumors (eg, immunodeficiency/dysregulation), and recent changes in the World Health Organization (WHO) classifications of CNS² and hematolymphoid tumors may have rendered some well-accepted concepts of the disease outdated. 5-8

The Research Ethics Committee of the Hospital Universitari de Bellvitge approved this article for publication (PR348/22).

Received December 6, 2022; accepted after revision January 19, 2023.

From the Radiology (A.P.-E., P.N.-B., C.M.) Pathology Departments (N.V.), Hospital Universitari de Bellvitge, Barcelona, Spain; Neurooncology Unit (A.P.-E., R.V., N.V., C.M.), Institut d'Investigació Biomèdica de Bellvitge, Barcelona, Spain; and Institute of Neurosciences and Department of Cell Biology, Physiology and Immunology (R.V.), Universitat Autònoma de Barcelona, Barcelona, Spain.

This work was partially supported by a grant from the Instituto de Salud Carlos III (P120/00360) to Carles Majós and Albert Pons-Escoda.

Please address correspondence to Albert Pons-Escoda, MD, Radiology Department, Institut de Diagnòstic per la Imatge, Hospital Universitari de Bellvitge, C/Feixa Llarga SN, L'Hospitalet de Llobregat, 08907, Barcelona, Spain; e-mail: albert.pons.idi@gencat.cat; @PonsEcoda

Om Indicates open access to non-subscribers at www.ajnr.org http://dx.doi.org/10.3174/ajnr.A7795

WHO Classification of Tumors, 5th Edition

Insights. Some basic concepts regarding WHO classifications need to be understood for an optimally up-to-date comprehension of lymphomas in the CNS. First, these tumors fall between two 5th edition WHO classifications: the CNS² and the hematolymphoid.⁴ Second, despite impressive advances in molecular pathology, the mainstay in lymphomas remains histology of biopsy specimens; this differs greatly from other brain tumors such as gliomas, for which molecular pathology is vital. Nevertheless, clinically relevant pathogenesis, mutation profiles, and genetic drivers have been characterized in recent years. Recurrent mutations frequently

activate the B-cell receptor, toll-like receptor, and NF- κ B pathways, and alterations in genes involved in chromatin structure and modification, cell-cycle regulation, and immune recognition are common. *MYD88* and *CD79B* mutations may be of clinical interest because they can be detected in several body fluids (plasma and CSF), potentially assisting in disease-monitoring under treatment and in minimally-invasive initial diagnosis. Also, knowledge of genetically activated pathways, tumor immune microenvironment, and expression of immune-response biomarkers may point to specific treatment targets. Finally, lymphoma classifications include clinical factors, especially regarding the immune status of patients, which plays an essential role in tumor classification with important treatment implications.^{2,4}

Updates. Thus, some changes may be identified in the updated WHO Classifications of CNS Tumors 2021 and Hematolymphoid Tumors 2022, first in CNS immunodeficiency-associated lymphoma. Whereas the prior CNS classification included a heterogeneous group of diseases primarily defined by the patient immunodeficiency setting, currently, it is exclusively defined as DLBCL and EBV positive (both essential criteria) lymphoma.² Moreover, the current spectrum of immunodeficiency includes immune-dysregulation according to the hematolymphoid classification, in which immunocompromised settings without a fully demonstrable immunodeficiency, such as immunosenescence (among others), are included.^{2,4}

Next, a change in terminology is recommended in the upcoming hematolymphoid classification, representing a paradigm shift. Currently, the type of immunodeficiency-associated lymphoma is not first determined by the immunodeficiency/dysregulation setting, as in the previous classification (eg, AIDS-related DLBCL). Instead, it is defined primarily by the tumor histology with the so-called 3-part nomenclature, composed of the following: 1) histologic lesion, 2) oncogenic virus status, and 3) immunodeficiency background of the patient (eg, DLBCL, EBV-positive, and autoimmune setting). This integrated nomenclature allows the grouping of specific types of immunodeficiency-associated lymphomas (such as DLBCL EBV-positive), despite the underlying immunodeficiency/dysregulation, to better define the unique shared pathogenetic mechanisms. 4,9,10

On the other hand, lymphomatoid granulomatosis is no longer considered an immunodeficiency-associated entity. It occurs exclusively in immunocompetent patients, and in the case of an underlying immunodeficiency, it should be considered a subtype of a polymorphic lymphoproliferative disorder.⁴

Also, according to the WHO classification of hematolymphoid tumors, the term primary CNS lymphoma may be considered imprecise, and it is no longer recommended for referring specifically to primary DLBCL of the CNS,⁴ which is the currently preferred term.^{2,4}

Finally, some tumors do not differ in their specific histology but rather in their precise location. This is because in the new WHO hematolymphoid classification, primary DLBCL of the CNS is classified together with DLBCL of the vitreoretina and of the testes of immunocompetent patients as primary DLBCL of immune-privileged sites. All these entities arise in so-called immune sanctuaries created by their anatomic and functional immune regulatory

barriers (eg, the blood-brain barrier). However, large B-cell lymphomas occurring in the dura (dural lymphoma) or inside the brain vessels (intravascular lymphoma) escape these immune privileges and are, therefore, classified separately.^{2,4}

With all these upgraded concepts in mind, the authors aim to provide a complete update-review of imaging features of the full spectrum of lymphomas involving the CNS, mainly based on those entities included in the 5th edition WHO Classification of Tumors of the CNS 2021. Primary DLBCL of the CNS, immunodeficiency-associated CNS lymphoma, lymphomatoid granulomatosis, intravascular large B-cell lymphoma of the CNS, mucosa-associated lymphoid tissue (MALT) lymphoma of the dura, other low-grade B-cell lymphomas of the CNS, anaplastic large-cell lymphoma (anaplastic lymphoma kinase positive and negative [ALK+/ALK-]), and T-cell and natural killer (NK)/T-cell lymphoma are discussed. Finally, the clinical-radiologic entity "lymphomatosis cerebri" and secondary lymphomas are also reviewed.

Imaging of CNS Lymphomas

Primary DLBCL of the CNS. Primary DLBCL of the CNS corresponds to 80%–85% of all CNS lymphomas, occurs almost always in immunocompetent patients, is EBV-negative, and is of unknown etiology.² The term primary CNS lymphoma may be considered imprecise, and it is no longer recommended by the WHO classification of hematolymphoid tumors⁴ for referring specifically to primary DLBCL of the CNS, which is the currently preferred term.^{2,4}

It usually appears as single or multiple (30%–35%) parenchymal lesions, located supratentorially (>80%), with a particular affinity for the basal ganglia, periventricular regions, midline, and corpus callosum (\approx 45%). It is also frequent in brain hemispheres (\approx 40%), rarely found in the posterior fossa, and exceptionally in the spinal cord (Fig 1). Associated leptomeningeal or subependymal enhancement is characteristic, but an exclusive presentation of the disease in this location may raise suspicion of secondary lymphoma. The typical perivascular histologic pattern also carries a characteristic perivascular enhancement on imaging (Fig 1). Parenchymal lesions are most frequently solid and homogeneous, but their presentation can range from well-defined expansive to ill-defined infiltrative lesions. $^{2,5-7,11}$

Notably, these lesions are frequently hyperattenuating on NCCT, ^{2,5-7,11} which is important to keep in mind because CT is the first-line radiologic examination and suspicion at this point may lead to corticoid avoidance (Fig 1). If administered, corticoids can complicate subsequent imaging and histologic diagnosis.^{2,3,12}

Regarding specific tumor MR imaging features, lymphoma typically appears hypointense on T2WI with marked diffusion restriction on DWI. Nevertheless, a T2-blackout effect consisting of a persistent hypointensity on b=1000 images due to very low T2 signal may lead to misinterpretation. Thus, ADC map hypointensity might be more reliable than b=1000 hyperintensity in assessing actual diffusion restriction.^{2,5-7,11} NCCT hyperattenuation, low T2 signal, and diffusion restriction correlate with high cellularity on histology, with Ki-67 proliferation indexes usually above 90% (Fig 1).¹³

Historically, the presence of hemorrhage or signs of necrosis on preoperative imaging in immunocompetent patients have been considered a factor arguing strongly against a diagnosis of lymphoma.¹⁴ However, the histologic appearance of tumor

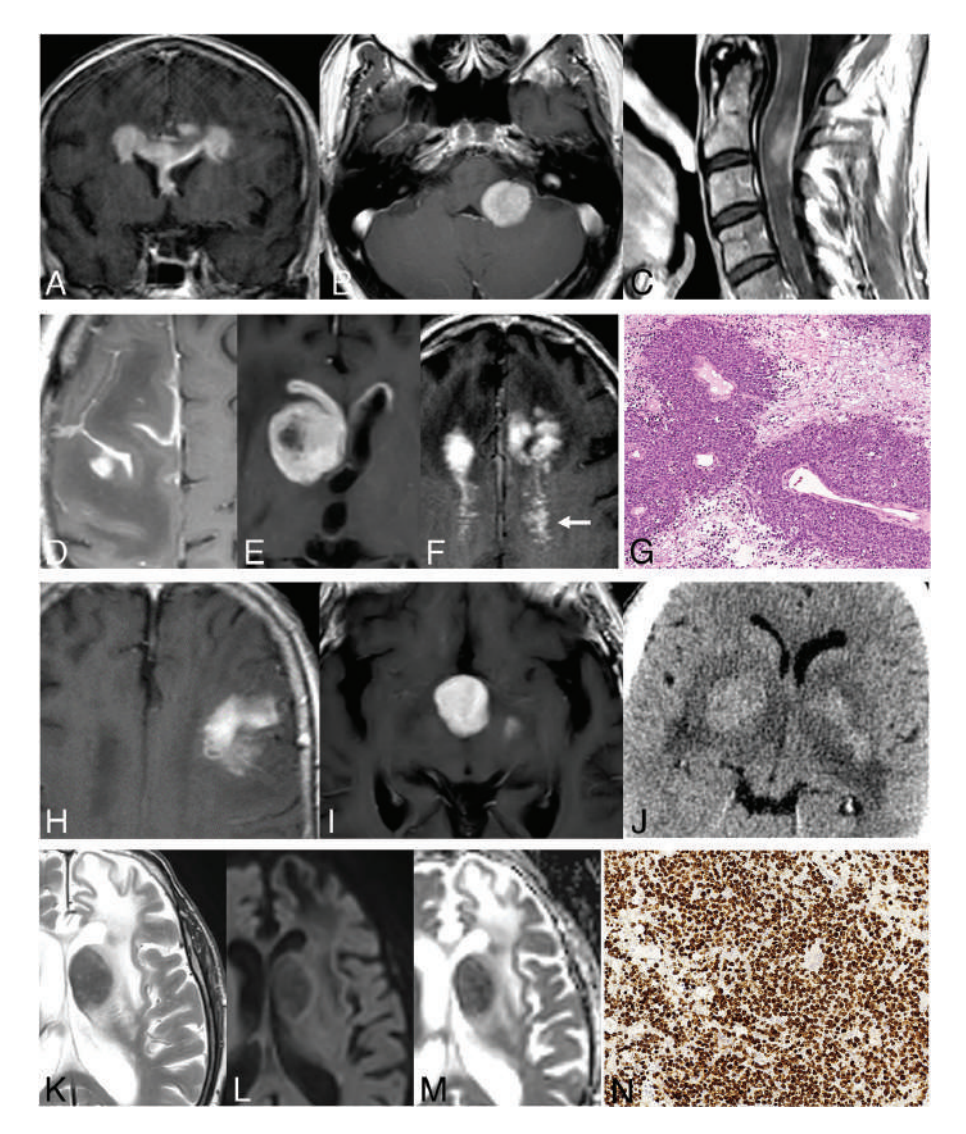


FIG 1. Primary DLBCLs of the CNS, EBV-negative. A-C: Usual deep, periventricular, corpus callosum, and midline location (A); a rare location in the posterior fossa (B); and exceptional in the spinal cord (C). D-G: Parenchymal lesions with associated characteristic leptomeningeal (D), subependymal (E), and perivascular (arrow, F) enhancement patterns. Histologic hematoxylin-eosin stain (original magnification \times 20) shows highly cellular, perivascular accumulation of lymphoma cells (G). H-J: Mass lesion with ill-defined infiltrative (H) or well-defined expansive (I) margins. Hyperattenuated lesions on NCCT (I). K-N: Deep T2 hypointensity of a lesion (I) with a T2-blackout effect at I000 image (I1) but a low signal of actual diffusion restriction on the ADC map (I1). I2 proliferation index by immunohistochemistry (original magnification I20) exceeding 90% (I1).

samples frequently includes hemorrhagic tumors with central necrosis.² Accordingly, recent literature reports the presence of hemorrhage on imaging in up to 50% of patients evaluated with SWI (20% with T2WI) and heterogeneous or ring enhancement (usually associated with necrosis) in up to 10%–15% of cases.^{3,15} Therefore, the authors discourage this classic assumption and believe that a certain degree of hemorrhage and heterogeneous or ring enhancements does not rule out suspicion of lymphoma, considering other imaging features as well (Fig 2).

Regarding quantitative imaging techniques beyond DWI, ¹H-MR spectroscopy and DSC-PWI, included in consensus recommendations for imaging CNS lymphoma, ¹⁶ have shown promising results for presurgical diagnosis. Attention must be paid to pulse-sequence parameters (TE, TR, flip angle), prebolus usage, and leakage corrections for DSC-PWI, but in general terms, this

tumor shows low-to-intermediate CBV, a high percentage of signal recovery (PSR), and characteristic time-intensity curve morphology. 7,17,18 Lower CBV values in lymphomas have paradoxically been related to a worse prognosis of survival. 19 1H-MR spectroscopy can also reinforce a presurgical suspicion in basically 2 ways: Short TE depicts much lower mIns (described as a glial marker) than that associated with enhancing non-necrotic astrocytoma (ie, grade 3), and long TE shows much lower mobile lipids (associated with necrosis) than glioblastoma or metastasis $(Fig 2).^{20}$

Brain FDG-PET may play a role in the presurgical differentiation of lymphoma and other malignant brain tumors such as glioblastoma and metastasis because most lymphoma lesions are highly FDG-avid, with homogeneous uptake. ¹⁶

As an additional comment on primary DLBCL of the CNS, it has been reported that "sentinel" inflammatory lesions, which may disappear after anti-inflammatory treatment, can precede the diagnosis of lymphoma by up to 2 years, ²¹ so attention must be paid to the patient's history of prior inflammatory brain lesions (Fig 3).

Immunodeficiency-Associated CNS Lymphoma. According to the latest WHO classification, the immunodeficiency-associated CNS lymphoma subtype specifically corresponds to primary DLBCL of the CNS, EBV-positive. Indeed, large B-cell histology and lymphotropic EBV tissue-positivity are currently the essential diagnostic criteria

for immunodeficiency-associated lymphoma of the CNS.² It represents 8%–10% of all primary CNS lymphomas. Despite being considered an infrequent entity, this is the second most frequent type of primary lymphoma of the CNS. Its clinical context has changed during recent decades. Whereas in the 1990s, AIDS due to HIV was the leading cause, currently and especially in more developed countries, other causes predominate, such as post transplant status, autoimmune disease, and iatrogenesis.²²⁻²⁸ This shift in the mechanisms of immunodeficiency and other developments in patient monitoring as well as in imaging techniques have also resulted in a change in the main differential diagnoses to consider. Currently, therefore, glioblastoma or metastases are more likely than opportunistic infections, in contrast to previous decades.^{8,29,30}

Morphologic imaging of this lymphoma is quite characteristic, and the opposite of that of the "typical" CNS lymphoma. It can

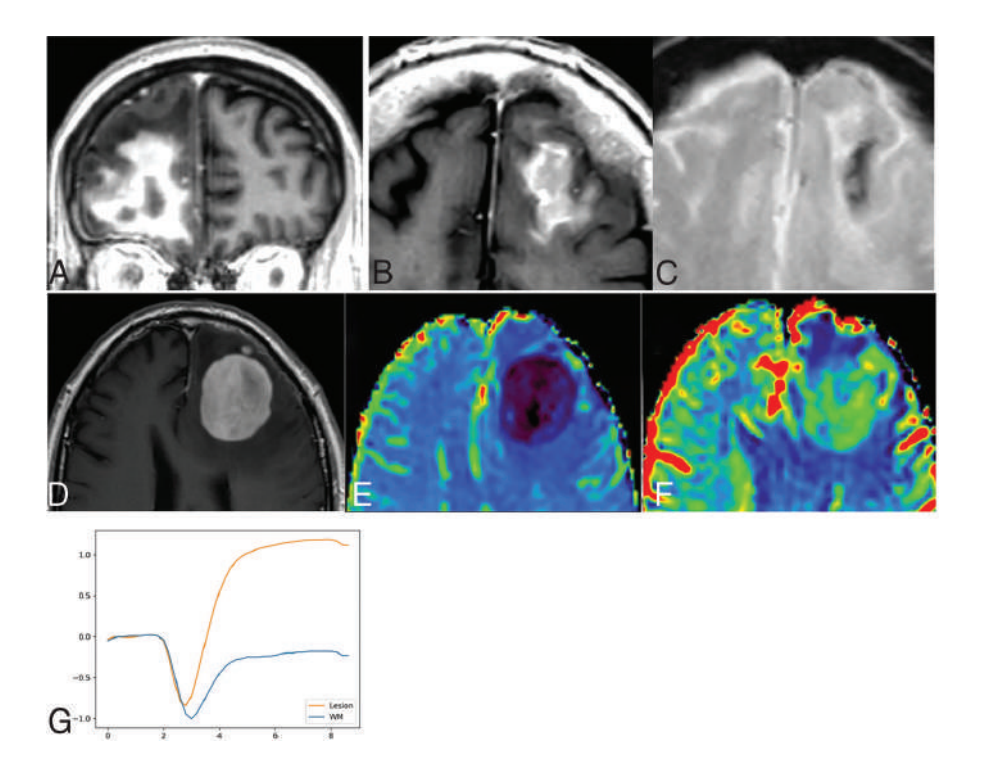


FIG 2. *A*—*C*: Primary DLBCLs of the CNS, EBV-negative, with imaging signs of central necrosis (A) and tumoral hemorrhage (*B* and *C*). *D*—*G*: DSC-PWI features of a left frontal primary DLBCL of the CNS, EBV-negative (*D*). Low-to-intermediate CBV on noncorrected (*E*) and corrected (*F*) color maps. Characteristic lymphoma DSC-PWI time-intensity curve morphology with ascending-part of the curve recovering signal intensity far above the baseline (high PSR) (*G*).

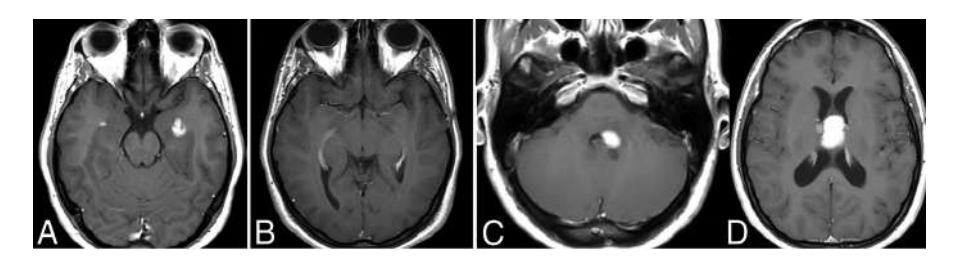


FIG 3. Sentinel inflammatory lesions preceding primary DLBCL of the CNS. Two enhancing periventricular temporal lesions were detected in a patient (*A*). A biopsy was obtained, and histopathology showed an inflammatory infiltrate without evidence of neoplasia. The lesions disappeared on further imaging controls during the following 2 years (*B*). In a subsequent MR imaging control, new masslike lesions reappeared (*C* and *D*). A biopsy of the new lesions yielded the final histopathologic diagnosis of primary DLBCL of the CNS.

be deep or hemispheric, with a slightly greater tendency to multiplicity. It is almost constantly highly necrotic with ring enhancement and intermediate-to-prominent signs of hemorrhage. T2WI and DWI signal patterns are both variable and inconsistent. In summary, it is a tumor that differs from the typical appearance of lymphoma and, rather, presents more like the main differential diagnoses, which are glioblastoma and metastasis. 8,29,30 A characteristic T2WI heterogeneous hypointensity of the nonenhancing "necrosis," not corresponding to blood products or mineralization, has recently been suggested in these tumors, in contrast to the usual hyperintense T2 signal of nonhemorrhagic necrosis in other tumors (Fig 4).8

While conventional imaging is often insufficient to reach a presurgical diagnosis of this challenging entity, quantitative imaging, especially DSC-PWI, can provide diagnostic clues. Indeed, the perfusion features of this lymphoma follow those of low-to-intermediate CBV, high PSR, and the characteristic time-intensity curve morphology when depicting an ROI in the solid parts of tumors (Fig 4).⁸ Finally, the ¹H-MR spectroscopy pattern seems of low value for presurgical characterization as lymphoma because this tumor has prominent mobile lipids overlapping with necrotic glioblastomas or metastasis.²⁰

In conclusion, we suggest that in dealing with a necrohemorrhagic tumor, potential immunodeficiency/dysregulation of the patient must be thoroughly examined. If this cannot be ruled out, DLBCL EBV-positive should be considered, and careful DSC-PWI assessment can provide a presurgical diagnostic clue.

Lymphomatoid Granulomatosis. According to the new WHO classification of hematolymphoid tumors, lymphomatoid granulomatosis is a lymphoproliferative disorder with large atypical EBV-positive B-cells, T-cell infiltration, and tissue necrosis occurring exclusively in immunocompetent patients.4 Previously, it was included in the group of immunodeficiency-associated entities, but currently, the identification of an underlying immunocompromised status rules out lymphomatoid granulomatosis, and it should instead be considered a subtype of a polymorphic lymphoproliferative disorder in the setting of immunodeficiency/dysregulation.4 Lymphomatoid granulomatosis is a very rare entity that exceptionally occurs primarily in the CNS, though CNS involvement is

usually secondary. It represents a spectrum of lymphoid disease graded from 1 to 3, with corresponding degrees of aggressiveness from indolent to very aggressive.^{2,4}

On imaging, typical findings are those of secondary lymphoma with frequent subependymal or leptomeningeal involvement and perivascular enhancement. Occasionally, it may be angiocentric and angiodestructive, resembling intravascular lymphoma. When there is isolated CNS involvement, it usually corresponds to grade 3 disease, and brain biopsy demonstrates DLBCL EBV-positive, 2,4 in which case imaging findings may consist of masslike lesions with hemorrhage and necrosis. 2,4,31,32

In the recent literature, lymphomatoid granulomatosis has been correlated with chronic lymphocytic inflammation with pontine perivascular enhancement responsive to steroids (CLIPPERS). Some authors hypothesize that this entity is a kind of a sentinel

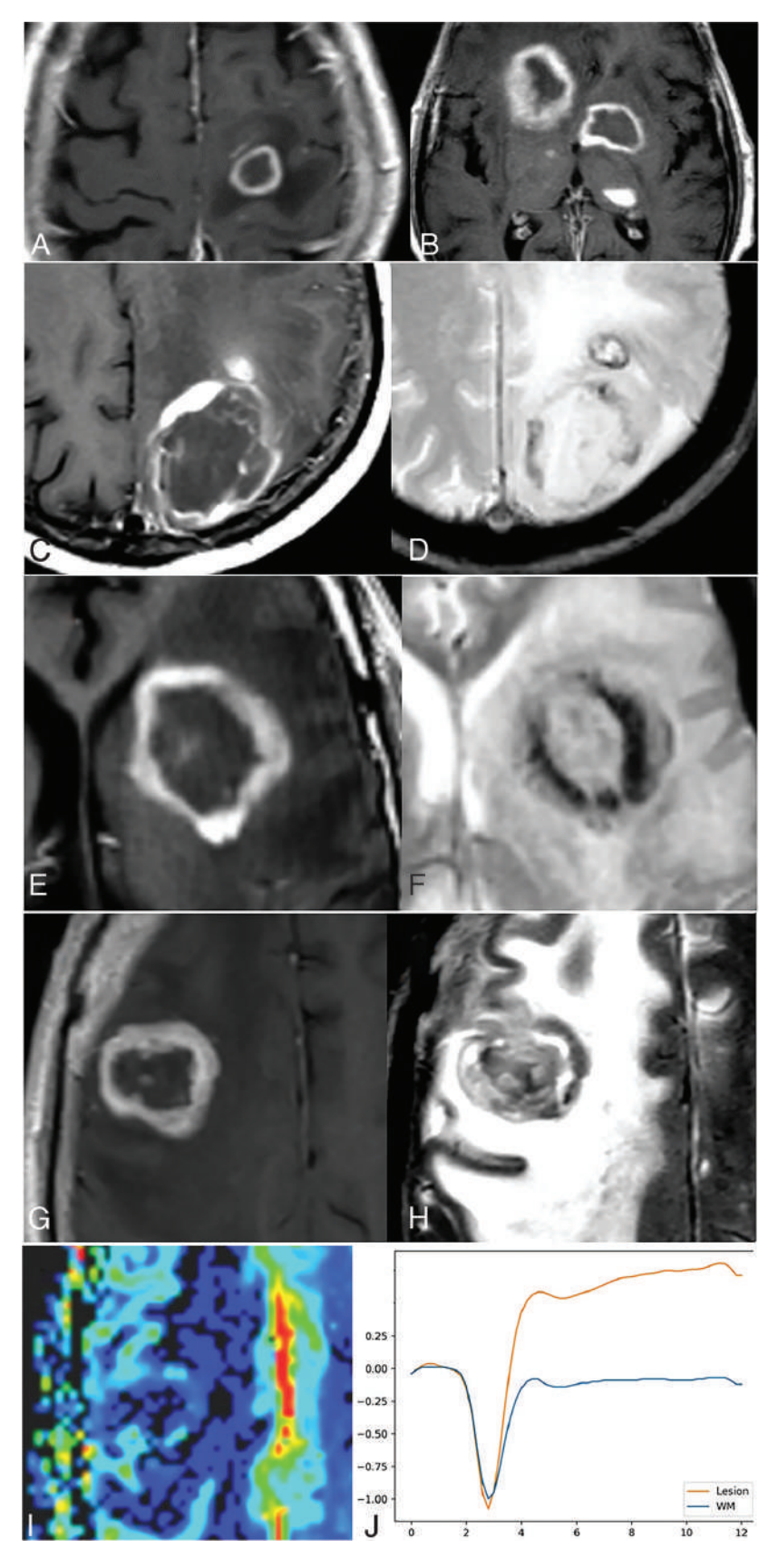


FIG 4. Primary DLBCLs of the CNS, EBV-positive (immunodeficiency/dysregulation-associated). Single (A) and multiple (B) lesions with prominent necrosis (C and E) and tumoral hemorrhage (D and F). Heterogeneous deep T2 hypointensity (H) of the nonenhancing central content (G) of lesions, so-called necrosis. Low-intermediate CBV on the corrected color map (I) and DSC-PWI time-intensity curve with high PSR (I), also very characteristic of this lymphoma subtype.

lesion, while others postulate that CLIPPERS may be an inflammatory response to lymphomatous tumor cells, responding to corticosteroids preceding the definitive tumor recurrence. 33,34

Intravascular Large B-Cell Lymphoma of the CNS. Intravascular large B-cell lymphoma of the CNS is defined by the selective proliferation of malignant B large-tumor cells within the brain vessels, particularly small- to medium-sized blood vessels, without or with minimal parenchymal extension. The tumor cells may occlude vessels causing patched bleeding and ischemia. Also, it is not exceptional for some tumor cells to extravasate beyond the vessels, focally reaching brain parenchyma. Regarding clinical presentation, strokelike symptoms are typical, though not always present.³⁵

The main phenomena detected on imaging are ischemic and hemorrhagic lesions, which usually suggest the differential with vasculitis, emboli, or hypercoagulability. The ischemia-like lesions appear dynamic and evanescent between near-in-time imaging followups. Furthermore, those possible tumor cells that extravasate beyond the vessels may focally reach the brain parenchyma, forming tumor islands that can appear as enlarging areas of parenchymal enhancement.^{2,36} Morphologic imaging features on these enhancing islands may be helpful for presurgical suspicion because they can express the signal characteristics of typical lymphoma. In addition, ependymal and leptomeningeal enhancement may also be present.^{36,37} Advanced imaging features may include a tumoral pattern on ¹H-MR spectroscopy with high Cho to NAA ratios, as well as a characteristic DSC-PWI pattern with shortened MTT (differing from ischemic lesions), low-to-intermediate CBV, high PSR, and the characteristic time-intensity curve morphology of lymphomas in the CNS. 7,18,20

In summary, this entity should be kept in mind whenever encountering MR imaging with hemorrhage and multiple dynamic ischemic lesions on T2WI and DWI, enlarging parenchymal enhancement, and possible associated leptomeningeal or subependymal disease (Fig 5). ^{36,37}

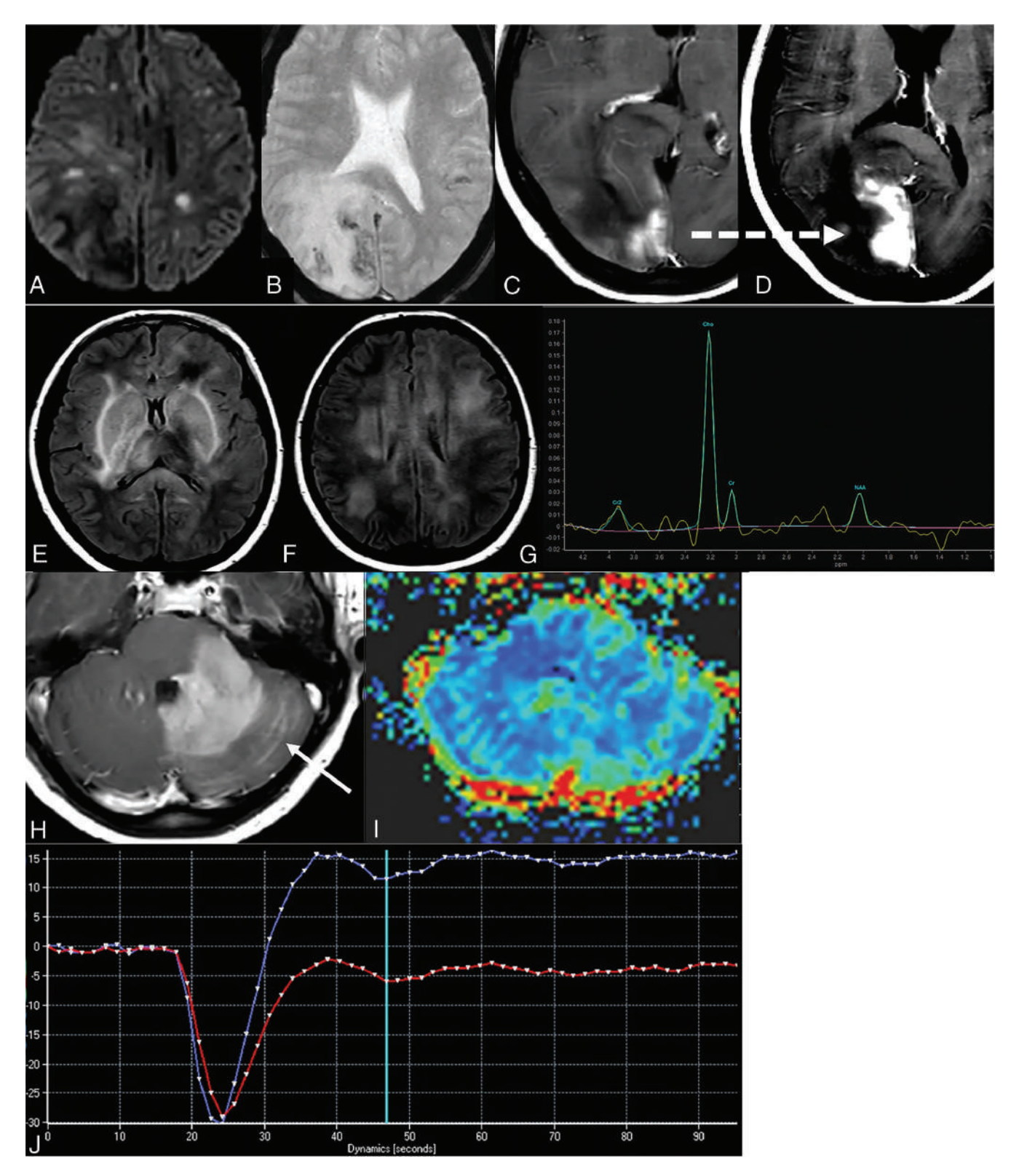


FIG 5. Intravascular lymphoma (A—D). Acute patched ischemia-like lesions on DWI (A), hemorrhages (β), and an area of enhancement (C), which grows on the subsequent few days of imaging control (D). Dashed arrow in C—D indicates the growth of the same enhancing-lesion in few days. DLBCL following a lymphomatosis cerebri pattern (E—I): extensive, patched, bilateral, and diffuse FLAIR hyperintensity on the basal ganglia (E) and white matter (F), with an area of enhancement in the left cerebellum (H) and associated leptomeningeal disease (arrow in H). Intermediate CBV in DSC-PWI color maps (I) and characteristic high PSR and time-intensity curve morphology (I). Tumoral pattern on H-MR spectroscopy at long TE with a high Cho-to-NAA ratio (H) and absent mins at the short TE (not shown), helpful in the differential diagnosis with nontumoral entities and gliomatosis cerebri, respectively.

MALT Lymphoma of the Dura. Lymphomas arising primarily in the dura are rare (\approx 1%) and usually correspond to MALT lymphoma. Occasionally, large B-cell lymphoma may also be primarily dural. Etiology and underlying associations are unknown.^{2,38}

On conventional imaging, they appear as extra-axial lesions with a wide dural base, soft attachment angles, and a possible CSF cleft between the lesion and brain parenchyma. In addition, edema or brain tissue infiltration can occur. They usually appear

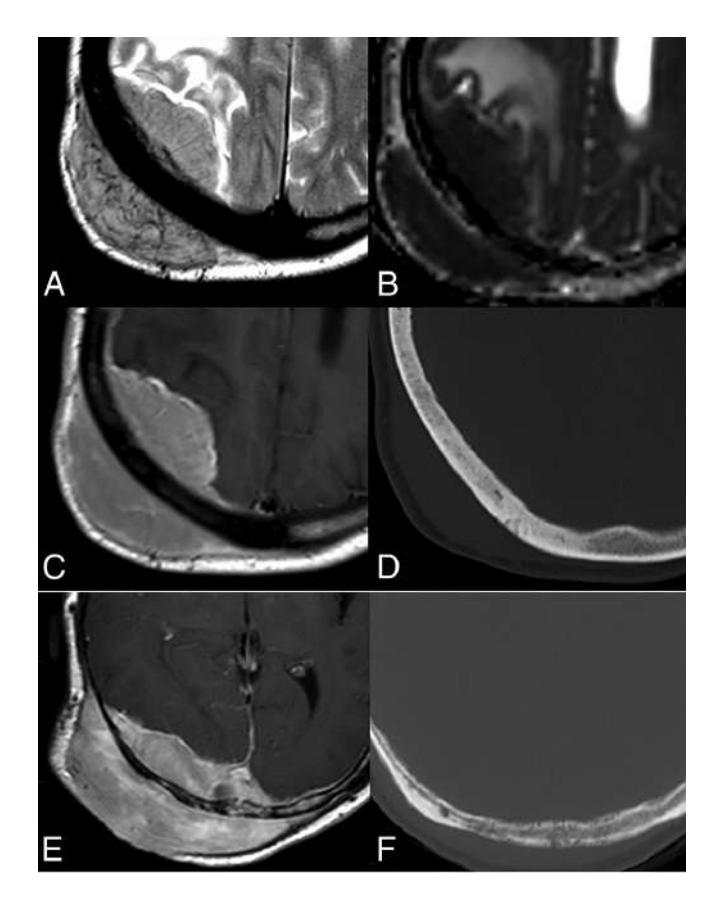


FIG 6. Dural lymphomas. MALT dural lymphoma (A-D) with extraaxial lesion features such as a CSF cleft (A) and a wide-implantation dural base with soft marginal angles (C), as well as T2-hypointensity (A) and diffusion restriction (B). Almost normal calvarial bone; only subtle sclerosis seen (D), despite the great soft-tissue component on both sides of the diploe (A-C). Similar imaging features with minimal bone destruction and a subtle permeative pattern (F) in comparison with the prominent soft-tissue component (E) in another diffuse large B-cell dural lymphoma (E) and (E)

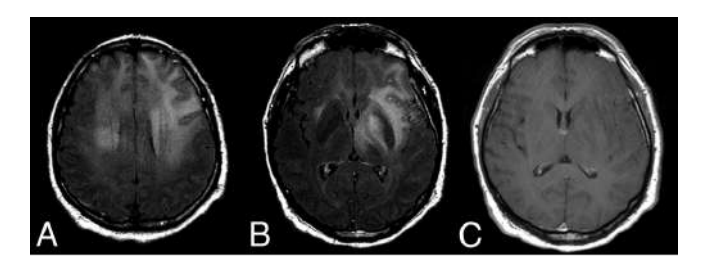


FIG 7. NK/T-cell lymphoma presenting with a lymphomatosis cerebri radiologic pattern (A–C). Patched and diffuse, bilateral and asymmetric, deep and subcortical, hyperintense lesions on FLAIR (A and B) without contrast enhancement (C).

homogeneous, NCCT hyperattenuated, T2WI hypointense, and with restricted diffusion; however, these features overlap with those of the most frequent extra-axial tumor in adults, meningioma (Fig 6). 39,40

Regarding advanced imaging, ¹H-MR spectroscopy can be of help for the differential diagnosis because meningiomas characteristically present with alanine, metastases present abundant mobile lipids, and the rarer solitary fibrous tumors (formerly termed hemangiopericytoma) show a high myo-inositol peak.³⁹

A clue for the presurgical suspicion of this tumor is provided by a characteristic pattern of bone infiltration or transdiploic extension. Characteristically, lymphoma presents as an extensive soft-tissue mass without bone destruction (normal bone to subtle permeative patterns) (Fig 6). This pattern is explained by the extension of tumor cells through Haversian canals. It differs from what is seen in meningiomas with hyperostosis or in plasmacytoma or metastasis with aggressive lytic destruction.³⁹

Other Low-Grade B-Cell Lymphomas of the CNS, Anaplastic Large Cell Lymphoma ALK+/ALK-, T-Cell and Natural Killer (NK)/T-Cell Lymphoma. The CNS WHO classification 2021 includes low-grade B-cell lymphoma of the CNS, ALK+/ALK-, T-Cell, and NK/T-cell lymphoma classified as miscellaneous, rare lymphomas in the CNS.² They represent a heterogeneous group of tumors with scarce evidence of concrete imaging findings. While low-grade B-cell lymphomas may occasionally appear as lymphoma-like lesions, other very different radiologic appearances are described, such as resembling edema, glial tumor, meningioma, and gliosis. 41 Regarding anaplastic large-cell and T-cell or NK/T-cell lymphomas, some authors postulate that they may resemble lymphoma or lymphomatosis cerebri on imaging, with other nonspecific presentations also possible (Fig 7). In summary, very heterogeneous imaging presentations, occasionally resembling lymphoma, can be seen in this heterogeneous group of exceptional entities. 41-43

Lymphomatosis Cerebri. Lymphomatosis cerebri corresponds to a clinical-radiologic pattern that is not included as a concrete histopathologic WHO entity. It may be observed in the context of different histologic lymphoma subtypes, but in most cases, it corresponds to primary DLBCL of the CNS. The typical clinical presentation is a subacute onset of dementia, cognitive impairment, and personality changes. 44,45

It consists of a nonenhancing or scarcely-enhancing (30%) T2-FLAIR hyperintense infiltration of brain tissue. It is usually located in white matter regions, with different distributions ranging from focal to patched or diffuse. The main differential includes gliomatosis cerebri (also considered a radiologic pattern and not a WHO entity) and inflammatory and toxic-metabolic diseases. Of note, in this form of CNS lymphoma, brain lesions may be highly variable and change between near-in-time follow-up scans. 44-47

In line with what was detailed in the intravascular lymphoma section, the detection of a tumoral pattern on ¹H-MR spectroscopy without relevant amount of mIns (potential glial marker present in gliomatosis) in abnormal areas of T2-FLAIR hyperintensity, as well as the above-described characteristic DSC-PWI pattern in the possible enhancing lesions, supports presurgical suspicion ^{46,47} (Fig 5).

Secondary Lymphomas of the CNS. Secondary lymphoma refers to the CNS spread of lymphoma that originated elsewhere. It may be as an isolated recurrence or as a synchronic systemic disease with an overall incidence of around 5%–10% in patients with systemic lymphomas, usually non-Hodgkins. Its occurrence is directly correlated with pathologic aggressiveness and ranges from <3% in the indolent, less-aggressive histologies to as high as 50% in the very aggressive ones such as Burkitt lymphoma. 48

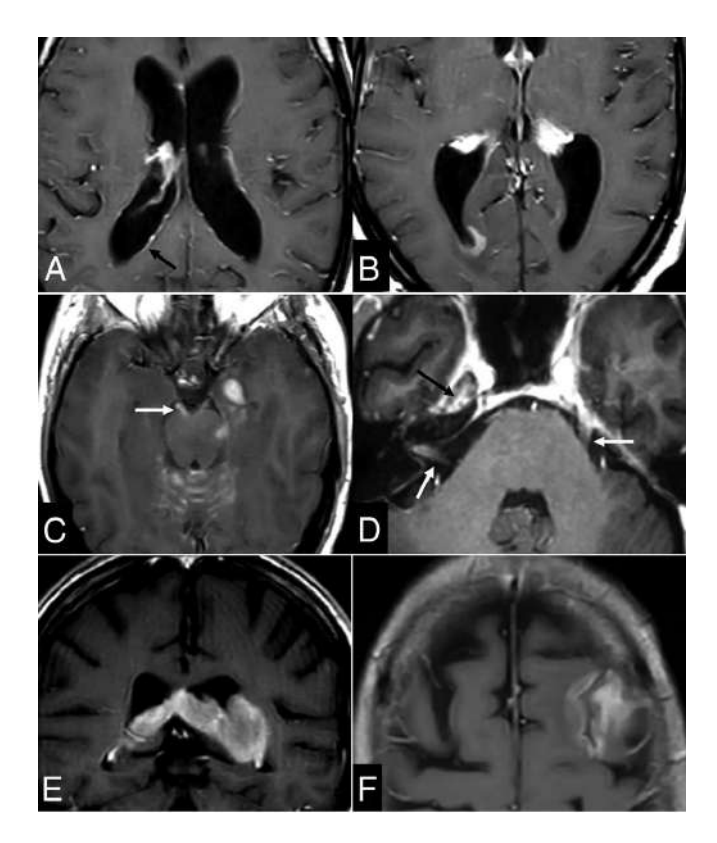


FIG 8. Imaging findings in secondary lymphomas of the CNS. *A–B*: Thin subtle linear (*arrow* in *A*) and nodular (*B*) subependymal enhancements. *C–D*: Prominent leptomeningeal disease along the superior vermian and cerebellar folia and third cranial nerve (*arrow* in *C*) as well as inside the right internal auditory canal—cranial nerves VII and VIII—and along the trigeminal nerve in the right Meckel cave and the left cisternal segment (*arrows* in *D*). Associated parenchymal mass in the left temporal lobe (*C*). *E–F*: Secondary lymphomas presenting as predominant intraparenchymal lesions with associated adjacent subependymal (*E*) and leptomeningeal (*F*) disease.

Although historically, it has been thought that secondary lymphomas presented with leptomeningeal involvement in a high proportion of cases (around 70%¹¹); more recent data differ, suggesting parenchymal involvement in 40%–60%, leptomeningeal in 20%–30%, and both in 10% (Fig 8).^{49,50} This higher proportion of parenchymal involvement in secondary lymphoma is important to consider in the radiologic interpretation because it is nonspecific for differentiation from primary CNS lymphoma, in which parenchymal lesions are almost constant.¹¹ Despite these differing disease distributions, imaging can frequently overlap, and differentiation between primary and secondary must rely on other staging examinations, such as a PET/CT scan, bone marrow aspiration, testicular sonography, vitreal examination, and the patient's history of systemic lymphoma.^{48,50}

CONCLUSIONS

The classification of CNS lymphomas is evolving. The radiologist plays a key role in the initial management of lymphomas, and a failure to suggest the possibility of this diagnosis on initial imaging may have a negative clinical impact. For this reason, the radiologist needs to be aware of the full spectrum of imaging presentations of CNS lymphoma. In this sense, we note some key points:

- Primary DLBCLs of the CNS present as homogeneous lesions, hyperdense on NECT, T2 hypointense, and with restricted diffusion. The presence of a certain degree of hemorrhage or signs of necrosis should not rule out their presurgical diagnosis.
- 2) Immunodeficiency-associated lymphomas (primary DLBCLs of the CNS, EBV-positive) appear as necrohemorrhagic tumors in potentially immunocompromised hosts. Special attention must be paid to the features of DSC-PWI, which may provide findings that suggest lymphoma.
- 3) Dural lymphoma should be suspected when a disproportionate soft-tissue mass without relevant bone destruction is identified in an extra-axial transdiploic tumor.
- 4) Intravascular lymphoma and lymphomatosis cerebri may be evolutive diagnoses of suspicion when dynamically changing T2-FLAIR areas of signal abnormality (and hemorrhage in intravascular lymphoma) are found. Also, attention must be paid to leptomeningeal and subependymal enhancement.
- 5) DSC-PWI and ¹H-MRS provide clues of great help in the differential diagnosis for each lymphoma subtype.
- 6) Secondary lymphomas often appear as parenchymal lesions. Isolated leptomeningeal or subependymal disease is characteristic but apparently less prevalent than formerly assumed.

ACKNOWLEDGMENTS

We thank CERCA Programme/Generalitat de Catalunya for institutional support.

Disclosure forms provided by the authors are available with the full text and PDF of this article at www.ajnr.org.

REFERENCES

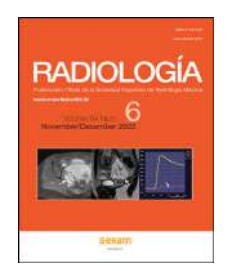
- Miller KD, Ostrom QT, Kruchko C, et al. Brain and other central nervous system tumor statistics, 2021. CA Cancer J Clin 2021;71:381– 406 CrossRef Medline
- 2. World Health Organization. **Central Nervous System Tumors.** *WHO Classification of Tumours Online. 5th ed.* https://tumourclassification.iarc.who.int/welcome/. Accessed January 16, 2023
- 3. Velasco R, Mercadal S, Vidal N, et al; GELTAMO and GENOSEN Group. Diagnostic delay and outcome in immunocompetent patients with primary central nervous system lymphoma in Spain: a multicentric study. *J Neurooncol* 2020;148:545–54 CrossRef Medline
- World Health Organization. Hematolymphoid Tumours. WHO Classification of Tumours Online. 5th ed. https://tumourclassification. iarc.who.int/welcome/. Accessed January 16, 2023
- Tang YZ, Booth TC, Bhogal P, et al. Imaging of primary central nervous system lymphoma. Clin Radiol 2011;66:768–77 CrossRef Medline
- Mansour A, Qandeel M, Abdel-Razeq H, et al. MR imaging features of intracranial primary CNS lymphoma in immune competent patients. Cancer Imaging 2014;14:1–9 CrossRef Medline
- Pons-Escoda A, Garcia-Ruiz A, Naval-Baudin P, et al. Presurgical identification of primary central nervous system lymphoma with normalized time-intensity curve: a pilot study of a new method to analyze DSC-PWI. AJNR Am J Neuroradiol 2020;41:1816–24 CrossRef Medline
- 8. Pons-Escoda A, García-Ruíz A, Naval-Baudin P, et al. **Diffuse large B-cell Epstein-Barr virus-positive primary CNS lymphoma in non- AIDS patients: high diagnostic accuracy of DSC perfusion metrics.** *AJNR Am J Neuroradiol* 2022;43:1567–74 CrossRef Medline
- 9. Cree IA. The WHO Classification of Haematolymphoid Tumours. Leukemia 2022;36:1701–02 CrossRef Medline
- 10. Li W. The 5(th) Edition of the World Health Organization Classification of Hematolymphoid Tumors. In: Li W. ed. Brisbane (AU) 2022

- Haldorsen IS, Espeland A, Larsson E-M. Central nervous system lymphoma: characteristic findings on traditional and advanced imaging. AINR Am I Neuroradiol 2011;32:984–92 CrossRef Medline
- Deckert M, Brunn A, Montesinos-Rongen M, et al. Primary lymphoma of the central nervous system: a diagnostic challenge. Hematol Oncol 2014;32:57–67 CrossRef Medline
- 13. Brunn A, Nagel I, Montesinos-Rongen M, et al. Frequent triple-hit expression of MYC, BCL2, and BCL6 in primary lymphoma of the central nervous system and absence of a favorable MYC(low)BCL2 (low) subgroup may underlie the inferior prognosis as compared to systemic diffuse large B cell lymphomas. Acta Neuropathol 2013;126:603-05 CrossRef Medline
- Jhaveri MD. Chapter 173: diffuse large B-cell lymphoma. In: Jhaveri MD, Osborn AG, Salzman KL. Diagnostic Imaging: Brain. 4th ed. Elsevier: 2020:602–06
- Sakata A, Okada T, Yamamoto A, et al. Primary central nervous system lymphoma: is absence of intratumoral hemorrhage a characteristic finding on MRI? Radiol Oncol 2015;49:128–34 CrossRef Medline
- 16. Barajas RF, Politi LS, Anzalone N, et al. Consensus recommendations for MRI and PET imaging of primary central nervous system lymphoma: guideline statement from the International Primary CNS Lymphoma Collaborative Group (IPCG). Neuro Oncol 2021;23:1056-71 CrossRef Medline
- 17. Lee MD, Baird GL, Bell LC, et al. Utility of percentage signal recovery and baseline signal in DSC-MRI optimized for relative CBV measurement for differentiating glioblastoma, lymphoma, metastasis, and meningioma. AJNR Am J Neuroradiol 2019;40:1145–450 CrossRef Medline
- 18. Xing Z, You RX, Li J, et al. Differentiation of primary central nervous system lymphomas from high-grade gliomas by rCBV and percentage of signal intensity recovery derived from dynamic susceptibility-weighted contrast-enhanced perfusion MR imaging. Clin Neuroradiol 2014;24:329–36 CrossRef Medline
- Valles FE, Perez-Valles CL, Regalado S, et al. Combined diffusion and perfusion MR imaging as biomarkers of prognosis in immunocompetent patients with primary central nervous system lymphoma. AJNR Am J Neuroradiol 2013;34:35–40 CrossRef Medline
- Mora P, Majós C, Castañer S, et al. 1H-MRS is useful to reinforce the suspicion of primary central nervous system lymphoma prior to surgery. Eur Radiol 2014;24:2895–905 CrossRef Medline
- Husseini L, Saleh A, Reifenberger G, et al. Inflammatory demyelinating brain lesions heralding primary CNS lymphoma. Can J Neurol Sci 2012;39:6–10 CrossRef Medline
- Levine AM. Lymphoma complicating immunodeficiency disorders.
 Ann Oncol 1994;5(5 Supple 2):29–35 CrossRef Medline
- Gandhi MK, Hoang T, Law SC, et al. EBV-associated primary CNS lymphoma occurring after immunosuppression is a distinct immunobiological entity. Blood 2021;137:1468–77 CrossRef Medline
- 24. Mahale P, Shiels MS, Lynch CF, et al. Incidence and outcomes of primary central nervous system lymphoma in solid organ transplant recipients. Am J Transplant 2018;18:453–61 CrossRef Medline
- Verdu-Bou M, Tapia G, Hernandez-Rodriguez A, et al. Clinical and therapeutic implications of Epstein-Barr virus in HIV-related lymphomas. Cancers (Basel) 2021;13:5534 CrossRef Medline
- Kaulen LD, Karschnia P, Dietrich J, et al. Autoimmune diseaserelated primary CNS lymphoma: systematic review and meta-analysis. J Neurooncol 2020;149:153–59 CrossRef Medline
- Mancuso S, Carlisi M, Santoro M, et al. Immunosenescence and lymphomagenesis. Immun Ageing 2018;15:1–7 CrossRef Medline
- 28. Barosi G. An immune dysregulation in MPN. Curr Hematol Malig Rep 2014;9:331–39 CrossRef Medline
- Suh CH, Kim HS, Lee SS, et al. Atypical imaging features of primary central nervous system lymphoma that mimics glioblastoma: utility of intravoxel incoherent motion MR imaging. Radiology 2014:272:504–13 CrossRef Medline
- Sauter A, Faul C, Bitzer M, et al. Imaging findings in immunosuppressed patients with Epstein Barr virus-related B cell malignant lymphoma. Am J Roentgenol 2010;194:W141–49 CrossRef Medline

- Patsalides AD, Atac G, Hedge U, et al. Lymphomatoid granulomatosis: abnormalities of the brain at MR imaging. Radiology 2005;237:265–73 CrossRef Medline
- Tateishi U, Terae S, Ogata A, et al. MR imaging of the brain in lymphomatoid granulomatosis. AJNR Am J Neuroradiol 2001;22:1283–90 Medline
- 33. De Graaff HJ, Wattjes MP, Rozemuller-Kwakkel AJ, et al. Fatal B-cell lymphoma following chronic lymphocytic inflammation with pontine perivascular enhancement responsive to steroids. *JAMA Neurol* 2013;70:915–18 CrossRef Medline
- 34. Dang YL, Kok HK, McKelvie PA, et al. Chronic lymphocytic infiltration with pontine perivascular enhancement responsive to steroids (CLIPPERS) and its association with Epstein-Barr virus (EBV)-related lymphomatoid granulomatosis: a case report. BMC Neurol 2021;21:80 CrossRef Medline
- Fonkem E, Dayawansa S, Stroberg E, et al. Neurological presentations of intravascular lymphoma (IVL): meta-analysis of 654 patients. BMC Neurol 2016;16:9 CrossRef Medline
- 36. Baehring JM, Henchcliffe C, Ledezma CJ, et al. Intravascular lymphoma: magnetic resonance imaging correlates of disease dynamics within the central nervous system. J Neurol Neurosurg Psychiatry 2005;76:540–44 CrossRef Medline
- 37. Yamamoto A, Kikuchi Y, Homma K, et al. Characteristics of intravascular large B-cell lymphoma on cerebral MR imaging. AJNR Am J Neuroradiol 2012;33:292–96 CrossRef Medline
- Quinn ZL, Zakharia K, Schmid JL, et al. Primary dural diffuse large B-cell lymphoma: a comprehensive review of survival and treatment outcomes. Clin Lymphoma Myeloma Leuk 2020;20:e105–12 CrossRef Medline
- 39. Pons Escoda A, Naval Baudin P, Mora P, et al. **Imaging of skull vault tumors in adults.** *Insights Imaging* 2020;11:23 CrossRef Medline
- Smith AB, Horkanyne-Szakaly I, Schroeder JW, et al. From the Radiologic Pathology Archives: mass lesions of the dura—beyond meningioma, radiologic-pathologic correlation. Radiographics 2014;34:295–312 CrossRef Medline
- Jahnke K, Schilling A, Heidenreich J, et al. Radiologic morphology of low-grade primary central nervous system lymphoma in immunocompetent patients. AJNR Am J Neuroradiol 2005;26:2446–54 Medline
- 42. Magaki S, Satyadev R, Chen Z, et al. Central nervous system ALKnegative anaplastic large cell lymphoma with IRF4/DUSP22 rearrangement. Brain Tumor Pathol 2022;39:25–34 CrossRef Medline
- 43. Menon MP, Nicolae A, Meeker H, et al. **Primary CNS T-cell lym- phomas: a clinical, morphologic, immunophenotypic, and molecular analysis.** *Am J Surg Pathol* 2015;39:1719–29 CrossRef Medline
- 44. Izquierdo C, Velasco R, Vidal N, et al. Lymphomatosis cerebri: a rare form of primary central nervous system lymphoma: analysis of 7 cases and systematic review of the literature. *Neuro Oncol* 2016;18:707–15 CrossRef Medline
- 45. Hatanpaa KJ, Fuda F, Koduru P, et al. Lymphomatosis cerebri: a diagnostic challenge. *JAMA Neurol* 2015;72:1066–67 CrossRef Medline
- 46. Li L, Rong JH, Feng J. Neuroradiological features of lymphomatosis cerebri: a systematic review of the English literature with a new case report. Oncol Lett 2018;16:1463–74 CrossRef Medline
- 47. Yu H, Gao B, Liu J, et al. Lymphomatosis cerebri: a rare variant of primary central nervous system lymphoma and MR imaging features. Cancer Imaging 2017;17:26 CrossRef Medline
- Nagpal S, Glantz MJ, Recht L. Treatment and prevention of secondary CNS lymphoma. Semin Neurol 2010;30:263–72 CrossRef Medline
- 49. Ferreri AJM, Doorduijn JK, Re A, et al; International Extranodal Lymphoma Study Group (IELSG). MATRix-RICE therapy and autologous haematopoietic stem-cell transplantation in diffuse large B-cell lymphoma with secondary CNS involvement (MARIETTA): an international, single-arm, phase 2 trial. Lancet Haematol 2021;8: e110-21 CrossRef Medline
- Bobillo S, Khwaja J, Ferreri AJM, et al. Prevention and management of secondary central nervous system lymphoma. Haematologica 2022. Nov 17 CrossRef Medline



RADIOLOGÍA



www.elsevier.es/rx

UPDATE IN RADIOLOGY

Presurgical diagnosis of diffuse gliomas in adults: Post-WHO 2021 practical perspectives from radiologists in neuro-oncology units



A. Pons-Escoda a,d,*, C. Majos a,b,c, M. Smits e,f,g, L. Oleaga h

- ^a Radiology Department, Hospital Universitari de Bellvitge, Barcelona, Spain
- ^b Neuro-Oncology Unit, Institut d'Investigació Biomèdica de Bellvitge-IDIBELL, Barcelona, Spain
- ^c Diagnostic Imaging and Nuclear Medicine Research Group, Institut d'Investigació Biomèdica de Bellvitge-IDIBELL, Barcelona, Spain
- d Facultat de Medicina i Ciencies de La Salut, Universitat de Barcelona (UB), Barcelona, Spain
- e Department of Radiology & Nuclear Medicine, Erasmus MC, Rotterdam, The Netherlands
- ^f Erasmus MC Cancer Institute, Erasmus MC, Rotterdam, The Netherlands
- g Medical Delta, Delft, The Netherlands
- ^h Radiology Department, Hospital Clínic Barcelona, Barcelona, Spain

Received 12 September 2023; accepted 31 October 2023 Available online 23 March 2024

KEYWORDS

Brain neoplasms; Glioma; Diagnostic imaging; Magnetic resonance imaging; World Health Organization; Histology; Molecular pathology Abstract The 2021 World Health Organization classification of CNS tumours was greeted with enthusiasm as well as an initial potential overwhelm. However, with time and experience, our understanding of its key aspects has notably improved. Using our collective expertise gained in neuro-oncology units in hospitals in different countries, we have compiled a practical guide for radiologists that clarifies the classification criteria for diffuse gliomas in adults. Its format is clear and concise to facilitate its incorporation into everyday clinical practice. The document includes a historical overview of the classifications and highlights the most important recent additions. It describes the main types in detail with an emphasis on their appearance on imaging. The authors also address the most debated issues in recent years. It will better prepare radiologists to conduct accurate presurgical diagnoses and collaborate effectively in clinical decision making, thus impacting decisions on treatment, prognosis, and overall patient care.

© 2024 The Authors. Published by Elsevier España, S.L.U. on behalf of SERAM. This is an open access article under the CC BY-NC-ND license (http://creativecommons.org/licenses/by-nc-nd/4.0/).

E-mail address: albert.pons@bellvitgehospital.cat (A. Pons-Escoda).

^{*} Corresponding author.

PALABRAS CLAVE

Neoplasias cerebrales; Glioma; Imagen diagnóstica; Imagen por resonancia magnética; Organización Mundial de la Salud; Histología; Patología molecular

Diagnóstico prequirúrgico de gliomas difusos en adultos: perspectivas prácticas de radiólogos de Unidades de neurooncología Post-WHO 2021

Resumen La Clasificación 2021 de tumores del SNC por la Organización Mundial de la Salud (OMS) fue acogida con entusiasmo, aunque al principio pudo parecer abrumadora. Con el tiempo, hemos comprendido los puntos clave, y basándonos en nuestra experiencia en unidades de neurooncología de hospitales internacionales, hemos elaborado una guía práctica para radiólogos. Esta guía esclarece los criterios de clasificación de los Gliomas Difusos en los adultos y presenta un formato claro para su aplicación diaria. El manuscrito repasa la evolución histórica de las clasificaciones y destaca las novedades más relevantes. Ofrece un análisis detallado de las entidades principales, centrándose en manifestaciones radiológicas. Además, discute los temas más controvertidos de los últimos años. Con este documento, los radiólogos estarán preparados para realizar diagnósticos prequirúrgicos, y sobre todo colaborar eficazmente en la toma de decisiones clínicas, con impacto directo sobre el tratamiento, el pronóstico o la atención personalizada.

© 2024 Los Autores. Publicado por Elsevier España, S.L.U. en nombre de SERAM. Este es un artículo Open Access bajo la licencia CC BY-NC-ND (http://creativecommons.org/licenses/by-nc-nd/4.0/).

Introduction

Following the launch of the World Health Organization (WHO) 2021 Classification for Central Nervous System (CNS) tumors, there was a sudden rise of related radiological papers. ¹⁻³ Initially, the wealth of these publications could seem daunting to many radiologists. But with time and practice, our grasp of the new key aspects has notably improved. By sharing our expertise, gathered in neuro-oncology units at international hospitals, we believe we can now provide a practical guide. This guide, aimed at radiologists (and other related clinicians), highlights the crucial components of the classification's 5th edition in a clear, comprehensible manner that can be promptly incorporated into daily practice.

The main aim of this paper is to offer a practical review based on the authors' firsthand experience in characterizing adult diffuse gliomas in multidisciplinary units. Ultimately it is done through visual assessments of radiological images, but it is essential not to overlook critical clinical concepts that are foundational for optimal imaging-guided knowledge implementation. While elucidating the fundamental concepts and foundations of the classification from a critical-applied perspective, the content is designed to be comprehensible to a wide audience. The more imaging-centric guide can be adapted to standard MRI protocols. 5-7 without requiring complex processing or data analysis, thereby ensuring its applicability, practicality and relevance.

Historical background

Back in 2007, the classification relied on the histological examination of surgical samples. Diffuse gliomas were classified as astrocytic, oligodendrocytic, or mixed oligoastrocytic. Thus, each tumor classification depended on pathologists' evaluations with a degree of subjectivity.

Especially, the consensus among pathologists did not achieve ideal precision when handling tumors with any oligoden-droglial elements. 10

Substantial progress in molecular pathology led to the integration of molecular criteria with histological evaluation in the WHO 2016 classification. A key update involved differentiating oligodendrogliomas from astrocytomas by mandating the presence of IDH mutation and 1p/19q codeletion in oligodendrogliomas, thereby reducing subjectivity in histological classification. ^{10,11} Another significant update involved categorizing astrocytomas based not only on histological grade but also on their IDH mutation status. This change was prompted by the recognition of substantial biological and prognostic distinctions between IDH-mutant and IDH-wildtype tumors, which transcend histological grading. ¹¹

After some years of growing influence from molecular pathology, 12 the paradigm shift completed in 2021, when the classification focused primarily on genetic entities.

WHO 2021 classification of diffuse gliomas in adults, key summary

The new classification system now centers around three primary genetically defined categories: IDH-wildtype Glioblastoma, IDH-mutant astrocytoma, and IDH-mutant 1p/19q-codeleted oligodendroglioma. Astrocytomas had grades 2 to 4, while oligodendrogliomas had grades 2 and 3. The term anaplastic was dropped and replaced by grade 3, and grade 4 IDH-mutant astrocytoma was no longer called Glioblastoma (reserved exclusively for IDH-wildtype). The grading system for each tumor still fundamentally relies on histology, with high mitosis and necrosis or microvascular proliferation indicating grade 4. However, new genetic criteria could upgrade a (solely) histological grade 2 or 3 to a WHO grade 4 (molecular grades 4): 1. A homozygous

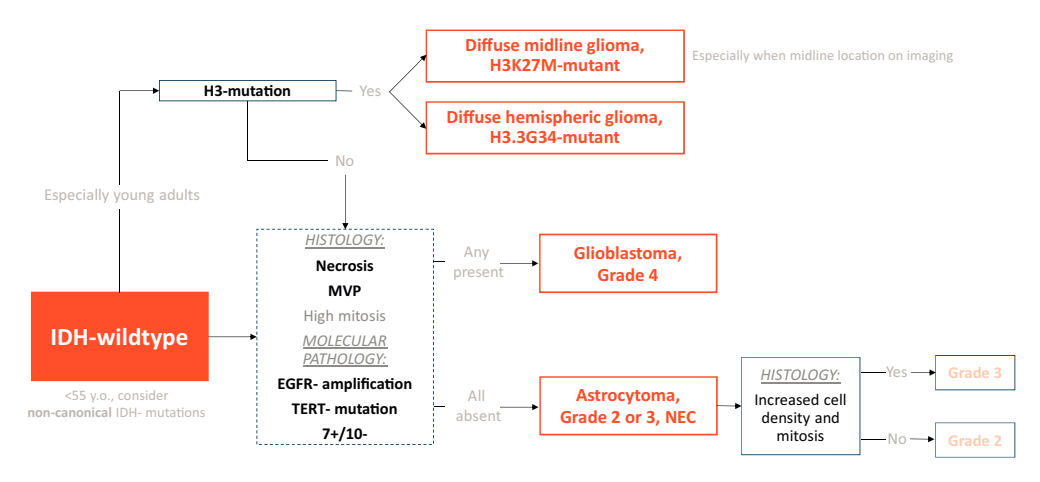


Figure 1 Classification Scheme for IDH-wildtype Gliomas in Adults. H3-mutations are considered pediatric-type gliomas, but they are included here due to their potential relevance in young adults. The dashed box highlights the stage at which molecular pathology can determine a Grade 4 tumor regardless histology. MVP stands for microvascular proliferation.

codeletion of CDKN2A or CDKN2B in IDH-mutant astrocytoma carries a grade 4 IDH-mutant astrocytoma, or 2. EGFR-amplification, TERT promoter-mutation, or 7+/10—concurrent gain of chromosome 7 and loss of chromosome 10 in IDH-wildtype carries a glioblastoma (WHO grade 4), regardless of histological traits.¹³ Therefore, in summary, the major key updates were: 1. Simplification of the classification to three genetically defined categories (IDH-wildtype glioblastoma, IDH-mutant astrocytoma, IDH-mutant 1p/19q-codeleted oligodendroglioma); and 2. Tumor grading incorporation of molecular grades 4 alongside traditional histological assessments.^{2,13}

Moreover, the latest classification notably differentiates between adult- and pediatric-type gliomas, acknowledging that certain pediatric types can occur in young adults. This adds another crucial molecular marker for classifying IDH-wildtype tumors in young adults, especially if midline-located: the histone H3-mutations. H3K27M mutations are frequently observed in diffusely infiltrating gliomas situated in midline structures. H3.3G34R/V mutations are found in a smaller group of high-grade gliomas in cerebral hemispheres, with a more favorable prognosis. Therefore, in young individuals, H3-mutations must be ruled out before confirming a glioblastoma. ¹³⁻¹⁵

Lastly, it is crucial to comprehend two terms: NOS (not otherwise specified) and NEC (not elsewhere classified). NOS indicates that the necessary tests for definitive classification are unavailable. NEC signifies that after performing all necessary tests, the tumor cannot be classified into any of the established WHO categories. ^{13,16} The primary focal entities in the NEC category are grade 2 or 3 IDH-wildtype astrocytic tumors. These tumors do not meet the histological or molecular criteria for grade 4 and thus cannot be classified as glioblastoma. ^{2,17} These somewhat enigmatic entities have attracted significant attention in academic discussions and will be debated here in a subsequent dedicated subsection.

A simplified framework of the classification is shown in Fig. 1 for IDH-wildtype and Fig. 2 for IDH-mutant.

Main molecular tests: immunohistochemistry, fluorescence in situ hybridization (FISH) and DNA sequencing

Understanding the available molecular tests, along with their strengths and limitations, is crucial. Immunohistochemistry is the most accessible to evaluate IDH-mutation status. However, it exclusively evaluates IDH1 p.R132H mutations, accounting for more than 90% of all IDH-mutations.

Gene sequencing, less accessible and more costly, extends the detection to other loci of IDH1 and IDH2, known as non-canonical IDH-mutations. Therefore, if the immunohistochemistry result is negative, DNA-sequencing is recommended. However, it is not required for grade 4 gliomas in patients aged ≥ 55 , where a negative immunohistochemistry result is sufficient to classify the tumor as IDH-wildtype^{13,18,19}

Also, regarding oligodendrogliomas and 1p/19q-codeletion; if the histology, IDH-mutation, and p53 and ATRX status are consistent with IDH-mutant astrocytoma, there is no additional need for FISH for 1p/19q-codeletion^{13,20,21} (Table1).

Understanding this, empowers radiologists to contribute effectively in reaching the most accurate diagnosis and recommending specific tests in unique scenarios. As an example, we might insist on non-canonical IDH-testing when a tumor presents with a T2-FLAIR mismatch, highly specific for IDH-mutants astrocytoma, if immunohistochemistry results are negative.

WHO 2021 diffuse gliomas imaging differential diagnosis in adults

Radiology in the era of genetic classification, current trends and critical perspective

Given the recent advances in the genetic characterization of gliomas, there is an increasing interest in radiogenomics:

^	ر
'n	٠
_	Ī

Method	Evaluated mutations	Accessibility/costs	Recommended for negative result	Comments
Immunohistochemistry	IDH1 p.R132H (canonical, 90% of all IDH mutations)	High/Low	DNA Sequencing	IDH1 p.R132H-negative results is enough to classify as Glioblastoma a CNS WHO grade 4 glioma > 55 years.
Immunohistochemistry	ATRX and p53 mutations	High/Low	FISH	IDH-mutant gliomas with astrocytic histology, ATRX loss and p53 mutation can be classified as Astrocytomas
FISH	1p 19q codeletion	High/Medium	N/A	without FISH
DNA sequencing	Non-IDH1 p.R132H IDH1 and IDH2 (non-canonical, 10%)	Low/High	N/A	Required in in gliomas < 55 years IDH1 p.R132H-negative to rule out non-canonical IDH-mutant Astrocytoma.
DNA sequencing	TERT, EGFR, 7+/10-	Low/High	N/A	Required in IDH-wildtype histological WHO grade 2–3, to detect molecular Glioblastoma. Initial evaluation possible through PCR and FISH.
DNA sequencing	CDKN2A/B	Low/High	N/A	Required in IDH-mutant histological WHO grade 2—3, to detect molecular grade 4 Astrocytoma.
DNA sequencing	H3	Low/High	N/A	Required in IDH-wildtype < 55 years, to rule-out H3-altered gliomas (pediatric-type). Initial evaluation possible through immunohistochemistry.

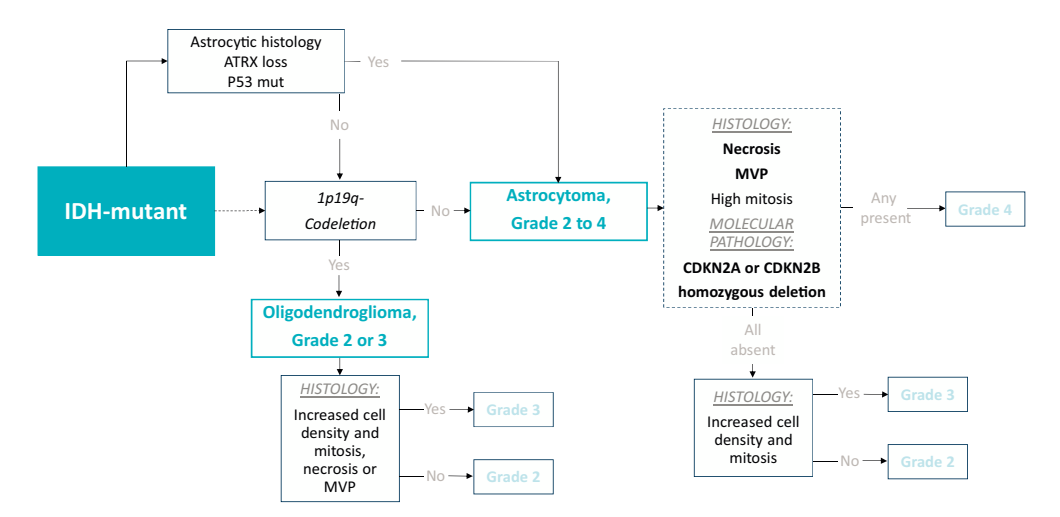


Figure 2 Classification Scheme for IDH-mutant Gliomas in Adults. The dashed box highlights the stage at which molecular pathology can determine a Grade 4 tumor regardless histology. MVP stands for microvascular proliferation.

categorizing genetically defined entities based on imaging phenotypes. Typically, it is quantitative and deals with big-data, and is widely represented in scientific literature. However, visual/qualitative radiogenomics is also feasible and useful; and, in fact, visual assessment continues to dominate in clinical practice. 23-28

When reviewing radiological literature on the 2021 classification, a critical perspective is essential. Many studies claim to distinguish between different genetic entities, but these claims often require careful interpretation because there is a strong correlation between genetic markers and histological grades. For instance, IDH wildtype tumors are mostly glioblastomas with histological grade 4, while IDH mutant astrocytomas are usually grade 2-3. Therefore, some studies' claims of differentiation of IDH-mutation status might actually be a more familiar distinction between grades 2-3 and 4. For example, is the presence of necrosis a marker of IDH-wildtype or is it just a grade 4 marker as we already knew it? All this invites debate. For example, in younger patients, where IDH-mutant and IDHwildtype coexists more evenly than in the elderly, 13,19,29 necrosis may be an unreliable marker of the IDH-status beyond the histological grade 4. Or conversely, an IDHwildtype grade 2-3 astrocytoma NEC should not present necrosis, 13 another situation in which the absence of this radiological marker would fail in determining IDH-status. Therefore, there is a delicate interplay between clinicalepidemiological data, histological grade, and genetic profile which the radiologist should skillfully manage when suggesting a specific diagnosis in clinical reports or neuro-oncology boards.

Preliminary key concepts

The first factor to consider when approaching the appropriate differential diagnosis may be the patient's age. IDH-mutations are much more common in patients under 55 years of age. ^{13,17,19,29} Therefore, in patients over 55, there exists a substantial likelihood of identifying an IDH-wildtype tumor, which is almost always a glioblastoma.

Imaging accuracy in detecting histological grade 4 in astrocytic gliomas, regardless of the IDH-mutation status, is crucial to remember for radiologists. Aligned with the WHO's histological criteria for grade 4, there are two primary methods. The first is by identifying necrosis on post-contrast T1-weighted (T1w) sequences. 30,31 The second involves assessing indirect signs of microvascular proliferation using DSC-PWI. 32,33 To simplify: unremarkable (without significant increases nor decreases) CBV maps are typically associated with grade 2 astrocytomas. In grade 3, one might observe a range from unremarkable to some foci of slightly elevated CBV. In contrast, clear nodular or diffuse frank elevations in CBV are more indicative of a grade 4.34 Additionally, Diffusion-Weighted-Imaging (DWI) can provide information on cellular density and therefore mitotic activity, important for histological grading. 35,36 All these imaging-based grading criteria are more controversial for oligodendrogliomas. 24,37

Finally, it is important to mention a well-known and extremely specific radiological sign for IDH-mutant astrocytomas: the T2-FLAIR mismatch. This consists of a high T2w and low FLAIR signal within solid tumor, often accompanied by a peripheral rim of FLAIR hyperintensity.³⁸ This sign serves as a specific marker for IDH-mutation and is absent in 1p19q-codeleted gliomas, facilitating the differentiation between astrocytomas (IDH-mutant, 1p19q- non codeleted) and oligodendrogliomas (IDH-mutant, 1p19q- codeleted). Additionally, it may function as a favorable prognostic indicator for astrocytomas.²³

IDH-wildtype, glioblastoma

Glioblastoma is the most common malignant primary tumor in adults, particularly affecting individuals over 55 years. 13,17,19,29,39 The clinical symptoms are acute to subacute. 40 It is an astrocytic glioma, IDH-wildtype and H3-wildtype, with: microvascular proliferation or necrosis; or altered TERT, EGFR, or 7+/10–. 13,15 It arises in the subcortical white matter and infiltrates cortex and deep grey matter. Extension through the corpus callosum is a well-known growth pattern. 41 Survival prog-

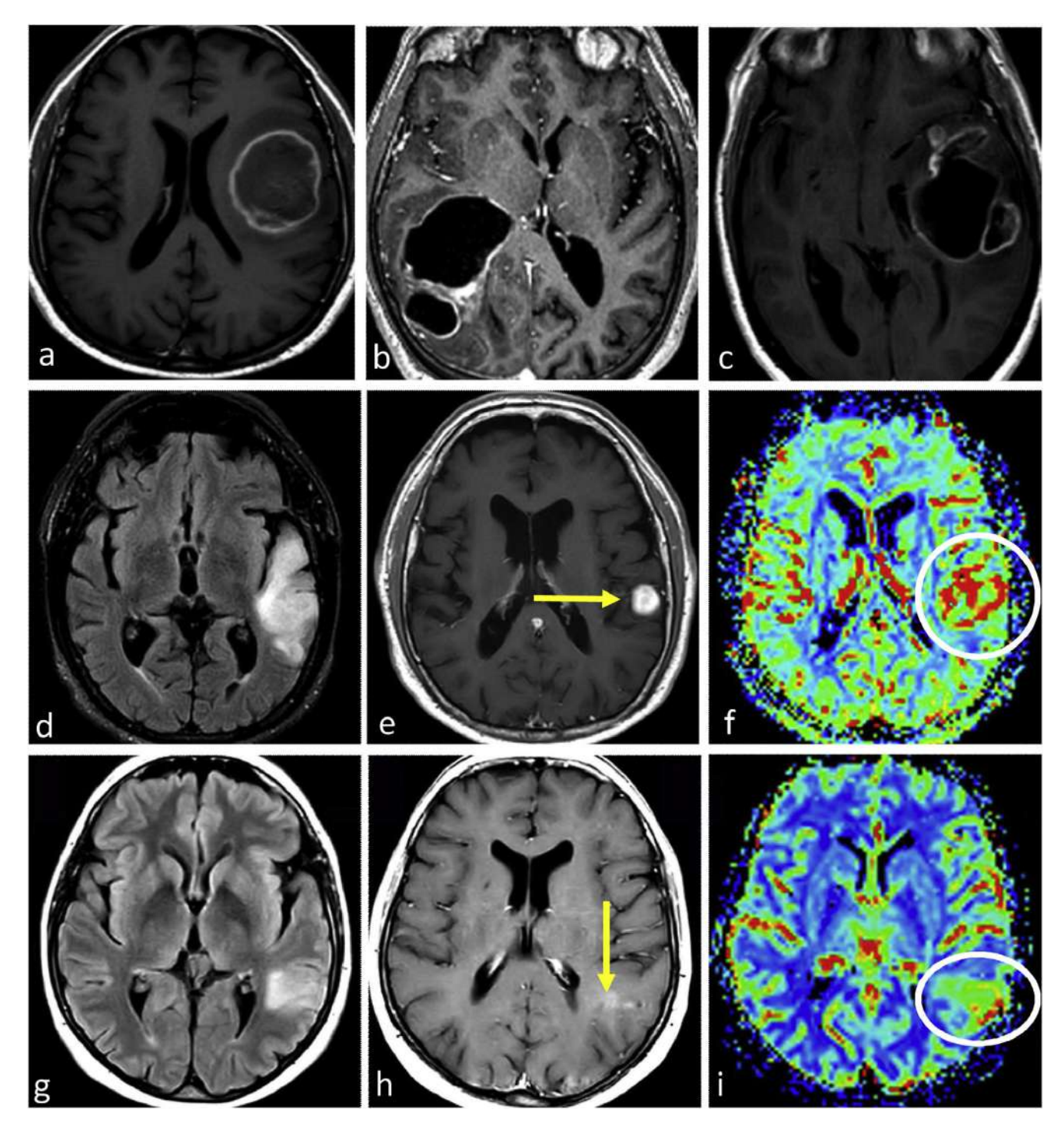


Figure 3 Three different typical presentations for IDH-wildtype glioblastoma in patients between 60- and 70 years old. In a-c, the most paradigmatic imaging features are seen in axial T1w-post contrast images of three different patients, with ring-enhancing irregular margins and extensive necrosis. In d-f: axial FLAIR, T1w-postcontrast, and CBV color maps from DSC-PWI. Extensive FLAIR left temporal infiltrative lesion (d) with associated solid nodular enhancement without necrosis (arrow in e) but with clearly elevated CBV (circle in f). In g-i: axial FLAIR, T1w-postcontrast, and CBV color maps from DSC-PWI. Focal FLAIR left temporal infiltrative lesion (g) with minimal enhancement and absent necrosis (arrow in h) but clearly elevated CBV (circle in i).

nosis is poor, around 15–18 months after therapy. 13 MGMTpromoter-methylation, is an independent predictor of longer survival beyond age and performance status. 42,43

Imaging

Glioblastoma characteristic imaging consists of an expansive-infiltrative lesion with prominent irregular

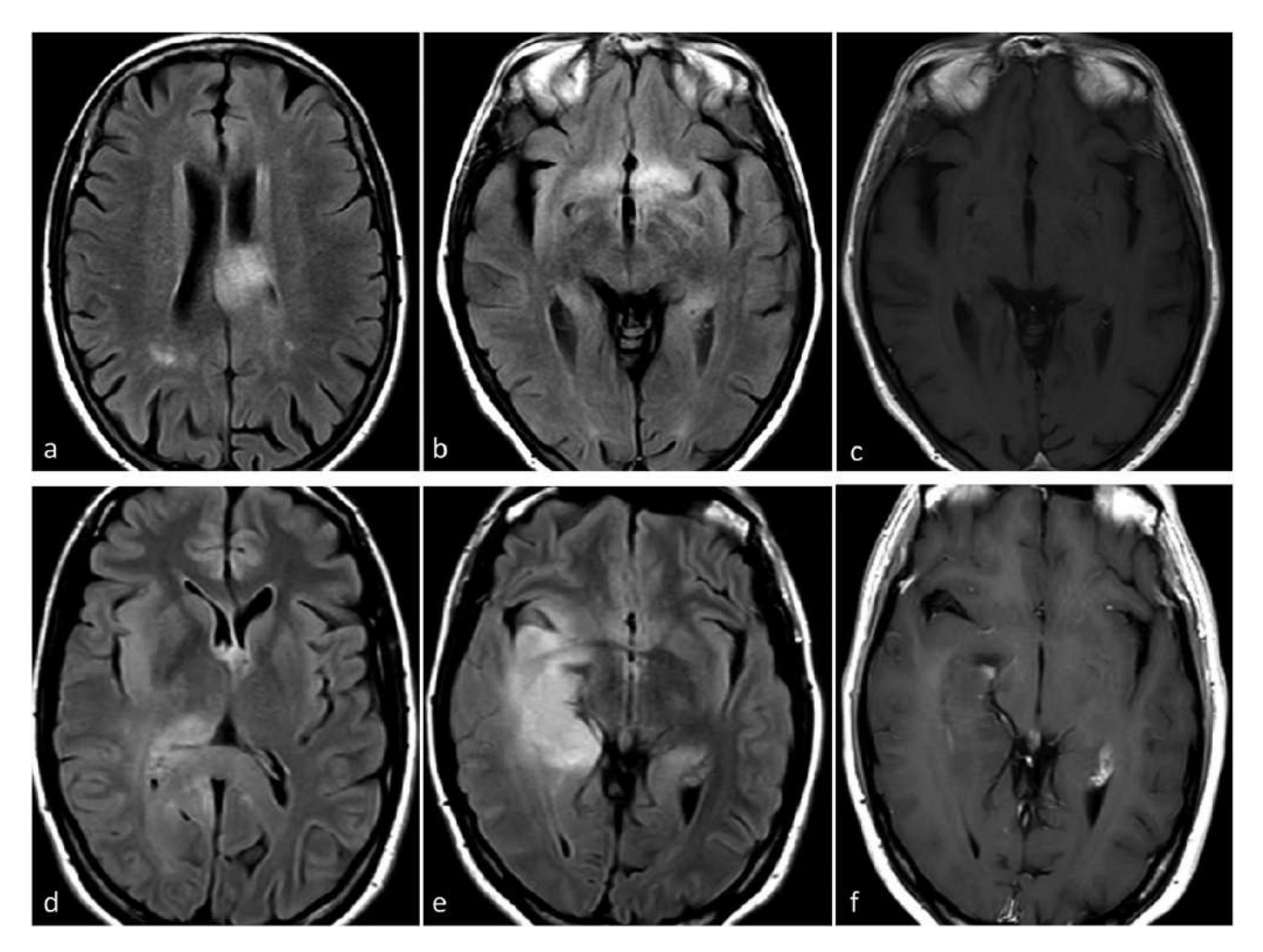


Figure 4 Possible Presentation of TERT or EGFR Altered Molecular IDH-wildtype glioblastoma. Two patients, 80-year-old (a-c) and 55-year-old (d-f). In axial FLAIR sequences (a-b and d-e), diffuse and extensive infiltrative hyperintensities reminiscent of a gliomatosis cerebri pattern in TERT promoter mutated glioblastomas. T1w post-contrast images (c and f) show no enhancement or signs of necrosis.

enhancement, extensive central necrosis and ill-defined margins. Different degrees of hemorrhage are frequently observed. Moderate to large areas of edema and mass effect are usual. 1-3,23 Signs of pial and ependymal invasion are frequent. 44 Non-enhancing T2w and FLAIR tumor components may be radiologically visible, although usually not the dominant part of the tumor. 45,46 Areas of clearly elevated CBV and restricted diffusion, within enhancing tumor, are very frequent. 47,48 Furthermore, the detection of these hyperperfused/diffusion restricted areas beyond the enhancing tumor is helpful in differentiating glioblastoma from solitary metastases 49-51 (Fig. 3).

In certain instances, glioblastoma can manifest without clear necrosis and predominantly display an infiltrative pattern. These tumors are characterized by large and poorly defined non-enhancing components, with absent or different degrees of enhancement. In these non-enhancing and non-necrotic tumors the presence of clear restricted diffusion or increased CBV are particularly relevant, as they strongly support the diagnosis of glioblastoma^{23,52} (Fig. 3).

In summary, when faced with an expansive-infiltrative lesion in an adult over 55, the neuroradiologist should thoroughly search for signs of histological grade 4 which should strongly suggest a diagnosis of glioblastoma. Specifically, necrosis in T1w post-contrast, hypercellularity on DWI and hypervascularization on DSC-PWI.

As an aside, no sound qualitative imaging markers for MGMTpromoter-methylation status have been elucidated. Nevertheless, according to one study, MGMTpromoter-methylated glioblastoma is more likely to show less edema, higher ADC, and lower CBV than unmethylated.⁵³

Molecular glioblastoma

The typical radiology for glioblastoma may not work for those that are not histologically but only molecularly defined (TERT, EGFR, 7+/10-), for which imaging remains relatively unknown. They can present as ill-defined infiltrative lesions on T2w and FLAIR sequences, with minimal or no-enhancement, absent necrosis, and unremarkable findings on DWI and DSC-PWI. In fact, they may present

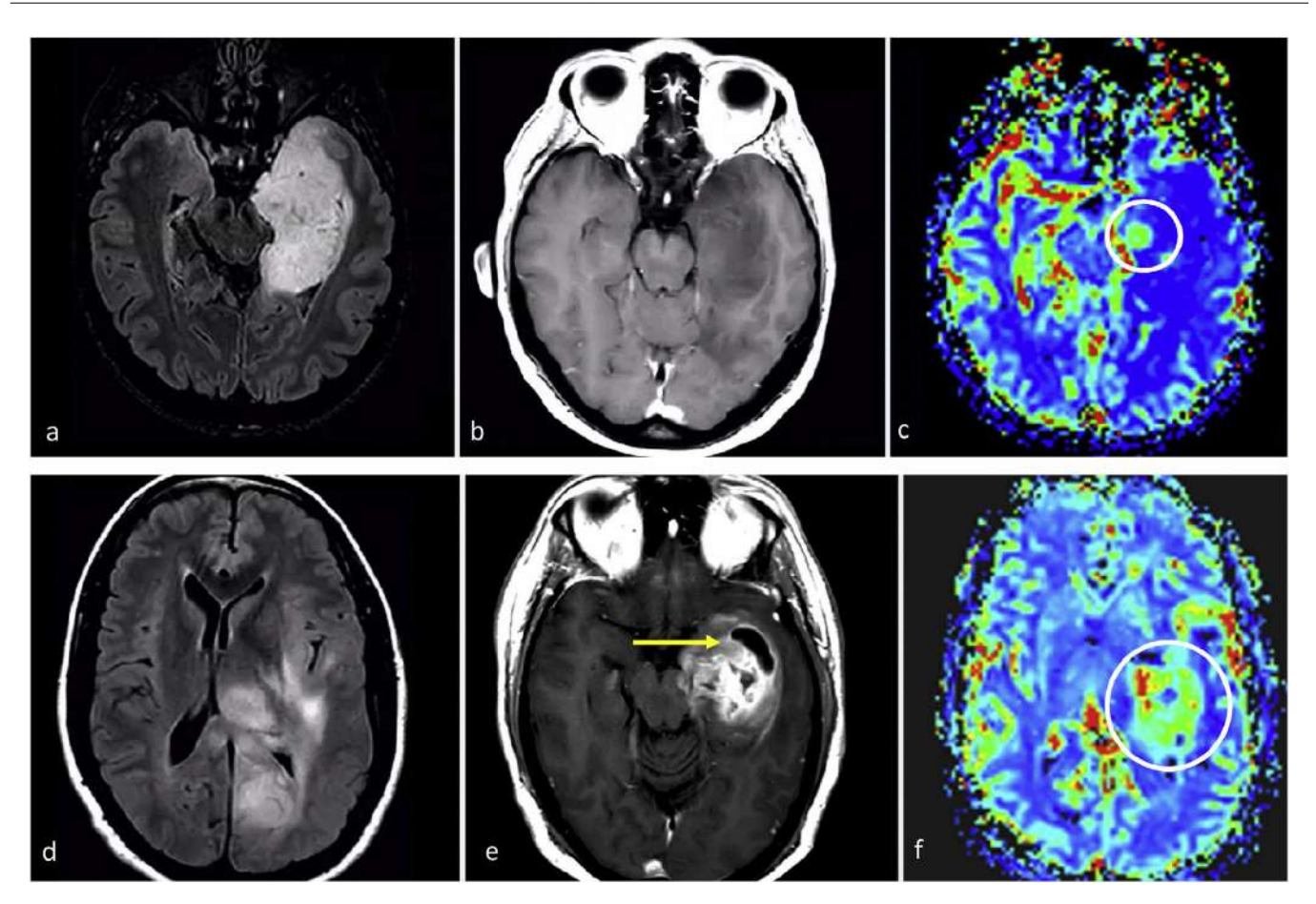


Figure 5 Two exemplifying cases in which biopsy results could render histological grade 2–3 results for an actual grade 4 tumor. Ac, 57-year-old patient. Axial FLAIR (a), T1w post-contrast (b) and DSC-PWI derived CBV color maps (c). Extensive FLAIR hyperintense medial left temporal infiltrative lesion (a), without enhancement or necrosis (b), and a subtle nodular focus of clearly elevated CBV (circle in c). i.e., a biopsy not capturing the high CBV foci would be at risk of undergrading this pathology proven IDH-wildtype astrocytic tumor as grade 2-3. (d-f), 58-year-old patient. Axial FLAIR (d), T1w post-contrast (e) and DSC-PWI derived CBV color maps (f). Extensive FLAIR hyperintense medial left temporal infiltrative lesion in (d), with a more focal area of prominent enhancement and necrosis (arrow in e) as well as high CBV (circle in f). i.e., a biopsy not capturing the necrosis and/or high CBV component would be at risk of undergrading this pathology proven IDH-wildtype astrocytic tumor as grade 2–3. Both patients were treated as IDH-wildtype glioblastomas under a tumor board's consensus decision.

as a classic histological grade 2-3 appearance. However, some studies have indicated a tendency towards multifocality and multicentricity, as well as a gyriform pattern of cortical infiltration in tumors with EGFR or TERT mutations. $^{54-56}$ From a practical perspective, the presence of a gliomatosis cerebri pattern (with some gyriform cortical infiltration) in an adult over 55 may raise suspicion of a molecular glioblastoma, particularly TERT mutated $^{54-56}$ (Fig. 4). No qualitative imaging description have been found for $^{7+}/10-$.

IDH-wildtype, astrocytoma grade 2-3, NEC

These tumors, not included as a distinct WHO entity, are the primary focal entities in the NEC category and have been subject of debate. They are diffuse, astrocytic gliomas IDH-wildtype and H3-wildtype, lacking histological and molecular markers of grade 4.

These somewhat enigmatic entities have attracted significant attention in the most recent academic discussions. In theory, such tumors should be exceptional, and any potential biases in their characterization need to be ruled out. For instance, there could be a biopsy bias: gliomas are heterogeneous, and different histological grades may coexist, so a focal sample from a biopsy may not reflect the highest histological grade within a tumor that might otherwise be undergraded. This bias can potentially be addressed with imaging: initially guiding the biopsy; and subsequently detecting necrosis or clear high vascularization possibly missed in the biopsied tissue, both of which would suggest a grade 4.31 Although this is not explicitly specified in the WHO 2021 classification, potential biopsy biases are not exceptional in neuro-oncology units. Therefore, radiologists need to be aware of this possibility and understand their crucial role in its prevention.

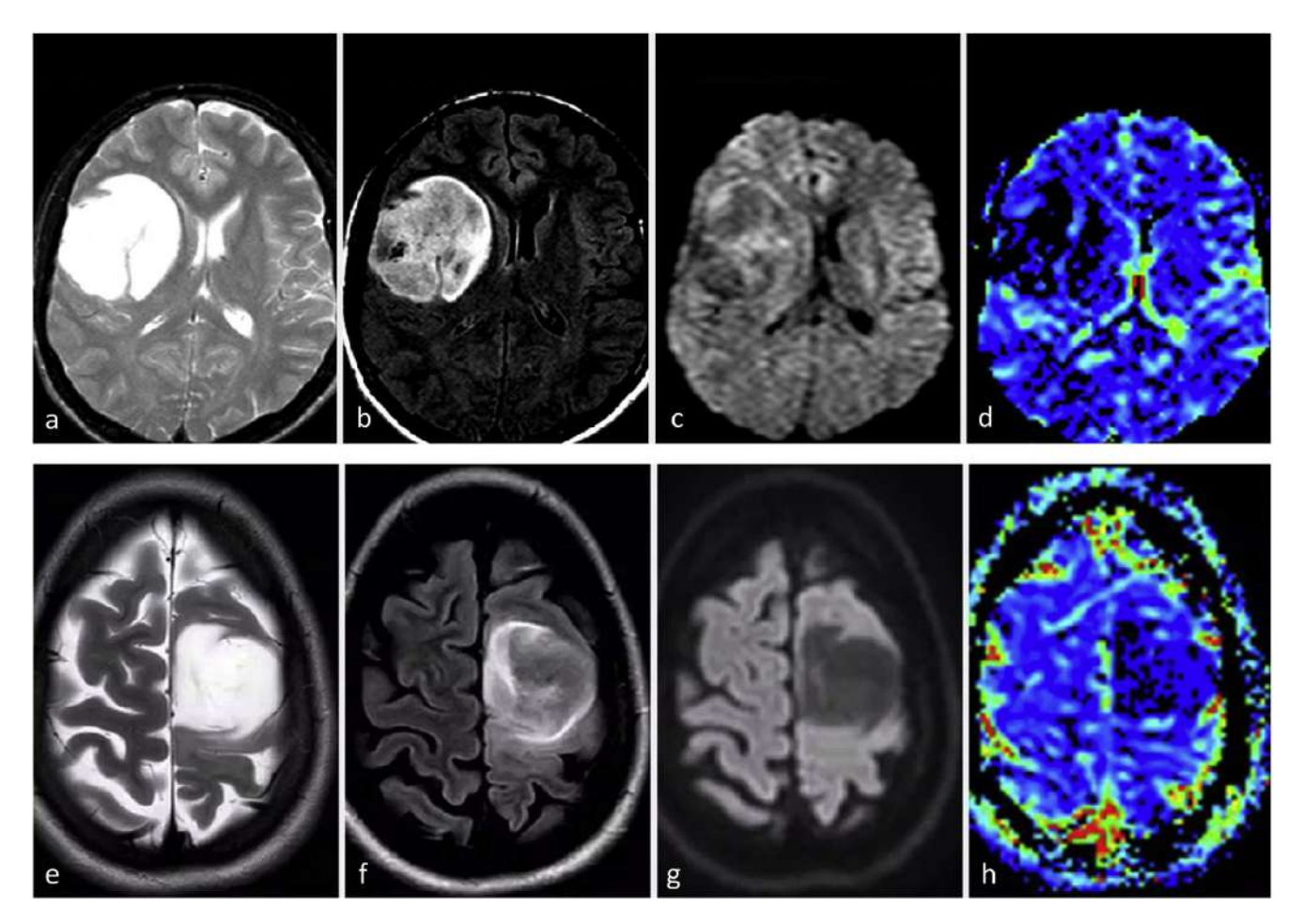


Figure 6 Two different patients with typical imaging features of IDH-mutant grade 2–3 astrocytoma. 31 (a–d) and 34 (e–h) years-old patients. Axial T2w (a and e), FLAIR (b and f), DWI (c and g), and DSC-PWI derived CBV color maps (d and h). Rounded, well-defined T2w hyperintense masses with corresponding FLAIR hypointensity, with a thin peripheral rim of hyperintensity: T2-FLAIR mismatch sign. Without significant diffusion restriction in DWI and low CBV in CBV color maps.

On imaging, based on assumptions from publications prior to the 5th edition, these tumors could present as ill-defined infiltrative lesions, with minimal or no-enhancement, absent necrosis, and unremarkable findings on DWI or DSC-PWI. They may present more ill-defined margins, and possible propensity for temporal location, as well as absent T2-FLAIR mismatch compared to IDH-mutant counterparts⁵⁷ (Fig. 5).

From a radiological management perspective, the authors recommend to keep in mind the radiologists' role in: 1. guiding biopsies to target the higher-grade regions of tumors, and 2. carefully analyzing the images to identify markers of histological grade 4 which may not have been captured in the biopsy. These practices should minimize potential biopsy biases and resultant undergrading.³¹

IDH-mutant, astrocytoma

Astrocytoma IDH-mutant is 1p/19q-non codeleted and frequently associated with ATRX loss and TP53 mutation.⁵⁸ Overall they mostly occur in patients under 55 years^{13,17,19,29}:

grade 2—3 between 30–40 years, and grade 4 in slightly older patients. ⁵⁹ They have a predilection for the frontal lobes ^{57,60} and symptoms are rarely abrupt unless they present with seizures. ⁶⁰

Focal oligodendroglioma-like components are possible and were a source of misclassifications prior to the establishment of molecular criteria. 9,10 Recent years have seen debate regarding the prognostic value of tumor grading among grade 2-3 IDH-mutant astrocytomas, with several scientific publications discussing these grades collectively. 18,59,61,62 According to the last WHO, 13 median overall survival is >5 and >10 years respectively. Conversely, grade 4 IDH-mutant astrocytomas show shorter survival rates (about 3 years¹³); yet longer than IDH-wildtype, despite sharing histological characteristics. 63 Molecular grade 4 are determined by homozygous deletion of CDKN2A or CDKN2B, even in the absence of necrosis and microvascular proliferation. 13,17 Finally, contrary to classical belief, recent work indicates that most grade 4 IDH-mutant astrocytomas occur de novo, rather than with a history of a lower-grade glioma, 13,64

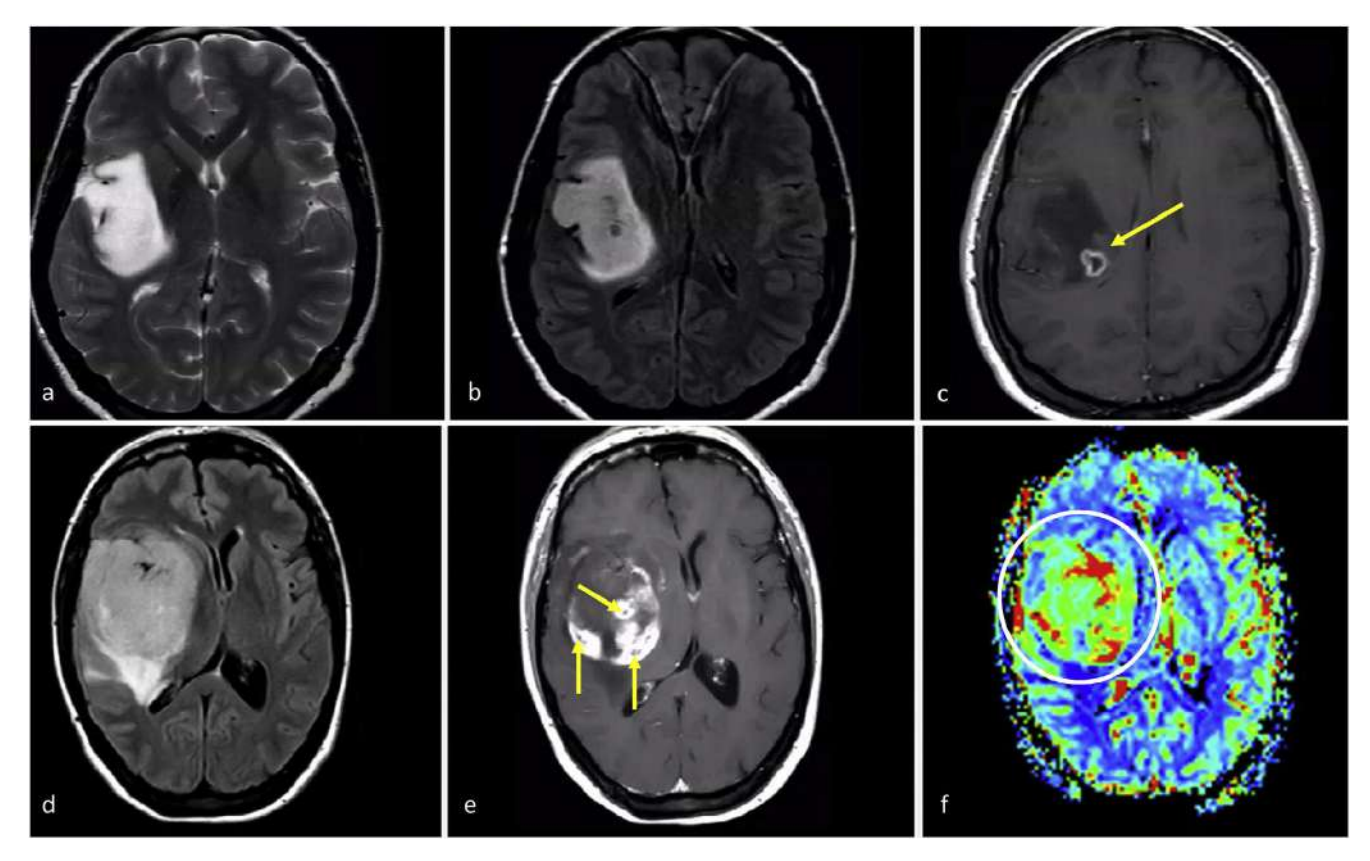


Figure 7 Imaging features in two patients with IDH-mutant astrocytoma grade 4. a-c, 37 years-old. Axial T2w, FLAIR, and T1w post-contrast. Extensive well-defined lesion hyperintense on T2w (a) with corresponding FLAIR hypointensity and thin peripheral hyperintense rim in (b), consistent with T2-FLAIR mismatch sign suggesting IDH-mutation. A small focus of enhancement and necrosis is seen within the deep margin of the tumor (c), suggesting grade 4. Also note that in this case, a biopsy not capturing the necrosis could undergrade the tumor as grade 2–3. Detection of grade 4 imaging features within a tumor with T2-FLAIR mismatch could be a specific presentation of IDH-mutant astrocytoma grade 4. d-f, 49 years-old. Axial FLAIR (d), T1w post-contrast (e), and DSC-PWI derived CBV color map (f). Well-defined, rounded tumor mass on FLAIR (d) with internal areas of solid enhancement (e) within non-enhancing tumor. Small foci of necrosis (arrows in e) and clearly elevated CBV (circle in f). Of note, more extensive necrosis existed in other parts of the tumor not captured in this figure. A grade 4 looking glioma in a patient under 55 with some atypical features for glioblastoma such as clear rounded morphology and well-defined margins could suggest an IDH-mutant astrocytoma grade 4.

Imaging

Grade 2-3 IDH-mutant, astrocytoma

These two different grades are usually treated together due to similar behaviours. 18,59,61,62 The most frequent imaging presentation is an infiltrative lesion, non- or scarcelyenhancing, with well-defined margins and nodular/oval morphology. Despite relatively low sensitivity, T2-FLAIR mismatch sign shows an almost perfect specificity in adults (when it represents at least >25-50% of tumor extent). The mass effect is relatively limited as well as the perilesional edema. They should lack imaging signs of necrosis. 4,23-27,38 DWI may vary between facilitated and homogeneous in grade 2 to slightly heterogeneous in grade 3. No frank CBV elevations should be seen with DSC-PWI³⁴⁻³⁶ (Fig. 6). Lack of calcification and cysts as well as the nodular/oval morphology instead of a gyriform pattern following the cortex may help in the main differential with oligodendrogliomas. 4,23-27

In summary, the neuroradiologist should consider this entity when encountering a young adult with a frontal lobe tumor that appears nodular or oval, exhibits well-defined borders, lacks necrosis, shows minimal to no contrast enhancement, and displays unremarkable DWI and DSC-PWI. If a T2-FLAIR mismatch is observed, it indicates a strong diagnostic possibility; and in the event of negative immunohistochemistry results, DNA-sequencing should be considered for additional assessment of IDH-mutations from a radiologist's perspective.

Grade 4 IDH-mutant, astrocytoma

This subgroup of IDH-mutant astrocytomas has been less extensively studied compared to grades 2–3, remaining a major radiological challenge. Unfortunately, these tumors often get grouped together (and consequently underrepresented) with grades 2–3 under the broader category of IDH-mutant astrocytomas. However, this generalized grouping may be counterproductive because: 1. The differences

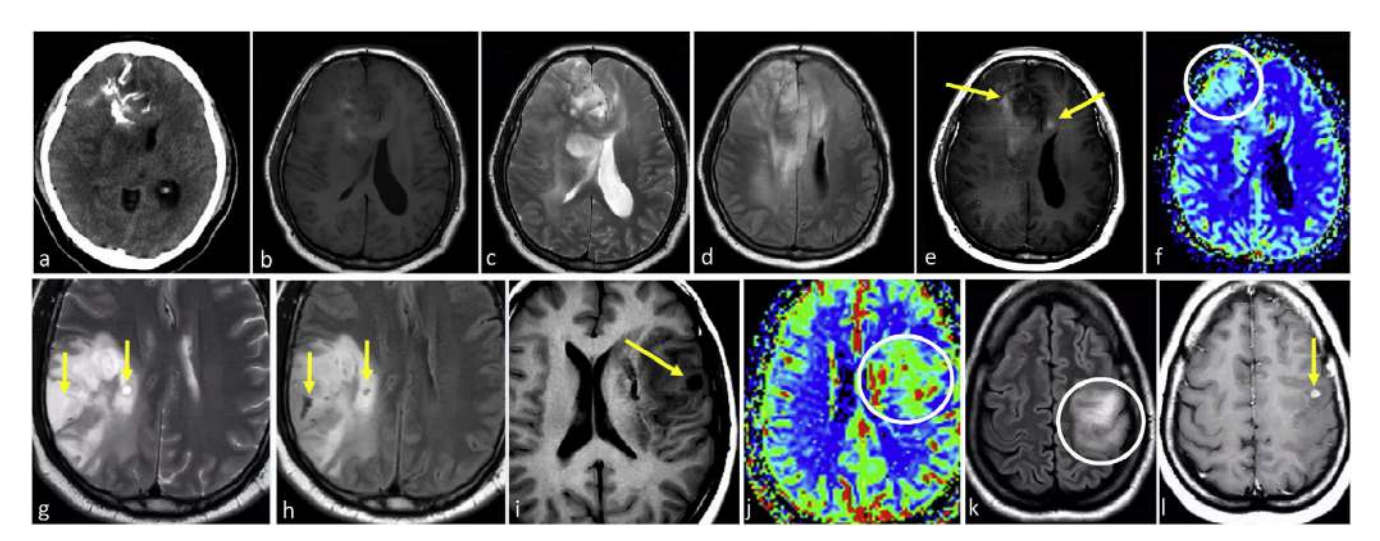


Figure 8 IDH-mutant 1p/19q-codeleted oligodendrogliomas grade 2–3. a–f, 53-year-old patient. Axial non-enhanced CT (a), T1w (b), T2w (c), FLAIR (d), T1w post-contrast (e), and CBV color map (f). Ill-defined diffuse bifrontal mass with extensive cortical infiltration (c and d) and heterogeneous signal on T1w and T2w (b and c). Prominent calcifications on CT (a). Very subtle irregular enhancement (arrows in e) and areas of elevated CBV (circle in f). (g and h) 52-year-old patient. Axial T2w (g) and FLAIR (h). Ill-defined infiltrative parietal mass with heterogeneous signal and extensive cortical infiltration (g–h). Presence of small characteristic intratumoral non-enhancing fluid signal intensity-like areas consistent with cystic foci (arrows in g and h). (I and j), 38-year-old patient. Axial T1w (i) and CBV color map (j). An example of a small intratumoral cyst on T1w (arrow in i) and clearly elevated CBV (j). K-l, 35-year-old patient. Axial FLAIR (k) and T1w post-contrast (l). Infiltrative ill-defined FLAIR hyperintense mass clearly centered on the cortex and following its gyriform morphology: continuous cortex sign (circle in k). Associated small foci of solid enhancement (arrow in l). Also note absent T2-FLAIR mismatch sign in c-d and g-h.

between IDH-mutant grades 2-3 and 4 are vital for patient management, and 2. The application of the same imaging indicators across grades 2-3 and 4 may not yield accurate results for grade 4, which share imaging characteristics with glioblastomas (also grade 4). Indeed, the imaging of grade 4 IDH-mutant astrocytomas is hypothesized to fall somewhere between that of grade 2-3 IDH-mutant astrocytomas (with which they share IDH-mutation status) and IDH-wildtype glioblastomas (with which they share grade). Therefore, based on histological grade this tumor should present necrosis, restricted diffusion and elevated CBV often; while based on its IDH-mutation status should appear in patients below 55 years, being well-defined and nodular/oval in morphology. Furthermore, the presence of a T2-FLAIR mismatch has been recently described specific also for grade 4 IDH-mutant astrocytoma. Added to prior knowledge, this suggests that if a tumor with a T2-FLAIR mismatch exhibits necrosis, prominent enhancement, restricted diffusion, or elevated CBV, it should be highly indicative of an IDH-mutant astrocytoma grade 4^{65,66} (Fig. 7).

Regarding molecular grade 4 IDH-mutant astrocytomas (CDKN2A/B homozygous deletion), to the authors' knowledge there are not described imaging features that allow presurgical detection.^{2,25}

Oligodendroglioma, IDH-mutant 1P/19Q-codeleted

These tumors are uncommon in patients >55 years. ^{13,17,19,29} Approximately two-thirds of patients present with seizures as initial symptom. ^{13,67} Survival data for genetically defined

oligodendrogliomas (only since WHO 2016) are lacking, because prior registries are confounded by the inclusion of gliomas without IDH-mutation or 1p/19q-codeletion. However, overall, they are associated with favorable response to therapy and possibly the highest median survival, above 10 years. 68,69 There is also a tendency in radiological literature to treat grade 2-3 together.

Imaging

These tumors often demonstrate a predilection for the frontal lobes. They typically present as mass lesions centered in the cortex and subcortical white matter. Their cortical epicenter is characteristic and often marked by a typical continuous-cortex sign. This term refers to the involvement of the cortex in more than 50% of the tumor extension. Calcifications (best detected on CT) and cysts are commonly seen and can be distinctive. Hemorrhage is possible. These three features are infrequent for IDHmutant astrocytomas. Also, they typically exhibit prominent heterogeneity on T1w and T2w images, with indistinct tumor margins. They most often appear non-enhancing, but some do enhance, possibly more common in grade 3. Their morphology often follows a gyriform pattern along the cortex, instead of the nodular/rounded appearance of IDH-mutant astrocytomas. 4,23-27 Additionally, oligodendrogliomas exhibit more heterogeneous DWI and DSC-PWI patterns, possibly presenting areas of higher CBV and restricted diffusion, 34-36 and imaging-based grading is not reliable^{24,37} (Fig. 8).

In summary, radiologists should suspect an oligodendroglioma in young adults presenting with a near-frontal mass that exhibits heterogeneity on T1w and T2w calcifications or cysts, ill-defined borders, gyriform morphology and continuous cortex sign. Radiologists should also be cognizant of possible heterogeneity on DWI and DSC-PWI.

Some authors postulate that additional molecular testing should be considered for IDH-mutant gliomas with discordant neuroimaging and FISH results. For instance, if imaging is highly suggestive of oligodendroglioma and FISH is negative for 1p19q co-deletion, other techniques, such as chromosomal microarray analysis can act as a tiebreaker.⁷⁰

Finally, leptomeningeal spread is occasionally seen in patients with oligodendroglioma, particularly at recurrence.⁷¹

Diffuse midline glioma H3K27-altered and diffuse hemispheric glioma, H3 G34-mutant

These pediatric-type gliomas, which lack IDH-mutations, can occasionally present in younger adults. Consequently, in this age group, without IDH-mutations in immunohistochemistry and DNA-sequencing, radiologists must be attentive. They should promptly inform clinical colleagues when a tumor is midline located, because it becomes crucial to rule out a diffuse midline glioma H3K27-altered before classifying the tumor as a glioblastoma. Moreover, in cases of hemispheric tumors in the same patient subset, it is also important to consider H3.3G34R/V-mutant diffuse hemispheric gliomas, as recommended in the latest classification. 13,15 In the authors' experience, H3K27-altered midline diffuse gliomas in adults may manifest as classic brainstem gliomas, occasionally with certain atypical features, that serve as red flags, such as clear enhancement and DWI or DSC-PWI anomalies. Alternatively, these tumors can present in brainstem or other midline structures (thalamus) with clear aggressive features, including avid heterogenous enhancement, restricted diffusion, high CBV, necrosis and hemorrhage (Fig. 9). This latter presentation has been described to be more frequent when they have extended outside the strict midline.⁷²

Imaging descriptions and key-features of all documented tumors can be found in Table 2.

Additional considerations

A subset of gliomas occurs with multiple lesions, termed multifocal or multicentric. Multifocal gliomas demonstrate contiguous pathways of spread between foci, whereas multicentric are widely separated. Also, widespread intracerebral dissemination may be referred to as gliomatosis cerebri. These pattern can be seen in IDH-wildtype glioblastomas and IDH-mutant 1p/19q-codeleted oligodendrogliomas. ^{13,73}

The terms primary and secondary gliomas should be used cautiously in radiological context, given current knowledge. It is now understood that most grade 4 IDH-mutant astrocytomas are de novo, 13,64 and the presence of non-

enhancing tumor components may not necessarily indicate subjacent lower aggressiveness. Therefore, radiologists should categorize a glioma as secondary only when a prior lower-grade tumor is demonstrable. Simply put, radiologists should avoid labeling a glioma as secondary just because they observe high-grade-looking foci accompanied by low-grade-looking areas, unless there is further evidence to support it.

Clinical relevance of non-invasive presurgical diagnosis

As radiologists, we could encounter the question: "which is the importance of attempting to diagnose specific entities non-invasively if the definitive diagnosis is ultimately based on pathology?" This perspective minimizes the radiologist's role and misrepresents the reality in neuro-oncology units. Although at face value this statement might seem valid, it overlooks the vital role radiologists play in securing a definitive diagnosis efficiently and safely.

The first-line molecular biology testing typically involves immunohistochemistry and FISH due to their wide availability. However, DNA-sequencing is the preferred method for detecting non-canonical IDH-mutations and other genetic alterations involved in classification. Unfortunately, in many centers worldwide, DNA-sequencing is either costly or unavailable. This lack of access to DNA-sequencing in many centers underscores the pivotal role of the radiologist in guiding testing procedures. ^{13,18–21,70}

Early identification of specific molecular subtypes is becoming increasingly important. This aids in selecting optimal candidates for specific treatments or clinical trials that evaluate novel targeted therapies. For example, a recent study showcased the significant efficacy of IDH-targeted therapy in managing IDH-mutant astrocytomas.⁷⁵

Accurate non-invasive imaging diagnosis, especially in certain locations like the brain stem, corpus callosum, or basal ganglia, can help avoid aggressive diagnostic or treatment interventions. It is essential to identify early those tumors that may benefit from aggressive and rapid treatment, and those that might not. Ultimately, in exceptional situations, treatment could be initiated without a definitive diagnosis, an option considered in European guidelines.¹⁵

Also, detecting and correcting possible biopsy biases can significantly impact treatment strategies. For example, if a patient is diagnosed with a grade 2–3 tumor, but the radiologist clearly identifies necrosis suggesting a grade 4, the treatment approach must be more aggressive than if we assume that pathology is the only truth. It is important for radiologists to be aware and speak up in such situations.³¹

Finally, although often also inherently linked to specific tumor presurgical classifications, radiological descriptions encompass relevant prognostic information. For example, a present T2-FLAIR mismatch can indicate a more favorable prognosis, while the presence of necrosis, enhancement,

 Table 2
 Summary of imaging features of diffuse gliomas in adults. The """ in "Molecular IDH-wildtype glioblastoma" indicates this is not a specific WHO category, but a subgroup within IDH-wildtype glioblastomas that can appear with different imaging patterns.

Tumor subtype	Age group	Typical imaging	Key imaging
IDH-wildtype glioblastoma	>55	Ill-defined margins, expansive-infiltrative, heterogeneously enhancing. Hemorrage possible. Large edema and mass effect	Prominent enhancement and necrosis, restricted diffusion, high CBV
*Molecular IDH-wildtype glioblastoma	>55	Ill-defined, infiltrative, minimal or no-enhancement, absent necrosis, predominant unremarkable DWI and PWI	Gliomatosis cerebri and gyriform pattern, associated with EGFR and TERT
DH-wildtype, astrocytoma grade 2–3, NEC	>55	Ill-defined, infiltrative, minimal or no-enhancement, absent necrosis, predominant unremarkable DWI and PWI	Temporal. Ill defined margins, absent T2-FLAIR mismatch. Special attention to potential biopsy biases
DH-mutant, astrocytoma grade 2—3	<55	Well-defined, homogeneous, infiltrative, minimal or no-enhancement, round/oval morphology, predominant unremarkable DWI and PWI. Low edema	Frontal. Well defined, homogeneous, round/oval. T2-FLAIR mismatch highly specific
DH-mutant, astrocytoma grade 4	<55	Well-defined, infiltrative to expansive infiltrative, minimal to prominent enhancement, round/oval morphology	Any degree of clear nodular enhancement, necrosis, restricted diffusion or high CBV within a tumor with T2-FLAIR mismatch highly specific
DH-mutant 1P19Q codeleted, oligodendroglioma	<55	Ill-defined, T1- and T2- heterogeneous, infiltrative. Different degrees of enhancement. Possible heterogeneity on DWI and DSC-PWI	Calcifications or cysts, heterogeneity, gyriform morphology, centered and following the continous cortex sign
13K27-altered, diffuse midline glioma	<55	Brain stem or midline, well to ill-defined, infiltrative to expansive- infiltrative. Possible prominent enhancement, necrosis, restricted diffusion and high CBV	Brain stem or midline glioma with any sign of 'agressiveness': enhancement, necrosis, restricted diffusion and high CBV

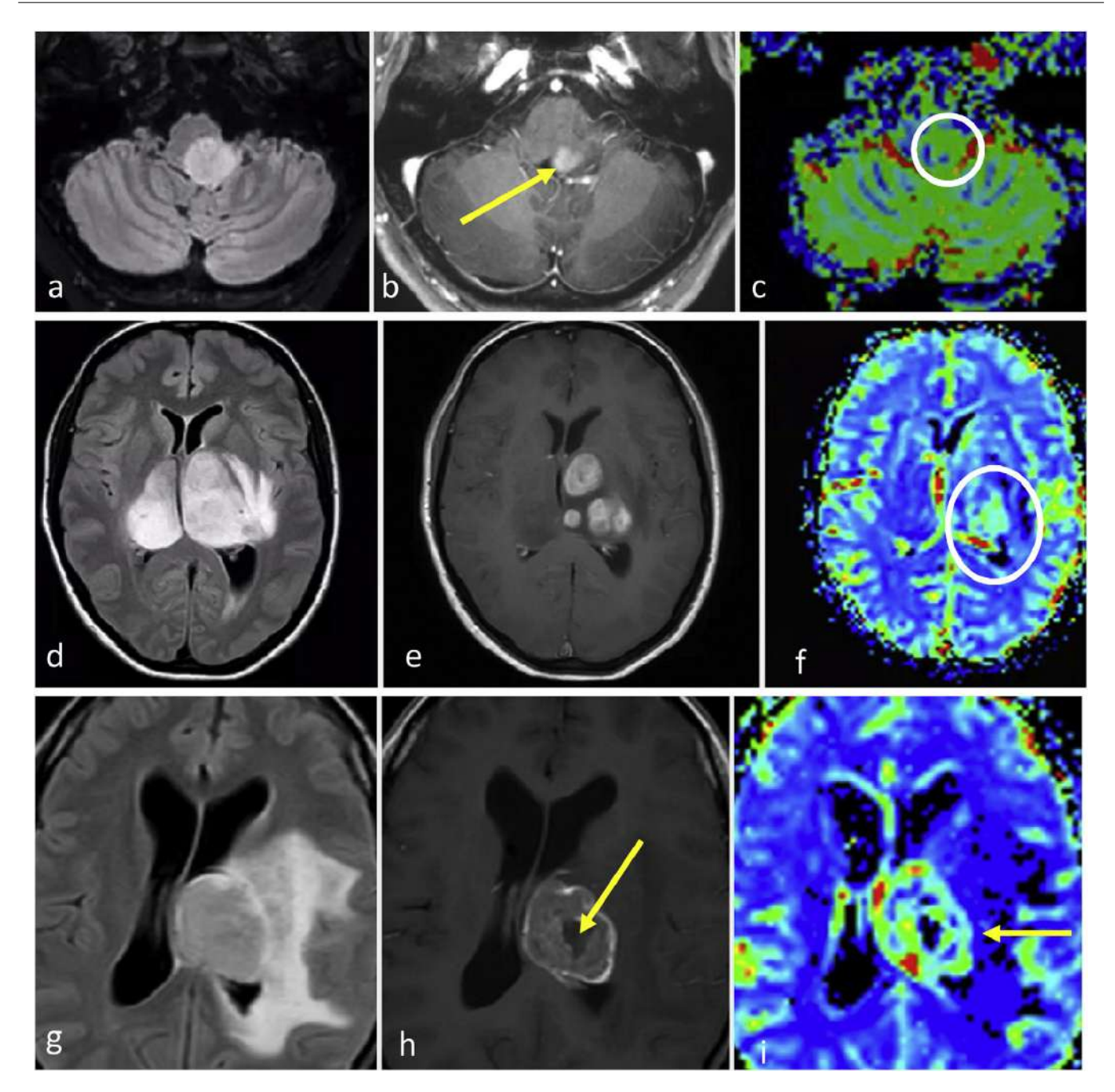


Figure 9 Diffuse mid-line gliomas H3K27-altered. a-c, 52-year-old patient. Axial FLAIR (a), T1w post-contrast (b), and CBV color map (c). Brain-stem glioma, slightly paramedian, nodular, and well-defined in FLAIR (a), with foci of enhancement (arrow in b) and slightly elevated CBV (circle in c). d-f, 48-year-old patient. Axial FLAIR (d), T1w post-contrast (e), and CBV color map (f). Bithalamic FLAIR hyperintense infiltrative mass (d) with multifocal solid nodular enhancements (e) and high CBV. G-i, 33-year-old patient. Axial FLAIR (g), T1w post-contrast (h), and CBV color map (i). Thalamic FLAIR hyperintense mass with extensive edema (g), irregular thick ring enhancement with central necrosis (arrow in h) and elevated CBV in the enhancing ring (arrow in i).

restricted diffusion, or elevated CBV usually implies less favorable outcomes. Radiologists should remain mindful of these prognostic indicators, recognizing that their significance goes beyond merely achieving an accurate non-invasive presurgical diagnosis aligned with the final pathology results.²³

Conclusions

Radiologists must have an in-depth understanding of the WHO classification, its strengths, and limitations, and recognize how radiology can contribute to ensuring optimal patient care.

This work highlights areas where further research is needed to optimize the role of radiology in the application of the WHO classification and its potential to improve patient outcomes

Finally, the authors wish to emphasize the pivotal role of radiology in optimally applying the WHO classification, and to express confidence in that future editions will incorporate radiology to a greater extent. Nonetheless, radiologists must be prepared to rise to such a responsibility.

Authorship

- 1 Responsible for study integrity: AP-E
- 2 Study conception: AP-E
- 3 Study design: AP-E
- 4 Data acquisition: AP-E
- 5 Data analysis and interpretation: AP-E
- 6 Statistical processing: NA
- 7 Literature search: AP-E
- 8 Drafting of the manuscript: AP-E
- 9 Critical review of the manuscript with intellectually significant contributions: AP-E, CM, MS, LO
- 10 Approval of the final version: AP-E, CM, MS, LO

Funding

This study did not receive any funding.

Conflicts of interest

Marion Smits declares consultancy fees from Bracco and Speaker fees from GE Healthcare, AuntMinnie and Fondazione Internazionale Menarini (all paid to institution). Albert Pons-Escoda, Carles Majos and Laura Oleaga confirm that they have no conflicts of interest to declare pertaining to this manuscript.

Acknowledgments

Albert Pons-Escoda and Carles Majos acknowledge support from the Instituto de Salud Carlos III (Proyectos de Investigación en Salud, PI20/00360).

References

- Johnson DR, Giannini C, Vaubel RA, Morris JM, Eckel LJ, Kaufmann TJ, et al. A radiologist's guide to the 2021 WHO central nervous system tumor classification: part I—key concepts and the spectrum of diffuse gliomas. Radiology. 2022;304:494–508, http://dx.doi.org/10.1148/radiol.213063.
- Osborn AG, Louis DN, Poussaint TY, Linscott LL, Salzman KL. The 2021 World Health Organization classification of tumors of the central nervous system: what neuroradiologists need to know. Am J Neuroradiol. 2022;43:928-37, http://dx.doi.org/10.3174/ajnr.A7462.
- Park YW, Vollmuth P, Foltyn-Dumitru M, Sahm F, Ahn SS, Chang JH, et al. The 2021 WHO classification for gliomas and implications on imaging diagnosis: part 1—key points of the fifth edition and summary of imaging findings on adulttype diffuse gliomas. J Magn Reson Imaging. 2023;58:677–89, http://dx.doi.org/10.1002/jmri.28743.

- 4. Zhou H, Vallières M, Bai HX, Su C, Tang H, Oldridge D, et al. MRI features predict survival and molecular markers in diffuse lower-grade gliomas. Neuro Oncol. 2017;19:862–70, http://dx.doi.org/10.1093/neuonc/now256.
- Ellingson BM, Bendszus M, Boxerman J, Barboriak D, Erickson BJ, Smits M, et al. Consensus recommendations for a standardized Brain Tumor Imaging Protocol in clinical trials. Neuro Oncol. 2015;17:1188–98, http://dx.doi.org/10.1093/neuonc/ nov095.
- Pons-Escoda A, Smits M. Dynamic-susceptibility-contrast perfusion-weighted-imaging (DSC-PWI) in brain tumors: a brief up-to-date overview for clinical neuroradiologists. Eur Radiol. 2023;33:8026–30, http://dx.doi.org/10. 1007/s00330-023-09729-3.
- Boxerman JL, Quarles CC, Hu LS, Erickson BJ, Gerstner ER, Smits M, et al. Consensus recommendations for a dynamic susceptibility contrast MRI protocol for use in high-grade gliomas. Neuro Oncol. 2020;22:1262-75, http://dx.doi.org/10.1093/neuonc/noaa141.
- Louis DN, Ohgaki H, Wiestler OD, Cavenee WK, Burger PC, Jouvet A, et al. The 2007 WHO Classification of tumours of the central nervous system. Acta Neuropathol. 2007;114:97–109, http://dx.doi.org/10.1007/s00401-007-0243-4.
- Lai A, Kharbanda S, Pope WB, Tran A, Solis OE, Peale F, et al. Evidence for sequenced molecular evolution of IDH1 mutant glioblastoma from a distinct cell of origin. J Clin Oncol. 2011;29:4482–90, http://dx.doi.org/10.1200/JCO.2010.33.8715.
- Kros JM, Gorlia T, Kouwenhoven MC, Zheng PP, Collins VP, Figarella-Branger D, et al. Panel review of anaplastic oligodendroglioma from European Organization for Research and Treatment of Cancer trial 26951. J Neuropathol Exp Neurol. 2007;66:545–51, http://dx.doi.org/10.1097/01.jnen.0000263869.84188.72.
- Louis DN, Perry A, Reifenberger G, von Deimling A, Figarella-Branger D, Cavenee WK, et al. The 2016 World Health Organization classification of tumors of the central nervous system: a summary. Acta Neuropathol. 2016;131:803–20, http://dx.doi.org/10.1007/s00401-016-1545-1.
- Gonzalez Castro LN, Wesseling P. The cIMPACT-NOW updates and their significance to current neuro-oncology practice. Neuro Oncol Pract. 2021;8:4–10, http://dx.doi.org/10.1093/nop/npaa055.
- WHO Classification of Tumours Editorial Board. Central nervous system tumours [Internet]. In: WHO classification of tumours series. 5th ed Lyon (France): International Agency for Research on Cancer; 2021 [cited 2023 Jul 13]. Available from: https://tumourclassification.iarc.who.int/chapters/45
- 14. Wang L, Shao L, Li H, Yao K, Duan Z, Zhi C, et al. Histone H3.3 G34-mutant diffuse gliomas in adults. Am J Surg Pathol. 2022;46:249–57, http://dx.doi.org/10.1097/PAS.000000000001781.
- 15. Weller M, van den Bent M, Preusser M, Le Rhun E, Tonn JC, Minniti G, et al. EANO guidelines on the diagnosis and treatment of diffuse gliomas of adulthood. Nat Rev Clin Oncol. 2021;18:170-86, http://dx.doi.org/10.1038/s41571-020-00447-z.
- Louis DN, Wesseling P, Paulus W, Giannini C, Batchelor TT, Cairncross JG, et al. cIMPACT-NOW update 1: Not Otherwise Specified (NOS) and Not Elsewhere Classified (NEC). Acta Neuropathol. 2018;135:481-4, http://dx.doi.org/10.1007/s00401-018-1808-0.
- Schaff LR, Mellinghoff IK. Glioblastoma and other primary brain malignancies in adults. JAMA. 2023;329:574, http://dx.doi.org/10.1001/jama.2023.0023.
- 18. Brat DJ, Verhaak RGW, Aldape KD, Yung WKA, Salama SR, Cooper LAD, et al. Comprehensive, integrative genomic analysis of dif-

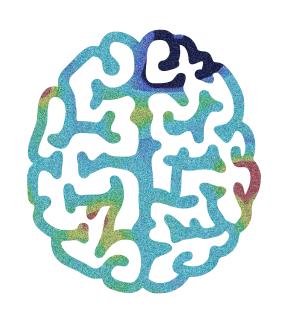
- fuse lower-grade gliomas. N Engl J Med. 2015;372:2481-98, http://dx.doi.org/10.1056/NEJMoa1402121.
- 19. Barresi V, Eccher A, Simbolo M, Cappellini R, Ricciardi GK, Calabria F, et al. Diffuse gliomas in patients aged 55 years or over: a suggestion for IDH mutation testing. Neuropathology. 2020;40:68–74, http://dx.doi.org/10.1111/neup.12608.
- 20. Tanboon J, Williams EA, Louis DN. The diagnostic use of immunohistochemical surrogates for signature molecular genetic alterations in gliomas. J Neuropathol Exp Neurol. 2016;75:4–18, http://dx.doi.org/10.1093/jnen/nlv009.
- 21. Velázquez Vega JE, Brat DJ. Incorporating advances in molecular pathology into brain tumor diagnostics. Adv Anat Pathol. 2018;25:143–71, http://dx.doi.org/10.1097/PAP.0000000000000186.
- 22. Badve C, Kanekar S. Radiogenomics of gliomas. Radiol Clin North Am. 2021;59:441–55, http://dx.doi.org/10.1016/j.rcl.2021.02.002.
- 23. Kamble AN, Agrawal NK, Koundal S, Bhargava S, Kamble AN, Joyner DA, et al. Imaging-based stratification of adult gliomas prognosticates survival and correlates with the 2021 WHO classification. Neuroradiology. 2023;65:41–54, http://dx.doi.org/10.1007/s00234-022-03015-7.
- 24. Joyner DA, Garrett J, Batchala PP, Rama B, Ravicz JR, Patrie JT, et al. MRI features predict tumor grade in isocitrate dehydrogenase (IDH)-mutant astrocytoma and oligodendroglioma. Neuroradiology. 2023;65:121-9, http://dx.doi.org/10.1007/s00234-022-03038-0.
- 25. Lasocki A, Buckland ME, Molinaro T, Xie J, Whittle JR, Wei H, et al. Correlating MRI features with additional genetic markers and patient survival in histological grade 2–3 IDH-mutant astrocytomas. Neuroradiology. 2023;65:1215–23, http://dx.doi.org/10.1007/s00234-023-03175-0.
- 26. Lasocki A, Buckland ME, Drummond KJ, Wei H, Xie J, Christie M, et al. Conventional MRI features can predict the molecular subtype of adult grade 2–3 intracranial diffuse gliomas. Neuroradiology. 2022;64:2295–305, http://dx.doi.org/10.1007/s00234-022-02975-0.
- 27. Park YW, Han K, Ahn SS, Bae S, Choi YS, Chang JH, et al. Prediction of IDH1-mutation and 1p/19q-codeletion status using preoperative MR imaging phenotypes in lower grade gliomas. Am J Neuroradiol. 2018;39:37-42, http://dx.doi.org/10.3174/ajnr.A5421.
- 28. Zhao K, Sun G, Wang Q, Xue Z, Liu G, Xia Y, et al. The diagnostic value of conventional MRI and CT features in the identification of the IDH1-mutant and 1p/19q co-deletion in WHO grade II gliomas. Acad Radiol. 2021;28:e189–98, http://dx.doi.org/10.1016/j.acra.2020.03.008.
- Robinson C, Kleinschmidt-DeMasters BK. IDH1-mutation in diffuse gliomas in persons age 55 years and over. J Neuropathol Exp Neurol. 2017;76:nlw112, http://dx.doi.org/10.1093/jnen/nlw112.
- 30. Pope WB, Sayre J, Perlina A, Villablanca JP, Mischel PS, Cloughesy TF. MR imaging correlates of survival in patients with high-grade gliomas. AJNR Am J Neuroradiol. 2005;26:2466–74.
- 31. Lasocki A, Tsui A, Tacey MA, Drummond KJ, Field KM, Gaillard F. MRI grading versus histology: predicting survival of World Health Organization grade II–IV astrocytomas. Am J Neuroradiol. 2015;36:77–83, http://dx.doi.org/10.3174/ajnr.A4077.
- 32. Law M, Yang S, Wang H, Babb JS, Johnson G, Cha S, et al. Glioma grading: sensitivity, specificity, and predictive values of perfusion MR imaging and proton MR spectroscopic imaging compared with conventional MR imaging. AJNR Am J Neuroradiol. 2003;24:1989–98.
- 33. Boxerman JL, Schmainda KM, Weisskoff RM. Relative cerebral blood volume maps corrected for contrast agent extravasa-

- tion significantly correlate with glioma tumor grade, whereas uncorrected maps do not. AJNR Am J Neuroradiol. 2006;27: 859–67.
- 34. Yang X, Xing Z, She D, Lin Y, Zhang H, Su Y, et al. Grading of IDH-mutant astrocytoma using diffusion, susceptibility and perfusion-weighted imaging. BMC Med Imaging. 2022;22:105, http://dx.doi.org/10.1186/s12880-022-00832-3.
- 35. Hirschler L, Sollmann N, Schmitz-Abecassis B, Pinto J, Arzanforoosh F, Barkhof F, et al. Advanced MR techniques for preoperative glioma characterization: part 1. J Magn Reson Imaging. 2023;57:1655-75, http://dx.doi.org/10.1002/jmri. 28662.
- 36. Villanueva-Meyer JE, Wood MD, Choi BS, Mabray MC, Butowski NA, Tihan T, et al. MRI features and IDH mutational status of grade II diffuse gliomas: impact on diagnosis and prognosis. Am J Roentgenol. 2018;210:621–8, http://dx.doi.org/10.2214/AJR.17.18457.
- Khalid L, Carone M, Dumrongpisutikul N, Intrapiromkul J, Bonekamp D, Barker PB, et al. Imaging characteristics of oligodendrogliomas that predict grade. Am J Neuroradiol. 2012;33:852-7, http://dx.doi.org/10.3174/ajnr.A2895.
- 38. Jain R, Johnson DR, Patel SH, Castillo M, Smits M, van den Bent MJ, et al. "Real world" use of a highly reliable imaging sign: "T2-FLAIR mismatch" for identification of IDH mutant astrocytomas. Neuro Oncol. 2020;22:936–43, http://dx.doi.org/10.1093/neuonc/noaa041.
- 39. Ostrom QT, Patil N, Cioffi G, Waite K, Kruchko C, Barnholtz-Sloan JS. CBTRUS statistical report: primary brain and other central nervous system tumors diagnosed in the United States in 2013–2017. Neuro Oncol. 2020;22:iv1–96, http://dx.doi.org/10.1093/neuonc/noaa200.
- Gilard V, Tebani A, Dabaj I, Laquerrière A, Fontanilles M, Derrey S, et al. Diagnosis and management of glioblastoma: a comprehensive perspective. J Pers Med. 2021;11:258, http://dx.doi.org/10.3390/jpm11040258.
- 41. Palmisciano P, Ferini G, Watanabe G, Ogasawara C, Lesha E, Bin-Alamer O, et al. Gliomas infiltrating the corpus callosum: a systematic review of the literature. Cancers (Basel). 2022;14:2507, http://dx.doi.org/10.3390/cancers 14102507.
- 42. Reifenberger G, Weber RG, Riehmer V, Kaulich K, Willscher E, Wirth H, et al. Molecular characterization of long-term survivors of glioblastoma using genome- and transcriptome-wide profiling. Int J Cancer. 2014;135:1822–31, http://dx.doi.org/10.1002/ijc.28836.
- 43. Weller M, Felsberg J, Hartmann C, Berger H, Steinbach JP, Schramm J, et al. Molecular predictors of progression-free and overall survival in patients with newly diagnosed glioblastoma: a prospective translational study of the German glioma network. J Clin Oncol. 2009;27:5743–50, http://dx.doi.org/10.1200/JCO.2009.23.0805.
- 44. Stoyanov GS, Petkova L, Dzhenkov DL. Hans Joachim Scherer and his impact on the diagnostic, clinical, and modern research aspects of glial tumors. Cureus. 2019;11:e6148, http://dx.doi.org/10.7759/cureus.6148.
- 45. Carrillo JA, Lai A, Nghiemphu PL, Kim HJ, Phillips HS, Kharbanda S, et al. Relationship between tumor enhancement, edema, IDH1 mutational status, MGMT promoter methylation, and survival in glioblastoma. Am J Neuroradiol. 2012;33:1349–55, http://dx.doi.org/10.3174/ajnr.A2950.
- 46. Lasocki A, Tsui A, Gaillard F, Tacey M, Drummond K, Stuckey S. Reliability of noncontrast-enhancing tumor as a biomarker of IDH1 mutation status in glioblastoma. J Clin Neurosci. 2017;39:170-5, http://dx.doi.org/10.1016/j.jocn.2017.01.007.

- 47. Salama GR, Heier LA, Patel P, Ramakrishna R, Magge R, Tsiouris AJ. Diffusion weighted/tensor imaging, functional mri and perfusion weighted imaging in glioblastoma—foundations and future. Front Neurol. 2018;8:660, http://dx.doi.org/10.3389/fneur.2017.00660.
- 48. Liesche-Starnecker F, Prokop G, Yakushev I, Preibisch C, Delbridge C, Meyer HS, et al. Visualizing cellularity and angiogenesis in newly-diagnosed glioblastoma with diffusion and perfusion MRI and FET-PET imaging. EJNMMI Res. 2021;11:72, http://dx.doi.org/10.1186/s13550-021-00817-3.
- Lee EJ, TerBrugge K, Mikulis D, Choi DS, Bae JM, Lee SK, et al. Diagnostic value of peritumoral minimum apparent diffusion coefficient for differentiation of glioblastoma multiforme from solitary metastatic lesions. Am J Roentgenol. 2011;196:71-6, http://dx.doi.org/10.2214/AJR.10.4752.
- Pons-Escoda A, Garcia-Ruiz A, Naval-Baudin P, Grussu F, Fernandez JJS, Simo AC, et al. Voxel-level analysis of normalized DSC-PWI time-intensity curves: a potential generalizable approach and its proof of concept in discriminating glioblastoma and metastasis. Eur Radiol. 2022;32:3705–15, http://dx.doi.org/10.1007/s00330-021-08498-1.
- 51. Blasel S, Jurcoane A, Franz K, Morawe G, Pellikan S, Hattingen E. Elevated peritumoural rCBV values as a mean to differentiate metastases from high-grade gliomas. Acta Neurochir (Wien). 2010;152:1893-9, http://dx.doi.org/10.1007/s00701-010-0774-7.
- Autry A, Phillips JJ, Maleschlijski S, Roy R, Molinaro AM, Chang SM, et al. Characterization of metabolic, diffusion, and perfusion properties in GBM: contrast-enhancing versus non-enhancing tumor. Transl Oncol. 2017;10:895–903, http://dx.doi.org/10.1016/j.tranon.2017.08.009.
- 53. Suh CH, Kim HS, Jung SC, Choi CG, Kim SJ. Clinically relevant imaging features for MGMT promoter methylation in multiple glioblastoma studies: a systematic review and meta-analysis. Am J Neuroradiol. 2018;39:1439–45, http://dx.doi.org/10.3174/ajnr.A5711.
- 54. Dono A, Wang E, Lopez-Rivera V, Ramesh AV, Tandon N, Ballester LY, et al. Molecular characteristics and clinical features of multifocal glioblastoma. J Neurooncol. 2020;148:389–97, http://dx.doi.org/10.1007/s11060-020-03539-z.
- 55. Izquierdo C, Barritault M, Poncet D, Cartalat S, Joubert B, Bruna J, et al. Radiological characteristics and natural history of adult IDH-wildtype astrocytomas with TERT promoter mutations. Neurosurgery. 2019;85:E448–56, http://dx.doi.org/10.1093/neuros/nyy513.
- 56. Mesny E, Barritault M, Izquierdo C, Poncet D, D'Hombres A, Guyotat J, et al. Gyriform infiltration as imaging biomarker for molecular glioblastomas. J Neurooncol. 2022;157:511–21, http://dx.doi.org/10.1007/s11060-022-03995-9.
- 57. Delfanti RL, Piccioni DE, Handwerker J, Bahrami N, Krishnan A, Karunamuni R, et al. Imaging correlates for the 2016 update on WHO classification of grade II/III gliomas: implications for IDH, 1p/19q and ATRX status. J Neurooncol. 2017;135:601-9, http://dx.doi.org/10.1007/s11060-017-2613-7.
- 58. Nishikawa T, Watanabe R, Kitano Y, Yamamichi A, Motomura K, Ohka F, et al. Reliability of IDH1-R132H and ATRX and/or p53 immunohistochemistry for molecular subclassification of Grade 2/3 gliomas. Brain Tumor Pathol. 2022;39:14–24, http://dx.doi.org/10.1007/s10014-021-00418-x.
- 59. Reuss DE, Mamatjan Y, Schrimpf D, Capper D, Hovestadt V, Kratz A, et al. IDH mutant diffuse and anaplastic astrocytomas have similar age at presentation and little difference in survival: a grading problem for WHO. Acta Neuropathol. 2015;129:867–73, http://dx.doi.org/10.1007/s00401-015-1438-8.
- 60. Stockhammer F, Misch M, Helms HJ, Lengler U, Prall F, von Deimling A, et al. IDH1/2 mutations in WHO

- grade II astrocytomas associated with localization and seizure as the initial symptom. Seizure. 2012;21:194-7, http://dx.doi.org/10.1016/j.seizure.2011.12.007.
- 61. Carstam L, Corell A, Smits A, Dénes A, Barchéus H, Modin K, et al. WHO grade loses its prognostic value in molecularly defined diffuse lower-grade gliomas. Front Oncol. 2022;11:803975, http://dx.doi.org/10.3389/fonc.2021.803975.
- 62. Aoki K, Nakamura H, Suzuki H, Matsuo K, Kataoka K, Shimamura T, et al. Prognostic relevance of genetic alterations in diffuse lower-grade gliomas. Neuro Oncol. 2018;20:66–77, http://dx.doi.org/10.1093/neuonc/nox132.
- 63. Hartmann C, Hentschel B, Simon M, Westphal M, Schackert G, Tonn JC, et al. Long-term survival in primary glioblastoma with versus without isocitrate dehydrogenase mutations. Clin Cancer Res. 2013;19:5146–57, http://dx.doi.org/10.1158/1078-0432.CCR-13-0017.
- 64. Korshunov A, Casalini B, Chavez L, Hielscher T, Sill M, Ryzhova M, et al. Integrated molecular characterization of IDH-mutant glioblastomas. Neuropathol Appl Neurobiol. 2019;45:108–18, http://dx.doi.org/10.1111/nan.12523.
- 65. Patel SH, Batchala PP, Muttikkal TJE, Ferrante SS, Patrie JT, Fadul CE, et al. Fluid attenuation in non-contrast-enhancing tumor (nCET): an MRI Marker for Isocitrate Dehydrogenase (IDH) mutation in Glioblastoma. J Neurooncol. 2021;152:523–31, http://dx.doi.org/10.1007/s11060-021-03720-y.
- 66. Lee MD, Patel SH, Mohan S, Akbari H, Bakas S, Nasrallah MP, et al. Association of partial T2-FLAIR mismatch sign and isocitrate dehydrogenase mutation in WHO grade 4 gliomas: results from the ReSPOND consortium. Neuroradiology. 2023;65:1343-52, http://dx.doi.org/10.1007/s00234-023-03196-9.
- 67. Buckner J, Giannini C, Eckel-Passow J, Lachance D, Parney I, Laack N, et al. Management of diffuse low-grade gliomas in adults use of molecular diagnostics. Nat Rev Neurol. 2017;13:340-51, http://dx.doi.org/10.1038/nrneurol.2017.54.
- 68. Tabouret E, Nguyen AT, Dehais C, Carpentier C, Ducray F, Idbaih A, et al. Prognostic impact of the 2016 WHO classification of diffuse gliomas in the French POLA cohort. Acta Neuropathol. 2016;132:625–34, http://dx.doi.org/10.1007/s00401-016-1611-8.
- 69. van den Bent MJ, Smits M, Kros JM, Chang SM. Diffuse infiltrating oligodendroglioma and astrocytoma. J Clin Oncol. 2017;35:2394-401, http://dx.doi.org/10.1200/JCO.2017.72.6737.
- 70. Patel SH, Batchala PP, Mrachek EKS, Lopes MBS, Schiff D, Fadul CE, et al. MRI and CT Identify Isocitrate Dehydrogenase (IDH)-mutant lower-grade gliomas misclassified to 1p/19q codeletion status with fluorescence in situ hybridization. Radiology. 2020;294:160-7, http://dx.doi.org/10.1148/radiol.2019191140.
- Andersen BM, Miranda C, Hatzoglou V, DeAngelis LM, Miller AM. Leptomeningeal metastases in glioma. Neurology. 2019;92:e2483-91, http://dx.doi.org/10.1212/WNL.0000000000007529.
- Zhao JP, Liu XJ, Lin HZ, Cui CX, Yue YJ, Gao S, et al. MRI comparative study of diffuse midline glioma, H3 K27altered and glioma in the midline without H3 K27-altered. BMC Neurol. 2022;22:498, http://dx.doi.org/10.1186/s12883-022-03026-0.
- Herrlinger U, Jones DTW, Glas M, Hattingen E, Gramatzki D, Stuplich M, et al. Gliomatosis cerebri: no evidence for a separate brain tumor entity. Acta Neuropathol. 2016;131:309–19, http://dx.doi.org/10.1007/s00401-015-1495-z.

- 74. Merenzon MA, Gómez Escalante JI, Prost D, Seoane E, Mazzon A, Bilbao ÉR. Preoperative imaging features: are they useful tools for predicting IDH1 mutation status in gliomas Grades II-IV? Surg Neurol Int. 2022;13:332, http://dx.doi.org/10.25259/SNI_373_2022.
- 75. Mellinghoff IK, van den Bent MJ, Blumenthal DT, Touat M, Peters KB, Clarke J, et al. Vorasidenib in IDH1- or IDH2-mutant low-grade glioma. N Engl J Med. 2023;389:589-601, http://dx.doi.org/10.1056/NEJMoa2304194.



2. HYPOTHESIS

2. HYPOTHESIS

DSC-PWI sequences allow differentiation, pre-surgically and noninvasively, between relevant tumor types and subtypes in adults.

DSC-PWI sequences contain significantly more diagnostic information than the primary CBV metric alone.

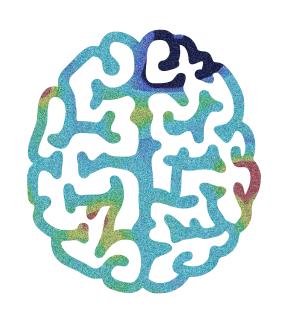
This additional information can be extracted through unsupervised analysis of time-intensity curves or by integrating multiple metrics (such as PSR and PH).

It is feasible and practical to develop a method for objective, quantitative, and visual analysis of DSC time-intensity curves.

Semi-automatic methods can be developed to extract this data, minimizing operator dependency and capturing tumor heterogeneity, in contrast to the current standard of manual region-of-interest selection for both tumor and normalization references.

Unsupervised analysis of voxel-wise information provides superior diagnostic accuracy compared to the standard single-metric (CBV) and single-value (mean/max) evaluation approach.

Incorporating additional DSC-PWI metrics — such as time-intensity curves, PSR, and PH — alongside CBV in a semi-automatic, unsupervised, and voxel-wise manner enhances the diagnostic capabilities of DSC-PWI sequences and enables the development of classifiers for pre-surgical brain tumor diagnosis that are useful in daily practice and have implications for patient management.



3. OBJECTIVES

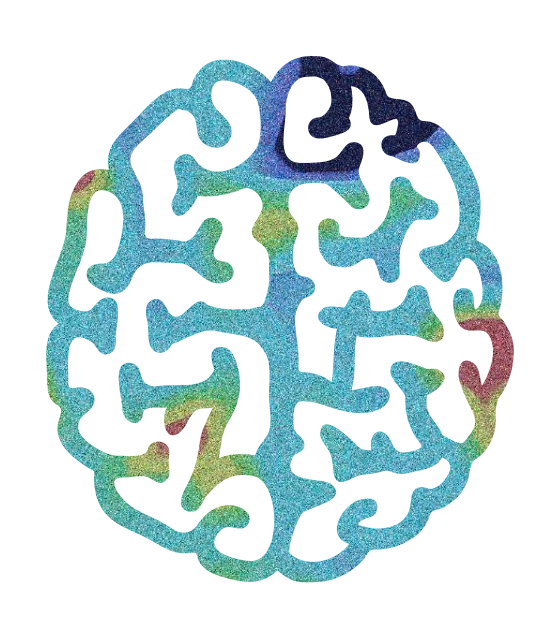
3. OBJECTIVES

Primary Objectives:

- To enhance the presurgical diagnostic accuracy of DSC-PWI sequences for brain tumor evaluation by incorporating a curvologic and multi-parametric approach.
- To differentiate between relevant tumor types and subtypes in adults presurgically and noninvasively, through improved DSC-PWI analysis methods.

Secondary Objectives:

- 1. To develop a feasible and practical framework for quantitative and visual analysis of DSC time-intensity curves that can be applied in routine clinical practice.
- To implement semi-automatic methods that minimize operator dependency in DSC-PWI analysis, allowing consistent data extraction and comprehensive tumor heterogeneity inclusion.
- 3. To apply curvologic and/or multi-parametric unsupervised and voxel-wise analysis for DSC-PWI that surpasses the diagnostic accuracy of standard single-metric (CBV) and single-value (mean/max) approaches.



4. MATERIAL, METHODS AND RESULTS

4. MATERIAL, METHODS AND RESULTS

This thesis was approved by the Research Ethics Committee of Hospital Universitari de Bellvitge under project number PR216/21.

This section comprises seven original research articles, presented in their published form and organized in the following order:

- Pons-Escoda A, Garcia-Ruiz A, Naval-Baudin P, Cos M, Vidal N, Plans G, Bruna J, Perez-Lopez R, Majos C. Presurgical Identification of Primary Central Nervous System Lymphoma with Normalized Time-Intensity Curve: A Pilot Study of a New Method to Analyze DSC-PWI. AJNR Am J Neuroradiol. 2020 Oct;41(10):1816-1824. doi: 10.3174/ajnr.A6761. Epub 2020 Sep 17. PMID: 32943424; PMCID: PMC7661072.
- 2. Pons-Escoda A, García-Ruíz A, Naval-Baudin P, Grussu F, Viveros M, Vidal N, Bruna J, Plans G, Cos M, Perez-Lopez R, Majós C. Diffuse Large B-Cell Epstein-Barr Virus-Positive Primary CNS Lymphoma in Non-AIDS Patients: High Diagnostic Accuracy of DSC Perfusion Metrics. AJNR Am J Neuroradiol. 2022 Nov;43(11):1567-1574. doi: 10.3174/ajnr.A7668. Epub 2022 Oct 6. PMID: 36202547; PMCID: PMC9731258.
- 3. Pons-Escoda A, Garcia-Ruiz A, Naval-Baudin P, Grussu F, Fernandez JJS, Simo AC, Sarro NV, Fernandez-Coello A, Bruna J, Cos M, Perez-Lopez R, Majos C. Voxel-level analysis of normalized DSC-PWI time-intensity curves: a potential generalizable approach and its proof of concept in discriminating glioblastoma and

metastasis. Eur Radiol. 2022 Jun;32(6):3705-3715. doi: 10.1007/s00330-021-08498-1. Epub 2022 Feb 1. PMID: 35103827.

- 4. Garcia-Ruiz A, Pons-Escoda A (co-first author), Grussu F, Naval-Baudin P, Monreal-Aguero C, Hermann G, Karunamuni R, Ligero M, Lopez-Rueda A, Oleaga L, Berbís MÁ, Cabrera-Zubizarreta A, Martin-Noguerol T, Luna A, Seibert TM, Majos C, Perez-Lopez R. An accessible deep learning tool for voxel-wise classification of brain malignancies from perfusion MRI. Cell Rep Med. 2024 Mar 19;5(3):101464. doi: 10.1016/j.xcrm.2024.101464. Epub 2024 Mar 11. PMID: 38471504; PMCID: PMC10983037.
- 5. Pons-Escoda A, Garcia-Ruiz A, Garcia-Hidalgo C, Gil-Solsona R, Naval-Baudin P, Martin-Noguerol T, Fernandez-Coello A, Flores-Casaperalta S, Fernandez-Viñas M, Gago-Ferrero P, Oleaga L, Perez-Lopez R, Majos C. MR dynamic-susceptibility-contrast perfusion metrics in the presurgical discrimination of adult solitary intra-axial cerebellar tumors. Eur Radiol. 2023 Dec;33(12):9120-9129. doi: 10.1007/s00330-023-09892-7. Epub 2023 Jul 13. PMID: 37439938.
- 6. Pons-Escoda A, Garcia-Ruiz A, Naval-Baudin P, Martinez-Zalacain I, Castell J, Camins A, Vidal N, Bruna J, Cos M, Perez-Lopez R, Oleaga L, Warnert E, Smits M, Majos C. Differentiating IDH-mutant astrocytomas and 1p19q-codeleted oligodendrogliomas using DSC-PWI: high performance through cerebral blood volume and percentage of signal recovery percentiles. Eur Radiol. 2024 Aug;34(8):5320-5330. doi: 10.1007/s00330-024-10611-z. Epub 2024 Jan 29. PMID: 38282078; PMCID: PMC11255054.

7. Pons-Escoda A, Naval-Baudin P, Viveros M, Flores-Casaperalta S, Martinez-Zalacaín I, Plans G, Vidal N, Cos M, Majos C. DSC-PWI presurgical differentiation of grade 4 astrocytoma and glioblastoma in young adults: rCBV percentile analysis across enhancing and non-enhancing regions. Neuroradiology. 2024 Aug;66(8):1267-1277. doi: 10.1007/s00234-024-03385-0. Epub 2024 Jun 5. PMID: 38834877; PMCID: PMC11246293.



This information is current as of January 9, 2025.

Presurgical Identification of Primary Central Nervous System Lymphoma with Normalized Time-Intensity Curve: A Pilot Study of a New Method to Analyze DSC-PWI

A. Pons-Escoda, A. Garcia-Ruiz, P. Naval-Baudin, M. Cos, N. Vidal, G. Plans, J. Bruna, R. Perez-Lopez and C. Majos

AJNR Am J Neuroradiol 2020, 41 (10) 1816-1824 doi: https://doi.org/10.3174/ajnr.A6761 http://www.ajnr.org/content/41/10/1816

Presurgical Identification of Primary Central Nervous System Lymphoma with Normalized Time-Intensity Curve: A Pilot Study of a New Method to Analyze DSC-PWI

🗓 A. Pons-Escoda, 🗓 A. Garcia-Ruiz, 🗓 P. Naval-Baudin, 🗓 M. Cos, 🗓 N. Vidal, 🗓 G. Plans, 🗓 J. Bruna, 🗓 R. Perez-Lopez, and



ABSTRACT

BACKGROUND AND PURPOSE: DSC-PWI has demonstrated promising results in the presurgical diagnosis of brain tumors. While most studies analyze specific parameters derived from time-intensity curves, very few have directly analyzed the whole curves. The aims of this study were the following: 1) to design a new method of postprocessing time-intensity curves, which renders normalized curves, and 2) to test its feasibility and performance on the diagnosis of primary central nervous system lymphoma.

MATERIALS AND METHODS: Diagnostic MR imaging of patients with histologically confirmed primary central nervous system lymphoma were retrospectively reviewed. Correlative cases of glioblastoma, anaplastic astrocytoma, metastasis, and meningioma, matched by date and number, were retrieved for comparison. Time-intensity curves of enhancing tumor and normal-appearing white matter were obtained for each case. Enhancing tumor curves were normalized relative to normal-appearing white matter. We performed pair-wise comparisons for primary central nervous system lymphoma against the other tumor type. The best discriminatory time points of the curves were obtained through a stepwise selection. Logistic binary regression was applied to obtain prediction models. The generated algorithms were applied in a test subset.

RESULTS: A total of 233 patients were included in the study: 47 primary central nervous system lymphomas, 48 glioblastomas, 39 anaplastic astrocytomas, 49 metastases, and 50 meningiomas. The classifiers satisfactorily performed all bilateral comparisons in the test subset (primary central nervous system lymphoma versus glioblastoma, area under the curve = 0.96 and accuracy = 93%; versus anaplastic astrocytoma, 0.83 and 71%; versus metastases, 0.95 and 93%; versus meningioma, 0.93 and 96%).

CONCLUSIONS: The proposed method for DSC-PWI time-intensity curve normalization renders comparable curves beyond technical and patient variability. Normalized time-intensity curves performed satisfactorily for the presurgical identification of primary central nervous system lymphoma.

ABBREVIATIONS: AUC = area under the curve; NAWM = normal-appearing white matter; nTIC = normalized time-intensity curve; MSID = maximal signal intensity drop; PCNSL = primary central nervous system lymphoma; PSR = percentage of signal recovery; TIC = time-intensity curve; CE-TIWI = contrastenhanced TIWI; TTA = time-to-arrival; rCBV = relative cerebral blood volume

he presurgical diagnosis of brain tumors is highly relevant to patient management. Although histopathology remains the

Received May 5, 2020; accepted after revision July 3.

From the Radiology Department (A.P.-E., P.N.-B., M.C., C.M.), Institut de Diagnòstic per la Imatge, Pathology Department (N.V.), Neurosurgery Department (G.P.), Neurology Department (J.B.), and Neurooncology Unit (A.P.-E., N.V., G.P., J.B., C.M.), Insitut Català d'Oncologia, Institut d'Investigació Biomèdica de Bellvitge, Hospital Universitari de Bellvitge, L'Hospitalet de Llobregat, Barcelona, Spain; and Radiomics Group (A.G.-R., R.P.-L.), Vall d'Hebron Institut d'Oncologia, Barcelona, Spain.

Please address correspondence to Albert Pons-Escoda, MD, Radiology Department, Institut de Diagnòstic per la Imatge (IDI), Hospital Universitari de Bellvitge. C/Feixa Llarga SN, L'Hospitalet de Llobregat, 08907, Barcelona, Spain; e-mail: albert.pons.idi @gencat.cat; @PonsEscoda

Indicates article with supplemental on-line tables.

Indicates article with supplemental on-line photo.

http://dx.doi.org/10.3174/ajnr.A6761

criterion standard, a presurgical suggestion of particular tumor types, such as primary central nervous system lymphoma (PCNSL) or metastasis, may greatly influence further procedures.1-4

MR imaging plays a pivotal role in the presurgical identification of brain tumors. Conventional MR imaging findings have been widely described; nevertheless, their performance is limited.⁵⁻¹¹ Given this limitation, an increasing number of studies have focused on monitoring physiologic and metabolic characteristics. In this sense, parameters derived from DSC-PWI have shown promising results in the diagnosis of brain tumors, and especially PCNSL. 12-20 DSC-PWI generates time-intensity curves (TICs) from dynamic monitoring of T2* signal intensity changes during contrast administration. Specific well-known parameters such as relative cerebral blood volume (rCBV) and percentage of signal recovery (PSR) are extracted from these TICs. Although visual evaluation of the entire TICs has been suggested by some authors, ²¹ to the best of our knowledge, there are no previous studies that have quantitatively evaluated the whole range of points that form the TIC altogether. This is probably because technical variability and patient physiologic characteristics hinder direct point-by-point comparisons. ²²⁻²⁴

Constructing normalized TICs (nTICs) would minimize the influence of physiologic and some technical parameters (especially regarding the timing of dynamics) on the TIC, offering interesting advantages: 1) It enables the possibility of performing a direct comparison of the entire nTIC between tumor types on a point-by-point basis, not limited to concrete parameters such as rCBV or PSR; and 2) it enhances the construction of user-friendly classifiers based on quantitative and visual comparison of particular cases to a data set of brain tumors.

The present article has 2 aims: first, to design an applicable method of processing TICs from DSC-PWI that allows obtaining normalized and comparable curves beyond technical and patient variability; and second, to test the applicability of this method by evaluating its diagnostic performance in a large series of patients with PCNSL.

MATERIALS AND METHODS

This article has been revised for publication by the research ethics committee of our tertiary hospital (Hospital Universitari de Bellvitge). The patient data were anonymized for this analysis. The confidential information of the patients was protected in accordance with national and European norms. Unspecific informed consent to participate in research projects was obtained from all patients. A waiver of a specific informed consent was provided by the ethics committee for this retrospective study.

Patients

Newly diagnosed patients with histologically confirmed PCNSL (2006–2019) were retrieved from our center database. Correlative cases by date and number, of glioblastoma, anaplastic astrocytoma, metastasis, and meningioma were retrieved from the same database for comparison.

Patients without PCNSL were selected to achieve the same number of patients with PCNSL, matched by year of acquisition. The rationale was to equalize the influence of technical differences of MR imaging sequences during such a long period (2006–2019) among tumor types. Inclusion criteria for the study were as follows: 1) confirmed tumor diagnosis by histology according to The World Health Organization 2007 or 2016 criteria, 2) an available diagnostic MR imaging examination including DSC-PWI and axial contrast-enhanced T1WI (CE-T1WI), 3) absence of previous oncospecific treatment at the time of the MR imaging examination, and 4) enhancing tumor on CE-T1WI with a shortest diameter of at least 10 mm. The flow diagram of study participants is shown in the On-line Figure.

Imaging

All the MR imaging examinations included in the study were acquired in the same tertiary hospital with 1 of 3 different scanners: Ingenia 3T with a 32-channel head coil, Ingenia or

Intera 1.5T with a 16-channel head coil (Philips Healthcare). Acquisition parameters for DSC-PWI sequences (all gradientecho) are summarized in On-line Tables 1 and 2. The intravenous contrast (gadobutrol; 1 mmol/mL, 0.1 mmol/kg) injection protocol was as follows: 18- or 20-ga peripheral intravenous access. No preload was performed. Baseline acquisition was on the order of 10 points. The start of the automatic injection (power injector at 4–5 mL/s) was by a manual setting. A final bolus of saline (25–50 mL) was injected at the same speed. The time and number of dynamics ranged from 1.26 to 3.55 seconds and 30 to 60, respectively.

The quality of the sequences was evaluated by visual inspection by 2 neuroradiologists (A.P.-E. and C.M.) with 5 years of experience in MR imaging of brain tumors. The examinations were labeled as poor quality and excluded from the study under the following circumstances: 1) artifacts prevented enhancing tumor segmentation on CE-T1WI or coregistration of CE-T1WI and DSC-PWI, or 2) an obvious low signal-to-noise ratio was observed in the raw TICs.

Postprocessing

Supervised semiautomatic volumetric segmentations (histogram thresholding and morphologic operations) of the enhancing tumor and normal-appearing white matter (NAWM) were performed on CE-T1WI and coregistered with DSC-PWI. Necrosis and nonenhancing components of the tumors were excluded from the segmentation. Semiautomatic volumetric segmentation of the whole enhancing lesion instead of partial, manual, or single-section ROI selection methods was chosen to minimize operator-dependency as well as to include all the intrinsic heterogeneity of the tumors in the analysis. 3D Slicer, Version 4.10 (http://www.slicer.org) was used for segmentation, 25 and the BRAINSFit module of 3D Slicer, for coregistering. 26

Two TICs for each case, 1 of the enhancing tumor and 1 of the NAWM, were obtained by averaging the TICs for all voxels within the segmented area. Baseline and the initial point of the descending curve were aligned. Signal intensity values (SI_i) of the enhancing tumor TIC were normalized by dividing by the maximal signal intensity drop (MSID) of the NAWM (SI_i/MSID_{NAWM}). Time values (T_i) were normalized as relative to the period of the descending curve on NAWM, which is the subtraction of time-to-peak (TTP) minus time-to-arrival (TTA) $[T_i / (TTP_{NAWM} - TTA_{NAWM})]$. We used TTP-TTA instead of TTP to normalize time values to avoid the potential human operator variability of TTA, mainly due to differences in the coordination between contrast infusion and sequence start. Finally, the same constant time points (0.2 TTP-TTA fractions from 0 to a total of 5, resulting in 26 constant time points) were extrapolated for all the curves (Fig 1). To detect the initial point of the descending curve necessary for alignment and TTA calculation, we calculated the average slope and SD of the 4 points before and after the MSID, and the first point where the curve slope became greater than the average minus the SD was established as the initial descending point.

The TICs were processed using Python 3.6 software (https://www.python.org/downloads/release/python-360/).

As a secondary subanalysis, to compare our method with conventional rCBV and PSR measures, we obtained mean rCBV and

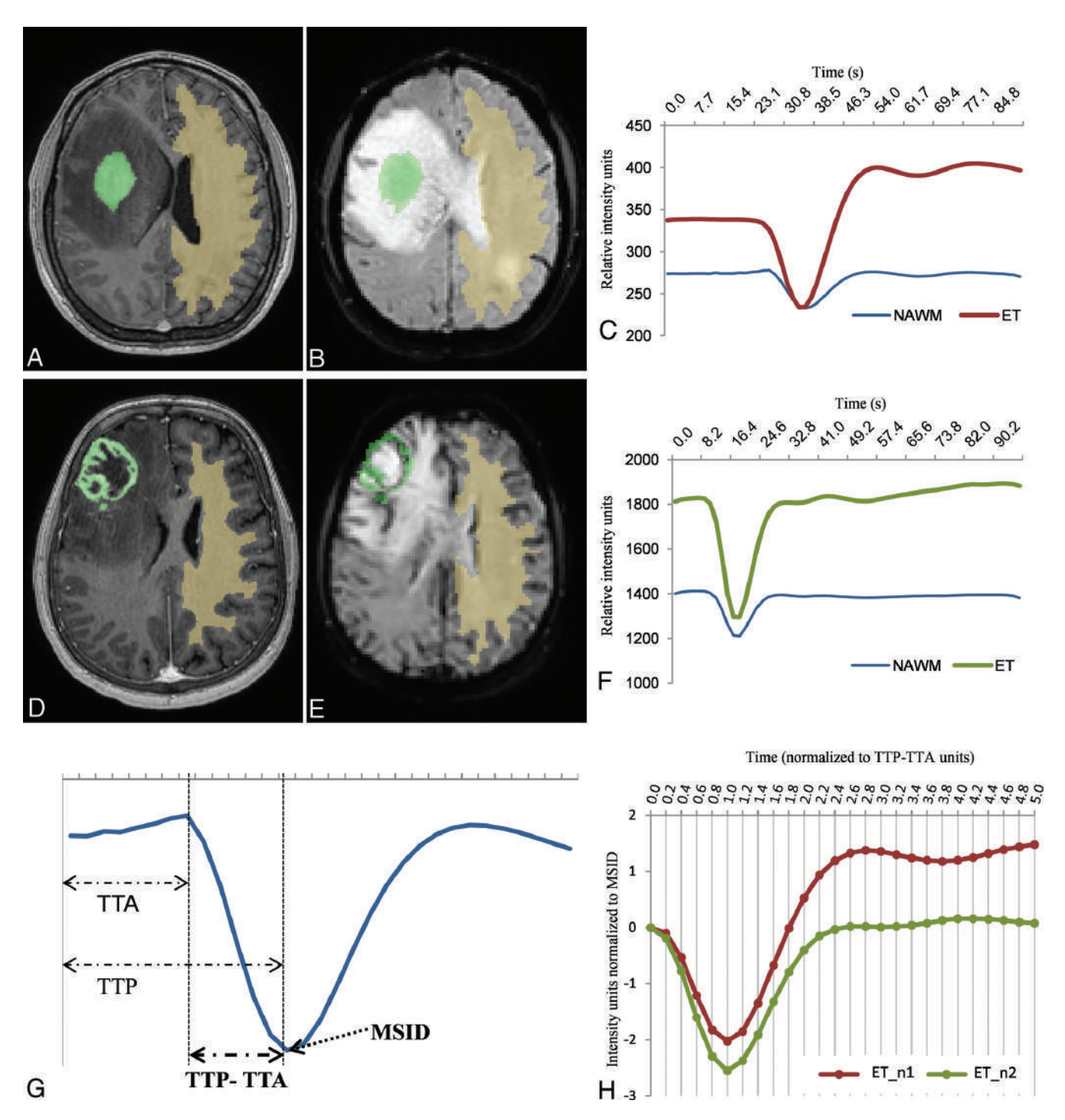


FIG 1. Solid (*A* and *B*) and necrotic (*D* and *E*) tumors and respective NAWM segmentations on axial CE-TIWI (*A* and *D*) and coregistered on DSC-PWI (*B* and *E*). Resultant raw curves by averaging the TIC for each voxel within the segmented areas (*C* and *F*), noncomparable due to differences in time, intensity, baseline, or initial point of the descending curve. Exemplification of the parameters used to normalize the curves, MSID, and TTP-TTA, relative to NAWM (*G*). Resultant normalized tumor curves, superimposable and comparable point by point (*H*). Curves with the exact same number of time-matching points and sharing common units of time (relative to TTP-TTA of the NAWM) and intensity (relative to MSID of the NAWM).

PSR values. rCBV was obtained with leakage correction²⁷ and normalized to the NAWM; PSR was obtained as described by Cha et al.²⁸ Both parameters were calculated using the same volumetric segmentation and coregistration as in the main analysis.

Statistics

The study sample was split into training (70%) and test (30%) subsets, which were balanced by the date of examination to

minimize the impact of quality and technical differences between TICs of the more distant-in-time examinations. For the statistical analysis, pair-wise comparisons between PCNSL and each of the other tumor types were made. First, a stepwise selection was run in the training set, which rendered the 5 best discriminatory points per comparison pair. Stepwise selection is an unsupervised automatic procedure for variable selection, which can be used in cases of a large number of potential explanatory variables but

with no underlying theory on which to base the model. Subsequently, predictive models were trained using logistic binary regression in each pair of the training set. Finally, the constructed classifiers based on the algorithms from the training set were applied to the test set.

All the statistical computations were performed with R statistical and computing software, Version 3.5.1 (http://www.r-project.org).²⁹

RESULTS

Patients

Fifty PCNSLs fulfilled the inclusion criteria and were included in the study. An additional 50 glioblastomas, 45 anaplastic astrocytomas, 50 metastases, and 50 meningiomas balanced with PCNSLs by date were included for comparison. The entire initial dataset included 245 patients (133 men; mean age, 59 years; range, 18–85 years). Demographics of the study sample are summarized in On-line Table 3.

Anaplastic astrocytoma was the only tumor type whose number of cases could not match the total of PCNSLs. Although the prevalence of anaplastic astrocytoma was higher than that of PCNSL, this was because only 45 cases fulfilled inclusion criterion number 4, "Enhancing tumor on CE-T1WI with a shortest diameter of at least 10 mm."

A total of 3 PCNSLs, 2 glioblastomas, 6 anaplastic astrocytomas, and 1 metastasis were ruled out by the quality filter. As a result, 47 PCNSLs, 48 glioblastomas, 39 anaplastic astrocytomas, 49 metastases, and 50 meningiomas were included in the final dataset (total n = 233). The patient dataset was split into training (70%) and test (30%) subsets balanced by the date of examination (training: 33 PCNSLs, 35 glioblastomas, 29 anaplastic astrocytomas, 36 metastases, and 36 meningiomas; test: 14 PCNSLs, 13 glioblastomas, 10 anaplastic astrocytomas, 13 metastases, and 14 meningiomas) (On-line Figure).

Normalized Curve Analysis and Pair-Wise Comparisons with PCNSL

Mean nTICs obtained from the training subset for each tumor type are shown in Fig 2. These mean curves are superimposable and comparable in a single graph due to the applied normalization method. This format provides a user-friendly tool for visual comparisons of nTICs. In this sense, notable differences were found between tumor-type nTICs on a first visual assessment, the most obvious around the MSID and the signal recovery segments. It is remarkable that all the curves in Fig 2 have the same number of time-matching points as well as sharing common units of time (relative to TTP-TTA of the NAWM) and intensity (relative to MSID of the NAWM). These features enable point-by-point absolute quantification of differences.

The 5 best discriminatory time points per pair of tumors achieved by stepwise selection are represented in Fig 2. The classifier algorithms, based on the logistic binary regression with the intercept and the relative power (coefficient) for each stepwise selected time point, are shown in On-line Tables 4 and 5.

Satisfactory results were obtained to enable segregating tumor types in all pair-wise comparisons in the training set. In summary, the area under the curve (AUC) values for all bilateral comparisons ranged between 0.86 (PCNSL versus anaplastic astrocytoma) and 1.00 (PCNSL versus meningioma), while the classification accuracies ranged between 74% (PCNSL versus anaplastic astrocytoma) and 97% (PCNSL versus meningioma). The same algorithms were applied to the test subset of tumors, confirming satisfactory classifications with AUC values between 0.83 (PCNSL versus anaplastic astrocytoma) and 0.96 (PCNSL versus glioblastoma) and accuracies between 71% (PCNSL versus anaplastic astrocytoma) and 96% (PCNSL versus meningioma) (Table).

The discriminating threshold of the constructed predictive model was set to zero to calculate the exposed results. Zero value corresponds to the point of maximum accuracy in binary logistic regressions. Nevertheless, this threshold can be easily modified, allowing the algorithm to be adapted to different clinical scenarios requiring specific sensitivity or specificity profiles.

Figures 3 and 4 are real clinical examples of the classifier user-friendly applicability. The nTIC curves of particular "problem" cases are overlapped on mean nTIC curves of each tumor type to visually assess similarities. The values after running the algorithm on the "problem" cases are depicted in a scatterplot to visually assess the likelihood of a particular diagnosis.

Regarding the rCBV and PSR subanalyses, the performance of these parameters is summarized in On-line Tables 6 and 7. In a general sense, mean rCBV and PSR showed inferior diagnostic performance to nTICs, with the only accuracies being slightly superior for PSR in PCNSL versus anaplastic astrocytoma and PCNSL versus metastasis in the test subgroups.

DISCUSSION

In this study, we have reported the design of an innovative method to obtain normalized TICs from DSC-PWI beyond patient and technical differences, which allows the following: 1) constructing mean curves for visual analysis, 2) performing point-by-point statistical comparisons between curves, and 3) building classifiers. We have tested its applicability in the presurgical identification of PCNSL and obtained satisfactory results.

DSC-PWI is an MR imaging technique that can be performed on most MR imaging units currently and provides noninvasive in vivo assessment of microvascular systems. It consists of a dynamic temporal acquisition during the vascular first pass of a contrast bolus. The injection of gadolinium results in an initial reduction in T2 signal intensity of tissues and subsequent signal recovery during contrast washout. TICs can be generated from this process. Well-studied parameters such as rCBV and PSR are extracted from these curves. The rCBV corresponds to the AUC, is usually measured relative to the NAWM, and has been related to histologic measurements of tumor vascularization. 22,24,30 The PSR is measured relative to the TIC baseline and may quantify the predominant T1 (signal recovery above baseline) or T2 (signal recovery below baseline) effects. These effects represent different leakage phenomena, which are explained by a complex combination of blood-brain barrier permeability, vascular volume fraction and vessel size, and tumor cell size and density. 22,30,31 The extraction of rCBV or PSR from TICs may represent an oversimplification of the information contained in the entire TIC. In fact, the curves have many other points that

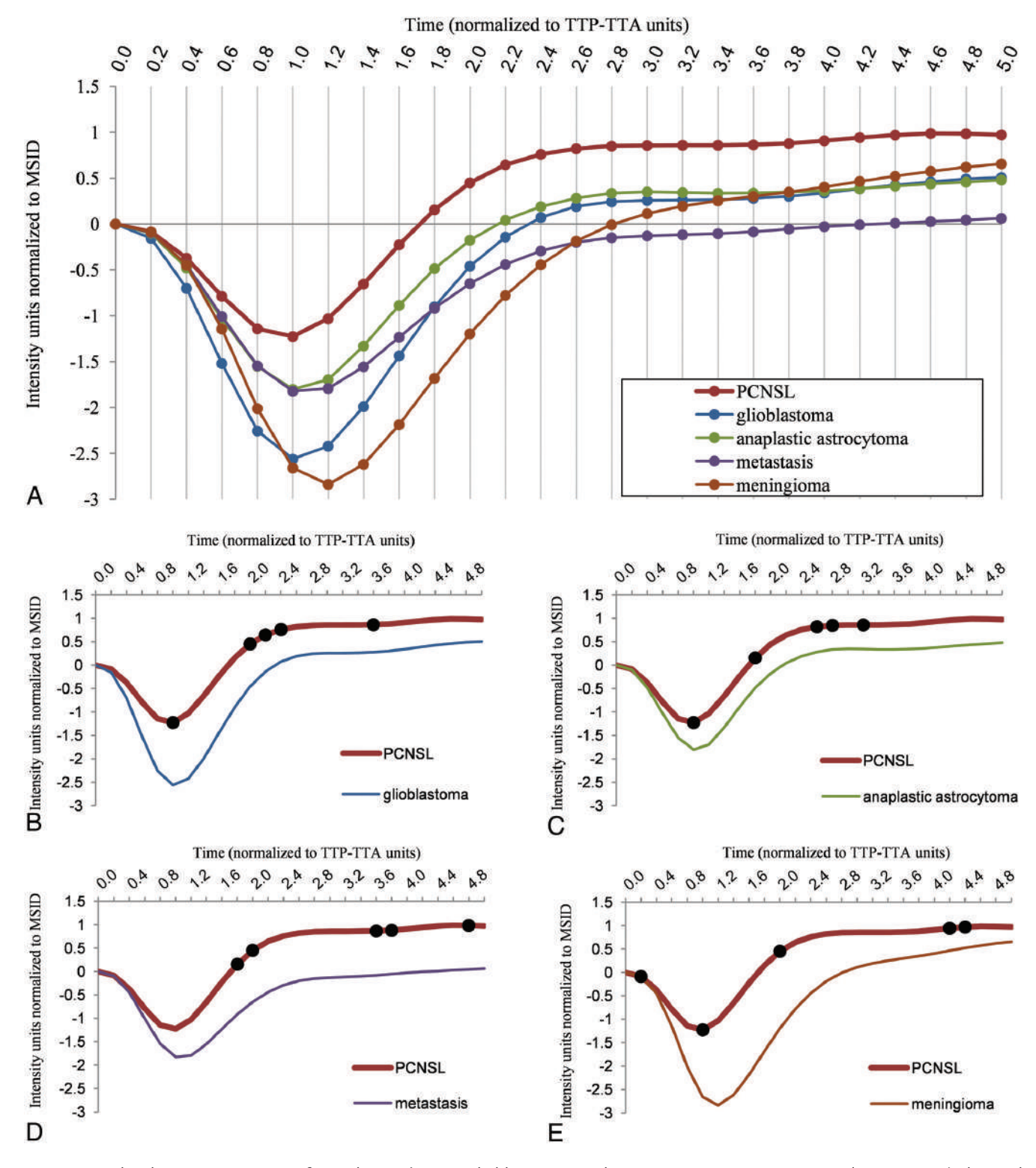


FIG 2. Normalized mean tumor curves for each type (PCNSL, glioblastoma, anaplastic astrocytoma, metastasis, and meningioma) obtained in the training subset (A). The curves are superimposable and comparable in a single graphic. This format provides a user-friendly tool for visual comparison of curves. Paired comparisons of normalized mean tumor curves for PCNSL against glioblastoma (B), anaplastic astrocytoma (C), metastasis (D), and meningioma (E), as well as representation of the 5 stepwise selected discriminatory TTP-TTA time points per pair (black dots).

remain excluded from these parameters. Along this line, some studies have suggested analyzing the whole curve to obtain improved information. Unfortunately, the proposed analysis was qualitative and limited to the visual pattern evaluation of the curve.²¹ Quantitative assessment of the entire curve has not been

accomplished to date, to our knowledge. This could be due to differences in the acquisition technique (including operator-dependency on some parameters) and patient physiologic features, which produce noncomparable TICs between different examinations or patients.^{22,23} For example, there may be differences in

the number and time of dynamics, in contrast injection start point and speed, or in patient heart rate preventing TICs from being comparable. 16,22-24

With these considerations in mind, we have developed a novel method for obtaining standardized, normalized, and comparable TICs independent of some technical and patient variability. We considered 2 parameters to be normalized to obtain comparable

Summary of the results in training and test subsets

	AUC	Accuracy	Sensitivity	Specificity
PCNSL vs GB				
Training	0.96	88% (60/68)	88% (29/33)	89% (31/35)
Test	0.96	93% (25/27)	93% (13/14)	92% (12/13)
PCNSL vs AA				
Training	0.86	74% (46/62)	76% (25/33)	72% (21/29)
Test	0.83	71% (17/24)	93% (13/14)	60% (6/10)
PCNSL vs MET				
Training	0.92	81% (56/69)	81% (26/32)	81% (30/37)
Test	0.95	93% (25/27)	100% (14/14)	85% (11/13)
PCNSL vs MEN				
Training	1.00	97% (67/69)	97% (32/33)	97% (35/36)
Test	0.93	96% (27/28)	100% (14/14)	93% (13/14)

Note:—GB indicates glioblastoma; AA, anaplastic astrocytoma; MET, metastasis; MEN, meningioma.

curves: time and intensity signal. Time was normalized as constant proportions of TTP-TTA from NAWM, and the time axis was re-dimensioned from seconds to fractions of 0.2 TTP-TTA units. Signal intensity was normalized to the MSID in NAWM. This normalization approach provided superimposable curves that could be visually analyzed and a list of point values that could be statistically compared among cases. Indeed, after normalization, mean curves for each tumor group could be constructed, allowing visual comparisons; the best discriminatory points with their optimal weighting for discrimination could be statistically determined, enabling the construction of classifiers; and particular cases could be displayed on scatterplots, providing visual representations of the likelihood of the diagnostic classification. Accordingly, we consider that this methodology could be further applied to construct user-friendly classifiers for the diagnosis of brain tumors. Examples of this potential application are shown in Figs 3 and 4.

We tested the performance of our method in the presurgical identification of PCNSL.

Reliable presurgical identification of PCNSL is vital because its management greatly differs from that of the other most prevalent enhancing brain tumors. ^{1-3,32} Maximal PCNSL resection is not recommended, and early stereotactic biopsy before

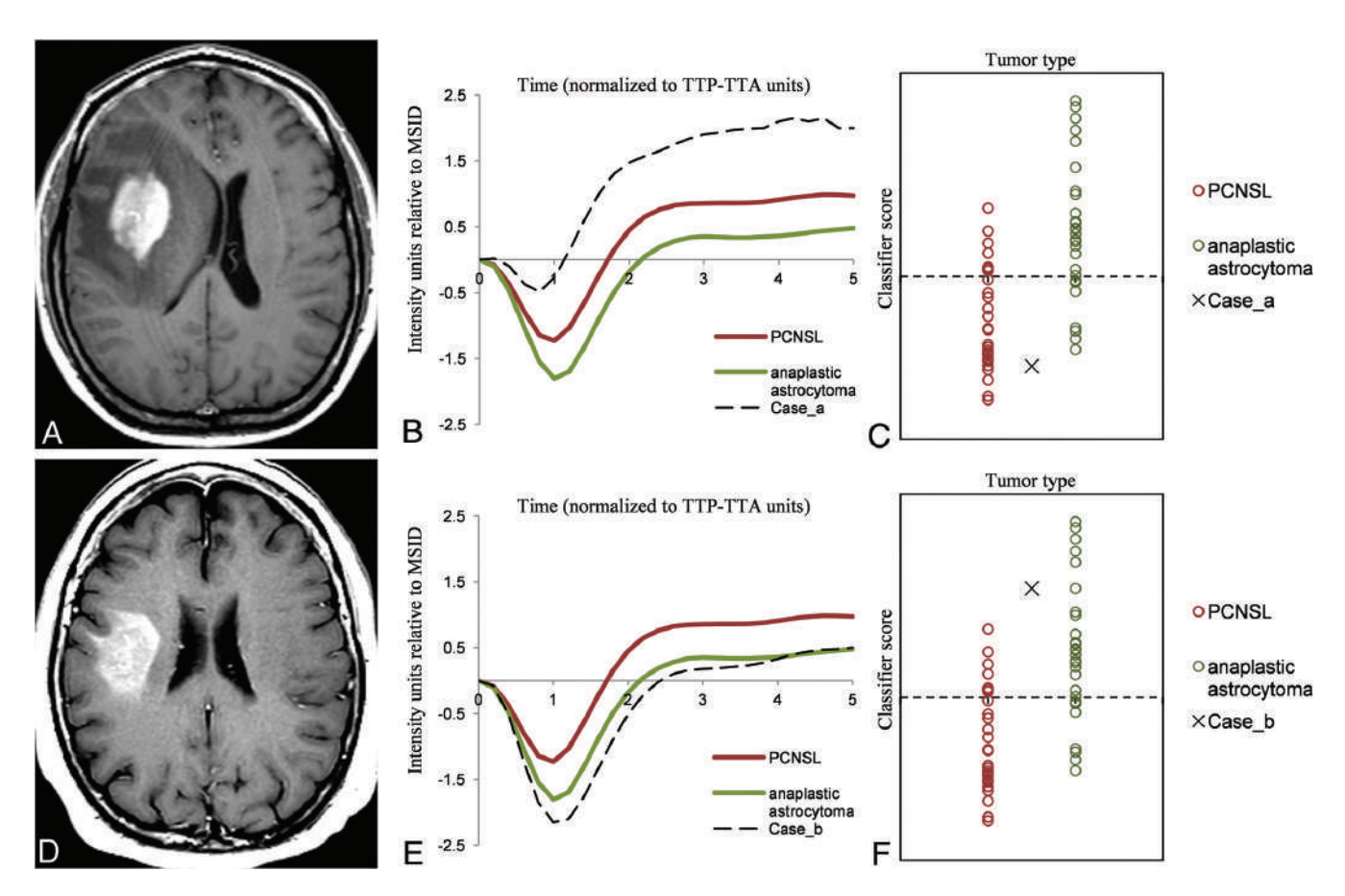


FIG 3. Example of clinical applicability on a "real" problem case. Axial CE-TIWI of 2 different patients (*A* and *D*) depicting 2 subcortical right frontal, solid enhancing tumors. PCNSL and anaplastic astrocytoma may be diagnostic possibilities to consider. Tumor normalized curves of each case overlapped to PCNSL, and anaplastic astrocytoma mean curves for visual assessment (*B* and *E*) show that the case in the upper row has similarities with PCNSL while in contrast, the case in the lower row has similarities with anaplastic astrocytoma. Representation of the classifier results on a scatterplot (*C* and *F*) demonstrates that the case in the upper row remains on the inferior side and may likely be a PCNSL, while the case in the lower row is more likely to be an anaplastic astrocytoma. We pathologically confirmed both diagnoses: case in the upper row, PCNSL; case in the lower row, anaplastic astrocytoma.

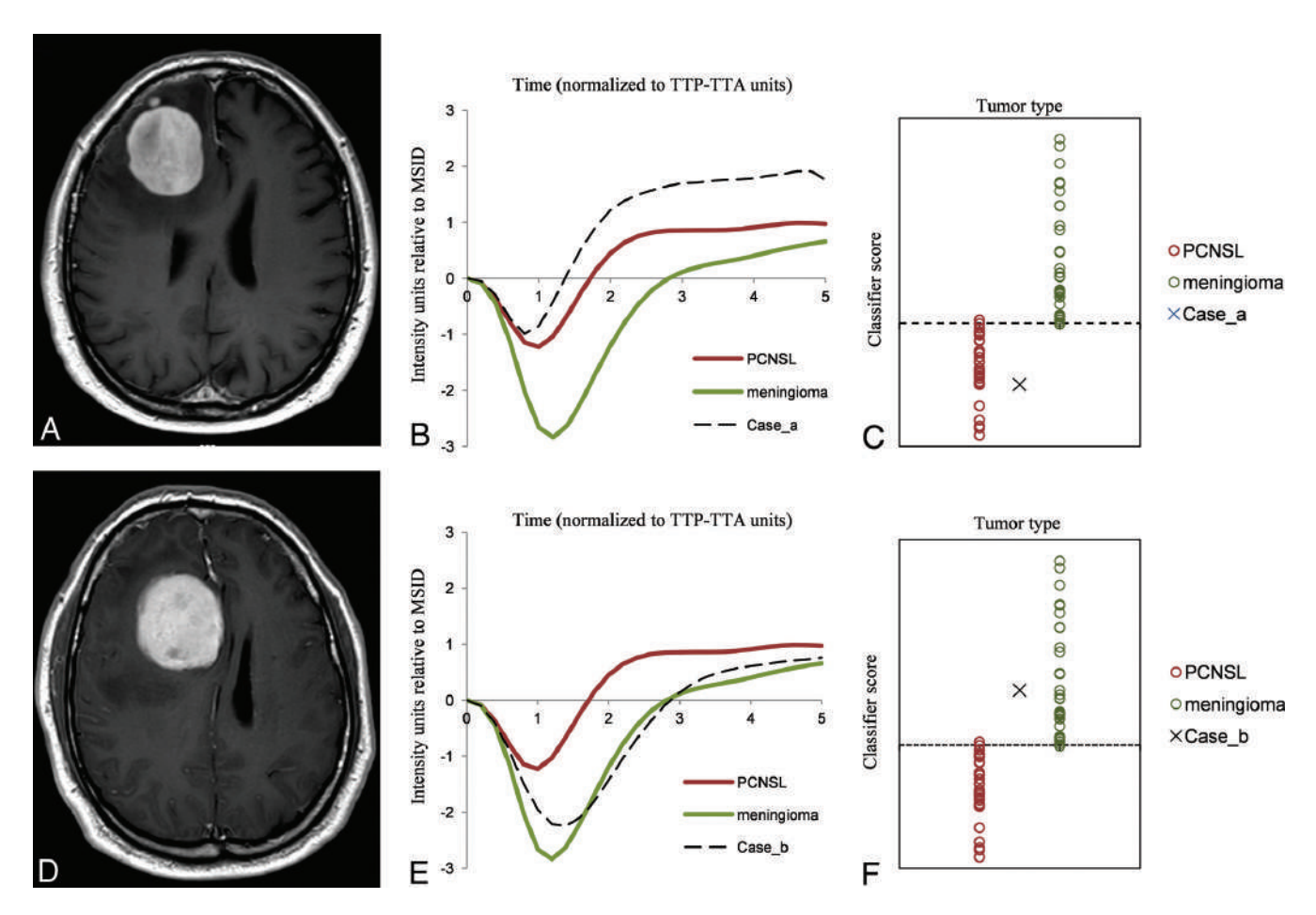


FIG 4. Example of clinical applicability on a "real" problem case. Axial CE-TIWI of 2 different patients with similar tumors (*A* and *D*): well defined, solid, avidly enhancing and right frontal peripherally located. PCNSL and meningioma were the 2 main diagnostic options considered. The tumor normalized curve of each case overlapping with PCNSL and meningioma mean curves (*B* and *E*) show that the case in the upper row is similar to PCNSL while the case in the lower row is close to meningioma. Representation of the classifier results on the scatterplot (*C* and *F*) suggests that the cases are likely to be PCNSL and meningioma, respectively. We pathologically confirmed both diagnoses: case in the upper row, PCNSL, case in the lower row, meningioma.

corticosteroid administration is mandatory when it is suspected from imaging.³²⁻³⁵ Conventional MR imaging in PCNSL has been widely analyzed and may be useful for guiding initial management.5-7 Nevertheless, these features may vary between patients and may overlap with other tumors. 8-11 Thus, radiologic diagnosis of PCNSL remains a challenge, and additional advanced imaging techniques such as DSC-PWI are increasingly being evaluated. Many articles have evaluated the potential of DSC-PWI for differentiating PCNSL from other tumors with excellent results. These studies focus on rCBV and PSR quantifications. Basically, PCNSL shows low rCBV and high PSR. 12-20 Some authors recently reported an additional parameter directly extracted from TICs termed "peak height," which has shown promising results. 12,15 However, the lack of technique standardization, which causes variability in the identification of the best discriminating parameter and its relevant thresholds between different studies, as well as the lack of a user-friendly way to depict the results, impedes the widespread clinical application of these perfusion parameters. 16,22-24

We obtained satisfactory accuracy values in the comparisons between PCNSL and glioblastoma, anaplastic astrocytoma, metastasis, and meningioma in the test subset. Accuracies ranged between 71% (versus anaplastic astrocytoma) and 96% (versus meningioma). Moreover, the performance of the new method is overall superior compared with the analysis of conventional rCBV or PSR measures in our dataset (On-line Tables 6 and 7). Visual differences between the standardized nTICs of the different tumors were noted, especially in the segments around the MSID and the return to baseline (Fig 2). Statistical analysis confirmed that the best discriminatory points were situated around those segments of the curves that may somehow be related to the traditional rCBV, peak height, and PSR, which can be evaluated on conventional raw TICs. Indeed, we hypothesize that our method evaluates a mixture of these known relevant values along with other potentially discriminatory and otherwise hidden values of the curve, all together in a single step. Additionally, the method enables a user-friendly representation of the results (Figs 3 and 4). For this, we used a pair-wise model that takes advantage of the radiologist's interaction by narrowing the most probable diagnoses. Then, the classifier is used as a support tool for diagnosis and not as an independent reader.

The variety of DSC pulse sequence parameters included in this retrospective study deserves special attention. Differences on these parameters (flip angle, TE, TR) affect the curve morphology and indeed seem to partially justify the variability in values and thresholds found in the literature regarding both rCBV and

PSR.³¹ In this sense, an overall predominantly high T1-weighting of the sequences in our study (On-line Table 1) seems to be carrying higher PSR values if compared with some prior studies.²⁰

Several limitations of our study must be considered. The single-site and retrospective character of the study may affect reproducibility. Nevertheless, the single-site origin may confer homogeneity that could be useful for this pilot study. At any rate, multicentric and prospective studies in new real clinical scenarios are needed for validation. The inclusion of a wide range of MR imaging examination dates and consequent technical differences may have affected the consistency of results. Some of them, such as the timing of dynamics or little heterogeneities in technical parameters, may be considered positive for the study by demonstrating the robustness of the method. Other parameters, such as variations in TE, TR, or flip angle, may be considered potentially confusing. In particular, higher T1-weighting of older sequences in our study may overestimate PSR values. 20,31 Balancing of cases between tumor types and training and test cohorts was an attempt to minimize its impact on the results. Finally, we did not stratify subtypes of tumors or DSC sequence parameters used to avoid excessive fragmentation of the dataset.

On the other hand, our study has several strong points. First, a large sample of PCNSL was included, which provides a robust method and very high accuracy rates despite heterogeneity. Second, a wide-but-logical differential diagnosis was considered in the comparisons, which emphasizes the clinical usefulness of the results. Third, there is the semiautomatization of the image segmentation and coregistration as well as the TIC processing, which minimized operator-dependency in favor of reproducibility. Last, the method allowed including all the nTIC point values in the analysis without supervision, which provides an objective approach to the classification process.

CONCLUSIONS

The novel proposed method of assessing DSC-PWI renders normalized point-by-point comparable TICs beyond technique and patient variability, enables the construction of classifiers that can be presented in user-friendly interfaces, and shows good performance when tested, with excellent results in the presurgical identification of PCNSL.

ACKNOWLEDGMENTS

We want to thank Marcel Vidal for assistance with statistics in an earlier version of the article.

Disclosures: Raquel Perez-Lopez—UNRELATED: Employment: Vall d'Hebron Institute of Oncology; Expert Testimony: Roche; Grants/Grants Pending: Astra Zeneca, CRIS Foundation, Prostate Cancer Foundation, FERO Foundation, Carlos III Research Institute*; Payment for Lectures Including Service on Speakers Bureaus: Roche. *Money paid to the institution.

REFERENCES

 Chiavazza C, Pellerino A, Ferrio F, et al. Primary CNS lymphomas: challenges in diagnosis and monitoring. Biomed Res Int 2018; 2018:3606970 CrossRef Medline

- 2. Altwairgi AK, Raja S, Manzoor M, et al. Management and treatment recommendations for World Health Organization grade III and IV gliomas. Int J Health Sci (Qassim) 2017;11:54–62 Medline
- Enrique GV, Irving SR, Ricardo BI, et al. Diagnosis and management of brain metastases: an updated review from a radiation oncology perspective. J Cancer Metastasis Treat 2019;5:54 CrossRef
- Euskirchen P, Peyre M. Management of meningioma. Presse Med 2018;47:e245–52 CrossRef Medline
- Tang YZ, Booth TC, Bhogal P, et al. Imaging of primary central nervous system lymphoma. Clin Radiol 2011;66:768–77 CrossRef Medline
- Giannini C, Dogan A, Salomão DR. et al. CNS lymphoma. J Neuropathol Exp Neurol 2014;73:478–94 CrossRef Medline
- Bühring U, Herrlinger U, Krings T, et al. MRI features of primary central nervous system lymphomas at presentation. Neurology 2001;57:393–96 CrossRef Medline
- Upadhyay N, Waldman AD. Conventional MRI evaluation of gliomas. Br J Radiol 2011;84:84 Spec No 2(Spec Iss 2);S107–11 CrossRef
- Fink K, Fink J. Imaging of brain metastases. Surg Neurol Int 2013;4:209 CrossRef
- Watts J, Box G, Galvin A, et al. Magnetic resonance imaging of meningiomas: a pictorial review. Insights Imaging 2014;5:113–22
 CrossRef Medline
- 11. Huang RY, Bi WL, Griffith B, et al; International Consortium on Meningiomas. Imaging and diagnostic advances for intracranial meningiomas. *Neuro Oncol* 2019;21:i44–61 CrossRef Medline
- 12. Lee MD, Baird GL, Bell LC, et al. Utility of percentage signal recovery and baseline signal in DSC-MRI optimized for relative CBV measurement for differentiating glioblastoma, lymphoma, metastasis, and meningioma. AJNR Am J Neuroradiol 2019;40:1145–50 CrossRef Medline
- 13. Xing Z, You RX, Li J, et al. Differentiation of primary central nervous system lymphomas from high-grade gliomas by rCBV and percentage of signal intensity recovery derived from dynamic susceptibility-weighted contrast-enhanced perfusion MR imaging. Clin Neuroradiol 2014;24:329–36 CrossRef Medline
- 14. Liang R, Li M, Wang X, et al. Role of rCBV values derived from dynamic susceptibility contrast-enhanced magnetic resonance imaging in differentiating CNS lymphoma from high grade glioma: a meta-analysis. Int J Clin Exp Med 2014;7:5573-77 Medline
- 15. Neska-Matuszewska M, Bladowska J, Saôsiadek M, et al. Differentiation of glioblastoma multiforme, metastases and primary central nervous system lymphomas using multiparametric perfusion and diffusion MR imaging of a tumor core and a peritumoral zone: searching for a practical approach. PLoS One 2018;13: e0191341 CrossRef Medline
- 16. Xu W, Wang Q, Shao A, et al. The performance of MR perfusion-weighted imaging for the differentiation of high-grade glioma from primary central nervous system lymphoma: a systematic review and meta-analysis. PLoS One 2017;12:e0173430 CrossRef Medline
- 17. Wang S, Kim S, Chawla S, et al. Differentiation between glioblastomas, solitary brain metastases, and primary cerebral lymphomas using diffusion tensor and dynamic susceptibility contrastenhanced MR imaging. AJNR Am J Neuroradiol 2011;32:507–14 CrossRef Medline
- 18. Lee IH, Kim ST, Kim HJ, et al. **Analysis of perfusion weighted image of CNS lymphoma.** *Eur J Radiol* 2010;76:48–51 CrossRef Medline
- Calli C, Kitis O, Yunten N, et al. Perfusion and diffusion MR imaging in enhancing malignant cerebral tumors. Eur J Radiol 2006; 58:394–403 CrossRef Medline
- 20. Mangla R, Kolar B, Zhu T, et al. Percentage signal recovery derived from MR dynamic susceptibility contrast imaging is useful to differentiate common enhancing malignant lesions of the brain. AJNR Am J Neuroradiol 2011;32:1004–10 CrossRef Medline
- 21. Chinchure S, Thomas B, Wangju S, et al. Mean intensity curve on dynamic contrast-enhanced susceptibility-weighted perfusion MR

- imaging: review of a new parameter to differentiate intracranial tumors. *J Neuroradiol* 2011;38:199–206 CrossRef Medline
- 22. Welker K, Boxerman J, Kalnin A, et al; American Society of Functional Neuroradiology MR Perfusion Standards and Practice Subcommittee of the ASFNR Clinical Practice Committee. ASFNR Recommendations for Clinical Performance of MR Dynamic Susceptibility Contrast Perfusion Imaging of the Brain. AJNR Am J Neuroradiol 2015;36:E41–51 CrossRef Medline
- 23. Willats L, Calamante F. The 39 steps: evading error and deciphering the secrets for accurate dynamic susceptibility contrast MRI. NMR Biomed 2013;26:913–31 CrossRef Medline
- Paulson ES, Schmainda KM. Comparison of dynamic susceptibilityweighted contrast-enhanced MR methods: recommendations for measuring relative cerebral blood volume in brain tumors. Radiology 2008;249:601–13 CrossRef Medline
- Fedorov A, Beichel R, Kalpathy-Cramer J, et al. 3D Slicer as an image computing platform for the Quantitative Imaging Network. Magn Reson Imaging 2012;30:1323–41 CrossRef Medline
- Johnson H, Harris G, Williams K. BRAINSFit: mutual information rigid registrations of whole-brain 3D images, using the insight toolkit. 2009. https://www.nitrc.org/docman/view.php/52/639/BRAINSFit. pdf. Accessed October 1, 2019
- 27. Hu LS, Baxter LC, Pinnaduwage DS, et al. Optimized preload leak-age-correction methods to improve the diagnostic accuracy of dynamic susceptibility-weighted contrast-enhanced perfusion MR imaging in posttreatment gliomas. AJNR Am J Neuroradiol 2010; 31:40–48 CrossRef Medline
- 28. Cha S, Lupo JM, Chen MH, et al. Differentiation of glioblastoma multiforme and single brain metastasis by peak height and

- percentage of signal intensity recovery derived from dynamic susceptibility-weighted contrast-enhanced perfusion MR imaging. *AJNR Am J Neuroradiol* 2007;28:1078–84 CrossRef Medline
- R Foundation. R: A language and environment for statistical computing. 2020. http://www.r-project.org/. Accessed October 15, 2019
- 30. Korfiatis P, Erickson B. **The basics of diffusion and perfusion imaging in brain tumors.** *Appl Radiol* 2014;43:22–29 Medline
- 31. Boxerman JL, Paulson ES, Prah MA, et al. The effect of pulse sequence parameters and contrast agent dose on percentage signal recovery in DSC-MRI: implications for clinical applications. AJNR Am J Neuroradiol 2013;34:1364–69 CrossRef Medline
- 32. Qian L, Tomuleasa C, Florian I-A, et al. **Advances in the treatment of newly diagnosed primary central nervous system lymphomas.** *Blood Res* 2017;52:159–66 CrossRef Medline
- 33. Hoang-Xuan K, Bessell E, Bromberg J, et al; European Association for Neuro-Oncology Task Force on Primary CNS Lymphoma. Diagnosis and treatment of primary CNS lymphoma in immunocompetent patients: guidelines from the European Association for Neuro-Oncology. Lancet Oncol 2015;16:e322-32 CrossRef Medline
- 34. Önder E, Arıkök AT, Önder S, et al. Corticosteroid pre-treated primary CNS lymphoma: a detailed analysis of stereotactic biopsy findings and consideration of interobserver variability. *Int J Clin Exp Pathol* 2015;8:7798–808 Medline
- Weller M, Martus P, Roth P, et al; German PCNSL Study Group.
 Surgery for primary CNS lymphoma? Challenging a paradigm.
 Neuro Oncol 2012;14:1481–84 CrossRef Medline



This information is current as of January 9, 2025.

Diffuse Large B-Cell Epstein-Barr Virus-Positive Primary CNS Lymphoma in Non-AIDS Patients: High Diagnostic Accuracy of DSC Perfusion Metrics

A. Pons-Escoda, A. García-Ruíz, P. Naval-Baudin, F. Grussu, M. Viveros, N. Vidal, J. Bruna, G. Plans, M. Cos, R. Perez-Lopez and C. Majós

AJNR Am J Neuroradiol 2022, 43 (11) 1567-1574 doi: https://doi.org/10.3174/ajnr.A7668 http://www.ajnr.org/content/43/11/1567

Diffuse Large B-Cell Epstein-Barr Virus—Positive Primary CNS Lymphoma in Non-AIDS Patients: High Diagnostic Accuracy of DSC Perfusion Metrics

DA. Pons-Escoda, DA. García-Ruíz, P. Naval-Baudin, F. Grussu, M. Viveros, N. Vidal, R. Perez-Lopez, and C. Majós

\equiv

ABSTRACT

BACKGROUND AND PURPOSE: Immunodeficiency-associated CNS lymphoma may occur in different clinical scenarios beyond AIDS. This subtype of CNS lymphoma is diffuse large B-cell and Epstein-Barr virus—positive. Its accurate presurgical diagnosis is often unfeasible because it appears as ring-enhancing lesions mimicking glioblastoma or metastasis. In this article, we describe clinicoradiologic features and test the performance of DSC-PWI metrics for presurgical identification.

MATERIALS AND METHODS: Patients without AIDS with histologically confirmed diffuse large B-cell Epstein-Barr virus—positive primary CNS lymphoma (December 2010 to January 2022) and diagnostic MR imaging without onco-specific treatment were retrospectively studied. Clinical, demographic, and conventional imaging data were reviewed. Previously published DSC-PWI time-intensity curve analysis methodology, to presurgically identify primary CNS lymphoma, was used in this particular lymphoma subtype and compared with a prior cohort of 33 patients with Epstein-Barr virus—negative CNS lymphoma, 35 with glioblastoma, and 36 with metastasis data. Normalized curves were analyzed and compared on a point-by-point basis, and previously published classifiers were tested. The standard percentage of signal recovery and CBV values were also evaluated.

RESULTS: Seven patients with Epstein-Barr virus—positive primary CNS lymphoma were included in the study. DSC-PWI normalized time-intensity curve analysis performed the best for presurgical identification of Epstein-Barr virus—positive CNS lymphoma (area under the receiver operating characteristic curve of 0.984 for glioblastoma and 0.898 for metastasis), followed by the percentage of signal recovery (0.833 and 0.873) and CBV (0.855 and 0.687).

CONCLUSIONS: When a necrotic tumor is found in a potentially immunocompromised host, neuroradiologists should consider Epstein-Barr virus-positive CNS lymphoma. DSC-PWI could be very useful for presurgical characterization, with especially strong performance of normalized time-intensity curves.

ABBREVIATIONS: AUC = area under the receiving operating characteristic curve; CE = contrast-enhanced; DLBC = diffuse large B-cell; EBV = Epstein-Barr virus; GE = gradient-echo; nTIC = normalized time-intensity curve; PCNSL = primary CNS lymphoma; PSR = percentage of signal recovery; rCBV = relative CBV; TIC = time-intensity curve; WHO = World Health Organization

Presurgical suspicion of CNS lymphoma is crucial for patient management. When it is suspected, initial corticosteroids

Received April 27, 2022; accepted after revision September 2.

From the Departments of Radiology (A.P.-E., P.N.-B., M.V., M.C., C.M.), Pathology (N.V.), and Neurosurgery (G.P.), Hospital Universitari de Bellvitge, Barcelona, Spain; Neurooncology Unit (A.P.-E., N.V., J.B., G.P., C.M.), Institut d'Investigació Biomèdica de Bellvitge-IDIBELL, Barcelona, Spain; Radiomics Group (A.G.-R., F.G., R.P.-L.), Vall d'Hebron Institut d'Oncologia, Barcelona, Spain; and Department of Radiology (R.P.-L.), Hospital Universitari Vall d'Hebron, Barcelona, Spain.

A.P.-E. and A.G.-R. are co-first authors of the manuscript. A.P.-E., P.N.-B., and C.M. created the experimental design. A.P.-E. led the investigation. A.P.-E. did the data collection. A.G.-R., F.G., and R.P.-L. led the data processing and statistical analysis in direct collaboration with A.P.-E., P.N.-B., and C.M. A.P.-E., P.N.-B., and C.M. wrote the manuscript and chose the best images. J.B. made important contributions to the final manuscript. A.P.-E. did the bibliographic research. M.V., M.C., N.V., G.P., and J.B. played an important role in imaging, patient data, or pathology sample acquisitions. All the authors have participated in the realization, review, and correction of the manuscript and its images, and all the authors have read and approved its submission to this journal.

should be avoided, and biopsy instead of surgical resection is recommended. $^{\!\!\!1,2}$

Conventional imaging features of CNS lymphoma are widely described,³⁻⁷ but they mainly refer to primary CNS lymphoma

This work was partially supported by a grant from the Instituto de Salud Carlos III (PI20/00360) to Carles Majós and Albert Pons-Escoda. Francesco Grussu has received funding from the postdoctoral fellowships program Beatriu de Pinós (2020 BP 00117), funded by the Secretary of Universities and Research (Government of Catalonia). Raquel Perez-Lopez is supported by a Prostate Cancer Foundation Young Investigator Award, CRIS Foundation Talent Award (TALENT-05), Fero Foundation, and the Instituto de Salud Carlos III.

Please address correspondence to Albert Pons-Escoda, MD, Radiology Department, Institut de Diagnòstic per la Imatge (IDI), Hospital Universitari de Bellvitge, C/Feixa Llarga SN, L'Hospitalet de Llobregat, 08907 Barcelona, Spain; e-mail: albert.pons.idi @gencat.cat: @PonsEscoda

Indicates article with online supplemental data.

http://dx.doi.org/10.3174/ajnr.A7668

(PCNSL), which specifically is Epstein-Barr virus (EBV)–negative and occurs in immunocompetent patients. However, less frequent subtypes of CNS lymphoma do not follow this imaging pattern. This is the case of immunodeficiency-associated CNS lymphoma, which usually appears as ring-enhancing lesions with central necrosis complicating accurate presurgical diagnosis. 9-14

The World Health Organization (WHO) Classification of Tumors of the CNS includes B-cell and EBV-positivity as essential criteria for immunodeficiency-associated CNS lymphoma. Diffuse large B-cell (DLBC) EBV positive^{8,15} lymphoma is considered a distinct immunobiologic entity and represents nearly 10% of all CNS lymphomas.¹⁶ In the scientific literature, DLBC EBV-positive CNS lymphoma is mainly described in the context of AIDS. However, while the AIDS incidence is decreasing, other causes of immunodeficiency are increasing. This is the case for iatrogenesis (treatment-induced immunosuppression) in the context of post-transplantation or for other causes such as autoimmune diseases, or even for other situations such as immunosenescence and chronic inflammation.¹⁷⁻²¹

DSC-PWI is a quantitative MR imaging technique that has shown promising results for presurgical identification of PCNSL. This tumor shows a characteristic time-intensity curve (TIC), which can be precisely evaluated with a new methodology that renders normalized TICs (nTICs)^{22,23} as well as by a lower relative CBV (rCBV) and a higher percentage of signal recovery (PSR) than glioblastoma or metastasis. ^{22,24-30} However, to the best of our knowledge, there is very little literature regarding DSC-PWI features specific to DLBC EBV-positive CNS lymphoma. ¹⁰

In summary, DLBC EBV-positive CNS lymphoma constitutes a unique clinical immunobiologic entity with particular imaging features that challenge its presurgical diagnosis. Conventional imaging is usually misleading, and comprehensive analysis of the full potential of DSC-PWI in this scenario is lacking.

In this article, the clinical and radiologic features of a homogeneous data set of patients with DLBC EBV-positive CNS lymphoma without AIDS are comprehensively described. The main objective of the study was to test the performance of DSC-PWI metrics (nTIC, PSR, CBV) for the presurgical differentiation of this entity from glioblastoma and metastasis.

MATERIALS AND METHODS

The research ethics committee of the Hospital Universitari de Bellvitge tertiary center approved this retrospective study and issued a waiver for a specific informed consent. Patient data were protected and anonymized in accordance with European Union General Data Protection Regulation legislation.

Patients

Records of patients with confirmed primary DLBC EBV-positive CNS lymphoma (December 2010 to January 2022) were retrieved from our center's database. Inclusion criteria were the following: 1) confirmed tumor diagnosis by histology (2016 WHO lymphoid neoplasm¹⁵ and 2021 WHO CNS tumor⁸ classification); 2) extension study without evidence of systemic lymphoma; and 3) available diagnostic MR imaging examination without onco-specific treatment.

Relevant clinical and demographic data were retrieved from the hospital records, including age, sex, underlying conditions, radiologic diagnosis, histopathologic diagnosis, and initial diagnostic-therapeutic patient management.

For comparison of the obtained perfusion metrics, we retrieved DSC-PWI data from previously published²² cases of EBV-negative PCNSL, glioblastoma, and metastasis, which are balanced by technique and demographic characteristics, as well as quality-filtered.

Imaging

The MR images included in the study were acquired in a single center with 1 of 2 scanners, either an Ingenia 1.5T or an Intera 1.5T (Philips Healthcare), both using a 16-channel head coil. MR imaging examinations included T1WI, contrast-enhanced (CE) T1WI, TSE-T2WI, gradient-echo (GE) T2*WI, DWI, and DSC-PWI.

Conventional Imaging. Two experienced neuroradiologists from our tertiary reference center neuro-oncology unit, A.P.-E. and C.M., with >8 and 25 years of experience in neuro-oncologic radiology, respectively, visually assessed T1WI, CE-T1WI, TSE-T2WI, GE-T2*WI, and DWI sequences. The assessment was done independently and included the number of lesions, location, ring enhancement, TSE-T2WI signal intensity, GE-T2*WI hemorrhagic components, and diffusion restriction. Discrepancies were resolved by consensus.

Perfusion Imaging Acquisition. Two GE DSC-PWI sequences were used. The first (2 cases) included 40 dynamic volumes with a temporal resolution of 1.9 seconds with the following parameters: flip angle = 7° , TE = 25–30 ms, TR = 16–20 ms, in-plane resolution = 1.72 mm, and section-thickness = 1.5 mm. The second (5 cases) included 60 dynamic volumes with a temporal resolution of 1.6 seconds with flip angle = 75° , TE = 40 ms, TR = 1522–1771 ms, pixel spacing = 1.75 mm, and section thickness = 5 mm. The intravenous contrast was gadobutrol, 1 mmol/mL, 0.1 mmol/kg. No contrast preload administered. Baseline acquisition was on the order of 10 points. The start of the automatic injection (4–5 mL/s) was by a manual setting.

Postprocessing. The segmentations of enhancing tumor and contralateral normal-appearing WM were performed on CE-T1WI semiautomatically (histogram intensity thresholding) and coregistered with DSC-PWI. Necrosis was not included in the segmentations. Segmentations were performed on 3D Slicer, Version 4.10 (http://www.slicer.org), and coregistration was with the BRAINSFit module (3D Slicer). TICs were preprocessed using the method proposed by Pons-Escoda et al,^{22,23} which renders nTICs: Signal-intensity values of the enhancing tumor TIC were normalized by dividing by the maximal signal intensity drop of the normal-appearing WM, and time values were normalized as relative to the period of the descending curve on normal-appearing WM. The resultant nTICs are timeand intensity-normalized, making them comparable among patients. The TICs were processed using Python 3.6 software (https://www.python.org/downloads/release/python-360/).

Visual evaluation of the average curves and point-by-point statistical comparison (Mann-Whitney U test) were performed.

Table 1: Clinical overview of the included patients with pathology-confirmed DLBC EBV-positive CNS lymphoma

					Diagnostic-Therapeutic Initial
	Age (yr)	Sex	Underlying Conditions	Radiologic Diagnosis ^a	Management
P 1	66	Male	Kidney transplant	Multiple metastases ^b	Biopsy: reason, multiple lesions
P 2	76	Male	Chronic myeloproliferative disorder; essential thrombocythemia	Glioblastoma	Biopsy: reason, patient basal clinical status
P 3	74	Male	Liver transplant	Single metastasis ^c	Biopsy: reason, second-look radiologic opinion
P 4	62	Female	Systemic sclerosis and discoid cutaneous lupus	Glioblastoma	Maximal safe surgical resection
P 5	70	Female	Immunosenescence	Multiple metastases or multifocal glioblastoma	Biopsy: reason, multiple lesions
P 6	63	Male	Autoimmune hepatitis	Metastasis or glioblastoma	Maximal safe surgical resection
P 7	78	Female	Kidney transplant	Single metastasis	Maximal safe surgical resection

Note:—P indicates patient

Table 2: Radiologic overview of the included patients with pathology-confirmed large B-cell EBV-positive primary CNS lymphoma

	No.	Location	Necrosis	CE-TIWI Ring	T2WI Solid Parts	T2*WI Hemorrhage	DWI Solid Parts
P1	Multiple	Bilateral basal ganglia and cortico-subcortical	Yes	Irregular thick and nodular	Heterogeneous hyperintense	Moderate	Heterogeneous restricted
P 2	Single	Parietal corticosubcortical	Yes	Irregular thick	Heterogeneous intermediate	Subtle	Heterogeneous intermediate
P 3	Single	Frontal cortico-subcortical	Yes	Irregular thick	Heterogeneous hypointense	Moderate	Heterogeneous restricted
P 4	Single	Parietal cortico-subcortical	Yes	Irregular thick	Heterogeneous hyperintense	Prominent	Heterogeneous restricted
P 5	Multiple	Cortico-subcortical unilateral	Yes	Irregular thin	Heterogeneous hypointense	Prominent	Heterogeneous intermediate
P 6	Single	Basal ganglia	Yes	Irregular thick	Homogenous hypointense	Prominent	Heterogeneous restricted
P 7	Single	Frontal subcortical	Yes	Regular thin	Homogenous hypointense	Moderate	Homogeneous restricted

Two previously published classifiers to differentiate PCNSL from glioblastoma and metastasis through nTICs were used to assess the performance in the particular group of DLBC EBV-positive CNS lymphomas.²² Also, we assessed the performance of mean rCBV and PSR. rCBV was obtained after leakage correction and normalized to the contralateral normal-appearing WM³¹ with 3D Slicer, Version 4.10, and PSR was obtained as described by Cha et al.³²

Additionally, replicating the same prior methodology²² (logistic binary regression on the 5 most discriminatory points of the curve), we trained a 1-way nTIC model to differentiate PCNSL and glioblastoma/metastasis as a single group and tested it for DLBC EBV-positive CNS lymphoma.

RESULTS

Patients

Seven patients fulfilled the inclusion criteria and were included in the study (4 men; mean age, 70 years; range, 62–78 years). The underlying conditions were the following: 3 iatrogenic in the context of posttransplant, 2 iatrogenic in the context of autoimmune disease, 1 chronic inflammation, and 1, elderly, related to immunosenescence. ^{15,17,19-21} The original radiologic diagnosis

was metastasis or glioblastoma in all patients. Initial biopsy was recommended in 4 cases, while the remaining patients were candidates for initial maximal safe resection. Patient characteristics are specified in Table 1. Four patients with DLBC EBV-positive CNS lymphoma were on corticosteroids at the time of MR imaging.

For perfusion metrics comparisons, DSC-PWI data from 33 patients with EBV-negative primary CNS lymphomas, 35 with glioblastomas, and 36 patients with metastases (total, 104; fifty-five men; mean age, 60 years; range, 18–82 years) were included. These data were previously acquired in the same center, with same technical parameters, 22 and there were no significant differences in their distributions with the currently analyzed cohort (χ^2 test, P=.108).

Imaging

Conventional Imaging. Conventional imaging findings are shown in Table 2. The most relevant findings on MR imaging were the following: single lesions and peripheral cortico-subcortical location; necrotic lesions with ring enhancement and different degrees of hemorrhage; and heterogeneous signal on DWI (Table 2 and Fig 1). An unexpected TSE-T2 heterogeneously iso-/hypointense signal of the central nonenhancing content of lesions was also described.

^a Based on a radiologic report from our neuro-oncology reference tertiary university hospital.

^b Atypical infection was considered, but as an unlikely option.

^c A second-look opinion raised the possibility of atypical lymphoma.

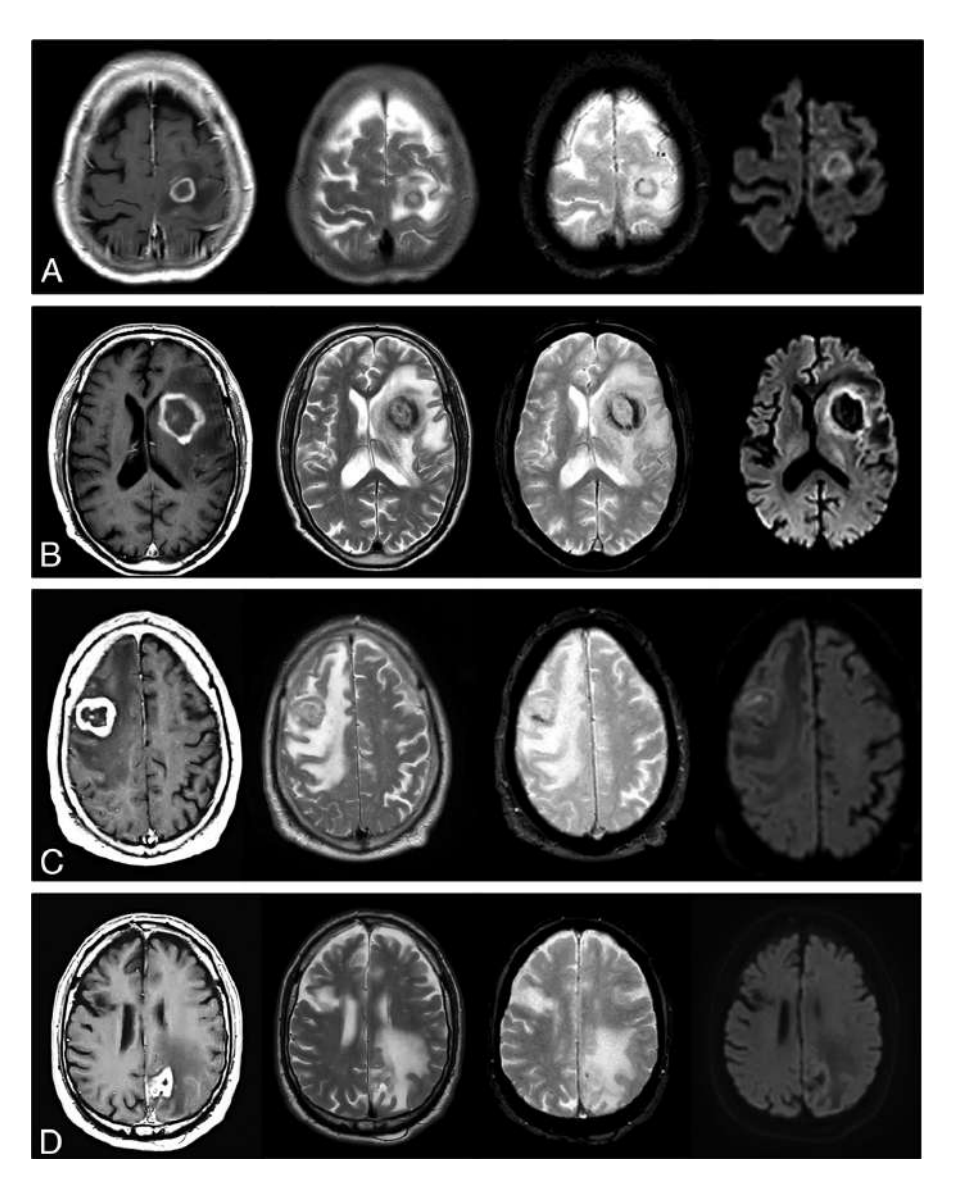


FIG 1. Visual summary of MR imaging features in 4 patients with pathology-confirmed DLBC EBV-positive CNS lymphoma. One patient in each row: CE-TIWI, TSE-T2WI, GE-T2*WI, and DWI at b=1000. Regular thin ring enhancement of a subcortical lesion in A, irregular thick ring enhancement of a basal-ganglia lesion in B. The solid walls of lesions show homogeneous TSE-T2WI low signal and restricted diffusion. Incidental right frontal chronic infarct in D. Irregular thick ring enhancement in cortico-subcortical lesions: frontal in C, parietal in D. Heterogeneous signal on TSE-T2WI: hypointense in C, iso- to hyperintense in D. Intermediate heterogeneous signal on DWI. Different amounts of hemorrhage in all cases are depicted by the GE-T2*WI. Note the TSE-T2WI heterogeneous iso- to hypointense signal of the nonenhancing central content of tumors in A-C, especially in B and C.

Perfusion Imaging. Figure 2 overlays the average nTIC for DLBC EBV-positive CNS lymphoma, PCNSL (EBV-negative), metastasis, and glioblastoma. Few differences were detected between DLBC EBV-positive CNS lymphoma and PCNSL. The most relevant visual differences with metastasis or glioblastoma were seen around the maximal-signal-intensity drop and signal-recovery segments of the curves. The Mann-Whitney *U* test found significant differences between DLBC EBV-positive CNS lymphoma and glioblastoma or metastasis at almost all time points of the curve, with the greatest level around the maximal-signal-intensity drop and signal-recovery segments, reinforcing the visual assessment.

Results of the 2 previously published classifier algorithms,²² along with the classification potential of PSR and rCBV, can be

found in Table 3, Fig 3, and the Online Supplemental Data. The 2 nTIC algorithms showed the most significant differences (P < .001 for glioblastoma and metastasis) and the best classification results. For glioblastoma, they yielded an area under the receiver operating curve (AUC) of 0.984, accuracy of 0.93, sensitivity of 1.0, and specificity of 0.91, while for metastasis, they yielded an AUC of 0.898, accuracy of 0.82, sensitivity of 1.0, and specificity of 0.78. Additionally, PSR was also significant for both comparisons, albeit slightly less so (P < .01) for both, AUC = 0.833 and 0.873). Finally, rCBV yielded significant differences for DLBC EBV-positive CNS lymphoma against glioblastoma (P = .003, AUC = 0.855), but not against metastasis (P =.122, AUC = 0.687).

Furthermore, when we compared DLBC EBV-positive CNS lymphoma and PCNSL, visual assessment of average nTICs showed very similar morphology, and statistical comparison confirmed no significant differences between them in the Mann-Whitney U test. Moreover, no significant differences were found in PSR, while rCBV showed a barely significant difference (P=.05). All results are summarized in Table 3, Fig 3, and the Online Supplemental Data.

Last, the 1-way adapted classifier results can be found in the Online Supplemental Data. The nTIC algorithm (Online Supplemental Data) discriminated between DLBC EBV-positive CNS lymphoma and glioblastoma/metastasis as a whole, with AUC = 0.90, while the AUC was 0.85 for PSR and 0.77 for rCBV.

No significant differences were found in all time points of nTICs, CBV, or PSR values among the different DSC-PWI

techniques (Mann-Whitney U test, P values = .245–1), neither among patients with nor without corticosteroids at the time of MR imaging (Mann-Whitney U test, P values = .157–.724).

DISCUSSION

In this study, we present a unique cohort of 7 patients with DLBC EBV-positive CNS lymphoma without AIDS in whom DSC-PWI was performed and compare them with those with PCNSL (EBV-negative), glioblastoma, and metastasis. While conventional imaging was misleading due to the strong similarity between DLBC EBV-positive CNS lymphoma and glioblastoma or metastasis, DSC-PWI metrics provided promising results, the best determined by nTIC analysis. Moreover, this is the first study to describe and

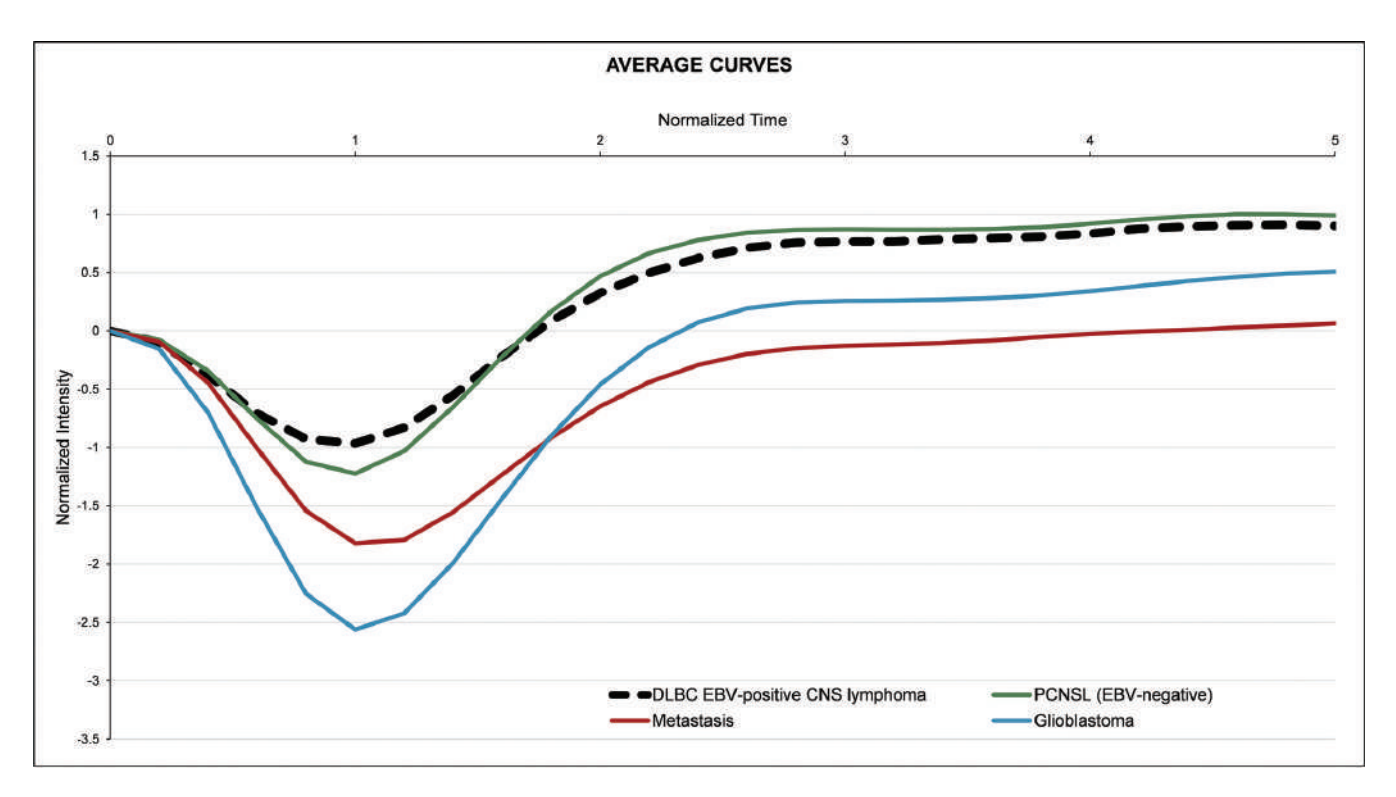


FIG 2. Average nTIC of DLBC EBV-positive CNS lymphoma, PCNSL (EBV-negative), metastasis, and glioblastoma. Few differences may be seen between DLBC EBV-positive CNS lymphoma and PCNSL. The most relevant visual differences between DLBC EBV-positive CNS lymphoma and metastasis or glioblastoma are seen around the maximal-signal-intensity drop and the signal-recovery segments of the curves.

Table 3: Summary of results

	P ^a	AUC
nTIC algorithms		
vs glioblastoma	<.001	0.984
vs metastasis	<.001	0.898
PSR		
vs glioblastoma	.006	0.833
vs metastasis	.002	0.873
rCBV		
vs glioblastoma	.003	0.855
vs metastasis	.122	0.687

^a Statistical significance, Mann-Whitney *U* test.

analyze DLBC EBV-positive CNS lymphoma nTIC features and PSR values, to the best of our knowledge.

Currently, it is recognized that DLBC EBV-positive CNS lymphoma is a specific subtype of CNS lymphoma associated with immunodeficiency. ^{8,15,16} AIDS-related CNS lymphoma appeared to become one of the most frequent brain tumors in the 1990s due to the explosion of the AIDS pandemic. ³³ However, with the advent of antiretroviral therapies, AIDS-related CNS lymphoma has gradually decreased in the 2000s. ^{34,35} Inherent to medical advances, other non-AIDS immunodeficiencies such as iatrogenic (posttransplantation and others), immunosenescence, and chronic inflammation have increased and probably overtaken AIDS as a cause of immunodeficiency-related CNS lymphoma. ^{17-21,36} Also, due to the differing underlying physiopathologies of these conditions, strict monitoring of patients, and the improvement in imaging techniques, necrotic tumors have become the main radiologic differentials. ^{14,37-39}

In the authors' opinion, radiology literature regarding DLBC EBV-positive CNS lymphoma without AIDS is scarce, probably due to the constantly evolving epidemiologic scenario and the relative rarity of the disease, making it difficult to pool these patients accurately. 14,16-21,33-35,37-39 However, DLBC EBV-positive CNS lymphoma without AIDS is a clear and specific clinical immunobiologic entity that is challenging to diagnose because of the uncommon signatures for the much more frequent PCNSL and its great similarity to glioblastoma and metastasis on conventional imaging. 14,37-39 Last, its identification before any surgical approach is crucial for optimal management because prompt biopsy without corticosteroids is the best choice, while surgical resection is not recommended. 1

In reference to the role of DSC-PWI, our literature search identified only 1 article that specifically assessed DSC-PWI of patients with DLBC EBV-positive CNS lymphoma without AIDS. 10 Another article¹⁴ analyzed a subgroup of CNS lymphomas under the term "atypical PCNSL" in patients without AIDS. Lee et al¹⁰ specifically assessed rCBV values of patients with DLBC EBV-positive CNS lymphoma and compared them with those in patients who were EBV-negative. They did not find differences between EBV-positive and EBV-negative CNS lymphomas, while we found a slightly significant difference. On the other hand, Suh et al¹⁴ reported relevant differences in rCBV values between their patients with atypical PCNSL and glioblastoma, congruent with our results. Nevertheless, in both articles the DSC-PWI analysis remained limited to rCBV, and the absence of AIDS is considered enough to rule out immunodeficiency, which raises the question of whether CNS lymphomas included in these articles could actually be "other

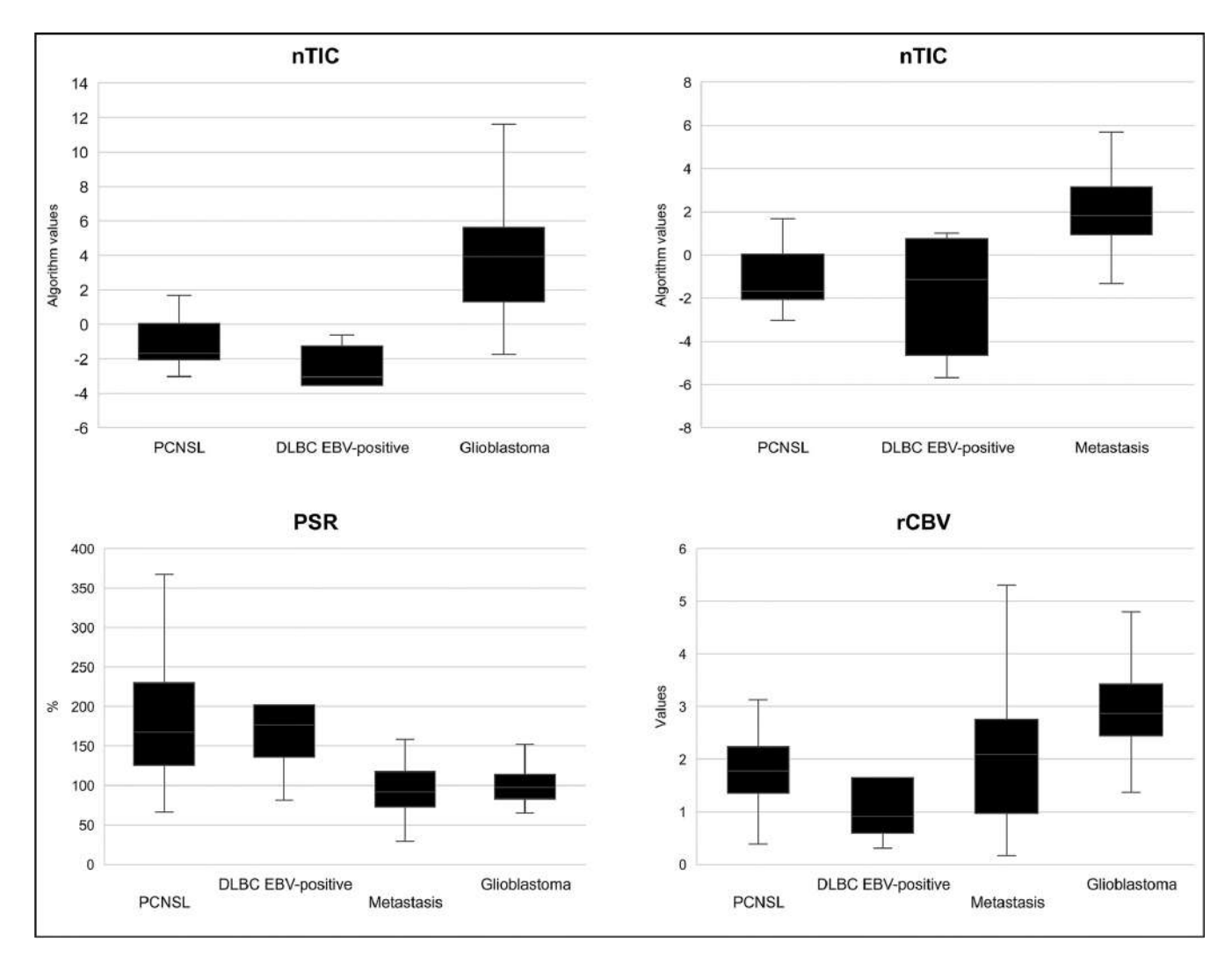


FIG 3. Boxplots depicting the results of the nTIC algorithms to differentiate PCNSL versus glioblastoma (*upper left*) and PCNSL versus metastasis (*upper right*) for each tumor subtype. *Lower row*: Boxplots depicting PSR and rCBV values for each tumor subtype.

immunodeficiency-associated," such as ours. Finally, the mere comparison of EBV-positive and EBV-negative CNS lymphoma¹⁰ and the noninclusion of metastasis in the differential¹⁴ may condition the lack of clinically relevant information from our point of view and experience. To overcome these issues, we present a unique cohort with comprehensive clinical and demographic information and pathologic diagnosis according to the 2016 WHO lymphoid neoplasm¹⁵ and the 2021 WHO CNS tumor⁸ classifications, and we systematically describe conventional imaging and analyze the full potential of DSC-PWI to presurgically identify DLBC EBV-positive CNS lymphoma.

In this study, standard DSC-PWI metrics of PSR and rCBV achieved good or acceptable results in pair-wise discrimination of DLBC EBV-positive CNS lymphoma and glioblastoma or metastasis. Nonetheless, the application of previously reported nTICs analysis methodology²² yielded improved diagnostic performance. We mainly applied the previously published PCNSL presurgical classifier algorithms²² to our data set; but as a secondary analysis, we generated a dedicated algorithm to differentiate PCNSL and glioblastoma/metastasis as a whole group, also obtaining excellent results. Additionally, the curve-normalization process allows overlaying the averaged nTICs of relevant differential diagnoses

(Fig 2), which offers radiologist-friendly visual evaluation of curve differences. An additional advantage of the nTIC classifier results is the high-sensitivity levels provided, which is ideal in this scenario in which the most relevant goal is to raise suspicion of CNS lymphoma to avoid prebiopsy corticosteroids and potentially harmful tumor resection.²

DSC-PWI pulse-sequence parameters are known to influence CBV and PSR values, often paradoxically (ie, those sequences optimized for CBV calculations may be suboptimal for PSR and vice versa). ⁴⁰ In this respect, we believe that the use of nTICs could be an alternative, especially in heterogeneous samples with nonstandardized technical acquisitions, which could be the situation among many neuroradiology departments worldwide such as ours because in this scenario, the evaluation of the whole normalized curve could surpass standard approaches such as CBV and PSR calculations. ^{22,23}

On the other hand, in our experience, conventional imaging findings were insufficient to raise suspicion of CNS lymphoma because these tumors appear almost consistently as ring-enhancing necrotic lesions, with differing amounts of hemorrhage, mimicking glioblastoma or metastasis. ⁹⁻¹⁴ We noted a prevalent heterogeneous low TSE-T2 signal from the central nonenhancing content of lesions,

not attributable to hemorrhage or calcification and, to the best of our knowledge, not usually seen in glioblastoma or metastasis.

Several considerations should be taken into account concerning this study. The single-site and retrospective character of the study may affect reproducibility. Nevertheless, they may also have conferred useful homogeneity to the study. Also, the limited number of cases of DLBC EBV-positive CNS lymphoma included may raise objections. However, this is a rare condition that needs to be detected presurgically, and the DSC-PWI characteristics have hardly been evaluated in the literature. At any rate, the data set suffices for a proof-of-concept demonstration, and our results warrant further multicentric prospective studies for validation. Furthermore, heterogeneous DSC-PWI technique acquisition parameters may compromise the generalizability of our concrete results. However, nTIC methodology is appliable elsewhere, and thresholds could be adapted in technically different cohorts.

Moreover, in our data set, no significant differences were found in nTICs among different DSC-PWI techniques, and indeed the nTIC method was created itself to hypothetically attenuate the impact of technical and physiologic variability on isolated parameter evaluation. Some of the data used in this investigation were part of previously published studies, ^{22,23} but the aims of the study were clearly differentiated, and prior data were used for comparisons and differential diagnoses. Moreover, the use of previously published algorithms conferred a certain robustness on the study. Additionally, the reliability of data is ensured because they are available, well-balanced, curated, and filtered for prior publication. Finally, the absence of infection and brain abscess in the differential is a limitation. However, in our clinical experience with this data set of patients, glioblastoma and metastasis were the main differential diagnoses considered.

CONCLUSIONS

DSC-PWI could be very useful to presurgically differentiate DLBC EBV-positive CNS lymphoma and glioblastoma or metastasis. Among DSC-PWI metrics, nTIC curvology assessment could surpass the performance of standard PSR and rCBV measures. Neuroradiologists should be aware of any risk factors for immunodeficiency when facing a necrotic tumor in the brain. In the event of potential immunodeficiency, careful assessment of DSC-PWI may raise the suspicion of DLBC EBV-positive CNS lymphoma, which would drastically alter patient management.

ACKNOWLEDGMENTS

We thank CERCA Programme/Generalitat de Catalunya for institutional support.

Disclosure forms provided by the authors are available with the full text and PDF of this article at www.ajnr.org.

REFERENCES

- Chiavazza C, Pellerino A, Ferrio F, et al. Primary CNS lymphomas: challenges in diagnosis and monitoring. Biomed Res Int 2018;2018:3606970 CrossRef Medline
- 2. Qian L, Tomuleasa C, Florian I-A, et al. **Advances in the treatment of newly diagnosed primary central nervous system lymphomas.** *Blood Res* 2017;52:159–66 CrossRef Medline

- Bühring U, Herrlinger U, Krings T, et al. MRI features of primary central nervous system lymphomas at presentation. Neurology 2001;57:393–96 CrossRef Medline
- Malikova H, Koubska E, Weichet J, et al. Can morphological MRI differentiate between primary central nervous system lymphoma and glioblastoma? Cancer Imaging 2016;16:40 CrossRef Medline
- Mansour A, Qandeel M, Abdel-Razeq H, et al. MR imaging features of intracranial primary CNS lymphoma in immune competent patients. Cancer Imaging 2014;14:22 CrossRef Medline
- Haldorsen IS, Espeland A, Larsson EM. Central nervous system lymphoma: characteristic findings on traditional and advanced imaging. AJNR Am J Neuroradiol 2011;32:984–92 CrossRef Medline
- Tang YZ, Booth TC, Bhogal P, et al. Imaging of primary central nervous system lymphoma. Clin Radiol 2011;66:768–77 CrossRef Medline
- 8. WHO Classification of Tumours Editorial Board. World Health Organization Classification of Tumours of the Central Nervous System. 5th ed. International Agency for Research on Cancer; 2021
- Sauter A, Faul C, Bitzer M, et al. Imaging findings in immunosuppressed patients with Epstein Barr virus-related B cell malignant lymphoma. AJR Am J Roentgenol 2010;194:141–49 CrossRef Medline
- Lee HY, Kim HS, Park JW, et al. Atypical imaging features of Epstein-Barr virus-positive primary central nervous system lymphomas in patients without AIDS. AJNR Am J Neuroradiol 2013;34:1562–67 CrossRef Medline
- 11. Jiménez de la Peña M del M, Vicente LG, Alonso RC, et al. The multiple faces of nervous system lymphoma. Atypical magnetic resonance imaging features and contribution of the advanced imaging. *Curr Probl Diagn Radiol* 2017;46:136–45 CrossRef Medline
- Lin X, Khan IRA, Seet YH, et al. Atypical radiological findings of primary central nervous system lymphoma. Neuroradiology 2020;62:669

 76 CrossRef Medline
- Shin DJ, Lee EJ, Lee JE, et al. Common and uncommon features of central nervous system lymphoma on traditional and advanced imaging modalities. Neurographics 2017;7:437–49 CrossRef
- 14. Suh CH, Kim HS, Lee SS, et al. Atypical imaging features of primary central nervous system lymphoma that mimics glioblastoma: utility of intravoxel incoherent motion MR imaging. Radiology 2014;272:504–13 CrossRef Medline
- Swerdlow SH, Campo E, Pileri SA, et al. The 2016 revision of the World Health Organization classification of lymphoid neoplasms. Blood 2016;127:2375–90 CrossRef Medline
- Gandhi MK, Hoang T, Law SC, et al. EBV-associated primary CNS lymphoma occurring after immunosuppression is a distinct immunobiological entity. Blood 2021;137:1468–77 CrossRef Medline
- 17. Mahale P, Shiels MS, Lynch CF, et al. **Incidence and outcomes of** primary central nervous system lymphoma in solid organ transplant recipients. *Am J Transplant* 2018;18:453–61 CrossRef Medline
- Verdu-Bou M, Tapia G, Hernandez-Rodriguez A, et al. Clinical and therapeutic implications of Epstein-Barr virus in HIV-related lymphomas. Cancers (Basel) 2021;13:5534 CrossRef Medline
- Kaulen LD, Karschnia P, Dietrich J, et al. Autoimmune diseaserelated primary CNS lymphoma: systematic review and meta-analysis. J Neurooncol 2020;149:153–59 CrossRef Medline
- Mancuso S, Carlisi M, Santoro M, et al. Immunosenescence and lymphomagenesis. Immun Ageing 2018;15:22 CrossRef Medline
- Barosi G. An immune dysregulation in MPN. Curr Hematol Malig Rep 2014;9:331–39 CrossRef Medline
- Pons-Escoda A, Garcia-Ruiz A, Naval-Baudin P, et al. Presurgical identification of primary central nervous system lymphoma with normalized time-intensity curve: a pilot study of a new method to analyze DSC-PWI. AJNR Am J Neuroradiol 2020;41:1816–24 CrossRef Medline
- Pons-Escoda A, Garcia-Ruiz A, Naval-Baudin P, et al. Voxel-level analysis of normalized DSC-PWI time-intensity curves: a potential generalizable approach and its proof of concept in discriminating glioblastoma and metastasis. Eur Radiol 2022;32:3705–15 CrossRef Medline

- 24. Lee MD, Baird GL, Bell LC, et al. Utility of percentage signal recovery and baseline signal in DSC-MRI optimized for relative CBV measurement for differentiating glioblastoma, lymphoma, metastasis, and meningioma. AJNR Am J Neuroradiol 2019;40:1445–50 CrossRef Medline
- 25. Xing Z, You RX, Li J, et al. Differentiation of primary central nervous system lymphomas from high-grade gliomas by rCBV and percentage of signal intensity recovery derived from dynamic susceptibilityweighted contrast-enhanced perfusion MR imaging. Clin Neuroradiol 2014;24:329–36 CrossRef Medline
- 26. Neska-Matuszewska M, Bladowska J, Saôsiadek M, et al. Differentiation of glioblastoma multiforme, metastases and primary central nervous system lymphomas using multiparametric perfusion and diffusion MR imaging of a tumor core and a peritumoral zone: searching for a practical approach. PLoS One 2018;13:e0191341 CrossRef Medline
- 27. Wang S, Kim S, Chawla S, et al. Differentiation between glioblastomas, solitary brain metastases, and primary cerebral lymphomas using diffusion tensor and dynamic susceptibility contrast-enhanced MR imaging. AJNR Am J Neuroradiol 2011;32:507–14 CrossRef Medline
- 28. Lee IH, Kim ST, Kim HJ, et al. **Analysis of perfusion weighted image of CNS lymphoma.** *Eur J Radiol* 2010;76:48–51 CrossRef Medline
- Calli C, Kitis O, Yunten N, et al. Perfusion and diffusion MR imaging in enhancing malignant cerebral tumors. Eur J Radiol 2006;58:394– 403 CrossRef Medline
- Mangla R, Kolar B, Zhu T, et al. Percentage signal recovery derived from MR dynamic susceptibility contrast imaging is useful to differentiate common enhancing malignant lesions of the brain. AJNR Am J Neuroradiol 2011;32:1004–10 CrossRef Medline
- Boxerman JL, Schmainda KM, Weisskoff RM. Relative cerebral blood volume maps corrected for contrast agent extravasation significantly correlate with glioma tumor grade, whereas uncorrected maps do not. AJNR Am J Neuroradiol 2006;27:859–67 Medline

- 32. Cha S, Lupo JM, Chen MH, et al. Differentiation of glioblastoma multiforme and single brain metastasis by peak height and percentage of signal intensity recovery derived from dynamic susceptibility-weighted contrast-enhanced perfusion MR imaging. AJNR Am J Neuroradiol 2007;28:1078–84 CrossRef Medline
- Corn BW, Marcus SM, Topham A, et al. Will primary central nervous system lymphoma be the most frequent brain tumor diagnosed in the year 2000? Cancer 1997;79:2409–13 Medline
- Kadan-Lottick NS, Skluzacek MC, Gurney JG. Decreasing incidence rates of primary central nervous system lymphoma. Cancer 2002;95:193–202 CrossRef Medline
- De Robles P, Fiest KM, Frolkis AD, et al. The worldwide incidence and prevalence of primary brain tumors: a systematic review and meta-analysis. Neuro Oncol 2015;17:776–83 CrossRef Medline
- 36. Adachi K, Yamaguchi F, Node Y, et al. Neuroimaging of primary central nervous system lymphoma in immunocompetent patients: comparison of recent and previous findings. J Nippon Med Sch 2013;80:174–83 CrossRef Medline
- 37. Wang ZD, Liu HH, Ma ZX, et al. Toxoplasma gondii infection in immunocompromised patients: a systematic review and metaanalysis. Front Microbiol 2017;8:1–12 CrossRef Medline
- 38. Arendt G, Maschke M. Update: opportunistic infections of the central nervous system in patients with iatrogenic immunosuppression: an update. Neurology International Open 2017;1:E316–25 CrossRef
- Morollón N, Rodríguez F, Duarte J, et al. Brain lesions in a longterm kidney transplant recipient: primary cerebral lymphoma or cerebral toxoplasmosis? Neurologia 2017;32:268–70 CrossRef Medline
- 40. Cindil E, Sendur HN, Cerit MN, et al. Validation of combined use of DWI and percentage signal recovery-optimized protocol of DSC-MRI in differentiation of high-grade glioma, metastasis, and lymphoma. Neuroradiology 2021;63:331–42 CrossRef Medline

NEURO



Voxel-level analysis of normalized DSC-PWI time-intensity curves: a potential generalizable approach and its proof of concept in discriminating glioblastoma and metastasis

Albert Pons-Escoda^{1,2} • Alonso Garcia-Ruiz³ • Pablo Naval-Baudin¹ • Francesco Grussu³ • Juan Jose Sanchez Fernandez¹ • Angels Camins Simo¹ • Noemi Vidal Sarro^{2,4} • Alejandro Fernandez-Coello^{5,6,7} • Jordi Bruna² • Monica Cos¹ • Raquel Perez-Lopez^{3,8} • Carles Majos^{1,2}

Received: 2 September 2021 / Revised: 22 November 2021 / Accepted: 9 December 2021 / Published online: 1 February 2022 © The Author(s), under exclusive licence to European Society of Radiology 2022

Abstract

Objective Standard DSC-PWI analyses are based on concrete parameters and values, but an approach that contemplates all points in the time-intensity curves and all voxels in the region-of-interest may provide improved information, and more generalizable models. Therefore, a method of DSC-PWI analysis by means of normalized time-intensity curves point-by-point and voxel-by-voxel is constructed, and its feasibility and performance are tested in presurgical discrimination of glioblastoma and metastasis.

Methods In this retrospective study, patients with histologically confirmed glioblastoma or solitary-brain-metastases and presurgical-MR with DSC-PWI (August 2007–March 2020) were retrieved. The enhancing tumor and immediate peritumoral region were segmented on CE-T1wi and coregistered to DSC-PWI. Time-intensity curves of the segmentations were normalized to normal-appearing white matter. For each participant, average and all-voxel-matrix of normalized-curves were obtained. The 10 best discriminatory time-points between each type of tumor were selected. Then, an intensity-histogram analysis on each of these 10 time-points allowed the selection of the best discriminatory voxel-percentile for each. Separate classifier models were trained for enhancing tumor and peritumoral region using binary logistic regressions.

Results A total of 428 patients (321 glioblastomas, 107 metastases) fulfilled the inclusion criteria (256 men; mean age, 60 years; range, 20–86 years). Satisfactory results were obtained to segregate glioblastoma and metastases in training and test sets with AUCs 0.71–0.83, independent accuracies 65–79%, and combined accuracies up to 81–88%.

Conclusion This proof-of-concept study presents a different perspective on brain MR DSC-PWI evaluation by the inclusion of all time-points of the curves and all voxels of segmentations to generate robust diagnostic models of special interest in heterogeneous diseases and populations. The method allows satisfactory presurgical segregation of glioblastoma and metastases. **Key Points**

- An original approach to brain MR DSC-PWI analysis, based on a point-by-point and voxel-by-voxel assessment of normal ized time-intensity curves, is presented.
- The method intends to extract optimized information from MR DSC-PWI sequences by impeding the potential loss of information that may represent the standard evaluation of single concrete perfusion parameters (cerebral blood volume, percentage of signal recovery, or peak height) and values (mean, maximum, or minimum).
- The presented approach may be of special interest in technically heterogeneous samples, and intrinsically heterogeneous diseases. Its application enables satisfactory presurgical differentiation of GB and metastases, a usual but difficult diagnostic challenge for neuroradiologist with vital implications in patient management.

Keywords Brain neoplasms · Glioblastoma · Metastases · Magnetic resonance imaging · Perfusion imaging

Albert Pons-Escoda and Alonso Garcia-Ruiz share joint first authorship.

Extended author information available on the last page of the article

Abbreviations

CBV Cerebral blood volume ET Enhancing tumor

NAWM Normal-appearing white matter nTIC Normalized time-intensity curve

PH Peak height



PR Peritumoral region

PSR Percentage of signal recovery

TIC Time-intensity curve

Introduction

Presurgical diagnosis of brain tumors is of vital importance for patient management. While histopathology remains the final reference standard, the presurgical approach mainly lays on neuroimaging with magnetic resonance (MR) as the lead actor. In this sense, one of the most challenging differentials for neuroradiologists is glioblastoma (GB) versus solitary brain metastasis, the two most common malignant intracranial tumors in adults [1, 2]. It is a cause of frequent debate in neurooncology units, whether the patient has a known extracranial primary tumor or not, and the ability to presurgically differentiate these two entities will significantly impact further steps on therapeutic decisions [3–8]. Consequently, achieving the highest diagnostic accuracy with non-invasive assays is an unmet critical need in the clinical practice.

Unfortunately, both tumor types are highly heterogeneous in their presentations, and morphological MR is too often limited to reach a trustable diagnosis [9, 10]. For this reason, the use of so-called advanced or functional MR imaging techniques in this context has been growing in recent years. These techniques go beyond morphology to offer information on the metabolic, cellular, or vascular environment levels. One of these MR techniques is dynamic susceptibility contrast–perfusion weighted imaging (DSC-PWI), which has shown promising results for the diagnosis of brain tumors [11–13].

DSC-PWI has been correlated with different histological features of tumor vascularization, microvascularity, and blood–brain barrier integrity [14–20]. In this respect, prior work has shown that tumor vasculature significantly differs between glioblastoma and metastasis. GB is characterized by heterogeneous blood–brain barrier disruption, while in metastasis, blood–brain barrier is absent and angiogenesis is the predominant phenomenon. Regarding the peritumoral region, metastases cause pure vasogenic edema, while in GB, infiltrative tumor cells may be found among edema [11, 21–24]. DSC-PWI exploits these tissular characteristics to try to monitor and discriminate different tumor types and environments.

Many authors have tried to presurgically differentiate GB and metastasis based on DSC-PWI [25–41]. Among the different studies, many different perfusion parameters are used, with a high heterogeneity in the results and thresholds. The most evaluated classical parameters are cerebral blood volume (CBV), percentage of signal recovery (PSR), and peak height (PH). These are all extracted from DSC-PWI

time-intensity curves (TICs). Prior work has suggested that analyzing and comparing the entire TIC instead of these concrete parameters may provide better information, by means of normalized TICs (nTICs) that can be compared individually or combined to train predictive models [42].

Furthermore, the standard parameters are usually evaluated in terms of mean or extreme (minimum or maximum) values obtained from the voxels in the region of interest (ROI). We consider this kind of approach further discards potentially useful information by not accounting for atypical distributions of these parameters. This atypical spatial distribution of perfusion may be, actually, common in some cases of predominant heterogeneity, as the current scenario of GB and metastases, which are proved highly heterogeneous tumors on histology [21–24].

We hypothesize that the study of the entire nTIC and the whole range of voxels included in the volumetric segmentations of enhancing tumor and peri-enhancing region could provide more accurate tissue characterization and improve tumor classification. Furthermore, the use of normalized perfusion data and model training based on all time-points and all voxels offers a new perspective in MR perfusion imaging which should facilitate the construction of more robust and generalizable models than isolated parameters such as CBV, PSR, or PH, by being able to take into account tumoral and technical heterogeneity more completely.

With these considerations in mind, we aim to present this novel method of DSC-PWI nTICs voxel-level percentile intensity-histogram analysis and test it for the clinical discrimination of glioblastoma and metastasis.

Material and methods

This work was approved by the Research Ethics Committee of Hospital Universitari de Bellvitge. A waiver of a specific informed consent was provided by the ethics committee for this retrospective study.

Patients

Newly diagnosed patients with histologically confirmed GB or solitary brain metastases (August 2007–March 2020) were retrospectively retrieved from our center's database. Inclusion criteria for the study were as follows: (1) confirmed tumor diagnosis by histology according to The World Health Organization 2007 or 2016 criteria [43, 44], (2) an available diagnostic presurgical MR imaging examination including DSC-PWI and contrast-enhanced T1WI (CE-T1WI), (3) enhancing tumor on CE-T1WI with the shortest diameter of at least 10 mm.



Imaging

All the MR imaging examinations included in the study were acquired in the same hospital with 1 of 3 different scanners: Ingenia 3 T with a 32-channel head coil, Ingenia 1.5 T, or Intera 1.5 T both with a 16-channel head coil (Philips Healthcare). Acquisition parameters for DSC-PWI (all gradient echo) and CE-T1WI sequences are summarized in Supplemental Table 1, and DSC-PWI technique distribution between groups is specified in Supplemental Table 2. The intravenous contrast (gadobutrol; 1 mmol/mL, 0.1 mmol/kg) injection protocol was as follows: 18- or 20-ga peripheral intravenous access. No preload was performed. Baseline acquisition was on the order of 10 points. The automatic injection start (power injector at 4-5 mL/s) was by a manual setting. A final bolus of saline (25-50 mL) was injected at the same speed. The time and number of dynamics ranged from 1.26 to 3.55 s and 30 to 60, respectively. The quality of the sequences was evaluated by visual inspection by 2 neuroradiologists (A.P.-E. and C.M.) with more than 6 and 25 years of experience in MR imaging of brain tumors. The examinations were labeled as poor quality and excluded from the study under the following circumstances: (1) artifacts prevented enhancing tumor segmentation on CE-T1WI or coregistration of CE-T1WI and DSC-PWI, or (2) an obvious low signal-to-noise ratio was observed in the raw TICs.

Postprocessing

The enhancing tumor (ET) and contralateral normal-appearing white matter (NAWM) were segmented on CE-T1WI using a supervised semiautomatic volumetric method with histogram thresholding and morphologic operations. The peritumoral region (PR) segmentation included a 2-cmwide rim of brain parenchyma immediately around the ET, excluding ventricles and extraaxial spaces and structures. Segmentations were then coregistered with DSC-PWI. Necrosis was excluded from the segmentations as it is avascular tissue which does not generate time-intensity curves. A 2-cm rim of PR was used because this is the distance around the enhancing tumor where it is assumed that most brain microinfiltration occurs in GB, and which is consequently used for concomitant radiotherapy planning as the "safetymargin" to be treated [45–48]. We used semiautomatic volumetric segmentations instead of partial, manual, or singlesection ROI selection methods in order to minimize operator dependency as well as to include all the intrinsic heterogeneity of the tumors in the analysis. 3D Slicer, Version 4.10 (http://www.slicer.org) was used for segmentation, and the BRAINSFit module of 3D Slicer, for coregistering.

All TICs included for analysis were normalized following the method proposed by Pons-Escoda et al. [42], generating multiple normalized TICs (nTICs). For each participant, we obtained the following nTICs: average curve of all ET voxels, average curve of all PR voxels, a matrix of nTICs for all segmented voxels in the ET, and another matrix in the PR. The matrices had as many nTICs as voxels included in the segmentations. All resultant nTICs are superimposable and comparable between patients in a single graph, as they are composed of the same number of time-matching points and intensity units normalized to NAWM.

The TICs were processed using Python 3.6 software (https://www.python.org/downloads/release/python-360/).

Data analysis

The study sample was split into "training" (70%) and "test" (30%) subsets. The groups were balanced by date of examination to minimize the impact of quality and technical differences between TICs of the more distant-in-time exams.

The 10 best discriminatory time-points were selected by performing area under the curve—receiver operating characteristic (AUC-ROC): the analysis was performed for all time-points on the segmentation-average ET and PR nTICs of the training subset, and those 10 points with the highest AUC were the chosen. Ten was selected semi-arbitrarily as the highest number of information to be included with acceptable AUC-ROCs and while avoiding overtraining [49, 50].

Then, an intensity histogram analysis was performed on each of these 10 time-points to select the voxel percentile which showed greater differences between groups. This produced 10 histograms for ET segmentation and 10 for the PR segmentation (1 histogram for each discriminatory time-point). These histograms depict the signal-intensity distribution of all the voxels included in the segmentations for each discriminatory time-point. For each time-point, the voxel percentile that showed greater differences between tumor-types was selected.

Subsequently, separate classifier models were trained for the ET and PR segmentations using binary logistic regression on these 10 variables on the "training" subset. The best discriminatory thresholds of the algorithms were obtained by receiver operating characteristic (ROC) analysis. Finally, the constructed classifiers and thresholds were applied to the "test" set.

Additionally, we also analyzed the classification performance of average nTICs, in order to compare the present method with a previous method that compared average nTICs, without performing the voxel-level percentile intensity-histogram analysis [42].

All the statistical computations were performed with R statistical and computing software, Version 3.5.1 (http://www.rproject.org).



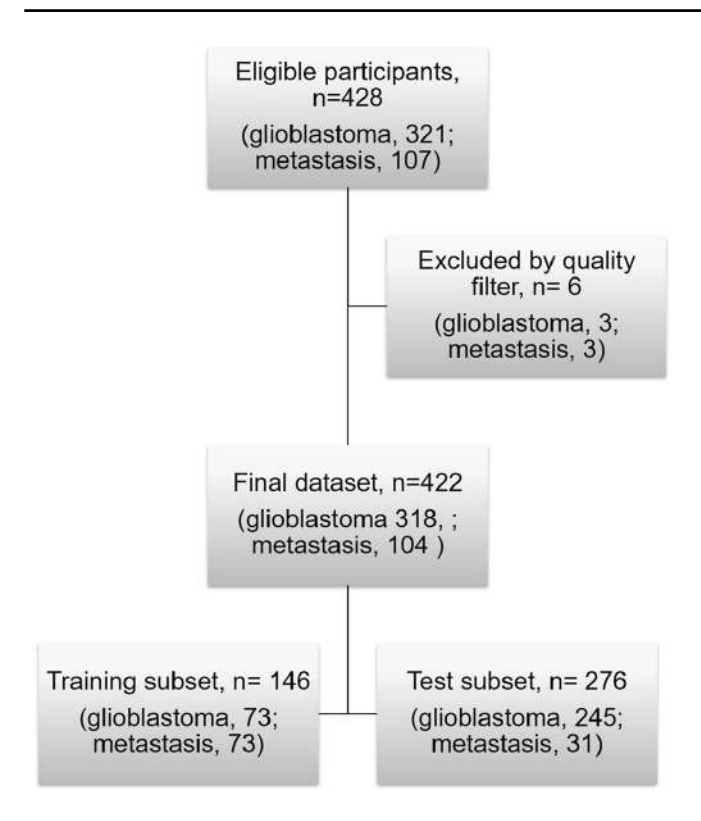


Fig. 1 Study participants flow chart

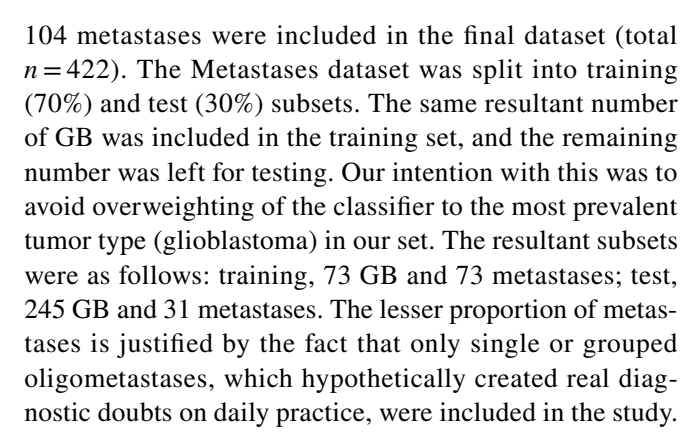
Table 1 Demographics of study participants

	Cases	Men	Women	Age
Tumor types				
Glioblastoma	321	197	124	60 (20-86)
Metastasis	107	59	48	60 (24–81)
Total	428	256	172	60 (20-86)
Study subgroups				
Train	146	93	53	59 (26–86)
Test	276	178	98	60 (20–86)
Total	422	253	169	60 (20–86)

Results

Patients

A total of 428 patients (321 glioblastomas and 107 metastases) fulfilled the inclusion criteria (256 men; mean age, 60 years; range, 20–86 years). A partial overlap of 48 glioblastomas and 49 metastases which participated in a prior published study with different objectives and methodology [42] is reported. The flow diagram of study participants is shown in Fig. 1. Demographics of the study sample are summarized in Table 1. Three GBs and 3 metastases were ruled out by the quality filter. As a result, 318 GB and



nTIC and percentile histogram analysis

Average ET and PR nTICs for each tumor type and the 10 discriminatory time-points are shown in Fig. 2. Notable differences were found between each tumor type nTICs on a first visual assessment. The most obvious were around the maximal signal intensity drop and the signal recovery segments.

The classifier algorithms are shown in Fig. 2 with the 10 best discriminatory points, the selected intensity-percentiles, and the model coefficients for each.

Satisfactory results were obtained to segregate GB and metastases with the constructed classifiers. In the training set (ET AUC=0.81, accuracy=79%; PR AUC=0.83, accuracy=78%). In the test set (ET AUC=0.79, accuracy=71%; PR AUC=0.71, accuracy=65%). Moreover, improved results were obtained when combining matching classifications of the ET and PR (72% of classifications matched in training set providing 88% accuracy. In the test set, 61% of classifications matched, providing 81% accuracy). Results are summarized in Table 2 and Fig. 3.

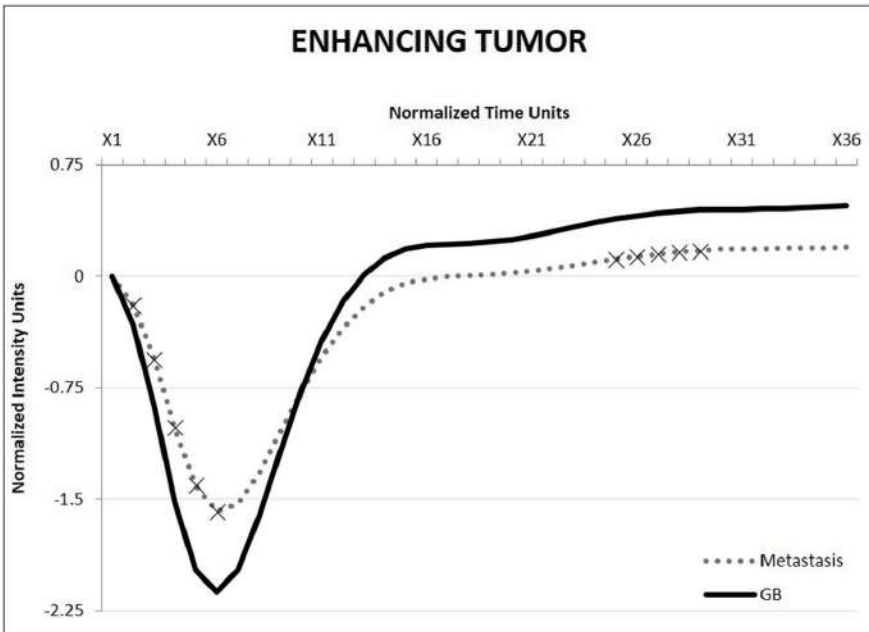
Additionally, the performance of whole segmented ROIs average nTICs was poorer in training and test sets for both the ET (training accuracy = 71%; test accuracy = 70%) and PR (training accuracy = 73%; test accuracy = 61%).

Figure 4 depicts an example of the classifier applicability.

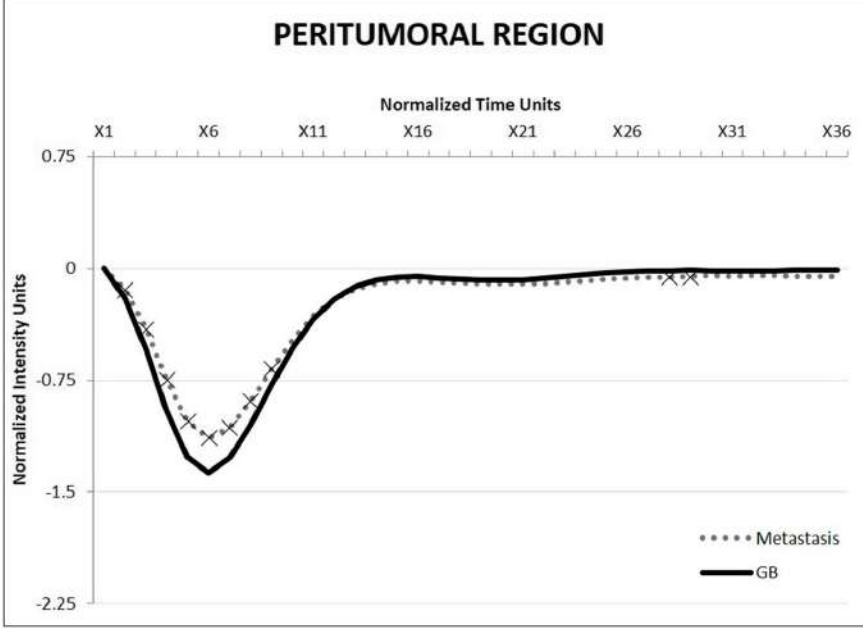
Discussion

In this study, we applied the previously reported nTIC methodology [42] to retrospectively analyze DSC-PWI studies of glioblastomas and metastasis, and explored its applicability for the discrimination between these two tumor types. We adapted the method to better approach the tumors' inherent high histological, vascular, and microvascular heterogeneity. The new modified method allows constructing classifiers that take into account the lesions' heterogeneity on a voxel-level by performing a point-by-point percentile intensity-histogram analysis of nTICs to generate a classifier





variables	coefficients
(Intercept)	1.6399319
p60 X2 _i	5.3447739
p70 X3 _i	-0.380345
p75 X4i	4.4540826
p85 X5 _i	-4.3117039
p95 X6 _i	3.9044655
p95 X25 _i	0.7014149
p60 X26 _i	-1.4883295
p60 X27 _i	-22.8331364
p60 X28i	20.3161906
p60 X29i	1.6134529



variables	coefficients
(Intercept)	2.936152
p70 X2i	-48.899096
p65 X3 _i	63.173447
p85 X4 _i	-3.468098
p90 X5 _i	10.997735
p90 X6 _i	-8.478254
p95 X7 _i	1.766047
p90 X8 _i	25.776699
p75 X9i	-13.559063
p20 X28i	5.333112
p20 X29i	-10.130743

Fig. 2 Overlapped average nTICs of glioblastoma (line) and metastasis (dashed line), discriminatory time-points highlighted by an X, and generated algorithms; everything obtained in the training set. Upper

row for enhancing tumor, lower row for peritumoral region. The algorithms depict the best percentile (p) for each time-point (X) and the relative power for each combination

model based on optimal time-points and optimal voxels. We obtained satisfactory results that provided up to 81% accuracy discrimination between glioblastoma and metastasis in the test set.

Reliable presurgical differentiation of GB and metastasis is crucial as management of these two entities differs significantly. While a suspected GB should undergo maximal safe gross surgical resection as treatment of choice, suspected metastases require systemic staging or re-staging before determining different local therapeutic approaches combined

with systemic treatments [3, 4]. For example, if a metastasis was surgically removed under the erroneous assumption of glioblastoma, the overall benefit of this potential morbid approach is lost or unknown [5, 6]. Moreover, improving the accuracy of the radiological assessment may be also relevant in patients with radiologically suspected GB, who are not candidates for specific therapeutic procedures due to their performance status or high basal morbidity, and in whom the final diagnostic assumption rests solely on neuroimaging [7]. This also applies in a vast majority of patients with

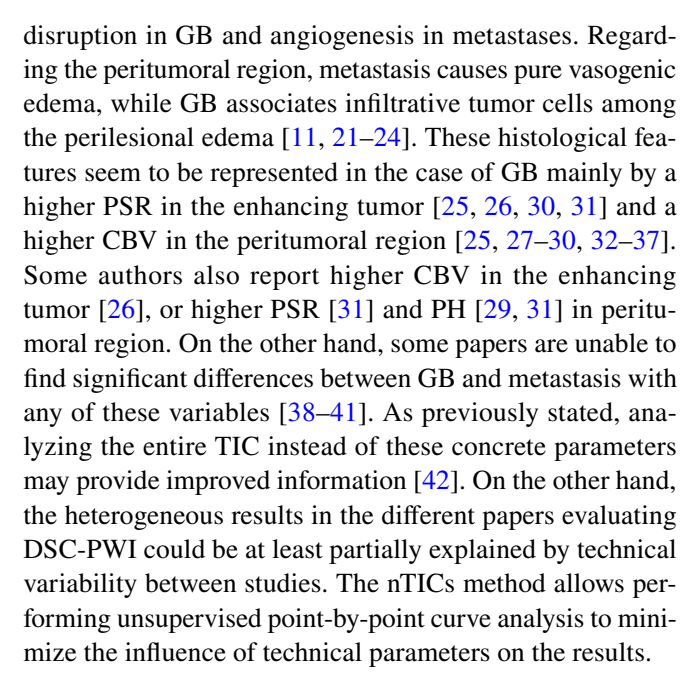


Table 2 Summary of the results in training and test subsets

	AUC	Accuracy	Sensitivity	Specificity
Enhancing t	umor	,		
Training	0.81	78% (114/146)	71% (52/73)	85% (62/73)
Test	0.79	71% (195/276)	84% (26/31)	69% (169/245)
Peritumoral	region			
Training	0.83	78% (114/146)	70% (51/73)	86% (63/73)
Test	0.71	65% (179/276)	55% (17/31)	66% (162/245)
Combined	Match	Accuracy	Sensitivity	Specificity
Training	72% (105/146)	88% (92/105)	86% (44/51)	89% (48/54)
Test	61% (169/276)	81% (135/169)	75% (13/16)	80% (122/153)

known systemic primary tumor and brain lesion suspicious of brain metastasis, who are directly treated for an assumed brain metastasis without confirmative histology [4], despite the knowledge that some of these tumors may end up not corresponding to the assumed histology [8]. These different scenarios in which the MR imaging diagnosis is the key to patient management warrant the highest possible diagnostic accuracy.

DSC-PWI is an MR imaging technique that can currently be performed on most MR imaging units and which provides a noninvasive in vivo assessment of microvascular systems. It consists of a dynamic temporal acquisition during the vascular first pass of a contrast bolus. The injection of gadolinium results in an initial reduction in T2 signal intensity of the tissue, followed by signal recovery during contrast washout. The TICs can be extracted from this process. Well-studied parameters such as CBV, PSR, or PH are generated from these curves. The CBV corresponds to the area under the curve and is usually measured relative to the NAWM (relative CBV). It has been correlated to histologic measurements of tumor vascularization [14, 20, 38]. The PSR and the PH are measured relative to the TIC baseline. PSR may quantify the predominant T1 effect (signal recovery above baseline) or T2 effect (signal recovery below baseline). These effects represent different leakage phenomena, which are explained by a complex combination of blood-brain barrier permeability, vascular volume fraction and vessel size, and tumor cell size and density [14, 17, 38]. The more recently popularized parameter PH is a measure with hypothetical parallelism to rCBV and also potentially related to tumor vascularization [29, 31]. Tumor vascularity is known to be different between GB and metastasis, and these differences could be monitored with DSC-PWI. Both tumors are heterogeneous, but their classical hallmarks are heterogeneous blood-brain barrier



DSC-PWI pulse-sequence parameters (flip angle and time of echo) influence curve morphology and thus affect the value of CBV and PSR, often paradoxically [16–18]. For this reason, the best results in the literature are obtained from homogeneous populations, but the best discriminatory parameters and thresholds vary between these studies. Meanwhile, those papers that do include technical heterogeneities, do not achieve optimal results. At this respect, our center's sample has changing DSC-PWI parameters between MRI scanners and between years, and may be a paradigm of heterogeneity, which is probably also the real-life scenario for most clinical centers worldwide. Indeed, this is why it is important to develop a method which can minimize the impact of technical variability on perfusion metrics. We hypothesize that in heterogeneous samples with non-standardized technical acquisition characteristics, the evaluation of the whole nTIC would be more powerful than standard approaches, as the paradoxical effects of pulse-sequence parameters would be better integrated.

Moreover, it is well known that GB and metastases are histologically highly heterogeneous tumors [21–24], so an approach which takes into account this heterogeneity by selecting the best predictive habitats seems necessary to obtain the best performing results. Most works in this field contemplate only mean, maximum, or minimum values for each evaluated parameter (CBV, PSR, PH). This kind of approach disregards most of the values contained within the whole tumor, even though the best discriminating value might not be one of these isolated metrics.

For all these reasons, we propose an approach for analyzing nTICs based on a volumetric voxel-by-voxel intensity-histogram evaluation of the enhancing tumor and the immediate peritumoral region with semi-unsupervised selection of the discriminatory time-points and



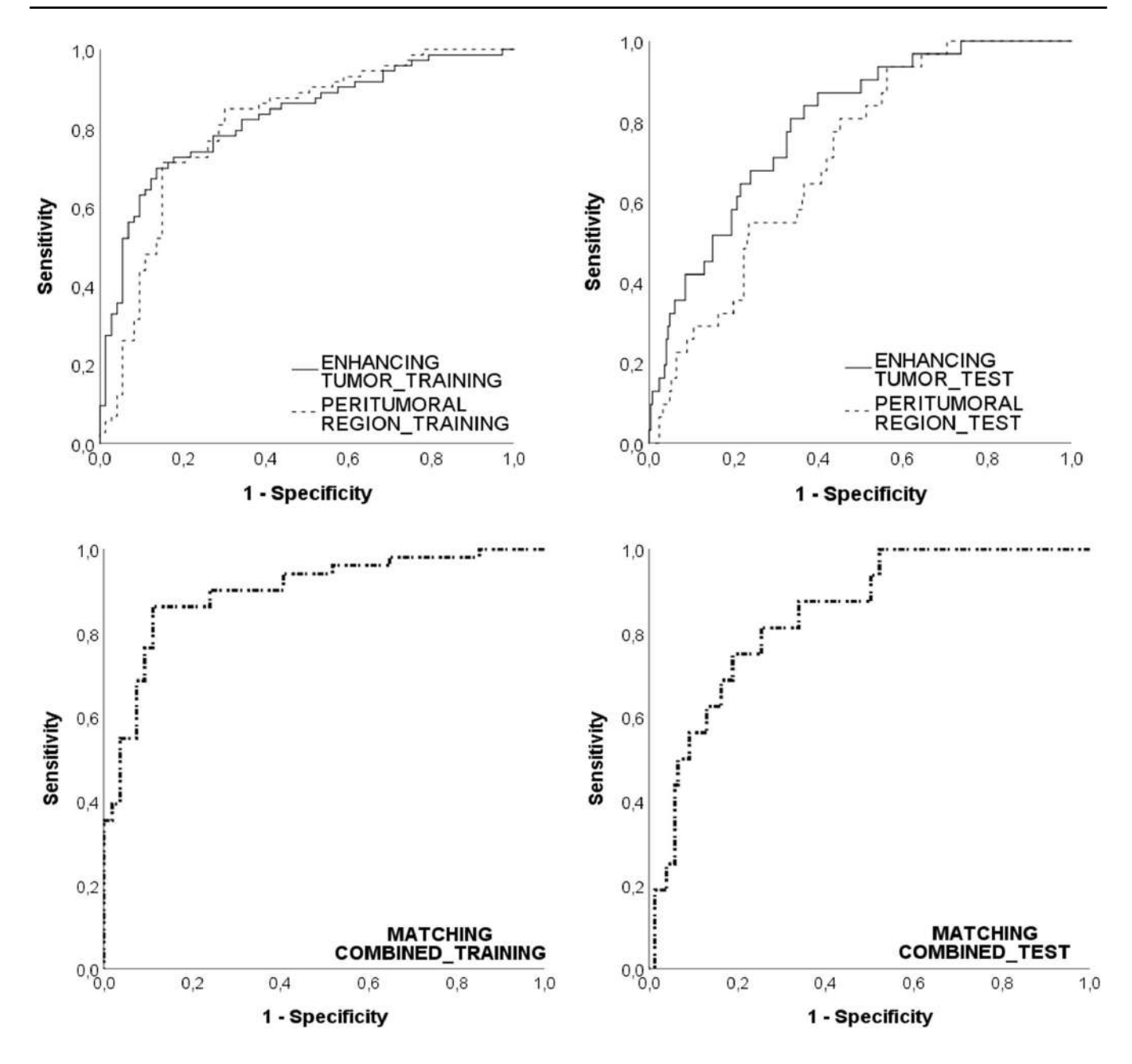


Fig. 3 Graphic representation of AUC-ROC in training (left) and test (right) groups, for enhancing tumor (line), peritumoral region (dashed line) and matching combinations (lower row). Training (enhancing tumor AUC=0.81, peritumoral region AUC=0.83, matching com-

bined AUC=0.90). Test (enhancing tumor AUC=0.79, peritumoral region AUC=0.71, matching combined AUC=0.84). All significant (p<0.00015)

voxel-intensity percentiles. With this approach, we aim to face the issue of tumors' vascular heterogeneity and maximize the discriminatory capacity of DSC-PWI. In summary, our approach not only minimizes the impact of physiological and technical variability, but also avoids the problem of choosing a concrete DSC-PWI parameter to analyze. We achieve these goals by selecting the most discriminatory time-points in the nTICs and then selecting the most discriminatory voxel-intensity percentile for those time-points.

Another potential weakness in DSC-PWI literature is the inhomogeneity in ROIs selection method. Many of these studies do not include the whole tumor, while others are operator dependent, focusing on extreme values such as "hot-spots" or tumor average. We minimized operator-dependent variability by performing volumetric segmentations of the whole enhancing tumor and statistical unsupervised selection of discriminatory variables without prior knowledge inputs.



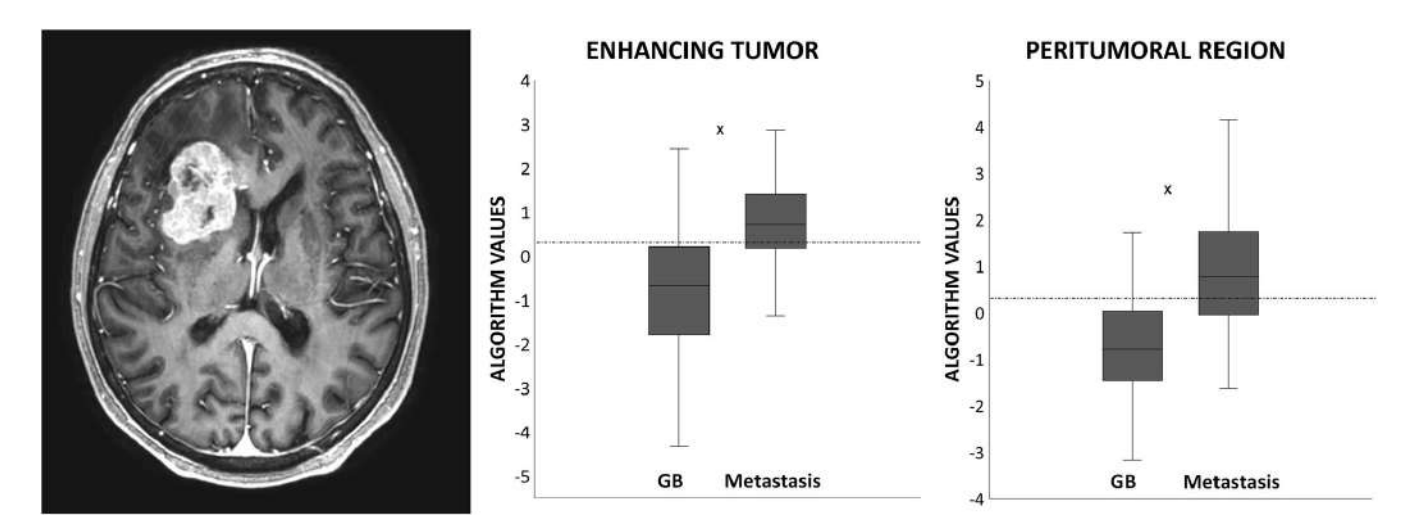


Fig. 4 Example problem case. Axial T1CE-wi shows an intraaxial, frontal and insular, enhancing, necrotic tumor which could correspond to a GB or to a single brain metastasis. The results of the algorithms applied to the problem case (represented by an X) are overlapped to scattered boxplots of our training set, those facilitating a

visual assessment of the diagnostic classification probability. In this problem case, the classification favors single brain metastasis for both the enhancing tumor and peritumoral region. Pathology confirmed this tumor corresponded to a renal cell carcinoma single brain metastasis

Some limitations of our paper must be considered. The single-site and retrospective character of the analysis may affect reproducibility, so multicentric and prospective studies in new real clinical scenarios are needed for validation. Nonetheless, our test subset results are promising in this regard. Secondly, the inclusion of a wide range of MR imaging examination dates and technical differences may have affected the consistency of results, although this could be considered a positive aspect in terms of generalizability of the method. Thirdly, balancing of cases between tumor types and training and test cohorts was necessary, to solve the biased excess of GB in our sample compared to the general population; however, our test data maintained the specific characteristics of our sample with excess GB, and nonetheless rendered still good results. Lastly, our method involves complex data processing, but we believe it is still easy to explain as a method intended to improve generalizability by means of nTIC methodology, and to extract the maximum information through the voxel-level percentile intensityhistogram analysis.

On the other hand, our study has several strengths: first, the large sample of patients included; second, the marked technical parameter heterogeneity, which supports credibility and generalizability; third, the minimal operator dependency with semiautomatic segmentation of enhancing components and automatization of the rest of the process; fourth, the use of a recently described method of perfusion-curve normalization, favoring reproducibility; fifth, the application of a completely novel perspective on perfusion-imaging analysis, which considers all time-points and all voxels for the diagnostic model generation, instead of isolated summary parameters; sixth, the aforementioned comprehensibility

which may lead to clinicians' trust in the method and results; and last, potential clinical implementation which could be achieved by developing user-friendly tools with visual displays similar to the one presented in Fig. 4.

Finally, we would like to highlight that we believe the currently proposed method is especially useful in situations in which tissue heterogeneity has important implications, such as this study's, but also in many others, such as radionecrosis versus tumor recurrence, progression versus pseudoprogression, or post-treatment high-grade tumor follow-up among others.

Conclusion

This proof-of-concept study presents a new perspective on DSC-PWI analysis beyond the interpretation of isolated parameters such as CBV, PSR, or PH and their mean or extreme values. Our novel method offers a minimally operator-dependent technique for analyzing every single time-point in the normalized perfusion curves and every single voxel in the tumor and peritumoral area to generate robust diagnostic models of special interest in heterogeneous tissues and heterogeneous populations. The method allowed satisfactory pre-surgical segregation of glioblastoma and metastases.

We also firmly believe that further development and application of this methodology may aid in bridging some of the many problems of comparability and heterogeneity in the field of MR perfusion imaging. It will facilitate data aggregation and result comparison between studies, promote



more robust and generalizable research, and ultimately favor large-scale analyses and clinical implementation.

Supplementary Information The online version contains supplementary material available at https://doi.org/10.1007/s00330-021-08498-1.

Acknowledgements The authors acknowledge support from the Instituto de Salud Carlos III (Proyectos de Investigación en Salud, PI20/00360).

Funding The authors state that this work has not received any funding.

Declarations

Guarantor The scientific guarantor of this publication is Albert Pons-Escoda.

Conflict of interest The authors declare no competing interests.

Statistics and biometry One of the authors has significant statistical expertise: Alonso Garcia-Ruiz (joint first author), Radiomics Group, Vall d'Hebron Institut d'Oncologia.

Informed consent Written informed consent was waived by the Institutional Review Board.

Ethical approval Institutional Review Board approval was obtained.

Study subjects or cohorts overlap Some study subjects or cohorts have been previously reported in Pons-Escoda A, Garcia-Ruiz A, Naval-Baudin P, Cos M, Vidal N, Plans G, Bruna J, Perez-Lopez R, Majos C. Presurgical Identification of Primary Central Nervous System Lymphoma with Normalized Time-Intensity Curve: A Pilot Study of a New Method to Analyze DSC-PWI. AJNR Am J Neuroradiol. 2020 Oct;41(10):1816-1824. https://doi.org/10.3174/ajnr.A6761. Epub 2020 Sep 17. PMID: 32943424; PMCID: PMC7661072.

Methodology

- retrospective
- diagnostic study
- performed at one institution

References

- Campos S, Davey P, Hird A et al (2009) Brain metastasis from an unknown primary, or primary brain tumour? A diagnostic dilemma. Curr Oncol 16:62–66. https://doi.org/10.3747/co.v16i1. 308
- Ostrom QT, Cioffi G, Gittleman H et al (2019) CBTRUS statistical report: primary brain and other central nervous system tumors diagnosed in the United States in 2012–2016. Neuro Oncol 21:v1–v100. https://doi.org/10.1093/neuonc/noz150
- Altwairgi AK, Raja S, Manzoor M et al (2017) Management and treatment recommendations for World Health Organization Grade III and IV gliomas. Int J Health Sci (Qassim) 11:54–62
- Enrique G-V, Irving S-R, Ricardo B-I, et al (2019) Diagnosis and management of brain metastases: an updated review from a radiation oncology perspective. J Cancer Metastasis Treat 5. https://doi. org/10.20517/2394-4722.2019.20
- 5. Morton LM, Onel K, Curtis RE, Hungate EA, Armstrong GT (2014) The rising incidence of second cancers: patterns of

- occurrence and identification of risk factors for children and adults. Am Soc Clin Oncol Educ B e57–e67. https://doi.org/10.14694/edbook_am.2014.34.e57
- Donin N, Filson C, Drakaki A et al (2016) Risk of second primary malignancies among cancer survivors in the United States, 1992 through 2008. Cancer 122:3075–3086. https://doi.org/10. 1002/cncr.30164
- Fuentes-Raspall R, Vilardell L, Perez-Bueno F et al (2011) Population-based incidence and survival of central nervous system (CNS) malignancies in Girona (Spain) 1994–2005. J Neurooncol 101:117–123. https://doi.org/10.1007/s11060-010-0240-7
- Patchell RA, Tibbs PA, Walsh JW et al (1990) A randomized trial of surgery in the treatment of single metastases to the brain. N Engl J Med 322:494–500. https://doi.org/10.1056/NEJM1 99002223220802
- Upadhyay N, Waldman AD (2011) Conventional MRI evaluation of gliomas. Br J Radiol 84:S107–S111. https://doi.org/10.1259/bjr/65711810
- Fink K, Fink J (2013) Imaging of brain metastases. Surg Neurol Int 4:209. https://doi.org/10.4103/2152-7806.111298
- Zhang J, Liu H, Tong H et al (2017) Clinical applications of contrast-enhanced perfusion MRI techniques in gliomas: recent advances and current challenges. Contrast Media Mol Imaging 1–27. https://doi.org/10.1155/2017/7064120
- Schmainda K (2016) Perfusion imaging for brain tumor characterization and assessment of treatment response. In: Handbook of neuro-oncology neuroimaging. Elsevier, pp 335–351
- 13. Shiroishi MS, Castellazzi G, Boxerman JL et al (2015) Principles of T 2 *-weighted dynamic susceptibility contrast MRI technique in brain tumor imaging. J Magn Reson Imaging 41:296–313. https://doi.org/10.1002/jmri.24648
- Welker K, Boxerman J, Kalnin A, Kaufmann T, Shiroishi M, Wintermark M (2015) ASFNR recommendations for clinical performance of MR dynamic susceptibility contrast perfusion imaging of the brain. AJNR Am J Neuroradiol 36:E41–E51. https://doi.org/10.3174/ajnr.A4341
- Willats L, Calamante F (2013) The 39 steps: evading error and deciphering the secrets for accurate dynamic susceptibility contrast MRI. NMR Biomed 26:913–931. https://doi.org/10.1002/nbm.2833
- Boxerman JL, Quarles CC, Hu LS et al (2020) Consensus recommendations for a dynamic susceptibility contrast MRI protocol for use in high-grade gliomas. Neuro Oncol 22:1262–1275. https://doi.org/10.1093/neuonc/noaa141
- Boxerman JL, Paulson ES, Prah MA, Schmainda KM (2013)
 The effect of pulse sequence parameters and contrast agent dose on percentage signal recovery in DSC-MRI: implications for clinical applications. AJNR Am J Neuroradiol 34:1364–1369. https://doi.org/10.3174/ajnr.A3477
- Leu K, Boxerman JL, Ellingson BM (2017) Effects of MRI protocol parameters, preload injection dose, fractionation strategies, and leakage correction algorithms on the fidelity of dynamic-susceptibility contrast MRI estimates of relative cerebral blood volume in gliomas. AJNR Am J Neuroradiol. https://doi.org/10.3174/ajnr.A5027
- Semmineh NB, Bell LC, Stokes AM, Hu LS, Boxerman JL, Quarles CC (2018) Optimization of acquisition and analysis methods for clinical dynamic susceptibility contrast MRI using a population-based digital reference object. AJNR Am J Neuroradiol 39:1981–1988. https://doi.org/10.3174/ajnr.A5827
- Paulson ES, Schmainda KM (2008) Comparison of dynamic susceptibility-weighted contrast-enhanced MR methods: recommendations for measuring relative cerebral blood volume in brain tumors. Radiology 249:601–613. https://doi.org/10.1148/ radiol.2492071659
- Pekmezci M, Perry A (2013) Neuropathology of brain metastases.
 Surg Neurol Int 4:245. https://doi.org/10.4103/2152-7806.111302



- Nduom EK, Yang C, Merrill MJ, Zhuang Z, Lonser RR (2013) Characterization of the blood-brain barrier of metastatic and primary malignant neoplasms. J Neurosurg 119:427–433. https://doi.org/10.3171/2013.3.JNS122226
- Klekner Á, Hutóczki G, Virga J et al (2015) Expression pattern of invasion-related molecules in the peritumoral brain. Clin Neurol Neurosurg 139:138–143. https://doi.org/10.1016/j.clineuro.2015. 09.017
- Fidler IJ (2015) The biology of brain metastasis. Cancer J 21:284– 293. https://doi.org/10.1097/PPO.000000000000126
- Mangla R, Kolar B, Zhu T, Zhong J, Almast J, Ekholm S (2011) Percentage signal recovery derived from MR dynamic susceptibility contrast imaging is useful to differentiate common enhancing malignant lesions of the brain. AJNR Am J Neuroradiol 32:1004–1010. https://doi.org/10.3174/ajnr.A2441
- Vallée A, Guillevin C, Wager M, Delwail V, Guillevin R, JV, (2018) Added value of spectroscopy to perfusion mri in the differential diagnostic performance of common malignant brain tumors. AJNR Am J Neuroradiol 39:1423–1431
- Blasel S, Jurcoane A, Franz K, Morawe G, Pellikan S, Hattingen E (2010) Elevated peritumoural rCBV values as a mean to differentiate metastases from high-grade gliomas. Acta Neurochir (Wien) 152:1893–1899. https://doi.org/10.1007/s00701-010-0774-7
- Tsougos I, Svolos P, Kousi E et al (2012) Differentiation of glioblastoma multiforme from metastatic brain tumor using proton magnetic resonance spectroscopy, diffusion and perfusion metrics at 3 T. Cancer Imaging 12:423–436. https://doi.org/10.1102/1470-7330.2012.0038
- Neska-Matuszewska M, Bladowska J, Sąsiadek M, Zimny A (2018) Differentiation of glioblastoma multiforme, metastases and primary central nervous system lymphomas using multiparametric perfusion and diffusion MR imaging of a tumor core and a peritumoral zone—searching for a practical approach. PLoS One 13:e0191341. https://doi.org/10.1371/journal.pone.0191341
- Cindil E, Sendur HN, Cerit MN et al (2021) Validation of combined use of DWI and percentage signal recovery-optimized protocol of DSC-MRI in differentiation of high-grade glioma, metastasis, and lymphoma. Neuroradiology 63:331–342. https://doi.org/10.1007/s00234-020-02522-9
- Cha S, Lupo JM, Chen MH et al (2007) Differentiation of glioblastoma multiforme and single brain metastasis by peak height and percentage of signal intensity recovery derived from dynamic susceptibility-weighted contrast-enhanced perfusion MR imaging. AJNR Am J Neuroradiol 28:1078–1084. https://doi.org/10.3174/ ajnr.A0484
- 32. Law M, Cha S, Knopp EA, Johnson G, Arnett J, Litt AW (2002) High-grade gliomas and solitary metastases: Differentiation by using perfusion and proton spectroscopic MR imaging. Radiology 222:715–721. https://doi.org/10.1148/radiol.2223010558
- 33. Rollin N, Guyotat J, Streichenberger N, Honnorat J, Tran Minh VA, Cotton F (2006) Clinical relevance of diffusion and perfusion magnetic resonance imaging in assessing intra-axial brain tumors. Neuroradiology 48:150–159
- 34. Wang S, Kim S, Chawla S et al (2011) Differentiation between glioblastomas, solitary brain metastases, and primary cerebral lymphomas using diffusion tensor and dynamic susceptibility contrast-enhanced MR imaging. AJNR Am J Neuroradiol 32:507–514. https://doi.org/10.3174/ajnr.A2333
- 35. Server A, Orheim TE, Graff BA, Josefsen R, Kumar T, Nakstad PH (2011) Diagnostic examination performance by using microvascular leakage, cerebral blood volume, and blood flow derived from 3-T dynamic susceptibility-weighted contrast-enhanced perfusion MR imaging in the differentiation of glioblastoma multiforme and brain me. Neuroradiology 53:319–330. https://doi.org/10.1007/s00234-010-0740-3

- Chiang IC, Kuo YT, Lu CY et al (2004) Distinction between high-grade gliomas and solitary metastases using peritumoral 3-T magnetic resonance spectroscopy, diffusion, and perfusion imagings. Neuroradiology 46:619–627. https://doi.org/10.1007/ s00234-004-1246-7
- Askaner K, Rydelius A, Engelholm S et al (2019) Differentiation between glioblastomas and brain metastases and regarding their primary site of malignancy using dynamic susceptibility contrast MRI at 3T. J Neuroradiol 46:367–372. https://doi.org/10.1016/j. neurad.2018.09.006
- Lee MD, Baird GL, Bell LC, Quarles CC, Boxerman JL (2019) Utility of percentage signal recovery and baseline signal in DSC-MRI optimized for relative CBV measurement for differentiating glioblastoma, lymphoma, metastasis, and meningioma. AJNR Am J Neuroradiol 40:1145–1450. https://doi.org/10.3174/ajnr.A6153
- Hakyemez B, Erdogan C, Bolca N, Yildirim N, Gokalp G, Parlak M (2006) Evaluation of different cerebral mass lesions by perfusion-weighted MR imaging. J Magn Reson Imaging 24:817–824
- Calli C, Kitis O, Yunten N, Yurtseven T, Islekel S, Akalin T (2006) Perfusion and diffusion MR imaging in enhancing malignant cerebral tumors. Eur J Radiol 58:394–403. https://doi.org/10.1016/j.ejrad.2005.12.032
- 41. Bulakbasi N, Kocaoglu M, Farzaliyev A, Tayfun C, Ucoz T, Somuncu I (2005) Assessment of diagnostic accuracy of perfusion MR imaging in primary and metastatic solitary malignant brain tumors. AJNR Am J Neuroradiol 26:2187–2189
- 42. Pons-Escoda A, Garcia-Ruiz A, Naval-Baudin P et al (2020) Presurgical identification of primary central nervous system lymphoma with normalized time-intensity curve: a pilot study of a new method to analyze DSC-PWI. AJNR Am J Neuroradiol 41:1816–1824. https://doi.org/10.3174/ajnr.A6761
- Louis DN, Ohgaki H, Wiestler OD et al (2007) The 2007 WHO classification of tumours of the central nervous system. Acta Neuropathol 114:97–109. https://doi.org/10.1007/s00401-007-0243-4
- Wen PY, Huse JT (2017) 2016 World Health Organization classification of central nervous system tumors. Contin Lifelong Learn Neurol 23:1531–1547. https://doi.org/10.1212/CON.00000000000000000000536
- Hochberg FH, Pruitt A (1980) Assumptions in the radiotherapy of glioblastoma. Neurology 30:907–907. https://doi.org/10.1212/ WNL.30.9.907
- Wallner KE, Galicich JH, Krol G, Arbit E, Malkin MG (1989) Patterns of failure following treatment for glioblastoma multiforme and anaplastic astrocytoma. Int J Radiat Oncol 16:1405–1409. https://doi.org/10.1016/0360-3016(89)90941-3
- 47. Gaspar LE, Fisher BJ, Macdonald DR et al (1992) Supratentorial malignant glioma: patterns of recurrence and implications for external beam local treatment. Int J Radiat Oncol 24:55–57. https://doi.org/10.1016/0360-3016(92)91021-E
- Liang BC, Thornton AF, Sandler HM, Greenberg HS (1991) Malignant astrocytomas: focal tumor recurrence after focal external beam radiation therapy. J Neurosurg 75:559–563. https://doi.org/10.3171/jns.1991.75.4.0559
- Mandrekar JN (2010) Receiver operating characteristic curve in diagnostic test ssessment. J Thorac Oncol 5:1315–1316. https:// doi.org/10.1097/JTO.0b013e3181ec173d
- 50. Tate AR, Underwood J, Acosta DM et al (2006) Development of a decision support system for diagnosis and grading of brain tumours usingin vivo magnetic resonance single voxel spectra. NMR Biomed 19:411–434. https://doi.org/10.1002/nbm.1016

Publisher's Note Springer Nature remains neutral with regard to jurisdictional claims in published maps and institutional affiliations.



Authors and Affiliations

Albert Pons-Escoda^{1,2} • Alonso Garcia-Ruiz³ • Pablo Naval-Baudin¹ • Francesco Grussu³ • Juan Jose Sanchez Fernandez¹ • Angels Camins Simo¹ • Noemi Vidal Sarro^{2,4} • Alejandro Fernandez-Coello^{5,6,7} • Jordi Bruna² • Monica Cos¹ • Raquel Perez-Lopez^{3,8} • Carles Majos^{1,2}

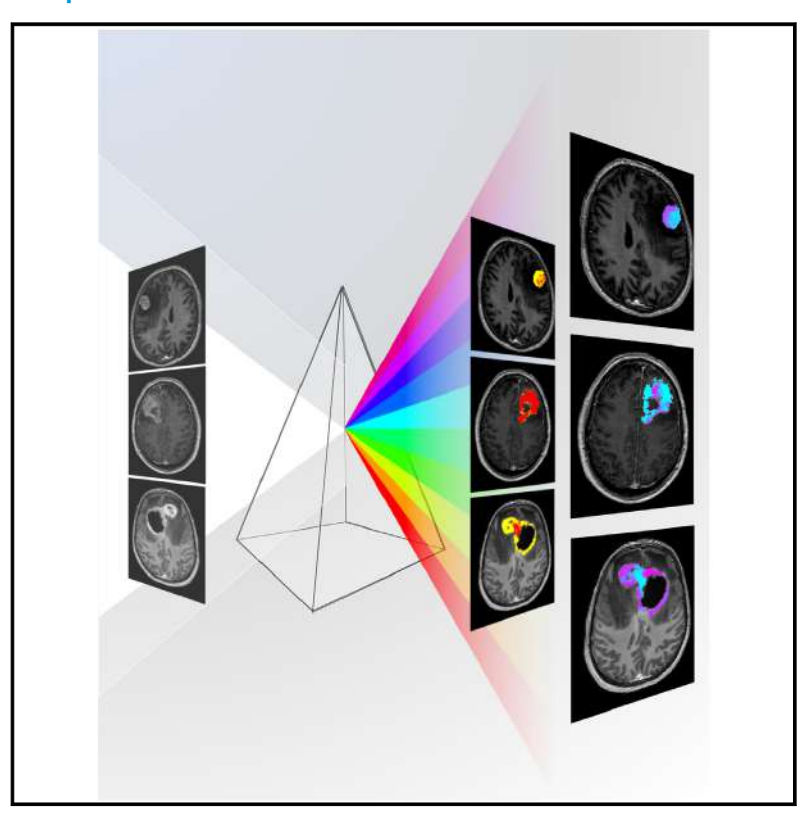
- Radiology Department, Institut de Diagnôstic per la Imatge-IDI, Hospital Universitari de Bellvitge, L'Hospitalet de Llobregat, Barcelona, Spain
- Neurooncology Unit, Institut d'Investigació Biomèdica de Bellvitge- IDIBELL, L'Hospitalet de Llobregat, Barcelona, Spain
- Radiomics Groups, Vall d'Hebron Institut d'Oncologia- VHIO, Barcelona, Spain
- Pathology Department, Hospital Universitari de Bellvitge, L'Hospitalet de Llobregat, Barcelona, Spain

- Neurosurgery Department, Hospital Universitari de Bellvitge, L'Hospitalet de Llobregat, Barcelona, Spain
- Pathology and Experimental Therapeutics Department, Anatomy Unit, University of Barcelona, Barcelona, Spain
- Biomedical Research Networking Centers of Bioengineering, Biomaterials and Nanomedicine (CIBER-BBN), Madrid, Spain
- ⁸ Radiology Department, Hospital Universitari Vall d'Hebron, Barcelona, Spain



An accessible deep learning tool for voxel-wise classification of brain malignancies from perfusion MRI

Graphical abstract



Authors

Alonso Garcia-Ruiz, Albert Pons-Escoda, Francesco Grussu, ..., Tyler M. Seibert, Carlos Majos, Raquel Perez-Lopez

Correspondence

rperez@vhio.net

In brief

Diagnosing brain tumors can be challenging, even with multiparametric MRI that includes vascular tumor evaluation through perfusion imaging. In this work, Garcia-Ruiz et al. developed a deep learning-based tool that leverages the full spatial and temporal information of perfusion MRI, outperforming conventional methods.

Highlights

- Voxel-wise approach enables training neural networks with limited patient cohorts
- DISCERN facilitates brain tumor classification to aid medical decisions
- DISCERN is a user-friendly tool designed for use with clinical perfusion MRI
- DISCERN enables accurate brain tumor diagnosis, surpassing conventional metrics







Article

An accessible deep learning tool for voxel-wise classification of brain malignancies from perfusion MRI

Alonso Garcia-Ruiz,^{1,10} Albert Pons-Escoda,^{2,3,10} Francesco Grussu,^{1,10} Pablo Naval-Baudin,² Camilo Monreal-Aguero,¹ Gretchen Hermann,⁴ Roshan Karunamuni,⁴ Marta Ligero,¹ Antonio Lopez-Rueda,⁵ Laura Oleaga,⁵ M. Álvaro Berbís,⁶ Alberto Cabrera-Zubizarreta,⁷ Teodoro Martin-Noguerol,⁷ Antonio Luna,⁷ Tyler M. Seibert,^{4,8,9} Carlos Majos,^{2,3} and Raguel Perez-Lopez^{1,11,*}

¹Radiomics Group, Vall d'Hebron Institute of Oncology (VHIO), 08035 Barcelona, Spain

²Radiology Department, Bellvitge University Hospital, 08907 Barcelona, Spain

³Neuro-Oncology Unit, Institut d'Investigacio Biomedica de Bellvitge (IDIBELL), 08907 Barcelona, Spain

⁴Radiation Medicine Department and Applied Sciences, University of California, San Diego, La Jolla, CA 92093, USA

⁵Radiology Department, Hospital Clínic de Barcelona, 08036 Barcelona, Spain

⁶Radiology Department, HT Medica, Hospital San Juan de Dios, 14012 Cordoba, Spain

⁷Radiology Department, HT Medica, 23008 Jaen, Spain

⁸Radiology Department, University of California, San Diego, La Jolla, CA 92093, USA

⁹Bioengineering Department, University of California, San Diego, La Jolla, CA 92093, USA

¹⁰These authors contributed equally

¹¹Lead contact

*Correspondence: rperez@vhio.net

https://doi.org/10.1016/j.xcrm.2024.101464

SUMMARY

Noninvasive differential diagnosis of brain tumors is currently based on the assessment of magnetic resonance imaging (MRI) coupled with dynamic susceptibility contrast (DSC). However, a definitive diagnosis often requires neurosurgical interventions that compromise patients' quality of life. We apply deep learning on DSC images from histology-confirmed patients with glioblastoma, metastasis, or lymphoma. The convolutional neural network trained on $\sim\!50,000$ voxels from 40 patients provides intratumor probability maps that yield clinical-grade diagnosis. Performance is tested in 400 additional cases and an external validation cohort of 128 patients. The tool reaches a three-way accuracy of 0.78, superior to the conventional MRI metrics cerebral blood volume (0.55) and percentage of signal recovery (0.59), showing high value as a support diagnostic tool. Our open-access software, Diagnosis In Susceptibility Contrast Enhancing Regions for Neuro-oncology (DISCERN), demonstrates its potential in aiding medical decisions for brain tumor diagnosis using standard-of-care MRI.

INTRODUCTION

Differential diagnosis between the most common brain malignancies (i.e., glioblastoma multiforme [GBM], brain metastasis from solid tumors, and primary CNS lymphoma [PCNSL]) represents a clinical unmet need because each of these entities requires a distinct therapeutic approach. 1–3 Although pathology evaluation of tumor samples remains the gold standard for diagnosis, it requires invasive neurosurgical procedures, with a significant risk of complications, and eventually can be confounded by the use of prior medication, such as steroids. 4,5

To overcome the need for surgery, magnetic resonance imaging (MRI) with intravenous contrast injection is being used as a noninvasive support system for differential diagnosis of brain malignancies. GBM, brain metastasis, and PCNSL represent up to 70% of all malignant brain tumors and more than 80% of contrast-enhancing tumors within the brain.⁶ Nevertheless, the

enhancing patterns on imaging exhibit a high degree of similarity across these tumor types, making differential diagnosis challenging even for experienced neuroradiologists.⁷⁻⁹

The noninvasive characterization of brain tumors on MRI has been an active subject of study for years, ^{10,11} gaining renewed interest with the application of recent machine learning techniques to imaging data. Among the existing literature, some studies have focused on differentiating GBM from solitary brain metastasis, either with anatomical GBM from solitary brain metastasis, either works have concentrated on the identification of PCNSL. Of particular significance is dynamic susceptibility contrast (DSC) perfusion MRI, which enables the visualization of vascular characteristics, including vascular density and permeability, and is proving to be valuable for brain tumor diagnosis. 9,10,18,20,22,27–37

DSC is a quantitative MRI technique that consists of a temporal T2*-weighted acquisition during the administration of a vascular





Cell Reports Medicine Article

contrast bolus. The contrast agent causes an initial decrease in the T2*-weighted signal intensity, followed by the signal recovery during washout. In DSC, every voxel in the image yields a unique dynamic curve that describes the temporal evolution of the T2*-weighted signal intensity and reflects local tissue vascular properties. The standard approach to analyze DSC is to derive metrics such as the relative cerebral blood volume (rCBV) and the percentage of signal recovery (PSR), both of which simplify the dynamic signal. The rCBV relates to the tumor vascular density with respect to normal tissue, and the PSR reflects the vascular permeability.³⁸ Both parameters remain the main focus of DSC analyses for tasks such as tumor type differentiation, grade stratification, and treatment response assessment. 28,39,40 However, among diverse clinically used DSC protocols, the performance of these parameters differs greatly, 38,41,42 which limits its use in routine clinical practice. Although recent multidisciplinary efforts have been made in the community to agree on a common procedure, 43-45 a global standardized DSC workflow is still lacking, regarding variations in the contrast preload settings, imaging parameters, and processing methods, all of which pose additional challenges to the generalizability of the technique and the establishment of reference rCBV/PSR values.

Regarding the use of DSC in aiding brain tumor diagnosis, it is worth noting that, with a few exceptions, ^{16,21,46} most studies to date have been designed to discriminate between two tumor types or pairs of malignancies. Furthermore, even fewer analyses can be found over large populations or validating external data, thus limiting the generalizability and clinical utility of the presented approaches.

DSC curve normalization and voxel-by-voxel analyses of the full dynamic range can overcome the limitations of conventional metrics and unlock the potential of DSC as a tool for differential diagnosis among the most common brain malignancies. Moreover, the application of deep learning techniques may enable new strategies of analysis and inference for dynamic data. In one of the first works exploring deep learning in DSC data, ⁴⁷ the authors described an end-to-end pipeline to obtain model-free perfusion metrics from the raw data. They used one-dimensional (1D) convolutional neural networks (CNNs) to characterize the dynamic DSC data of individual voxels. Park et al. ³⁴ developed an autoencoder and a clustering strategy to distinguish different brain areas, including pathologies, from the 1D dynamic data.

In this work, we describe the development and validation of an innovative, comprehensive framework for differential diagnosis of GBM, brain metastasis, and PCNSL, taking advantage of all of the time points of the normalized DSC (nDSC) data. The proposed Diagnosis In Susceptibility Contrast Enhancing Regions for Neuro-oncology (DISCERN) app provides voxel-by-voxel signatures of tumor type and is based on training 1D deep CNNs, with only a small number of pilot scans for a given DSC protocol. In the present study, we demonstrate the feasibility and accuracy of the method and show its superior performance compared to classifiers based on conventional DSC metrics. In addition, our method exhibits on par or higher diagnostic capabilities in comparison to those of expert neuroradiologists. The potential of DISCERN is to aid radiologists in interpreting brain MRI data, thereby enhancing the diagnostic capacity of experienced neuroradiologists and allowing less experienced radiologists to achieve a higher level of proficiency. To facilitate ease of use, we have designed a user-friendly interface with the ultimate goal of minimizing the need for invasive brain biopsies and guiding the selection of optimal treatment strategies in clinical practice.

RESULTS

Population demographics

In this multicenter, retrospective study, we analyzed MRI data from a total of 568 patients with biopsy-confirmed GBM, brain metastasis, or PCNSL. The classification model was developed and tested with 440 patients from a single center, and additional independent cohorts with varying imaging protocols were processed for external validation (Figure 1A). Further information about the study cohorts and classification results can be found in the STAR Methods and in Table S1. No statistically significant differences (p > 0.05) in terms of age and gender were observed between the three tumor types.

Development of a CNN for brain tumor classification

We trained our CNN classifier on a development cohort in which patients were randomly split into training and test sets. For the training set, we included 20 patients with PCNSL and 20 non-PCNSL patients (10 with GBM and 10 with metastasis). This provides a comparable number of voxels for each tumor type and each binary classification (i.e., PCSNL vs. non-PCNSL; GBM vs. metastasis for the non-PCNSL cases). The test set consisted of 25 patients with PCNSL, 85 with metastasis, and 290 with GBM (Figure 1). Approximately 50,000 nDSC curves from voxels of the enhancing region in the training group were used to train the classifier. Each nDSC curve corresponds to a specific spatial voxel of the enhancing tumor.

DISCERN outperforms standard classifiers for brain tumor diagnosis

Following a hierarchical classification approach, our CNN method successfully achieved three-way tumoral classification, outperforming the traditional perfusion metrics (i.e., rCBV and PSR) and standing out from simpler binary classifiers. Specifically, for the task of PCNSL diagnosis, DISCERN achieved superior performance, with an accuracy of 0.94 (95% confidence interval [CI]: 0.93-0.94), and mean rCBV and mean PSR classified patients with accuracies of 0.72 (95% CI: 0.70-0.74) and 0.84 (95% CI: 0.83-0.85), respectively. In a second step, patients not classified as PCNSL were categorized as GBM or brain metastasis. DISCERN differentiated GBM from metastases, with an accuracy of 0.81 (95% CI: 0.79-0.82). By contrast, the performance of standard DSC-derived metrics was markedly lower: rCBV classification achieved an accuracy of 0.69 (95% CI: 0.67-0.71) and a mean PSR of 0.65 (95% CI: 0.63-0.67). In Figure 2, the area under the receiver operating characteristic (AUC ROC) curves of the binary classifiers and 3-way average ROC curves are shown for both the DISCERN classifier and conventional rCBV/PSR. For PCNSL vs. non-PCNSL, the CNN provided a significantly higher AUC than rCBV (DeLong test against rCBV: p = 0.0019, against PSR, p = 0.4615). For GBM vs. metastasis, the CNN resulted in a higher AUC than rCBV and also than PSR (against rCBV: p = 0.0049, against PSR, p < 0.001).

Article



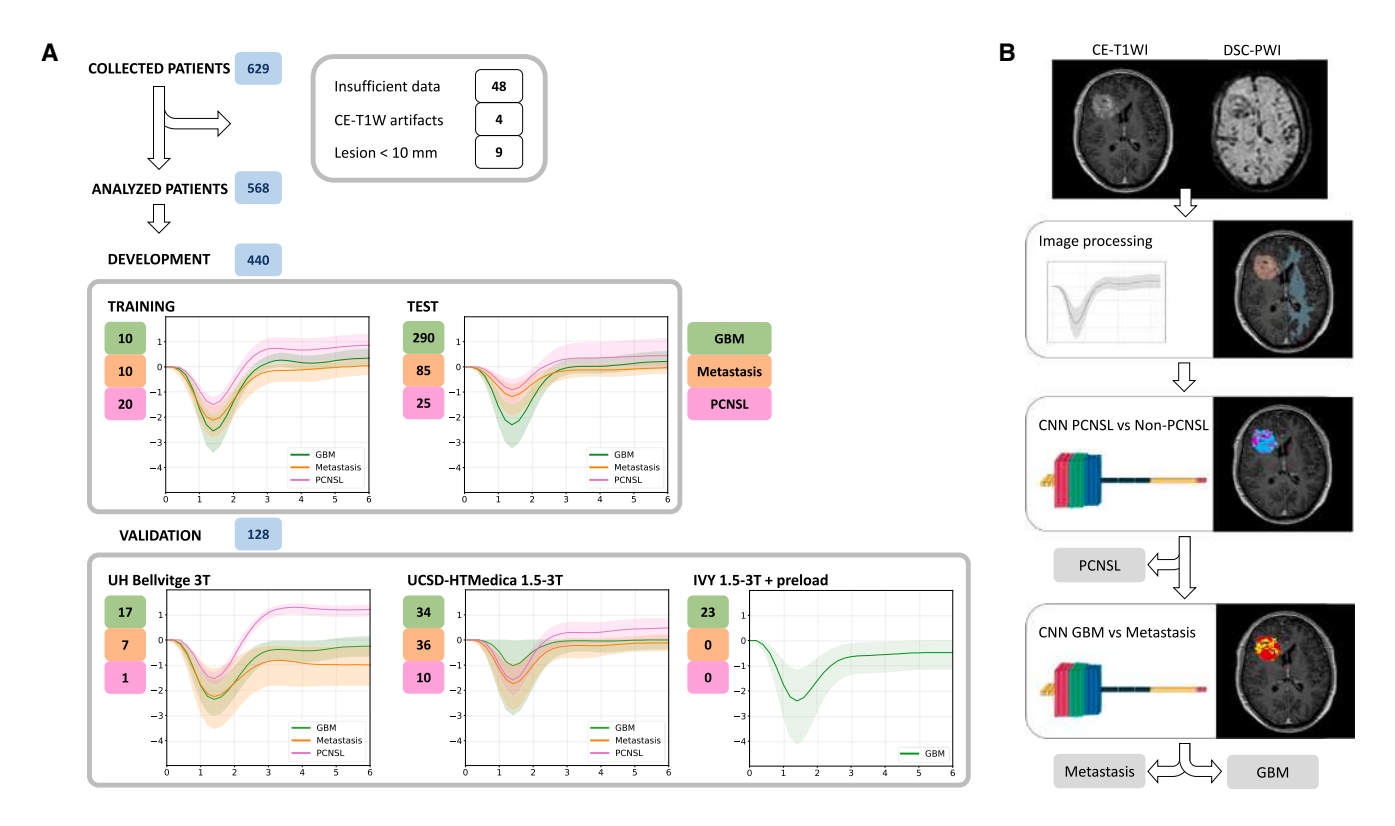


Figure 1. Summary of the population and study design

(A) Collected, excluded, and included data for analysis and further split into the development cohort and external validation cohorts. The number of patients for each tumor type and the respective nDSC perfusion distribution are shown for each cohort.

(B) Processing pipeline of the DISCERN app for 3-way tumor classification of DSC data. At the top, the input images of CE-T1WI for automated region of interest selection and DSC for classification are provided. DSC curves are then extracted voxel-wise from the enhancing tumor and normal white matter in the contralateral hemisphere. The dynamic DSC signals from the enhancing tumor are normalized (nDSC) to the white matter. Every nDSC is classified by 2 sequential CNNs, obtaining a probability map and an overall tumor classification. CE-T1WI, contrast-enhanced T1-weighted imaging.

Lastly, we mimicked a real-world clinical scenario in which our diagnostic support system is confronted with brain lesions comprising the three most common malignancies, in this case represented by the internal test dataset (unseen in the training). In this setting, DISCERN achieved an accuracy of 0.78 (95% CI: 0.76-0.79), which is substantially better than the three-way accuracy achieved using mean rCBV, 0.59 (95% CI: 0.57-0.60) and mean PSR, 0.55 (95% CI: 0.53-0.56). Furthermore, the combination of rCBV and PSR into a logistic regression model also yielded poor performance (Table S2). When validating DISCERN, the tool obtained a three-way classification accuracy of 0.71 evaluating 80 scans of patients from external centers, 0.72 on 25 cases from a 3T scanner (same center as the 1.5T development data), and 0.78 on 23 patients with GBM from the Ivy GAP public dataset (Table S3). These data underscore the potential of DISCERN for differentiating among the three most common clinical diagnostic challenges in patients with enhancing brain lesions.

Voxel-wise explainable representation of the CNN decision process

DISCERN provides spatial probability maps of tumor classification, which are then used to obtain a voxel proportion and a patient classification label. In Figure 2A, we present three examples per tumor type of the voxel-wise probability maps according to the DISCERN classifier. The probability maps are shown overlaid onto the CE-T1W MRI for anatomical references. Overall, the tumor type probability maps are smooth and identify the tumor type with high confidence in most voxels, even when intratumor signal heterogeneity is seen in the contrast-enhanced T1W scan. Voxels exhibiting a high probability of belonging to the incorrect tumor class tend to be located either in the boundary of the enhancing area or around necrotic intratumoral spots. This potentially reflects partial volume (i.e., inclusion of signal from tumor and nontumor areas within a voxel) or intratumoral heterogeneity.

Visual interpretation of the CNN classification

We further sought to implement Class Activation Mapping (CAM) to provide a visual explanation of the DISCERN classification network. The ScoreCAM⁴⁸ method yields a normalized score of the contribution of every input to the final classification of a CNN. This allows us to identify the most discriminative time points for nDSC differentiation. ScoreCAM spatial maps were obtained for each binary classification (Figure 3A). The CNN focuses mostly on the bolus passage to classify the central tumor region (middle row for PCNSL vs. non-PCNSL and lower row for GBM vs. metastasis



Cell Reports Medicine Article

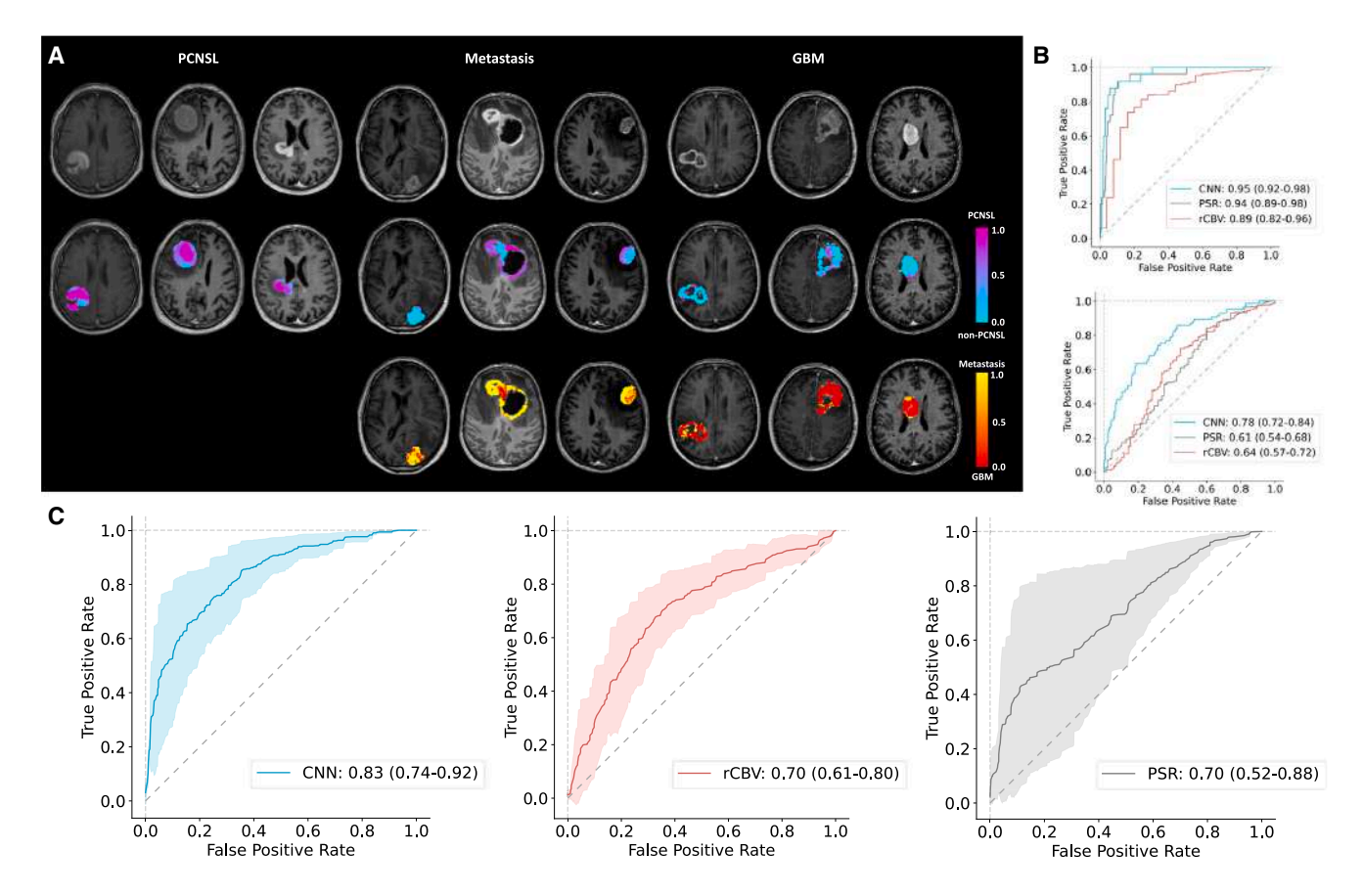


Figure 2. Probability maps and diagnostic performance of DISCERN

(A) Nine cases (3 per tumor type) correctly classified by DISCERN are shown, from left to right: PCNSL, metastasis, and GBM. In the upper row, a representative 2D slice of the CE-T1WI registered to the DSC with overlaid probability maps for PCNSL vs. non-PCNSL (center row) and for GBM vs. metastasis (lower row) of non-PCNSL cases

(B) ROC curves for binary classifiers PCNSL vs. non-PCNSL (top) and GBM vs. metastasis (bottom) for the proposed CNN, rCBV, and PSR. The CNN provided significantly higher AUC than rCBV for PCNSL vs. non-PCNSL and higher than rCBV and PSR for GBM vs. metastasis.

(C) Three-class ROC curves showing mean and SD of 2-class combinations, from left to right: the proposed CNN, rCBV, and PSR.

differentiation in Figure 3A). In contrast, the bolus passage seems less important for some voxels in surrounding regions. This suggests that the CNN effectively considered the bolus passage as a discerning characteristic, but also that it provides additional tissue perfusion differences compared to the raw perfusion signal (top row in Figure 3A).

The average ScoreCAM values per tumor type and per CNN classifier can be found in Figure 3B (upper row for PCNSL vs. non-PCNSL and lower row for GBM vs. metastasis differentiation). Overall, the sharper signal changes of the nDSC (i.e., steep slopes during contrast arrival and washout) have a higher contribution score. This is especially true for GBM, with greater differences in these time points with respect to the other two tumor types (average nDSC shown in black in Figure 3B). For PCNSL and metastasis, the last part of the signal is also considered important, which can be expected given the overall higher signal magnitude reached in these cases. Importantly, applying 1D CNNs over nDSC signals allowed analysis of the local changes of the signal over time. In this regard, methods that only consider the signal magnitude of specific time points, such as PSR, or a derived measurement such as rCBV, may overlook local nDSC

changes occurring over time that reflect specific physiological traits of the tumor.

A user-friendly app to aid brain tumor diagnosis

The DISCERN app was successfully implemented at the participating institutions for validating the tool in external cohorts, as illustrated in Figure 4 and Table S3. The tool requires approximately 2 min to process a new case and provides a classification outcome, in the form of (1) voxel-wise tumor type probability maps and (2) patient-wise tumor type. In addition, it shows the average nDSC for the enhancing tumor and white matter, as well as a visualization of the segmentation for the user to safely check the process. The mask can be automatically segmented from the enhancing tumor by DISCERN or it can be provided by the user. The DISCERN app provides a classification label with balanced sensitivity and specificity (Youden's index) by default, but a given clinical scenario may require a different classification threshold. To that end, sensitivities and specificities for every threshold are displayed, and the default settings can be changed.

In the benchmark study assessing the diagnostic efficacy of our tool in comparison to two neuroradiologists, notable





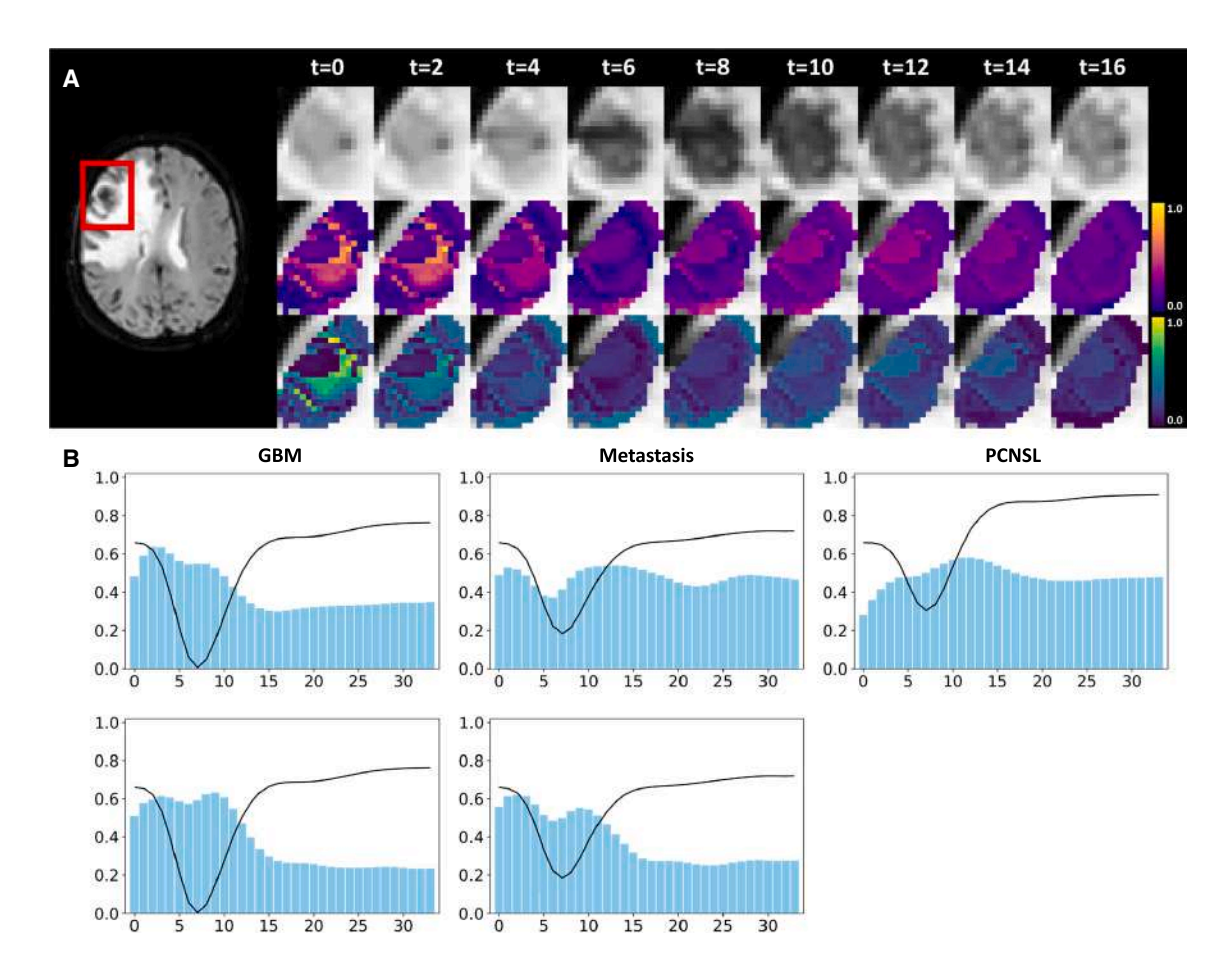


Figure 3. Visual interpretation of the CNN classification

(A) ScoreCAM spatial maps to further understand what the most discriminative nDSC time points for classification per voxel are. We show here a representative case of a metastasis in a 2D slice of the DSC (red box at leftmost). In the upper row, consecutive DSC dynamic time points, zoomed in on the lesion. In the center row, spatial importance score maps obtained with ScoreCAM for PCNSL vs. non-PCNSL and for GBM vs. metastasis in the lower row; the score was scaled to sum 1 over all time points in each voxel to observe relative importance in space.

(B) The average importance of each time point obtained from ScoreCAM that contributes to the tumor classification of nDSC curves, for PCNSL vs. non-PCNSL (upper row) and GBM vs. metastasis (lower row) differentiation; average tumor type nDSC in the training set is overlaid as a black solid line.

distinctions were observed between the senior and junior radiologists, achieving accuracies of 0.80 and 0.40, respectively (it is worth noting that a random chance accuracy is 0.33 in the three-way classification scenario). Within this subset, our tool demonstrated a commendable performance with an accuracy of 0.73, effectively identifying all of the instances of PCNSL by relying solely on perfusion-based information. Furthermore, in cases in which the radiologists exhibited elevated levels of uncertainty (16 out of 30 cases), our tool accurately diagnosed 11 out of these 16 instances (Figure S1). These results underscore the potential of the tool to enhance diagnostic accuracy and reliability, particularly in scenarios characterized by increased diagnostic complexity.

DISCUSSION

We present a voxel-wise method for analyzing perfusion scans with CNNs and improve brain cancer diagnosis, built upon prior DSC signal normalization.⁴⁹ By applying this method, we were

able to surpass the performance of previous models for noninvasive differential diagnosis of the most frequent malignant brain tumors (i.e., GBM, metastasis, and PCNSL, representing up to 70% of all malignant tumors in the brain⁶), which is critical to define an optimal treatment approach. Notably, our method showcases superior diagnostic capabilities compared to those of neuroradiologists. The potential of DISCERN is to assist radiologists in interpreting brain MRI data, amplifying the diagnostic proficiency of expert neuroradiologists and enabling less experienced counterparts to attain a heightened level of expertise.

Our deep learning framework takes advantage of the large amount of information provided by the thousands of voxelwise nDSC signals available in each individual DSC MRI scan, 47,50 and achieves optimal performance through training with a limited number of scans from a few patients at fixed DSC protocol (on the order of 30-40 cases). Our approach is particularly appealing for medical imaging applications, in which the design of robust deep learning methods is challenged by the limited number of scans available. In addition, our method



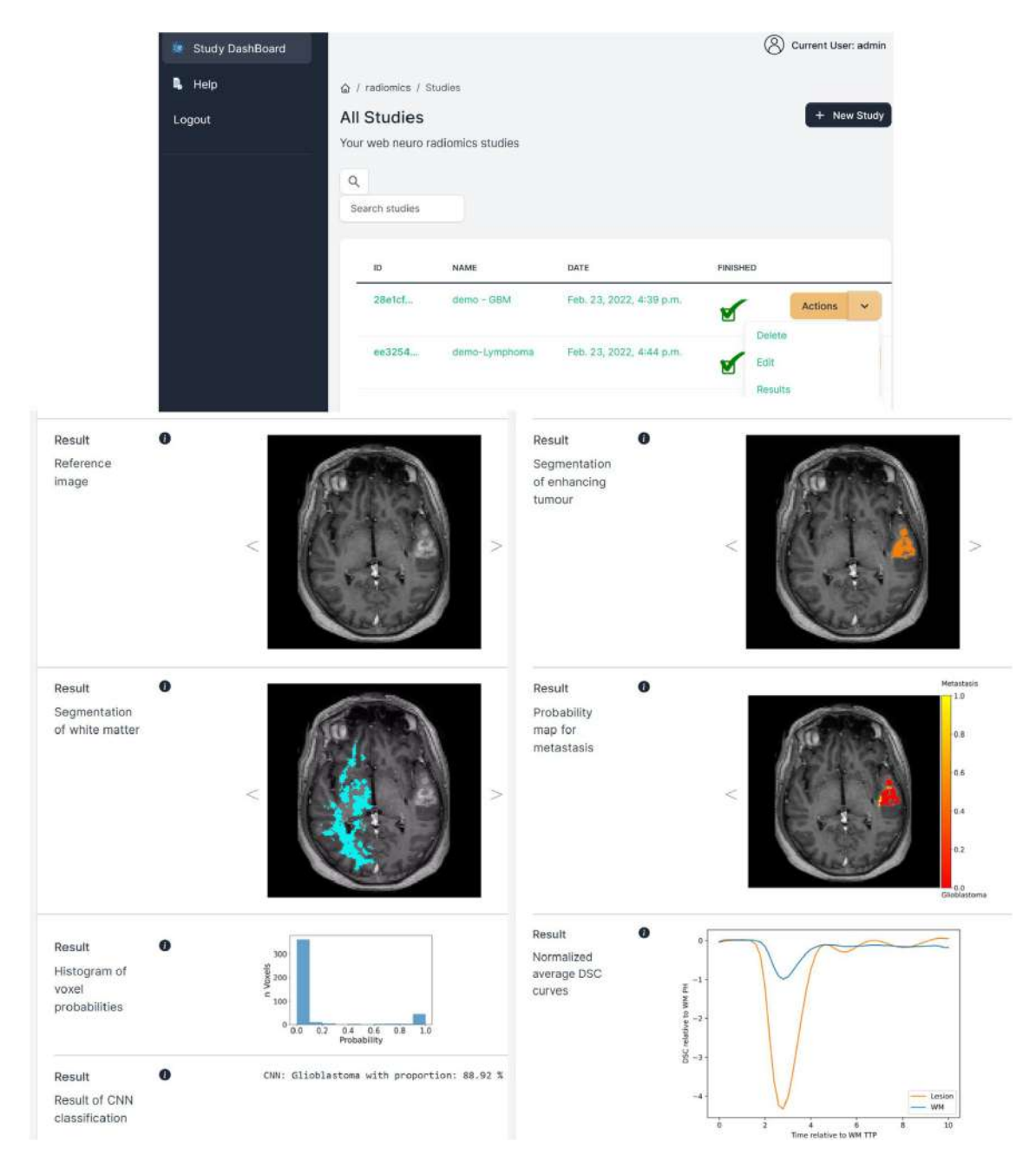


Figure 4. Implementation of the app with an easy-to-use interface

The image illustrates the web interface of the DISCERN app Docker, used to infer results for external validation cohorts. In the uppermost tile, the user dashboard shows the ongoing and finished studies in which to run the pipeline. The next tiles show the results, namely the reference image used for segmentation and respective enhancing tumor and white matter regions, the average nDSC curves of those regions, the tumor probability map and distribution, and a final classification result.

distinguishes between tumor types in a three-way classification task. This can be of particular relevance as a support tool for differential diagnosis in clinical practice, and is a considerable step forward as compared to the current literature, which is dominated by binary classification studies. 11-14,28

Although three other published works 16,21,46 have included different kinds of three-way classifications among the most common brain tumors (GBM, metastases, and lymphoma), they show some limitations. Liu et al. 16 used the three-way classification as a first step to select the metrics for further pairwise classifications. They considered T1w and T2w anatomical images, with DSC regarded as a future step to improve their results. Tariciotti et al.46 developed a three-way classification with multiparametric MRI data, using a 2D ResNet model, which would only take advantage of spatial information, but not of dynamic temporal information of DSC, and the reported performance of

Article



the model was only moderate. Wang et al.²¹ reported a two-step classification scheme similar to ours, and using only conventional DSC metrics, with the main limitation being the lack of validation in external cohorts.

In contrast, we present the largest dataset reported in this context. The voxel-by-voxel approach to the classification of DSC data takes advantage of inherently redundant information. Furthermore, the 1D CNN takes into account the changes in the temporal profile of the bolus passage, which other methods ignore or simplify. It also produces probability maps, facilitating the visual inspection of the spatial distribution of the classification. Finally, we have validated the results in external cohorts, demonstrating the generalizability and potential utility of our findings.

A noninvasive diagnostic support tool is especially relevant when considering PCNSL among potential diagnoses. Corticosteroids are a reasonable therapeutic option for mitigating neurological symptoms secondary to edema in patients with malignant brain tumors. However, early stereotactic biopsy before corticosteroid administration is mandatory when a brain PCNSL is suspected, because medication with steroids can alter the histological pattern of PCNSL.⁵ Moreover, PCNSL is highly sensitive to chemoradiotherapy instead of resection, which is contraindicated, as opposed to GBM or metastasis. Therefore, a reliable characterization of the tumor type by imaging is critical to devise the appropriate management of patients.

The DISCERN app provides voxel-wise tumor type probability maps, which are then used to obtain a voxel proportion and a patient classification label. The default Youden's index (tradeoff between sensitivity and specificity) can be changed to the needs of different clinical scenarios. For instance, some medical cases may require a very high specificity for suspected GBM and metastases with respect to PCNSL and, if all evidence supports it, then an additional intervention for a biopsy could be prevented. Therefore, the voxel proportion can be adjusted in the app to match the user's needs.

The presented method successfully achieved three-way tumoral classification, outperforming the traditional perfusion metrics, and standing out from simpler binary classifiers. When tested, our method performed with accuracies of 0.94 for PCNSL identification, 0.81 for differentiation of GBM from metastasis, and 0.78 for three-way classification.

Of note, the DSC protocol used for model development did not include contrast preload. Contrast preload is a common approach described in the literature to achieve a better estimate of the rCBV. 42 However, preload can be undesirable for a number of reasons. First, it delivers a higher contrast dose to the patient. Second, it can introduce potential variability sources, affecting the nDSC signal morphology. As countermeasures, leakage correction and acquisition parameters that minimize the T1 effect, such as low flip angle, have been shown to effectively yield reliable rCBV estimates without preload. 42,44 In this study, we only had access to retrospective data with high flip angle; consequently, rCBV was estimated with leakage correction, obtaining results comparable to those of PSR. The combination of both rCBV and PSR in logistic regression was explored for completeness, but it did not improve the results of the individual parameters. It is noteworthy that even though the DSC protocol used a nonoptimal flip angle for PSR or rCVB quantification, DISCERN achieved a good level of discriminatory performance. This was further confirmed by validating the results using heterogeneous external validation data, indicating a high level of robustness in the method.

A key feature of our CNN approach is the computation of voxel-wise spatial representations of perfusion curve characteristics in the form of maps describing the probability of a voxel to belong to a specific tumor type. Such spatial probability maps provide an explainable representation of the CNN decision process and may enable further studies of intratumor heterogeneity, making them an appealing tool for integrative multi-omics research and also of potential clinical interest to plan surgical procedures. Few studies have applied deep learning to voxelwise DSC signals in neuro-oncological applications. A recent study³⁴ used a deep autoencoder to derive a set of five descriptors of DSC that could differentiate between pairs of tumor types. However, the reconstructed time signals from such a minimal set of descriptors, in contrast to the original signal, produce a smooth perfusion curve morphology, which may omit relevant details for diagnostic applications.

In conclusion, the presented CNN framework for three-class brain tumor classification based on voxel-wise DSC signal analysis is feasible and outperforms classifiers built on conventional rCBV and PSR metrics. The method can be trained using a limited number of scans, which most centers are likely to have available, with notable generalization to external data. In addition, it provides voxel-wise maps of tumor type signatures that could be useful to visualize the CNN classification process and for tumor spatial characterization. As a way to make this tool more accessible and eventually make an impact in clinical practice, the proposed method has been implemented on the user-friendly DISCERN application, which is made freely accessible at http://84.88.64.102:5000/discern-app, to enhance study reproducibility and accelerate its adoption in future clinical studies.

Limitations of the study

The diagnostic tool DISCERN was trained with perfusion MRI data from scans without preload contrast injection, which may limit its performance on preloaded MRI scans. Tests on all eligible external 3T scans with a contrast preload of 23 patients with GBM from the IvyGAP⁵¹ dataset yielded 18 cases correctly classified as GBM (0.78 accuracy). Further testing in preload MRI scans should be performed to explore the generalizability of the results in this context.

The study used automatically segmented regions of interest, revised by an experienced neuroradiologist. However, the variability in segmentations among different neuroradiologists has not been explored. The proposed future segmentation methods aim to minimize manual input, but this aspect requires further development.

The training data were obtained from only 40 patients, which may introduce a bias toward the inherent characteristics of this subpopulation. To account for patient and scanner biases, we normalized the signals to those of white matter and we trained with an equal number of patients for every malignancy. As a limitation of the retrospective nature of this study, older diagnostic



Cell Reports Medicine Article

standards were in place and isocitrate dehydrogenase mutation status was missing from this study, which would provide a cleaner glioblastoma cohort.

The current algorithm is limited to certain MRI sequences (T1-weighted and perfusion MRI) and does not yet incorporate other potentially useful image data, such as diffusion MRI,⁵² which may offer more detailed insights into tumor microstructure and potentially improve the performance of the tool.

DISCERN is user-friendly and can classify three common brain tumors, but its application to other tumor types is still under development. In addition, although the framework shows promise, it requires further clinical qualification and approval for use as a medical diagnostic tool.

STAR*METHODS

Detailed methods are provided in the online version of this paper and include the following:

- KEY RESOURCES TABLE
- RESOURCE AVAILABILITY
 - Lead contact
 - Materials availability
 - O Data and code availability
- EXPERIMENTAL MODEL AND STUDY PARTICIPANT DETAILS
 - Cohort and clinical characteristics
- METHOD DETAILS
 - Patient eligibility
 - Imaging acquisition parameters
 - Data pre-processing
 - O Conventional DSC-PWI metrics
 - CNN architecture
 - O Classification scheme
 - Classification performance
 - O CNN interpretation
 - Utility in aiding medical decisions for brain tumor diagnosis
 - O Development of the online app DISCERN
- QUANTIFICATION AND STATISTICAL ANALYSIS

SUPPLEMENTAL INFORMATION

Supplemental information can be found online at https://doi.org/10.1016/j.xcrm.2024.101464.

ACKNOWLEDGMENTS

This project was supported by "La Caixa" Foundation (RTI2018-095209-B-C21) and the Spanish Ministry of Science and Innovation (FIS-G64384969). R.P.-L. is supported by the Prostate Cancer Foundation Young Investigator Award, the FERO Foundation, the CRIS Foundation Talent Award (TALENT19-05), the Instituto de Salud Carlos III Investigacion en Salud (PI21/01019), and the Asociacion Espanola Contra el Cancer (PRYCO211023-SERR). F.G. was funded by the Government of Catalonia (Beatriu de Pinos 2020 00117 BP) and by the Fundacio LaCaixa (ID 100010434, code LCF/BQ/PR22/11920010). C.M. and A.P.-E. acknowledge support from the Instituto de Salud Carlos III-Investigación en Salud (PI20/00360). We would like to express our sincere appreciation to Javier Carmona for his valuable support and assistance in reviewing the manuscript.

AUTHOR CONTRIBUTIONS

Conceptualization, C.M., A.P.-E., and R.P.-L. Methodology, A.G.-R., F.G., and A.P.-E. Software, C.M.-A. and R.K. Validation, G.H., R.K., T.M.S., A.L.-R., L.O., M.A.B., A.C.-Z., T.M.-N., A.L., and T.M.S. Formal analysis, A.G.-R. Investigation, A.G.-R., L.O., and A.C.-Z. Resources, C.M., A.P.-E., M.L., G.H., T.M.S., A.L.-R., L.O., M.A.B., A.C.-Z., T.M.-N., and A.L. Data curation, P.N.-B., A.P.-E., G.H., and M.A.B. Writing – original draft, A.G.-R. Writing – review & editing, R.P.-L., C.M., A.P.-E., P.N.-B., F.G., T.M.S., and A.G.-R. Funding acquisition, R.P.-L., C.M., and A.P.-E. Supervision, R.P.-L., C.M., and F.G.

DECLARATION OF INTERESTS

The authors declare no competing interests.

Received: August 30, 2023 Revised: November 16, 2023 Accepted: February 15, 2024 Published: March 11, 2024

REFERENCES

- Young, R.M., Jamshidi, A., Davis, G., and Sherman, J.H. (2015). Current trends in the surgical management and treatment of adult glioblastoma. Ann. Transl. Med. 3, 121.
- Hatiboglu, M.A., Wildrick, D.M., and Sawaya, R. (2013). The role of surgical resection in patients with brain metastases. Ecancermedicalscience 7:308.
- Hoang-Xuan, K., Bessell, E., Bromberg, J., Hottinger, A.F., Preusser, M., Rudà, R., Schlegel, U., Siegal, T., Soussain, C., Abacioglu, U., et al. (2015). Diagnosis and treatment of primary CNS lymphoma in immunocompetent patients: guidelines from the European Association for Neuro-Oncology. Lancet Oncol. 16, e322–e332.
- Dammers, R., Haitsma, I.K., Schouten, J.W., Kros, J.M., Avezaat, C.J.J., and Vincent, A.J.P.E. (2008). Safety and efficacy of frameless and frame-based intracranial biopsy techniques. Acta Neurochir. 150, 23–29.
- Chiavazza, C., Pellerino, A., Ferrio, F., Cistaro, A., Soffietti, R., and Rudà, R. (2018). Primary CNS Lymphomas: Challenges in Diagnosis and Monitoring. BioMed Res. Int. 2018, 3606970.
- Miller, K.D., Ostrom, Q.T., Kruchko, C., Patil, N., Tihan, T., Cioffi, G., Fuchs, H.E., Waite, K.A., Jemal, A., Siegel, R.L., and Barnholtz-Sloan, J.S. (2021). Brain and other central nervous system tumor statistics. CA A Cancer J. Clin. 71, 381–406.
- Leung, D., Han, X., Mikkelsen, T., and Nabors, L.B. (2014). Role of MRI in primary brain tumor evaluation. J. Natl. Compr. Cancer Netw. 12, 1561–1568.
- Arita, K., Miwa, M., Bohara, M., Moinuddin, F.M., Kamimura, K., and Yoshimoto, K. (2020). Precision of preoperative diagnosis in patients with brain tumor A prospective study based on "top three list" of differential diagnosis for 1061 patients. Surg. Neurol. Int. 11, 55.
- Chakravorty, A., Steel, T., and Chaganti, J. (2015). Accuracy of percentage
 of signal intensity recovery and relative cerebral blood volume derived
 from dynamic susceptibility-weighted, contrast-enhanced MRI in the preoperative diagnosis of cerebral tumours. NeuroRadiol. J. 28, 574–583.
- Law, M., Cha, S., Knopp, E.A., Johnson, G., Arnett, J., and Litt, A.W. (2002). High-grade gliomas and solitary metastases: differentiation by using perfusion and proton spectroscopic MR imaging. Radiology 222, 715–721.
- Fordham, A.J., Hacherl, C.C., Patel, N., Jones, K., Myers, B., Abraham, M., and Gendreau, J. (2021). Differentiating Glioblastomas from Solitary Brain Metastases: An Update on the Current Literature of Advanced Imaging Modalities. Cancers 13, 2960.

Article



- Artzi, M., Bressler, I., and Ben Bashat, D. (2019). Differentiation between glioblastoma, brain metastasis and subtypes using radiomics analysis. J. Magn. Reson. Imag. 50, 519–528.
- Bae, S., An, C., Ahn, S.S., Kim, H., Han, K., Kim, S.W., Park, J.E., Kim, H.S., and Lee, S.K. (2020). Robust performance of deep learning for distinguishing glioblastoma from single brain metastasis using radiomic features: model development and validation. Sci. Rep. 10, 12110.
- Qian, Z., Li, Y., Wang, Y., Li, L., Li, R., Wang, K., Li, S., Tang, K., Zhang, C., Fan, X., et al. (2019). Differentiation of glioblastoma from solitary brain metastases using radiomic machine-learning classifiers. Cancer Lett. 451, 128–135.
- Maurer, M.H., Synowitz, M., Badakshi, H., Lohkamp, L.N., Wüstefeld, J., Schäfer, M.L., and Wiener, E. (2013). Glioblastoma multiforme versus solitary supratentorial brain metastasis: differentiation based on morphology and magnetic resonance signal characteristics. Röfo 185, 235–240.
- Liu, D., Chen, J., Ge, H., Hu, X., Yang, K., Liu, Y., Hu, G., Luo, B., Yan, Z., Song, K., et al. (2022). Differentiation of malignant brain tumor types using intratumoral and peritumoral radiomic features. Front. Oncol. 12, 848846.
- Liu, Y., Xu, X., Yin, L., Zhang, X., Li, L., and Lu, H. (2017). Relationship between Glioblastoma Heterogeneity and Survival Time: An MR Imaging Texture Analysis. AJNR. Am. J. Neuroradiol. 38, 1695–1701.
- Lee, E.J., Ahn, K.J., Lee, E.K., Lee, Y.S., and Kim, D.B. (2013). Potential role of advanced MRI techniques for the peritumoural region in differentiating glioblastoma multiforme and solitary metastatic lesions. Clin. Radiol. 68, e689–e697.
- Yang, G., Jones, T.L., Barrick, T.R., and Howe, F.A. (2014). Discrimination between glioblastoma multiforme and solitary metastasis using morphological features derived from the p:q tensor decomposition of diffusion tensor imaging. NMR Biomed. 27, 1103–1111.
- Bauer, A.H., Erly, W., Moser, F.G., Maya, M., and Nael, K. (2015). Differentiation of solitary brain metastasis from glioblastoma multiforme: a predictive multiparametric approach using combined MR diffusion and perfusion. Neuroradiology 57, 697–703.
- 21. Wang, S., Kim, S., Chawla, S., Wolf, R.L., Knipp, D.E., Vossough, A., O'Rourke, D.M., Judy, K.D., Poptani, H., and Melhem, E.R. (2011). Differentiation between glioblastomas, solitary brain metastases, and primary cerebral lymphomas using diffusion tensor and dynamic susceptibility contrast-enhanced MR imaging. AJNR. Am. J. Neuroradiol. 32, 507–514.
- 22. Neska-Matuszewska, M., Bladowska, J., Sasiadek, M., and Zimny, A. (2018). Differentiation of glioblastoma multiforme, metastases and primary central nervous system lymphomas using multiparametric perfusion and diffusion MR imaging of a tumor core and a peritumoral zone-Searching for a practical approach. PLoS One 13, e0191341.
- 23. Swinburne, N.C., Schefflein, J., Sakai, Y., Oermann, E.K., Titano, J.J., Chen, I., Tadayon, S., Aggarwal, A., Doshi, A., and Nael, K. (2019). Machine learning for semi-automated classification of glioblastoma, brain metastasis and central nervous system lymphoma using magnetic resonance advanced imaging. Ann. Transl. Med. 7, 232.
- 24. Priya, S., Ward, C., Locke, T., Soni, N., Maheshwarappa, R.P., Monga, V., Agarwal, A., and Bathla, G. (2021). Glioblastoma and primary central nervous system lymphoma: differentiation using MRI derived first-order texture analysis - a machine learning study. NeuroRadiol. J. 34, 320–328.
- Alcaide-Leon, P., Dufort, P., Geraldo, A.F., Alshafai, L., Maralani, P.J., Spears, J., and Bharatha, A. (2017). Differentiation of Enhancing Glioma and Primary Central Nervous System Lymphoma by Texture-Based Machine Learning. AJNR. Am. J. Neuroradiol. 38, 1145–1150.
- Ahn, S.J., Shin, H.J., Chang, J.H., and Lee, S.K. (2014). Differentiation between primary cerebral lymphoma and glioblastoma using the apparent diffusion coefficient: comparison of three different ROI methods. PLoS One 9, e112948.
- Toh, C.H., Wei, K.C., Chang, C.N., Ng, S.H., and Wong, H.F. (2013). Differentiation of primary central nervous system lymphomas and glioblastomas: comparisons of diagnostic performance of dynamic susceptibility

- contrast-enhanced perfusion MR imaging without and with contrast-leakage correction. AJNR. Am. J. Neuroradiol. 34, 1145–1149.
- Cha, S., Lupo, J.M., Chen, M.H., Lamborn, K.R., McDermott, M.W., Berger, M.S., Nelson, S.J., and Dillon, W.P. (2007). Differentiation of glioblastoma multiforme and single brain metastasis by peak height and percentage of signal intensity recovery derived from dynamic susceptibility-weighted contrast-enhanced perfusion MR imaging. AJNR. Am. J. Neuroradiol. 28, 1078–1084.
- Lee, M.D., Baird, G.L., Bell, L.C., Quarles, C.C., and Boxerman, J.L. (2019). Utility of Percentage Signal Recovery and Baseline Signal in DSC-MRI Optimized for Relative CBV Measurement for Differentiating Glioblastoma, Lymphoma, Metastasis, and Meningioma. AJNR. Am. J. Neuroradiol. 40. 1445–1450.
- Barajas, R.F., Jr., Chang, J.S., Segal, M.R., Parsa, A.T., McDermott, M.W., Berger, M.S., and Cha, S. (2009). Differentiation of recurrent glioblastoma multiforme from radiation necrosis after external beam radiation therapy with dynamic susceptibility-weighted contrast-enhanced perfusion MR imaging. Radiology 253, 486–496.
- 31. Hu, L.S., Baxter, L.C., Pinnaduwage, D.S., Paine, T.L., Karis, J.P., Feuerstein, B.G., Schmainda, K.M., Dueck, A.C., Debbins, J., Smith, K.A., et al. (2010). Optimized preload leakage-correction methods to improve the diagnostic accuracy of dynamic susceptibility-weighted contrastenhanced perfusion MR imaging in posttreatment gliomas. AJNR. Am. J. Neuroradiol. 31, 40–48.
- 32. Kim, Y.E., Choi, S.H., Lee, S.T., Kim, T.M., Park, C.K., Park, S.H., and Kim, I.H. (2017). Differentiation between Glioblastoma and Primary Central Nervous System Lymphoma Using Dynamic Susceptibility Contrast-Enhanced Perfusion MR Imaging: Comparison Study of the Manual versus Semiautomatic Segmentation Method. Investig. Magn. Reson. Imaging 21, 9
- 33. Mangla, R., Kolar, B., Zhu, T., Zhong, J., Almast, J., and Ekholm, S. (2011). Percentage signal recovery derived from MR dynamic susceptibility contrast imaging is useful to differentiate common enhancing malignant lesions of the brain. AJNR. Am. J. Neuroradiol. 32, 1004–1010.
- Park, J.E., Kim, H.S., Lee, J., Cheong, E.N., Shin, I., Ahn, S.S., and Shim, W.H. (2020). Deep-learned time-signal intensity pattern analysis using an autoencoder captures magnetic resonance perfusion heterogeneity for brain tumor differentiation. Sci. Rep. 10, 21485.
- Pons-Escoda, A., Garcia-Ruiz, A., Naval-Baudin, P., Grussu, F., Fernandez, J.J.S., Simo, A.C., Sarro, N.V., Fernandez-Coello, A., Bruna, J., Cos, M., et al. (2022). Voxel-level analysis of normalized DSC-PWI time-intensity curves: a potential generalizable approach and its proof of concept in discriminating glioblastoma and metastasis. Eur. Radiol. 32, 3705–3715.
- 36. Surendra, K.L., Patwari, S., Agrawal, S., Chadaga, H., and Nagadi, A. (2020). Percentage signal intensity recovery: A step ahead of rCBV in DSC MR perfusion imaging for the differentiation of common neoplasms of brain. Indian J. Cancer 57, 36–43.
- Zhang, J., Liu, H., and Tong, H. (2017). Clinical Applications of Contrast-Enhanced Perfusion MRI Techniques in Gliomas: Recent Advances and Current Challenges. Contrast Media Mol. Imaging 2017, 7064120.
- 38. Bell, L.C., Hu, L.S., Stokes, A.M., McGee, S.C., Baxter, L.C., and Quarles, C.C. (2017). Characterizing the Influence of Preload Dosing on Percent Signal Recovery (PSR) and Cerebral Blood Volume (CBV) Measurements in a Patient Population With High-Grade Glioma Using Dynamic Susceptibility Contrast MRI. Tomography 3, 89–95.
- 39. Bell, L.C., Semmineh, N., An, H., Eldeniz, C., Wahl, R., Schmainda, K.M., Prah, M.A., Erickson, B.J., Korfiatis, P., Wu, C., et al. (2020). Evaluating the Use of rCBV as a Tumor Grade and Treatment Response Classifier Across NCI Quantitative Imaging Network Sites: Part II of the DSC-MRI Digital Reference Object (DRO) Challenge. Tomography 6, 203–208.
- Fu, R., Szidonya, L., Barajas, R.F., Jr., Ambady, P., Varallyay, C., and Neuwelt, E.A. (2022). Diagnostic performance of DSC perfusion MRI to



- distinguish tumor progression and treatment-related changes: a systematic review and meta-analysis. Neurooncol. Adv. 4, vdac027.
- 41. Boxerman, J.L., Paulson, E.S., Prah, M.A., and Schmainda, K.M. (2013). The effect of pulse sequence parameters and contrast agent dose on percentage signal recovery in DSC-MRI: implications for clinical applications. AJNR. Am. J. Neuroradiol. 34, 1364–1369.
- 42. Paulson, E.S., and Schmainda, K.M. (2008). Comparison of dynamic susceptibility-weighted contrast-enhanced MR methods: recommendations for measuring relative cerebral blood volume in brain tumors. Radiology 249, 601-613.
- 43. Boxerman, J.L., Quarles, C.C., Hu, L.S., Erickson, B.J., Gerstner, E.R., Smits, M., Kaufmann, T.J., Barboriak, D.P., Huang, R.H., Wick, W., et al. (2020). Consensus recommendations for a dynamic susceptibility contrast MRI protocol for use in high-grade gliomas. Neuro Oncol. 22, 1262-1275.
- 44. Schmainda, K.M., Prah, M.A., Hu, L.S., Quarles, C.C., Semmineh, N., Rand, S.D., Connelly, J.M., Anderies, B., Zhou, Y., Liu, Y., et al. (2019). Moving Toward a Consensus DSC-MRI Protocol: Validation of a Low-Flip Angle Single-Dose Option as a Reference Standard for Brain Tumors. AJNR. Am. J. Neuroradiol. 40, 626-633.
- 45. Open Science Initiative for Perfusion Imaging (OSIPI). (2023). OSIPI/osipi.github.io. GitHub. https://github.com/OSIPI.
- 46. Tariciotti, L., Ferlito, D., Caccavella, V.M., Di Cristofori, A., Fiore, G., Remore, L.G., Giordano, M., Remoli, G., Bertani, G., Borsa, S., et al. (2022). A Deep Learning Model for Preoperative Differentiation of Glioblastoma, Brain Metastasis, and Primary Central Nervous System Lymphoma: An External Validation Study. NeuroSci 4, 18-30.
- 47. Hess A, Meier R, Kaesmacher J Jung, S., Scalzo, F., Liebeskind, D., Wiest, R. and McKinley, R. Synthetic Perfusion Maps: Imaging Perfusion Deficits in DSC-MRI with Deep Learning. InBrainlesion: Glioma, Multiple Sclerosis, Stroke and Traumatic Brain Injuries: 4th International Workshop, BrainLes 2018, Held in Conjunction with MICCAI 2018, Granada, Spain, September 16, 2018, Revised Selected Papers, Part I 4 2019 (pp. 447-455). Springer International Publishing.
- 48. Wang, H., Wang, Z., Du, M., Yang, F., Zhang, Z., Ding, S., Mardziel, P., and Hu, X. (2020). Score-CAM: Score-Weighted Visual Explanations for Convolutional Neural Networks. In Paper presented at: 2020 IEEE/CVF Conference on Computer Vision and Pattern Recognition Workshops (CVPRW).
- 49. Pons-Escoda, A., Garcia-Ruiz, A., Naval-Baudin, P., Cos, M., Vidal, N., Plans, G., Bruna, J., Perez-Lopez, R., and Majos, C. (2020). Presurgical Identification of Primary Central Nervous System Lymphoma with Normalized Time-Intensity Curve: A Pilot Study of a New Method to Analyze DSC-PWI. AJNR. Am. J. Neuroradiol. 41, 1816–1824.
- 50. Grussu, F., Blumberg, S.B., Battiston, M., Kakkar, L.S., Lin, H., Ianuş, A., Schneider, T., Singh, S., Bourne, R., Punwani, S., et al. (2021). Feasibility

- of Data-Driven, Model-Free Quantitative MRI Protocol Design: Application to Brain and Prostate Diffusion-Relaxation Imaging. Front. Physiol. 9.
- 51. Shah, N., Feng, X., Lankerovich, M., Puchalski, R.B., and Keogh, B. (2016). Data from Ivy Glioblastoma Atlas Project (IvyGAP): The Cancer Imaging
- 52. Nilsson, M., Englund, E., Szczepankiewicz, F., van Westen, D., and Sundgren, P.C. (2018). Imaging brain tumour microstructure. Neuroimage 182, 232-250.
- 53. Puchalski, R.B., Shah, N., Miller, J., Dalley, R., Nomura, S.R., Yoon, J.G., Smith, K.A., Lankerovich, M., Bertagnolli, D., Bickley, K., et al. (2018). An anatomic transcriptional atlas of human glioblastoma. Science 360, 660-663.
- 54. Clark, K., Vendt, B., Smith, K., Freymann, J., Kirby, J., Koppel, P., Moore, S., Phillips, S., Maffitt, D., Pringle, M., et al. (2013). The Cancer Imaging Archive (TCIA): maintaining and operating a public information repository. J. Digit. Imag. 26, 1045-1057.
- 55. Data from the Multi-Institutional Paired Expert Segmentations and Radiomic Features of the Ivy GAP Dataset. The Cancer Imaging Archive (TCIA), (2020). https://wiki.cancerimagingarchive.net/pages/viewpage.action?pageId= 70222827.
- 56. Pati, S., Verma, R., Akbari, H., Bilello, M., Hill, V.B., Sako, C., Correa, R., Beig, N., Venet, L., Thakur, S., et al. (2020). Reproducibility analysis of multi-institutional paired expert annotations and radiomic features of the Ivy Glioblastoma Atlas Project (Ivy GAP) dataset. Med. Phys. 47, 6039-6052.
- 57. Fedorov, A., Beichel, R., Kalpathy-Cramer, J., Finet, J., Fillion-Robin, J.C., Pujol, S., Bauer, C., Jennings, D., Fennessy, F., Sonka, M., et al. (2012). 3D Slicer as an image computing platform for the Quantitative Imaging Network. Magn. Reson. Imaging 30, 1323-1341.
- 58. Louis, D.N., Ohgaki, H., Wiestler, O.D., Cavenee, W.K., Burger, P.C., Jouvet, A., Scheithauer, B.W., and Kleihues, P. (2007). The 2007 WHO classification of tumours of the central nervous system. Acta Neuropathol. 114,
- 59. van Gelderen, P., Duyn, J.H., Ramsey, N.F., Liu, G., and Moonen, C.T.W. (2012). The PRESTO technique for fMRI. Neuroimage 62, 676-681.
- 60. Tustison, N.J., Avants, B.B., Cook, P.A., Zheng, Y., Egan, A., Yushkevich, P.A., and Gee, J.C. (2010). N4ITK: improved N3 bias correction. IEEE Trans. Med. Imag. 29, 1310-1320.
- 61. Pohl, K.M., Bouix, S., Nakamura, M., Rohlfing, T., McCarley, R.W., Kikinis, R., Grimson, W.E.L., Shenton, M.E., and Wells, W.M. (2007). A hierarchical algorithm for MR brain image parcellation. IEEE Trans. Med. Imag. 26, 1201-1212.



STAR*METHODS

KEY RESOURCES TABLE

REAGENT or RESOURCE	SOURCE	IDENTIFIER
Deposited data		
Ivy GAP imaging dataset	Shah et al. 51,53,54	https://doi.org/10.7937/K9/TCIA.2016. XLwaN6nL
Segmentations for the Ivy GAP dataset	Pati et al. ^{55,56}	https://doi.org/10.7937/9j41-7d44
Trained models for DISCERN ("models" folder)	This paper; Zenodo; GitHub	https://doi.org/10.5281/zenodo.8301141 https://github.com/radiomicsgroup/ discern-app
Software and algorithms		
Code for DISCERN	This paper; Zenodo; GitHub	https://doi.org/10.5281/zenodo.8301141 https://github.com/radiomicsgroup/ discern-app
Dcm2niix	GitHub	https://github.com/rordenlab/dcm2niix
3D Slicer	Fedorov et al. ⁵⁷ ; website	https://doi.org/10.1016/j.mri.2012.05.001 https://slicer.org/
Python v3	Python Software Foundation	https://www.python.org

RESOURCE AVAILABILITY

Lead contact

All inquiries for further information regarding this work should be directed to and will be fulfilled by the lead contact, Raquel Perez-Lopez, 115-117 Natzaret, 08035 Barcelona, Spain (rperez@vhio.net).

Materials availability

No materials such as reagents or other products were generated in this study.

Data and code availability

- The datasets used in this study from Bellvitge Hospital, UC San Diego, and HT Medica health centers are not publicly available due to patient privacy concerns. To request access to the data, please contact the lead contact, who will connect you with the responsible researcher at each of the centers. Data will be accessible only if the Ethics Committee of each center where the data were collected grants permission. Therefore, the requester must describe the project for which data access is requested, detailing the objectives and data management plan. Data access will be considered for research purposes and non-commercial use only. To ensure patient privacy, access to personally identifiable information or sensitive clinical information (including medical histories) will not be provided, and requests for data access must rigorously adhere to the consent agreements established with study participants. Additional terms and conditions for accessing data by collaborating institutions may apply, as defined by the institutional Ethics Committee. The Ivy GAP dataset including MR DSC and T1w scans is publicly available and can be accessed through The Cancer Imaging Archive (https://doi.org/10.7937/K9/TCIA.2016.XLwaN6nL), as well as the annotated brain regions for the same dataset (https://doi.org/10.7937/9j41-7d44). The references and links for the datasets are listed in the key resources table.
- All the original codes and the trained models generated in this study are available under the folder "models" both in a repository at Zenodo (https://doi.org/10.5281/zenodo.8301141) and in a mirroring repository at GitHub (https://github.com/ radiomicsgroup/discern-app), both publicly accessible as of the date of publication. The DOIs and links are listed in the key resources table. Instructions for use can be found on the GitHub readme file.
- Any additional information required to reanalyse the data reported in this paper is available from the lead contact upon request.

EXPERIMENTAL MODEL AND STUDY PARTICIPANT DETAILS

Cohort and clinical characteristics

Data was retrospectively collected from multiple centers from patients with biopsy-confirmed GBM, brain metastasis or PCNSL. A total of 568 patients from three institutions (Bellvitge University Hospital, Spain; UC San Diego Health Center, USA; HT Medica Jaen, Spain) were included in the study.



Four hundred and forty patients (45 for PCNSL, 95 for metastasis and 300 for GBM) diagnosed from 2007 (2007 WHO criteria⁵⁸) to 2020 at Bellvitge University Hospital (Spain) with MRI available were included in the development cohort after image quality inspection and exclusion (Figure 1A). Patient demographics and clinical characteristics per groups are shown in Table S1.

Additional independent cohorts were included and processed for external validation: a) 80 patients from UC San Diego Health Center (USA) and HT Medica Jaen (Spain), b) 25 patients from Bellvitge University Hospital (Spain), acquired at magnet strength of 3T and c) 23 patients from the IvyGAP⁵¹ open database of patients with GBM and MRI scan with pre-bolus contrast administration, to account for the effect of different DSC protocols in the tool performance.

The research ethics committee of Bellvitge University Hospital (Barcelona, Spain) approved the study and informed consent was waived. The confidential data from patients were anonymized and protected in accordance with national and European regulations.

METHOD DETAILS

Patient eligibility

Eligibility criteria included: i) histologically confirmed diagnosis of GBM, single brain metastasis or PCNSL, ii) diagnostic MR scan on 1.5T or 3T including DSC and contrast-enhanced T1-weighted imaging (CE-T1WI) acquired prior to any oncological treatment and iii) a minimum of 10 mm of diameter of enhancing tumor in the CE-T1WI. Exclusion criteria included missing imaging data and poor image quality. The number of patients included can be seen in Figure 1A.

Imaging acquisition parameters

For the training and internal testing cohort, acquisitions were performed with 1.5T Philips scanners. The DSC dynamic sequences (gradient-echo echo-planar imaging and PRESTO⁵⁹) salient parameters were: TE of 24-40 ms, and FA of 75° (PRESTO 7°), acquired during a bolus administration of gadolinium contrast agent (gadobutrol 0.1 mmol/kg) without contrast preload.

The MRI scans from the development set were performed in 1.5T Philips scanners (219 on Ingenia and 221 on Intera). The DSC-PWI dynamic sequences (gradient-echo echo-planar imaging and PRESTO⁵⁹) salient parameters were: temporal sampling of 1.26-1.93 s, 40-60 timepoints, TR of 1640 ms (PRESTO 16 ms) TE of 24-40 ms, FA of 75° (PRESTO 7°) and in-plane resolution of 1.7 mm, acquired during a bolus administration of gadolinium contrast agent (gadobutrol 0.1 mmol/kg) without contrast preload.

The CE-T1WI main parameters were gradient-echo with repetition time (TR) of 6.58-25 ms, echo time (TE) of 3.17-5.49 ms, flip angle (FA) of 8°-30°, and spin-echo with TR of 535–625 ms, TE of 10–15 ms, FA of 70°-90°, all with in-plane resolution of 0.9 mm.

The acquisition details of the external datasets were as follows. The DSC-PWI protocol did not include contrast preload, the acquisition parameters were: TR of 1123-3031 ms, TE of 28-60 ms, FA of 40°-90° and in-plane resolution of 0.9 mm. Imaging was performed on Philips Achieva or Intera 1.5T (n = 55), Siemens Essenza (n = 4), Toshiba Vantage Elan 1.5T (n = 2), GE Signa HDxt 1.5T (n = 2), Philips Achieva 3T (n = 9), GE Signa Architect 3T (n = 5), GE Discovery 3T (n = 2) and Philips Panorama HFO 1T (n = 1).

Data pre-processing

The DSC dynamic sequence was motion-corrected by rigid registration of all DSC volumes. Bias field correction 60 was applied to the CE-T1WI, which was rigidly registered to the DSC. Brain region masking was obtained on the CE-T1WI using a hierarchical approach, 61 used for normal-appearing white matter segmentation and to split the brain into hemispheres. The white matter in the hemisphere contralateral to the tumor was selected once the tumor segmentation was available. Segmentations of the enhancing tumor were first obtained automatically by intensity thresholding on the image histogram. Specifically, an intensity threshold was set on the histogram right tail (voxels with high intensities) at the intensity where the histogram density falls below the mean histogram density. This result was followed by morphological operations to remove spurious voxels and small objects such as vessels. The segmentations were afterward revised by an experienced neuroradiologist.

The DSC signal reflecting the bolus passage in every voxel of the MRI sequence were extracted for the aforementioned enhancing tumor and white matter regions. According to a previously presented normalisation method, 23 the intensity and timescale of the DSC curves from the enhancing tumor were normalised (nDSC) to the white matter, interpolating to the same time resolution, providing comparable data among voxels of the same patient and between patients. The minimum peak point of the nDSC signals was retrieved, the curves were aligned to this point and signals with points within the average plus and minus standard deviation were used for training the CNNs, to avoid training on low signal or high noise data. Slicer⁵⁷ (www.slicer.org) and Python 3.8 were used for segmentation, processing, training, inference and statistical tests.

Conventional DSC-PWI metrics

Standard metrics of DSC analyses were obtained to compare against our voxel-trained CNN. The T2*-weighted signal S from a DSC-PWI sequence can be expressed as:

$$S \propto e^{-\frac{TE}{T2^*}}; \frac{1}{T2^*} = R2^*$$

Article



With R2* representing the relaxation rate. In a dynamic acquisition, a signal S(t) is acquired at n discrete time points t = [0,1,2,...,n]during the contrast bolus passage. The change in relaxation rate $\Delta R2^*(t)$ is proportional to the contrast concentration C(t), and can be obtained as follows:

$$C_t \propto \Delta R2_t^* = R2_t^* - R2_0^* = -\frac{1}{TE} ln \frac{S_t}{S_0}$$

The relative cerebral blood volume (rCBV) was obtained as the area under the ΔR2* curve with leakage correction using Slicer.⁵⁷ The percentage of signal recovery (PSR) was defined as the ratio of the recovered DSC-PWI signal over the baseline signal, as follows:

$$PSR = \frac{(S_r - S_{min})}{(S_b - S_{min})} \cdot 100$$

Where Smin is the minimum peak point reached by the perfusion curve, Sb is the baseline perfusion signal before contrast bolus arrival and Sr is the recovered signal after bolus passage.

CNN architecture

A 1D convolutional neural network (CNN) allows to take advantage of the convolution operation over the dynamic nDSC curves, considering the intensity change in a window of neighboring timepoints of size equal to the kernel size.

To take into account the information over different time windows, a CNN was designed with three 1D convolutional layers with kernel sizes [3,5,7]. A small size would mean looking at the closest neighbor timepoints and considering immediate changes in the dynamic signal, while bigger kernel sizes would consider further neighbor timepoints, therefore capturing the signal change over a longer time period. By including three possible kernel sizes, we expected to make the model more flexible toward heterogeneous nDSC input signals.

The convolutional layers were followed by a 10% dropout layer and max pooling layer (pool size 2). Because in the previous layers we extracted many features, these layers act as a filter to retain only relevant information: the dropout layer discards data from the previous layer and the max pooling layer down-samples the information into a smaller size. By reducing the number of features, these steps are meant to prevent overfitting and improve generalizability.

Finally, the output was concatenated into a dense layer with 100 nodes of rectified linear units and a final binary output layer with softmax activation, cross-entropy loss function and Adam optimizer. The internal parameters of the CNN were self-optimised during training and internal validation, and hyper-parameters were set experimentally as: batch size of 5000, maximum number of epochs of 3000 with a stopping condition of 50 iterations without validation loss improvement. The CNN was built using Tensorflow v2 with Keras frontend. The CNN classifier receives a given nDSC as input and outputs a binary probability.

Classification scheme

By applying the CNN classifier voxel-by-voxel, a probability map is obtained over the enhancing tumor region. These voxel-wise probabilities are then converted into a patient-wise classification as:

$$voxel\ proportion = \frac{n_{confident\ type\ 1}}{n_{confident\ type\ 1} + n_{\ confident\ type\ 2}}\ . \tag{Equation\ 1}$$

Above, $n_{confident type \ 1}$ is the number of voxels with a probability higher than 0.9 for one tumor type and $n_{confident type \ 2}$ is the number of voxels with a probability higher than 0.9 for the second tumor type on the binary classifier. The tumor type of each patient was inferred by applying Youden's index (highest sum of specificity and sensitivity in the training set) to the voxel proportion above. In practice, a 3-class classifier differentiating between PCNSL, GMB and metastases was implemented by concatenating two 2-class classifiers. The first classifier distinguishes PCNSL from non-PCNSL cases, the least frequent of the three malignancies, while the second classifier differentiates the non-PCNSL cases into GBM or metastasis (Figure 1). This allows obtaining binary classification performance to compare with other binary methods and to apply ROC curves.

Classification performance

Classification accuracy, sensitivity and specificity were obtained for 100 groups of 25 randomly-selected patients from the test cohort in order to obtain average classification performance and 95% confidence intervals (CI) for all classifiers, as reported in Table S2.

In addition, the area under the ROC curve was obtained for binary classifications, which shows the trade-off between sensitivity and specificity of different classification thresholds (Figure 2B). The thresholds were set by Youden's index as described above, but the app allows users to change them to meet different clinical needs, as discussed. Average ROC curves were obtained for the 3-class problem (Figure 2C).

Classification metrics and ROC curves were obtained for PSR and rCBV applying the same classification structure used for the CNN-based approach.



To compare the proposed approach with the performance of different machine learning algorithms, we built Random Forests and Support Vector Machine models from the rCBV and PSR values, following the classification scheme described for the CNN, i.e., applying binary classifications consecutively. Training was performed on the 40 subjects of the training dataset and tested on the test set of 400 subjects. A Random Forests hyperparameter search was performed with 5-fold cross-validation and the best parameters applied were maximum depth of 1 and 500 trees, and an overall 3-way accuracy of 0.61. A Support Vector Machine classification model with radial kernel was also trained with 5-fold cross-validation and the best hyperparameters found were gamma = 1 and C = 10, with a three-way accuracy of 0.37 (Table S4).

CNN interpretation

The CNN provides a tumour-type probability value from each nDSC signal found in each voxel. The map inherently informs about the decision process of the CNN classifier toward one tumor type or another and, more importantly, about the confidence of the classification in spatial regions.

To further explore the features that the CNN associated with each tumor type, down to the individual timepoints of the nDSC curve, we applied a score-weighted visual explanation for CNNs (ScoreCAM⁴⁸). On Figure 3A, the importance score was scaled to sum 1 over all timepoints in every voxel, in order to see the spatial relative importance. On Figure 3B, the average importance score is shown in each timepoint for each tumor type, with the average tumor nDSC from the training data overlaid in black, in order to see the temporal differences.

Utility in aiding medical decisions for brain tumor diagnosis

A benchmark diagnostic study was conducted to assess and compare the performance of DISCERN with that of expert neuroradiologists. The study also aimed to evaluate the potential improvement in diagnostic accuracy when DISCERN was utilised to support medical decision-making. For this purpose, two expert neuroradiologists with 10 and more than 20 years of experience in the field were selected. They were blinded to each other's assessments and also to the histopathological diagnosis results. The participants evaluated 30 cases, corresponding to 10 per each tumor type randomly distributed. The neuroradiologists had access to the MRI scans, given all imaging sequences (including T1w pre and post-contrast and the DSC maps), age and gender. To facilitate the evaluation process, each case was labeled by the neuroradiologists across four categories, ranging from "very unlikely" to "very likely," based on the likelihood and confidence of their diagnosis for each tumor type. A final diagnosis per radiologist was reached by considering the malignancy for which each radiologist estimated the highest likelihood, and then compared with the results from the tool. To measure the confidence in diagnosing, accounting for multiple answers for a given patient, we assigned scores (0.75 to "very likely", 0.25 to "likely" and "unlikely", 0 to "very unlikely") and applied:

Confidence =
$$max\{A\} * \left(1 + max\{A\} - \sum_{a \in A} a\right)$$

Where 'A' is the set of answers 'a' for each patient. This function gives a maximum confidence score when assigning "very likely" to one malignancy and "very unlikely" to the others. The results of this subanalysis are shown in Figure S1.

Development of the online app DISCERN

The processing and classification pipeline was bundled into a Docker image which can run as a standalone application in any system (Figure 4). The user can input their anonymized DSC and CE-T1WI scans in raw DICOM, Nifti or NRRD formats and, optionally, their own segmentations. When the study is processed, the tool shows the average nDSC curve, the result of the classification and the spatial probability map. For demonstrative purposes, the DISCERN app can be accessed at http://84.88.64.102:5000/ discern-app for research purposes.

QUANTIFICATION AND STATISTICAL ANALYSIS

Statistical tests were performed to compare: (i) patient age distribution between training and test sets of each tumor type (Welch's t-test), as well as among tumor types (one-way ANOVA); (ii) patient gender distribution between training and test sets of each tumor type (Fisher's exact test), as well as among tumor types (Chi-square test). Relations are shown in Table S1. The DeLong test was used to compare differences in AUC between ROC curves. Statistical significance was considered for p < 0.05. Variable names and abbreviations are explained in each figure or table legend, numbers in tables are explained in the heading of each column.

NEURO





MR dynamic-susceptibility-contrast perfusion metrics in the presurgical discrimination of adult solitary intra-axial cerebellar tumors

Albert Pons-Escoda^{1,2} • Alonso Garcia-Ruiz³ • Clemente Garcia-Hidalgo⁴ • Ruben Gil-Solsona⁵ • Pablo Naval-Baudin¹ • Teodoro Martin-Noguerol⁶ • Alejandro Fernandez-Coello^{2,7,8} • Susanie Flores-Casaperalta¹ • Montserrat Fernandez-Viñas¹ • Pablo Gago-Ferrero⁵ • Laura Oleaga⁹ • Raquel Perez-Lopez³ • Carles Majos^{1,2}

Received: 27 April 2023 / Revised: 16 May 2023 / Accepted: 30 May 2023 / Published online: 13 July 2023 © The Author(s), under exclusive licence to European Society of Radiology 2023

Abstract

Objectives Adult solitary intra-axial cerebellar tumors are uncommon. Their presurgical differentiation based on neuroimaging is crucial, since management differs substantially. Comprehensive full assessment of MR dynamic-susceptibility-contrast perfusion-weighted imaging (DSC-PWI) may reveal key differences between entities. This study aims to provide new insights on perfusion patterns of these tumors and to explore the potential of DSC-PWI in their presurgical discrimination.

Methods Adult patients with a solitary cerebellar tumor on presurgical MR and confirmed histological diagnosis of metastasis, medulloblastoma, hemangioblastoma, or pilocytic astrocytoma were retrospectively retrieved (2008–2023). Volumetric segmentation of tumors and normal-appearing white matter (for normalization) was semi-automatically performed on CE-T1WI and coregistered with DSC-PWI. Mean normalized values per patient tumor-mask of relative cerebral blood volume (rCBV), percentage of signal recovery (PSR), peak height (PH), and normalized time-intensity curves (nTIC) were extracted. Statistical comparisons were done. Then, the dataset was split into training (75%) and test (25%) cohorts and a classifier was created considering nTIC, rCBV, PSR, and PH in the model.

Results Sixty-eight patients (31 metastases, 13 medulloblastomas, 13 hemangioblastomas, and 11 pilocytic astrocytomas) were included. Relevant differences between tumor types' nTICs were demonstrated. Hemangioblastoma showed the highest rCBV and PH, pilocytic astrocytoma the highest PSR. All parameters showed significant differences on the Kruskal–Wallis tests (p < 0.001). The classifier yielded an accuracy of 98% (47/48) in the training and 85% (17/20) in the test sets.

Conclusions Intra-axial cerebellar tumors in adults have singular and significantly different DSC-PWI signatures. The combination of perfusion metrics through data-analysis rendered excellent accuracies in discriminating these entities.

Clinical relevance statement In this study, the authors constructed a classifier for the non-invasive imaging presurgical diagnosis of adult intra-axial cerebellar tumors. The resultant tool can be a support for decision-making in the clinical practice and enables optimal personalized patient management.

Albert Pons-Escoda and Alonso Garcia-Ruiz are first authors with equal contributions.

Twitter: @PonsEscoda

- Albert Pons-Escoda albert.pons@bellvitgehospital.cat
- Radiology Department, Hospital Universitari de Bellvitge, Feixa Llarga SN, 08907 L'Hospitalet de Llobregat, Barcelona, Spain
- Neuro-Oncology Unit, Institut d'Investigació Biomedica de Bellvitge, IDIBELL, Barcelona, Spain
- Radiomics Group, Vall d'Hebron Institut d'Oncologia, Barcelona, Spain

- ⁴ Universidad de Murcia, Murcia, Spain
- Institut de Diagnostic Ambiental i Estudis de l'Aigua (IDAEA) – CSIC, Barcelona, Spain
- Magnetic Resonance Unit, HT Medica, Jaen, Spain
- Neurosurgery Department, Hospital Universitari de Bellvitge, Barcelona, Spain
- Biomedical Research Networking Centers of Bioengineering, Biomaterials and Nanomedicine (CIBER-BBN), Madrid, Spain
- ⁹ Radiology Department, Hospital Clinic de Barcelona, Barcelona, Spain



Key Points

- Adult intra-axial cerebellar tumors exhibit specific, singular, and statistically significant different MR dynamic-susceptibility-contrast perfusion-weighted imaging (DSC-PWI) signatures.
- Data-analysis, applied to MR DSC-PWI, could provide added value in the presurgical diagnosis of solitary cerebellar metastasis, medulloblastoma, hemangioblastoma, and pilocytic astrocytoma.
- A classifier based on DSC-PWI metrics yields excellent accuracy rates and could be used as a support tool for radiologic diagnosis with clinician-friendly displays.

Keywords Brain · Perfusion magnetic resonance imaging · Cerebellar neoplasms

Abbreviations

DSC-PWI Dynamic-susceptibility-contrast perfusion-

weighted imaging

nTIC Normalized time-intensity curves

PH Peak height

PSR Percentage of signal recovery rCBV Relative cerebral blood volume

Introduction

Solitary intra-axial cerebellar tumors in adults are infrequent, representing 2–2.5% of all CNS tumors [1], but deserve dedicated attention [1, 2]. Their differential diagnosis is limited and specific but diverges from that of the much more prevalent intra-axial supratentorial brain tumors. In the cerebellum, the most common malignancy in adults is metastasis. Meanwhile, the most common primary tumor is hemangioblastoma, followed by medulloblastoma and pilocytic astrocytoma, both more prevalent in the pediatric population [1, 2].

Due to the small volume of the posterior fossa, a slight mass effect can cause fatal tonsillar herniation or hydrocephalus. This emphasizes the importance of a rapid diagnostic imaging workup in which magnetic resonance (MR) plays a pivotal role. The presurgical differentiation of these tumors will greatly impact patient management [2–6]. A systemic staging study should follow a metastasis suspicion. A presurgical embolization would minimize the risk of bleeding during the standard-of-care surgery in a suspected hemangioblastoma. The possibility of a medulloblastoma requires a complete neuroaxis extension study to evaluate leptomeningeal dissemination, before deciding on surgery and chemo-radiotherapy schemes. Or lastly, a tumor consistent with a pilocytic astrocytoma can be cured with an excellent prognosis only with direct surgical removal [3–6].

Despite classic imaging pearls, such as the cystic appearance with a solid mural nodule of hemangioblastomas and pilocytic astrocytomas, or the strikingly restricted diffusion of solid medulloblastomas, morphological imaging is often insufficient to reach a reliable presurgical suspicion [2, 7]. Indeed, metastases are very heterogeneous in presentations

with different patterns depending on the primary tumor histology, among other factors. Hemangioblastoma and pilocytic astrocytoma often escape the classical image and appear heterogeneously solid-cystic or solid. And meduloblastoma can appear cystic, compromising the value of their characteristic homogeneous diffusion restriction [2, 7].

Functional and quantitative imaging techniques such as DSC-PWI have shown promising results in discriminating some cerebellar tumors [8–11]. This technique offers in vivo information on tumor vascular and microvascular environments. However, its full potential for the pre-surgical discrimination of cerebellar tumors might not have been achieved. Previous papers in this regard are based on the evaluation of isolated metrics extracted from the time-T2* intensity curves generated during contrast administration. Relative cerebral blood volume (rCBV) is the most widely studied perfusion parameter. However, some more recently described metrics such as percentage of signal recovery (PSR) and peak height (PH) [12] are more scarcely investigated in these groups of tumors [9]. In summary, the PSR mainly reflects changes in capillary blood-brain barrier permeability, whereas the PH is thought to reflect the total capillary volume [12]. Moreover, the analysis of the whole normalized time-intensity curve (nTIC), qualitatively and quantitively assessable with recently described methodologies [13–15], remains unknown. In summary, previous studies only considered isolated DSC-PWI metrics and limit their analysis to descriptive statistics [10] or pairwise comparisons [8, 9, 11] but multiple-way classifications have not been performed.

Also, the rarity of adult intra-axial cerebellar tumors results in the relatively scarce literature regarding their DSC-PWI features [8, 9, 11]. Moreover, most of these publications involve only two entities (i.e., metastasis versus hemangioblastoma [11] or pilocytic astrocytoma versus hemangioblastoma [9]) but not the full differential of tumors that can be encountered in this location.

To overcome these limitations, the evaluation and combination of all cited DSC-PWI features could allow the construction of robust classifiers. These tools would be of great added value in the presurgical differentiation of these tumors, and ultimately would optimize therapeutic management.



This study aims to explore the full potential of DSC-PWI in the presurgical diagnosis of adult intra-axial cerebellar tumors (a) by evaluating and comparing rCBV, PSR, PH, and TIC between the most frequent adult intra-axial cerebellar tumors, and (b) by combining these metrics, to construct a classifier that can be applied in clinical practice with radiologist-friendly displays.

Material and methods

This retrospective study was approved by the research ethics committee of Hospital Universitari de Bellvitge (PR306/22). The confidential data from patients were anonymized and protected following national and European regulations.

Patients

Adult patients with a solitary, enhancing, intra-axial (inside the pia mater [2]) cerebellar tumor on presurgical MR and confirmed histological diagnosis of metastasis, medulloblastoma, hemangioblastoma, or pilocytic astrocytoma were retrospectively retrieved from the database of Hospital Universitari de Bellvitge and HT Medica, Spain, between January 2008 and January 2023. Patients with extra-axial, brainstem, or ventricular tumors were not considered. Inclusion criteria were (1) histopathological confirmed tumor diagnosis; (2) available presurgical diagnostic MR examination including DSC-PWI and axial contrast-enhanced T1WI (CE-T1WI); and (3) enhancing tumor on CE-T1WI with the shortest diameter of at least 10 mm. Exclusion criterion was low quality of the sequences preventing DSC-PWI data extraction.

Imaging

All MR imaging examinations included in the study were acquired in 1.5- and 3-T scanners. All DSC-PWI sequences were gradient-echo, with different technical parameters specified in Supplementary Table 1. A single bolus of intravenous gadolinium-based contrast agent 1 mmol/mL was used at a standard dose of 0.1 mmol/kg with an injection rate of 4–5 mL/s. No contrast preload was administered. Two experienced neuroradiologists, A.P.-E. and CM., evaluated the quality of the sequences.

DSC-PWI postprocessing and data extraction

Volumetric segmentations of enhancing tumor and contralateral normal-appearing white matter (NAWM) (for normalization) were performed on CET1WI semi-automatically (histogram intensity thresholding) and coregistered with DSC-PWI. Cysts, calcifications, hemorrhage, and necrosis were excluded from the segmented lesion masks to ensure that the perfusion metrics represent viable tumor tissue.

All segmentations were performed on 3D Slicer, version 5.0 (http://www.slicer.org), and coregistration was with the BRAINSFit module. Time-intensity curves were preprocessed using the method proposed by Pons-Escoda et al [13] which renders normalized nTICs: Signal-intensity values of the enhancing tumor TIC were normalized by dividing by the maximal signal intensity drop of the NAWM, and time values were normalized as relative to the period of the descending curve on NAWM. The resultant nTICs are comparable among different patients and techniques. The TICs were processed using Python 3.11 software (https://www.python.org/ downloads/release/python-3110/). Mean normalized values per patient tumor-mask of nTICs, rCBV, PSR, and PH were extracted. rCBV was obtained as described by Boxerman et al [16] after leakage correction with 3D Slicer. PSR and PH were obtained as described by Cha et al [12]. All postprocessing and data extraction were performed employing a whole semi-automatized in-house pipeline. All segmentations and perfusion curves were visually supervised and quality filtered by a neuroradiologist (A.P.-E.) with 10 years of experience in neuro-oncologic imaging. Those DSC-PWI registrations that did not show a clear time-intensity curve or an excessive signal-to-noise ratio were excluded.

DSC-PWI metrics comparisons

Visual assessment of each tumor type nTIC and point-bypoint statistical comparisons (Kruskal–Wallis test) of the four different tumor curves was performed. Visual assessment of each tumor group rCBV, PSR, and PH value distributions and dispersions represented on box plots, as well as statistical comparisons (Kruskal–Wallis test), was done.

In addition, we performed pairwise comparisons between tumor types using the Mann–Whitney U test, and calculated the area under the receiver operating characteristic curve (AUC-ROC) for each comparison.

DSC-PWI classifier construction

To construct the classifier, the sample set was randomly divided into training and holdout test sets, with 75% of each tumor type allocated to the former and the remaining 25% to the latter. The training set was used to develop the classifier model, while the holdout set was utilized to test it. Additionally, a leave-one-out cross-validation (LOOCV) was conducted to further evaluate the performance of the model.

Time point intensity values of the mean nTICs and mean values of rCBV, PSR, and PH per patient tumor-mask were the variables included in the primary model. Making use of "Caret" R package [17] (https://cran.r-project.org/package=caret), a boosted tree classifier (stochastic gradient boosting) was constructed. All the details on the model generation are



Table 1 Demographics of the study sample

Tumor type	Number	Sex (male:female)	Age in years (mean, range)
Metastasis	31	15:16	61, 30–83
Medulloblastoma	13	8:5	32, 21–44
Hemangioblastoma	13	9:4	46, 31–61
Pilocytic astrocytoma	11	3:8	38, 21–69
Total	68	35:33	49, 21–83

available in the R script in the Supplementary Material. The model performance in both training and holdout sets was assessed in terms of accuracy (% of correct assignation).

Finally, for comparison, two secondary boosted tree models were tested following the exact same methods. In the first model, only the nTICs were considered. The second model considered rCBV, PSR, and PH.

All data computations were performed with R statistical and computing software, R package version 4.2.2 [18] (http://www.r-project.org).

Results

Patients

Seventy-six patients were considered eligible for the study. Eight patients were excluded by the quality filter. Therefore, a total of 68 patients (35 men; mean age 49, range 21–83)

Fig. 1 Average nTICs of solitary posterior fossa metastasis (Met), medulloblastoma (Mdl), hemangioblastoma (Hbl), and pilocytic astrocytoma (P-a) in adults. Evident visual and significant statistical differences between the time point values of each tumor type curve, Kruskal–Wallis test, p < 0.005. The X-axis and the Y-axis correspond to normalized time and signal intensity units, relative to the period of the descending curve and the maximal signal intensity drop of the NAWM respectively

were enrolled for the study: 31 metastases, 13 medulloblastomas, 13 hemangioblastomas, and 11 pilocytic astrocytomas. The training set included 22 metastases, 9 medulloblastomas, 9 hemangioblastomas, and 8 pilocytic astrocytomas. The rest of the cases were set apart for testing. Patient selection flowchart is summarized in Supplementary Fig. 1 and demographics are in Table 1.

The primary tumor location of the metastatic cases was lung in 20 patients, followed by breast in 6, colorectal in 4, and renal in 1.

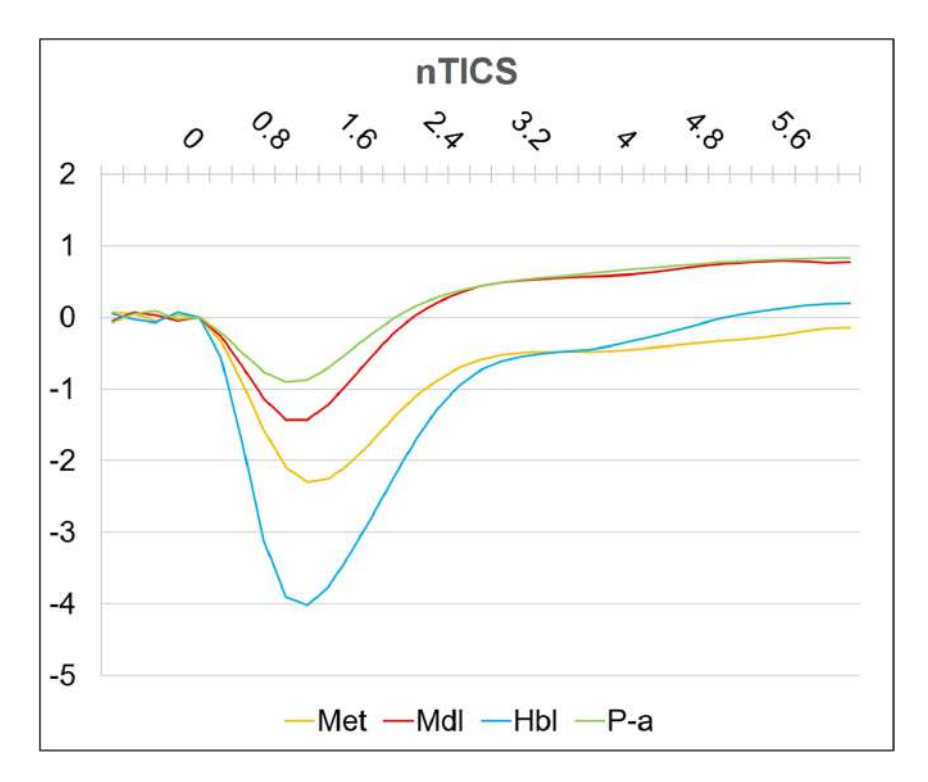
Significant differences were found in patients' age among the four tumor types (Kruskal–Wallis test, p < 0.001).

DSC-PWI comparisons

Mean nTICs, as well as box plots for rCBV, PSR, and PH values for each tumor type, are shown in Figs. 1 and 2. There were differences between tumor-type nTICs morphology and rCBV, PSR, and PH values on a visual assessment. Mean values of rCBV, PSR, and PH are shown in Table 2 and overlaid on Fig. 2 box plots. The Kruskal–Wallis tests demonstrated significant differences (p < 0.001) in all points (since the first descending point) of the curves and in rCBV, PSR, and PH between the four tumor types.

For pairwise comparisons, the Mann–Whitney U test results are shown in Supplementary Table 2 and the AUC-ROC analysis in Table 3.

Finally, no significant differences were found for different primary tumor origins of metastases nor for different DSC-PWI techniques among each tumor subgroup.





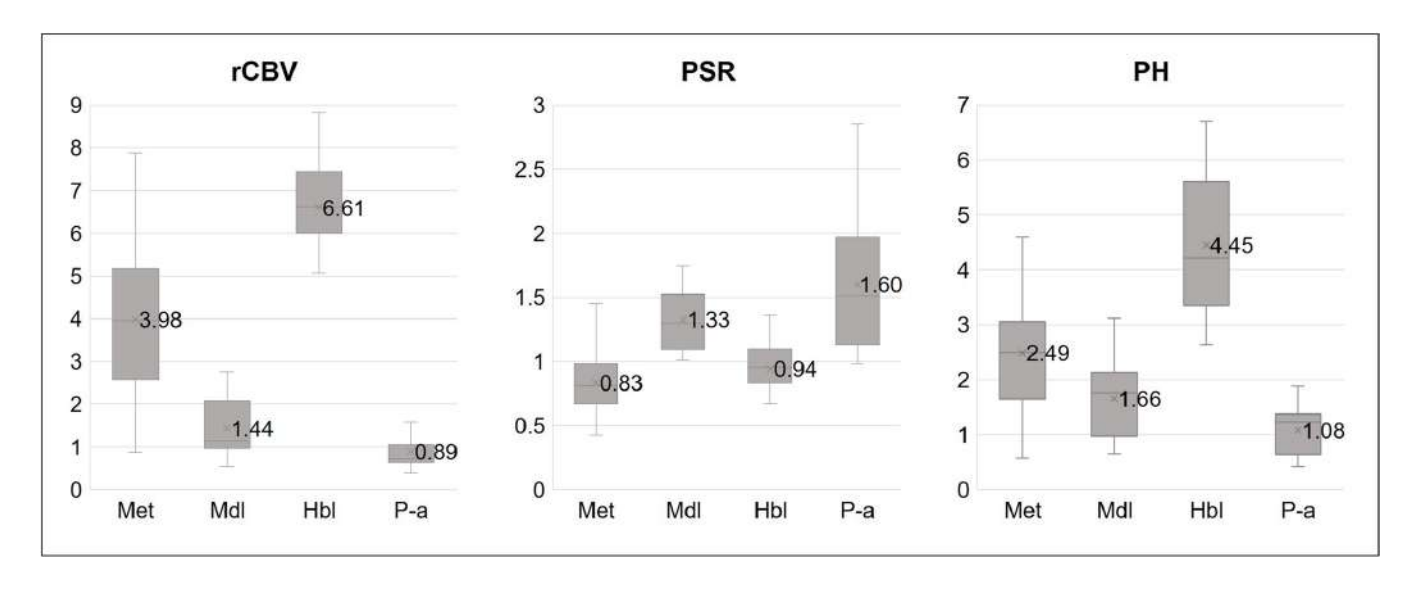


Fig. 2 Box plots for rCBV, PSR, and PH values of solitary posterior fossa metastasis (Met), medulloblastoma (Mdl), hemangioblastoma (Hbl), and pilocytic astrocytoma (P-a) in adults. "x" represents

average values. Evident visual and significant statistical differences between each tumor type values of the three evaluated metrics, Kruskal–Wallis test, p < 0.001

DSC-PWI classifier performance

The primary classifier demonstrated high accuracy rates, with 98% accuracy (47/48) in the training set and 85% accuracy (17/20) in the test set. The relative weighting assigned to each variable in the model can be found in Supplementary Table 3. Additional specific classification results are available in the confusion matrices in Supplementary Fig. 2. The classifier misclassified between metastasis and hemangioblastoma (1 in the training set, 2 in the test set), as well as between medulloblastoma and pilocytic astrocytoma (1 in the test set). The LOOCV produced an average accuracy of 76%.

Regarding the two secondary classifiers created for comparison, they rendered poorer accuracy results than the primary model. The first model considering only the nTIC provided 100% accuracy in the training set, which lowered to 70% (14/20) in the test. The second, considering only rCBV, PSR, and PH values, obtained accuracies of 94% (45/48) and 75% (15/20) respectively.

An additional classifier was developed using all DSC-PWI metrics and patient age, which was found to be significantly

Table 2 rCBV, PSR, and PH mean values [$\pm 95\%$ confidence interval] for each tumor subtype. Kruskal–Wallis test, p < 0.001

Tumor type	rCBV	PSR	PH
Metastasis	3.98 [±0.66]	$0.83 [\pm 0.10]$	2.49 [±0.35]
Medulloblastoma	$1.44 [\pm 0.36]$	$1.33 [\pm 0.13]$	$1.66 [\pm 0.38]$
Hemangioblastoma	$6.61 [\pm 0.82]$	$0.94 [\pm 0.12]$	$4.45 [\pm 0.67]$
Pilocytic astrocytoma	$0.89 [\pm 0.20]$	$1.6 [\pm 0.31]$	$1.08 [\pm 0.26]$

different among the tumor groups. The accuracy of this classifier was 100% in the training set, but it decreased to 70% (14/20) in the test set. Thus, the inclusion of age in the model did not improve its accuracy in the test set.

Tool display for clinical applicability

Finally, the authors present a radiologist-friendly display that could be incorporated into a diagnostic support tool which would be applicable in daily practice (see examples in Figs. 3 and 4 where two new "problem" cases are given a specific classification, but they are also overlapped on mean nTIC curves as well as rCBV, PSR, and PH plots of each tumor type). This allows for visual assessment of differences of new "problem" cases with each tumor type and ensures radiologist interactivity to achieve the final diagnostic clinical decision.

Table 3 Summary of area under the receiver operating characteristic curve (AUC-ROC) analysis for pairwise comparisons. *The nTIC results are determined by the highest AUC achieved by a single time point, from among all the points of the curve

Pair of tumors	CBV	PSR	PH	nTIC*
Met vs Mdl	0.893	0.913	0.734	0.931
Met vs Hbl	0.854	0.675	0.882	0.897
Met vs P-a	0.953	0.935	0.9	0.960
Mdl vs P-a	0.734	0.622	0.748	0.762
Mdl vs Hbl	1	0.899	0.988	0.988
Hbl vs P-a	1	0.902	1	1



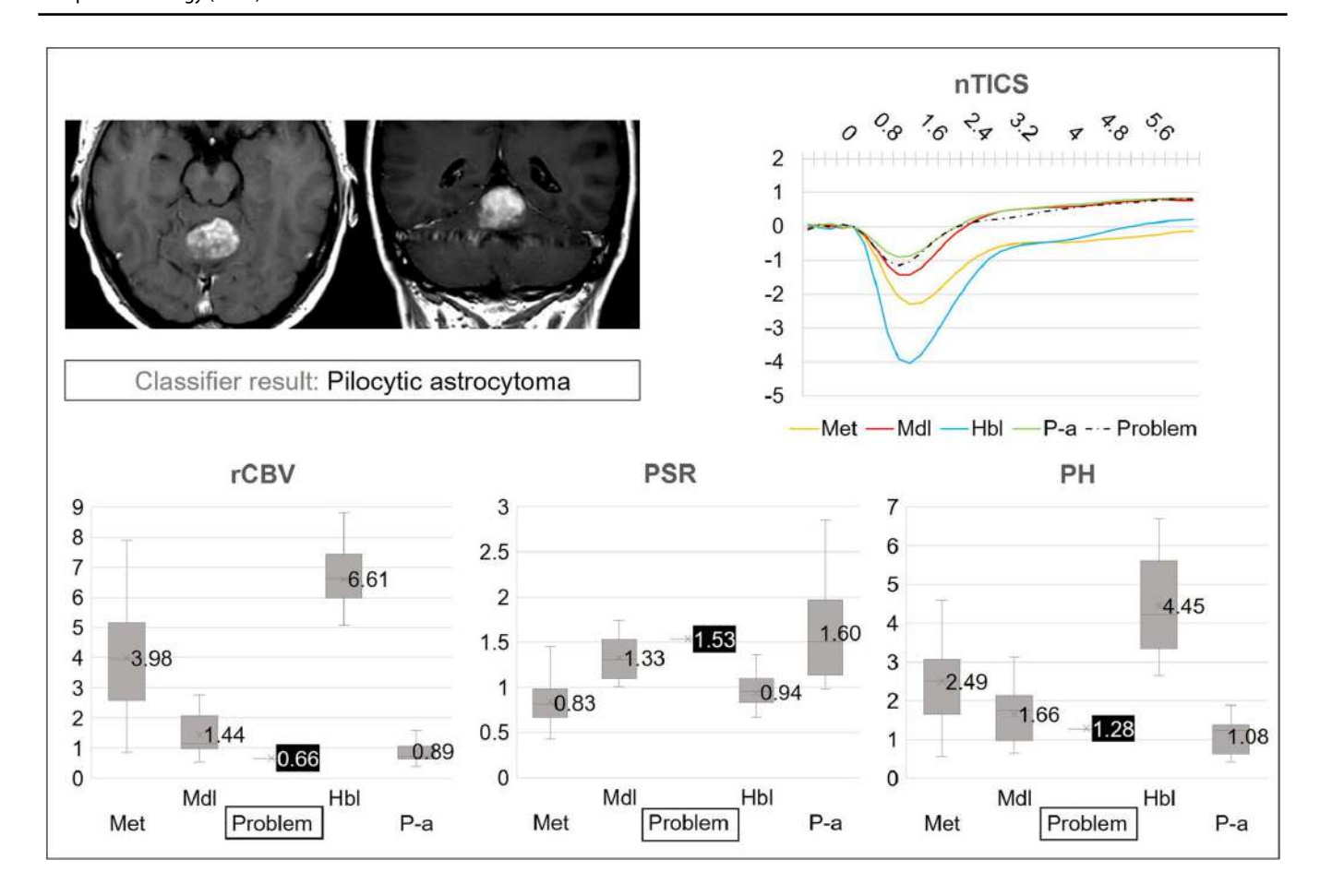


Fig. 3 Real clinical example of the user-friendly applicability of results. The classifier assigns a diagnostic suggestion of pilocytic astrocytoma for this new "problem" case of a solid homogeneously enhancing tumor. The nTIC curves as well as rCBV, PSR, and PH values of the "problem" case overlap with those

of pilocytic astrocytoma. Therefore, the neuroradiologist can suggest the final diagnostic prediction of pilocytic astrocytoma considering all the displayed data. Histopathology furtherly confirmed the definitive diagnostic of pilocytic astrocytoma

Discussion

In this manuscript, we studied a large series of the wide differential of adult intra-axial cerebellar tumors. We evidenced that they have different and characteristic DSC-PWI patterns in terms of nTIC morphology as well as of rCBV, PSR, and PH values. Combining all these variables enabled the creation of a robust and highly accurate classifier which provides a single diagnostic suggestion with 85% accuracy in the independent test set. Furthermore, taking advantage of the significant differences between tumor types, we designed an interactive and intuitive visual-friendly display. This interface supports clinicians' reliability on the model by facilitating explainability of conclusions and potential misclassifications.

Figures 3 and 4 are real clinical examples of the classifier's user-friendly applicability. For visual evaluation of a new "problem" case, its nTIC and rCBV, PSR, and PH values are overlapped on mean nTICs and box plots of each tumor type. Parallelly, the classifier assigns a diagnostic

suggestion for the new case. This supportive and interactive format increases reliability, promotes explainability, and keeps away the feared "black-box" issue.

DSC-PWI, which is included in the optimal brain tumor imaging protocols according to the most recent consensus [19–21], has shown promising results in discriminating some cerebellar tumors [8-11, 22]. Previous papers are based on evaluating isolated metrics, mainly rCBV, and in one single case, PSR and PH [9]. Furthermore, the whole nTIC [13–15] has not yet been investigated in these groups of tumors. Also, the most frequent single-parameter DSC-PWI analysis has not allowed multiclass predictions to date. This paper demonstrates that the combination of multiple DSC-PWI variables (rCBV, PSR, PH, and the nTIC) allows the creation of highly accurate multiclass classifiers, of great added value in this complex clinical scenario. Finally, the rarity of adult intraaxial cerebellar tumors results in the relatively scarce literature on this topic, especially considering altogether a complete differential such as the one presented in this study.



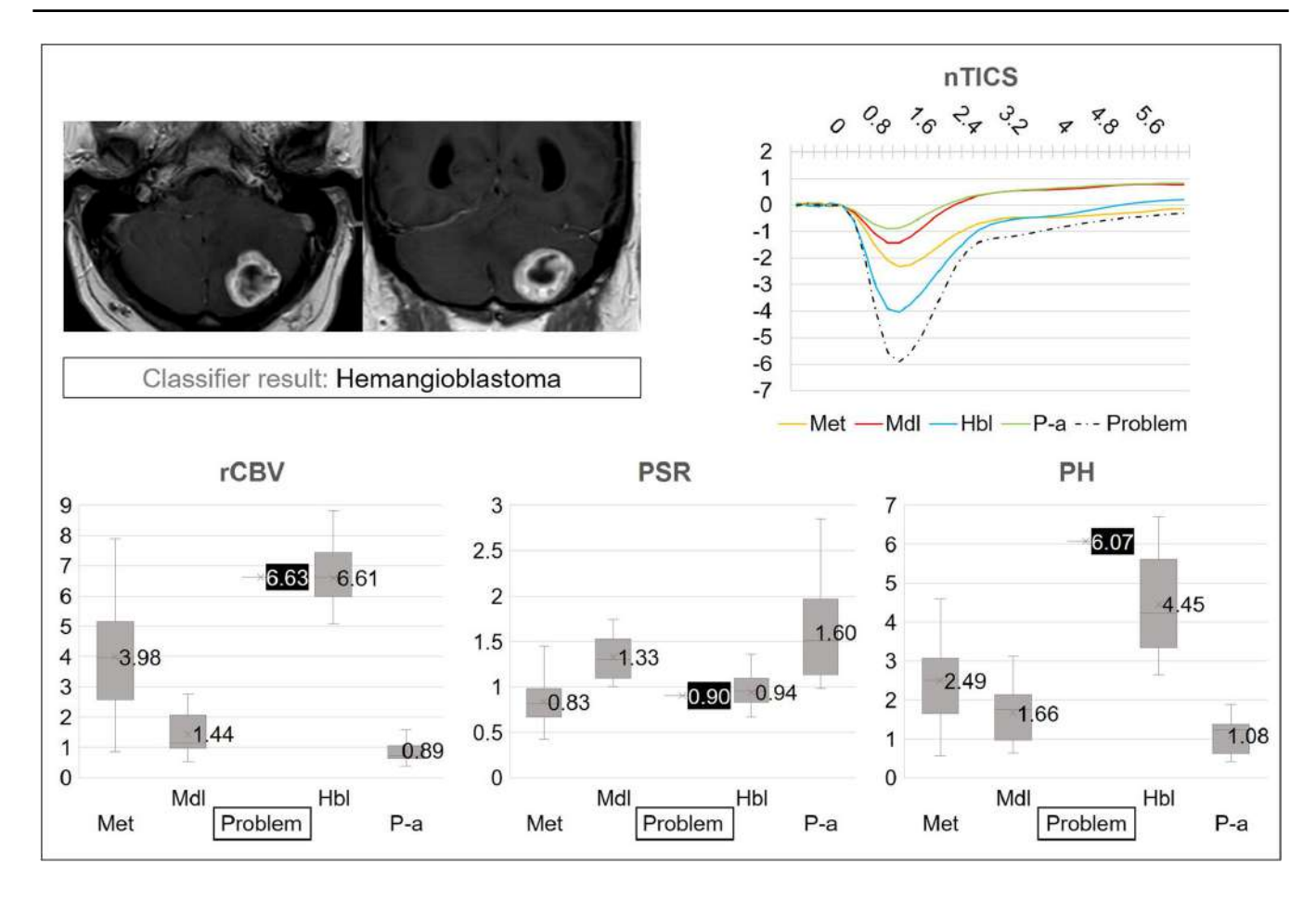


Fig. 4 Real clinical example of the user-friendly applicability of results. The classifier assigns a diagnostic suspicion of hemangioblastoma for this new "problem" case of a heterogeneous solid-cystic/necrotic tumor. The nTIC curves as well as rCBV, PSR, and PH values of the "problem" case

overlap with those of hemangioblastoma. Therefore, the neuroradiologist can suggest the final diagnostic prediction of hemangioblastoma considering all the displayed data. The definitive diagnostic of hemangioblastoma was furtherly confirmed by histopathology

The paramount importance of this study is the introduction of several new insights about DSC-PWI of adult cerebellar tumors. From our results, we summarize the following statements about specific DSC-PWI signatures of adult cerebellar tumors. Regarding "perfusion curvology," nTICs are different between all tumor types, save for only partial overlap on the signal-recovery part of the curve between medulloblastoma and pilocytic astrocytoma. Hemangioblastoma and metastasis T2* dynamic-signal decays pronounced and fast (more so in hemangioblastoma), while recovers slowly, remaining below the baseline during the whole curve of metastasis, and only reaching the baseline in the last time points of hemangioblastoma. Medulloblastoma and pilocytic astrocytoma signal decays much less (a bit more in medulloblastoma) and slower, while recovers far above the baseline. Metastasis and hemangioblastoma show high rCBV and PH, and low PSR, while medulloblastoma and pilocytic astrocytoma exhibit low rCBV and PH, and high PSR. Hemangioblastoma demonstrates the highest rCBV and PH, and pilocytic astrocytoma the highest PSR. Overall, these DSC-PWI characteristics primarily reflect

a higher degree of vascularization in hemangioblastoma and metastasis, whereas a higher degree of blood—brain barrier disruption in pilocytic astrocytoma and medulloblastoma.

The DSC-PWI metrics evaluated in our study are not new, as they have been studied in brain tumor imaging studies such as glioblastoma, metastasis, or lymphoma [13–15], which usually involve a different differential and are supratentorial. However, the importance of our study lies in the specific evaluation of these parameters for adult solitary intra-axial cerebellar tumors, which is a less studied area. The fact that already known metrics, usually used in neuro-oncology, were evaluated in this study is positive because it allows clinicians to apply the results using familiar and precisely interpretable metrics, promoting direct clinical implementation and comprehensibility of results. Those limited metrics that have already been evaluated in the scarce previous literature are aligned with our results, e.g., very high rCBV [8-11] and PH [9] of hemangioblastoma, as well as low rCBV [8, 9] and high PSR [9] for pilocytic astrocytoma. DSC-PWI features in adult medulloblastoma seemed the less described in the literature, with the only reference reporting



partial overlap in rCBV values with adult pilocytic astrocytoma [8]. Also, Ho et al [22] described overlapping low rCBV and high PSR values in the pediatric population.

Previous studies have reported differences in DSC-PWI features of metastases depending on the primary tumor of origin [11]. However, in our dataset of metastases from lung, breast, colorectal, and renal origins, we did not observe significant differences in these features. It is important to note that this finding should be interpreted with caution, given the relatively small sample size of some primary cancer origins in our dataset. Furthermore, it is possible that other less common primary cancer origins may exhibit different DSC-PWI features that were not directly captured in our study. Nonetheless, examining metastases as a collective entity, as done in this study, can hold significant clinical value: it is not uncommon for a solitary metastasis to be the initial manifestation of an unknown tumor, leading to the clinician being unaware of its primary origin. Additionally, while variations among primary types exist, several characteristics of metastases are universal, such as the lack of a blood-brain barrier or a proclivity for angiogenesis [15].

Regarding our classifier model mistakes, they consisted of misclassifications between metastasis and hemangioblastoma (1 in the training set, 2 in the test set), and medulloblastoma and pilocytic astrocytoma (1 in the test set). Importantly for the classifier trustability, these mistakes seem explainable, as these pairs of tumors showed lesser significant differences in DSC-PWI features at pairwise comparisons.

While age is an essential factor to consider in distinguishing cerebellar tumors in clinical practice, our secondary analysis combining age with nTICs, PSR, CBV, and PH did not enhance the accuracy of our classifier. This could be attributed to the partially overlapping age ranges among the entities: metastases are more prevalent in elderly patients, whereas both pilocytic astrocytoma and medulloblastoma occur in younger individuals, and hemangioblastoma can occur in both age groups. Nevertheless, we acknowledge that clinicians must always consider this clinical factor while making diagnostic decisions, especially in pairwise comparisons involving metastasis or elderly patients. In this regard, we would like to highlight the relevance of the pairwise comparisons also included in our study. In certain cases, the differential diagnosis could be between two entities rather than among all four, and this supplementary approach can aid clinicians in making even more accurate diagnoses.

The authors acknowledge that attention must be paid to DSC-PWI technical parameters. Especially preloaded DSC-PWI sequences minimize the leakage effects and change the curve morphology, theoretically, to optimize rCBV measures [20]. In this regard, our model was trained with DSC-PWI data without preload and it is possible that the performance lowered when applied to preloaded data. However, we have included a notable technical variability with a wide range of

FA values (which also theoretically impacts curves morphology), and the model still generalizes reaching excellent accuracies in an independent test set. It is important to note that in order to mitigate the effects of technical and patient-related variability, we implemented well-described specific methods to normalize and relativize the DSC-PWI data. These steps ensure that our results were not biased or influenced by such variabilities. Also, to maintain rCBV reliability in our study, it was estimated with leakage correction [16], obtaining comparable statistical results to those of PSR or PH. Importantly, no significant differences were found among the different DSC-PWI techniques within each tumor type, confirming robust DSC-PWI pattern for each histology. Heterogeneity in the DSC-PWI technique may be common in clinical practice among neuroradiology departments worldwide, and approaches that mitigate this variability, such as ours, may be of great interest for improving applicability. Of note, although consensus for DSC-PWI parameters in glioma clinical trials [20] recommends intermediate FA and pre-bolus usage for accurate rCBV measures, there is evidence that non-preloaded sequences may provide greater information for presurgical differential diagnosis purposes [22, 23]. In fact, non-preloaded sequences better depict the leakage effects that could be of interest in differing between tumor entities, while preserving acceptable performances of rCBV [23]. This may also be the case for the discrimination of intra-axial cerebellar tumors in adults. In any case, the proposed method could accommodate different DSC-PWI protocols by training the models with new imaging samples.

Some limitations should be considered in this work. First, this is a retrospective study, and the sample size may seem small. However, the dataset used in this study is comparatively large when compared to previous studies, and considering the prevalence of the diseases under investigation. The higher number of metastases in the test may be criticized, but it also reflects the reality where metastasis is the most prevalent. In any instance, the studied population suffices to provide insights into these tumors and for a pilot classification study. Second, the wide range of pulse-sequence parameters included in the study could raise concerns about the consistency of results. However, it is also worth noting that this aspect of the study has a positive implication: the inclusion of various pulse-sequence parameters demonstrates the generalizability and robustness of the study despite technical differences. This is noteworthy because it suggests that the findings of the study are likely to be applicable and relevant in realworld clinical settings. Finally, we focused solely on DSC-PWI features, while in clinical practice multiple sequences are evaluated together for a final diagnostic suggestion. Therefore, additional studies could incorporate a broader range of imaging features to achieve even better diagnostic accuracies. At any rate, further development of methods and multicentric prospective studies remain needed for validation.



In contrast, our study has remarkable strengths. First, it provides a robust method with excellent accuracy rates despite sample heterogeneity. Second, the complete differential diagnosis of adult intra-axial cerebellar tumor is considered, which, jointly with the proposed results' display, emphasizes the clinical usefulness. Third, semi-automatization of image processing and data extraction minimizes operator dependency in favor of reproducibility. Lastly, the presented tool's display combines the strength of machine learning with the comprehensibility of classic statistics to preserve the clinical user trust.

As conclusions, adult intra-axial cerebellar tumors have specific, singular, and statistically significant different DSC-PWI patterns regarding nTIC, rCBV, PSR, and PH values. The combination of these different metrics through data analysis allowed the creation of a classifier which renders 85% accuracy in an independent test cohort. The classic statistics' differences, together with the classifier results, can be displayed in a radiologist-friendly interface that ensures interactivity and reliability of the clinical user and provides an added support to the radiologic diagnosis.

Supplementary Information The online version contains supplementary material available at https://doi.org/10.1007/s00330-023-09892-7.

Acknowledgements Albert Pons-Escoda and Carles Majos acknowledge a grant from the Instituto de Salud Carlos III (PI20/00360). Pablo Gago-Ferrero acknowledges a Ramón y Cajal grant (RYC2019-027913-I). The authors want to acknowledge Pilar Lopez-Ubeda, PhD, from HT Medica. She participated in retrospective patient recruitment through advanced natural language processing methods. The authors thank CERCA Programme/Generalitat de Catalunya for institutional support.

Funding No funding was received.

Declarations

 $\label{lem:condition} \textbf{Guarantor} \ \ \textbf{The scientific guarantor of this publication is Albert Pons-Escoda}.$

Conflict of interest Albert Pons-Escoda is a member of the *European Radiology* Scientific Editorial Board. He has not taken part in review or selection process for this article. The remaining authors of this manuscript declare no relationships with any companies whose products or services may be related to the subject matter of the article.

Statistics and biometry Several authors have significant statistical expertise; mainly Alonso Garcia-Ruiz and Ruben Gil-Solsona have expertise in statistics, data analysis, and machine learning.

Informed consent Written informed consent was waived by the institutional review board.

Ethical approval Institutional review board approval was obtained. This study has been approved by The Research Ethics Committee of the Hospital Universitari de Bellvitge (PR306/22).

Study subjects or cohorts overlap None of the study subjects or cohorts has been previously reported.



- retrospective
- · diagnostic study
- performed at one institution

References

- Ostrom QT, Patil N, Cioffi G et al (2020) CBTRUS statistical report: primary brain and other central nervous system tumors diagnosed in the United States in 2013–2017. Neuro Oncol 22:iv1-iv96. https://doi.org/10.1093/neuonc/noaa200
- Shih RY, Smirniotopoulos JG (2016) Posterior fossa tumors in adult patients. Neuroimaging Clin N Am 26:493–510. https://doi. org/10.1016/j.nic.2016.06.003
- Wade A, Hayhurst C, Amato-Watkins A et al (2013) Cerebellar pilocytic astrocytoma in adults: a management paradigm for a rare tumour. Acta Neurochir (Wien) 155:1431–1435. https://doi.org/ 10.1007/s00701-013-1790-1
- Sunderland GJ, Jenkinson MD, Zakaria R (2016) Surgical management of posterior fossa metastases. J Neurooncol 130:535–542. https://doi.org/10.1007/s11060-016-2254-2
- Kuharic M, Jankovic D, Splavski B et al (2018) Hemangioblastomas of the posterior cranial fossa in adults: demographics, clinical, morphologic, pathologic, surgical features, and outcomes. A systematic review. World Neurosurg 110:e1049–e1062. https://doi.org/10.1016/j.wneu.2017.11.173
- Franceschi E, Giannini C, Furtner J et al (2022) Adult medulloblastoma: updates on current management and future perspectives. Cancers (Basel) 14. https://doi.org/10.3390/cancers14153708
- Jhaveri M, Osborn A, Salzman K (2020) Diagnostic imaging: brain, 4th ed. Elsevier, Salt Lake City, UT
- Kurokawa R, Kurokawa M, Baba A et al (2022) Differentiation of pilocytic astrocytoma, medulloblastoma, and hemangioblastoma on diffusion-weighted and dynamic susceptibility contrast perfusion MRI. Medicine (Baltimore) 101:e31708. https://doi.org/10. 1097/MD.00000000000031708
- Neska-Matuszewska M, Zimny A, Bladowska J et al (2018) The role of diffusion and perfusion magnetic resonance imaging in differentiation of haemangioblastomas and pilocytic astrocytomas. Polish J Radiol 83:e197–e203. https://doi.org/10.5114/pjr.2018.75870
- Hakyemez B, Erdogan C, Bolca N et al (2006) Evaluation of different cerebral mass lesions by perfusion-weighted MR imaging. J Magn Reson Imaging 24:817–824
- 11. She D, Yang X, Xing Z, Cao D (2016) Differentiating hemangioblastomas from brain metastases using diffusion-weighted imaging and dynamic susceptibility contrast-enhanced perfusion-weighted MR imaging. AJNR Am J Neuroradiol 37:1844–1850. https://doi.org/10.3174/ajnr.A4809
- Cha S, Lupo JM, Chen MH et al (2007) Differentiation of glioblastoma multiforme and single brain metastasis by peak height and percentage of signal intensity recovery derived from dynamic susceptibility-weighted contrast-enhanced perfusion MR imaging. AJNR Am J Neuroradiol 28:1078–1084. https://doi.org/10.3174/ajnr.A0484
- Pons-Escoda A, Garcia-Ruiz A, Naval-Baudin P et al (2020) Presurgical identification of primary central nervous system lymphoma with normalized time-intensity curve: a pilot study of a new method to analyze DSC-PWI. AJNR Am J Neuroradiol 41:1816–1824. https://doi.org/10.3174/ajnr.A6761
- Pons-Escoda A, García-Ruíz A, Naval-Baudin P et al (2022)
 Diffuse large B-cell Epstein-Barr virus-positive primary CNS lymphoma in non-AIDS patients: high diagnostic accuracy of DSC perfusion metrics. AJNR Am J Neuroradiol 43:1567–1574. https://doi.org/10.3174/ajnr.A7668
- Pons-Escoda A, Garcia-Ruiz A, Naval-Baudin P et al (2022)
 Voxel-level analysis of normalized DSC-PWI time-intensity



- curves: a potential generalizable approach and its proof of concept in discriminating glioblastoma and metastasis. Eur Radiol. https://doi.org/10.1007/s00330-021-08498-1
- Boxerman JL, Schmainda KM, Weisskoff RM (2006) Relative cerebral blood volume maps corrected for contrast agent extravasation significantly correlate with glioma tumor grade, whereas uncorrected maps do not. AJNR Am J Neuroradiol 27:859–867
- 17. Kuhn M, Wing J, Weston S, Williams A (2022) "Caret": classification and regression training. R package version 6.0–93
- Team R R Core Team (2020) R: a language and environment for statistical computing. R Foundation for Statistical Computing, Vienna, Austria
- Barajas RF, Politi LS, Anzalone N et al (2021) Consensus recommendations for MRI and PET imaging of primary central nervous system lymphoma: guideline statement from the International Primary CNS Lymphoma Collaborative Group (IPCG). Neuro Oncol 23:1056–1071. https://doi.org/10.1093/neuonc/noab020
- Boxerman JL, Quarles CC, Hu LS et al (2020) Consensus recommendations for a dynamic susceptibility contrast MRI protocol for use in high-grade gliomas. Neuro Oncol 22:1262–1275. https://doi.org/10.1093/neuonc/noaa141

- Kaufmann TJ, Smits M, Boxerman J et al (2020) Consensus recommendations for a standardized brain tumor imaging protocol for clinical trials in brain metastases. Neuro Oncol 22:757–772. https://doi.org/10.1093/neuonc/noaa030
- Ho CY, Cardinal JS, Kamer AP et al (2016) Contrast leakage patterns from dynamic susceptibility contrast perfusion MRI in the grading of primary pediatric brain tumors. AJNR Am J Neuroradiol 37:544–551. https://doi.org/10.3174/ajnr.A4559
- Cindil E, Sendur HN, Cerit MN et al (2021) Validation of combined use of DWI and percentage signal recovery-optimized protocol of DSC-MRI in differentiation of high-grade glioma, metastasis, and lymphoma. Neuroradiology 63:331–342. https://doi.org/10.1007/s00234-020-02522-9

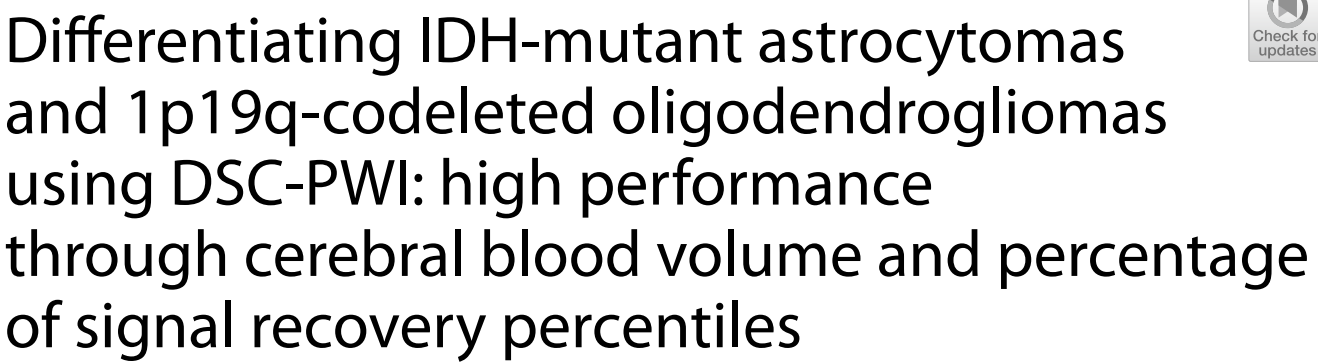
Publisher's note Springer Nature remains neutral with regard to jurisdictional claims in published maps and institutional affiliations.

Springer Nature or its licensor (e.g. a society or other partner) holds exclusive rights to this article under a publishing agreement with the author(s) or other rightsholder(s); author self-archiving of the accepted manuscript version of this article is solely governed by the terms of such publishing agreement and applicable law.





NEURO





Abstract

Objective Presurgical differentiation between astrocytomas and oligodendrogliomas remains an unresolved challenge in neuro-oncology. This research aims to provide a comprehensive understanding of each tumor's DSC-PWI signatures, evaluate the discriminative capacity of cerebral blood volume (CBV) and percentage of signal recovery (PSR) percentile values, and explore the synergy of CBV and PSR combination for pre-surgical differentiation.

Methods Patients diagnosed with grade 2 and 3 IDH-mutant astrocytomas and IDH-mutant 1p19q-codeleted oligodendrogliomas were retrospectively retrieved (2010–2022). 3D segmentations of each tumor were conducted, and voxel-level CBV and PSR were extracted to compute mean, minimum, maximum, and percentile values. Statistical comparisons were performed using the Mann-Whitney *U* test and the area under the receiver operating characteristic curve (AUC-ROC). Lastly, the five most discriminative variables were combined for classification with internal cross-validation.

Results The study enrolled 52 patients (mean age 45-year-old, 28 men): 28 astrocytomas and 24 oligodendrogliomas. Oligodendrogliomas exhibited higher CBV and lower PSR than astrocytomas across all metrics (e.g., mean CBV = 2.05 and 1.55, PSR = 0.68 and 0.81 respectively). The highest AUC-ROCs and the smallest p values originated from CBV and PSR percentiles (e.g., PSRp70 AUC-ROC = 0.84 and p value = 0.0005, CBVp75 AUC-ROC = 0.8 and p value = 0.0006). The mean, minimum, and maximum values yielded lower results. Combining the best five variables (PSRp65, CBVp70, PSRp60, CBVp75, and PSRp40) achieved a mean AUC-ROC of 0.87 for differentiation.

Conclusions Oligodendrogliomas exhibit higher CBV and lower PSR than astrocytomas, traits that are emphasized when considering percentiles rather than mean or extreme values. The combination of CBV and PSR percentiles results in promising classification outcomes.

*Correspondence: Albert Pons-Escoda albert.pons@bellvitgehospital.cat Full list of author information is available at the end of the article



Clinical relevance statement The combination of histogram-derived percentile values of cerebral blood volume and percentage of signal recovery from DSC-PWI enhances the presurgical differentiation between astrocytomas and oligodendrogliomas, suggesting that incorporating these metrics into clinical practice could be beneficial.

Key Points

- The unsupervised selection of percentile values for cerebral blood volume and percentage of signal recovery enhances pre surgical differentiation of astrocytomas and oligodendrogliomas.
- Oligodendrogliomas exhibit higher cerebral blood volume and lower percentage of signal recovery than astrocytomas.
- Cerebral blood volume and percentage of signal recovery combined provide a broader perspective on tumor vasculature and yield promising results for this preoperative classification.

Keywords Brain neoplasms, Astrocytoma, Oligodendroglioma, Perfusion imaging, Magnetic resonance imaging

Introduction

The imaging-based presurgical differentiation between astrocytomas and oligodendrogliomas represents an unsolved challenge in neuro-oncology. This differentiation has potential implications for diagnosis and initial patient management in several ways. First, accurate radiological classification allows for the selection of the most time- and cost-effective diagnostic test sequence in histopathology and molecular pathology [1-5]. In certain situations, it can further enhance the accuracy of the final diagnostic process. For instance, some researchers advocate for additional molecular testing for 1p19q co-deletion when there is a discrepancy between neuroimaging and fluorescence in situ hybridization results [5]. Secondly, the differentiation between these two entities assists in choosing the most appropriate surgical approach (e.g., total resection vs. partial resection or biopsies), predicting prognosis, and deciding the necessity and intensity of different adjuvant therapies, all of which can vary between astrocytomas and oligodendrogliomas [1-4].

Despite significant advances in imaging techniques, achieving accurate differentiation preoperatively remains complex. This emphasizes the need for innovative approaches that can enhance current diagnostic capabilities [6]. Qualitative morphological imaging, particularly through the T2-FLAIR mismatch sign, provides valuable insights and is highly specific for identifying IDH-mutant astrocytomas [7]. However, this method has low sensitivity, and its interpretation remains largely visual and subjective, reliant on the experience of the neuroradiologist with possible uncertain cases, especially for those less experienced. As a result, there has been an increasing interest in quantitative sequences. These offer the potential for more objective and reproducible results, enhancing the precision and reliability of presurgical tumor differentiation [8].

Dynamic susceptibility contrast perfusion-weighted imaging (DSC-PWI) is one such quantitative sequences

that has received extensive attention in neuro-oncology. Widely available and included in the most recent brain tumor imaging consensus, DSC-PWI monitors T2* signal changes dynamically during the vascular passage of a gadolinium-based contrast agent (GBCA), thereby generating time-intensity curves. The standard evaluation involves calculating the area under the curves to obtain cerebral blood volume (CBV), which estimates the overall vascularization of the tumors [9–11]. However, the potential information embedded in these time-intensity curves goes beyond just CBV. For instance, the percentage of signal recovery (PSR) is another metric that has received significant attention and demonstrated promising results for differential diagnosis of brain tumors [12–14].

The PSR provides an indirect measure of T1 and T2* leakage effects, which notably influence the time-intensity curve after the first pass of GBCA. It has been extensively studied in tumors with well-known prominent blood-brain barrier (BBB) disruption like glioblastoma or lymphoma [13–20]. However, in the context of a more preserved BBB, such as in grade 2–3 gliomas [21], PSR biological meaning may be different and it is scarcely investigated.

Commonly, CBV (and PSR) calculations focus on mean values from two-dimensional (2D) regions of interest (ROIs), or whole-tumor three-dimensional (3D) volumes of interest (VOIs). Some authors suggest using extreme (maximum/minimum) values, either automatically generated or manually identified via hot-spots of CBV. Nevertheless, some of these methods have their shortcomings. First, 2D ROIs only evaluate isolated regions of the whole tumor and overlook tumor heterogeneity [12]. Second, relying on preselected single values, such as the mean or maximum, may overlook potential significant differences within the entire spectrum of voxel-wise values. These values can be further investigated using histogram-derived percentiles [22].

Finally, when CBV and PSR are evaluated, they are treated separately and their performances are compared as if one must choose between them. However, the reality is that they offer distinct information that characterizes tumor vascular-microvascular habitats from different perspectives. Therefore, CBV and PSR could be integrated, providing additive rather than mutually exclusive information [23].

Taking all these considerations together, the authors' objectives in the context of pre-surgical DSC-PWI evaluation of astrocytomas and oligodendrogliomas are:

- to characterize each tumor's DSC-PWI features, assess the discriminative power of CBV and PSR, and compare the performance of common preselected values (mean, extreme) with unsupervised voxel-level percentile values derived from 3D tumors' segmentations and
- 2. to unlock the potential value of combining CBV and PSR for these tumors' pre-surgical differentiation.

Material and methods

This retrospective study was approved by the Research Ethics Committee of Hospital Universitari de Bellvitge.

Patients

Patients diagnosed with IDH-mutant astrocytomas and IDH-mutant 1p19q-codeleted oligodendrogliomas, grades 2 or 3, were retrospectively retrieved from our center's database spanning the years 2010–2022. The stud's inclusion criteria were as follows: (1) confirmed tumor diagnosis in accordance with the World Health Organization classification of CNS Tumors 2021 [24], and (2) availability of a diagnostic pre-surgical MR examination including DSC-PWI, T1WI, T2WI, FLAIR, and contrast-enhanced T1WI (CE-T1WI). The study's exclusion criterion was sequences of such low quality that prevented tumor segmentation or DSC-PWI data extraction.

All tumors were classified following the WHO 2021 classification criteria. The classification process encompassed histopathological examination, immunohistochemical analysis for IDH, p53, and ATRX, as well as fluorescence in situ hybridization (FISH) for detecting 1p19q codeletion. The missing tests were retrospectively conducted for tumors with incomplete records using archived samples from the pathology department's biobank at our hospital as part of a national research project.

Imaging

All the MR imaging examinations included in the study were acquired in the same tertiary hospital with 2 different scanners: Ingenia 3.0- or Ingenia 1.5-T (Philips

Healthcare). All DSC-PWI sequences were gradient-echo, with the following technical parameters: time of echo, 40 ms; time of repetition, 1500–1700 ms; flip angle, 75°; pixel size, 1.75 mm²; slice thickness, 5mm; matrix size, 128 × 128; number of slices, 20–25; number and duration of dynamics, 60 and 1.5s. A single dose of 0.1 mmol/kg of intravenous GBCA (1 mmol/mL) was injected at a rate of 4–5 mL/s. No preload was administered. The baseline was in the order of 10–15 points. The quality of the sequences was assessed by two experienced neuroradiologist, i.e., A.P-E. and C.M., with more than one and two decades of experience in neuro-oncological radiology. Technical details of the morphological sequences (T1WI, T2WI, and FLAIR) are summarized in Supplemental Material 1.

Post-processing and DSC-PWI data extraction

The volumetric segmentations of the entire tumors, considering axial T1WI, T2WI, FLAIR, and CE-T1WI, were carried out semi-automatically (histogram thresholding) and checked by two experienced neuroradiologists: A.P-E. and C.M. The segmentations encompassed the entire signal abnormality in T2-FLAIR. The additional sequences were used as support to identify macroscopically normal brain vessels, cysts, calcifications, hemorrhage, or necrosis, which were all excluded from segmentations. Simultaneously, ten ROIs of 5-mm diameter were selected in the contralateral normal appearing white matter for normalization. The ten ROIs were consistently and homogeneously placed across all patients through a consensus approach by two experienced neuroradiologists (A.P-E. and C.M.). The ROIs were positioned within the centrum semiovale [25], covering two contiguous slices, each 5 mm in thickness. All segmentations and ROIs were done using 3D Slicer (http://www. slicer.org), and co-registered with DSC-PWI using the BRAINSFit module. The extraction of DSC-PWI metrics was streamlined using an in-house pipeline. CBV maps were produced with the DSC MRI analysis module in 3D Slicer. This software calculates CBV in accordance with consensus methodologies [11]. Time-intensity curves were converted into time-concentration curves and the area under the curve was calculated to obtain relative CBV, applying leakage correction using the Boxerman-Schmainda-Weiskoff (BSW) method. The PSR was captured early in the theoretical end of the first vascular pass of gadolinium on the time-intensity curve, automatically detected when the mean ascending slope of the curve fell below its standard deviation. This early PSR was then computed as described by Cha et al [26]. For each voxel within the tumors, normalized relative CBV leakage-corrected (from now on, nrCBV) and PSR were calculated. For each tumor, the mean, maximum, and minimum values of all the voxels as well as percentile values in increments of five were calculated.

Description and comparison of DSC-PWI metrics

Statistical analyses were conducted to compare astrocytomas and oligodendrogliomas nrCBV and PSR mean, minimum, maximum, and percentiles via Mann-Whitney *U* test. Simultaneously, we calculated the area under the receiver operating characteristic curve (AUC-ROC) for all variables, with tenfold stratified cross-validation to enhance robustness [27]. Finally, box-plots were constructed to visually assess the segregation potential of all these variables. In addition, a subanalysis was performed to compare differences between histological grades within each tumor type statistically.

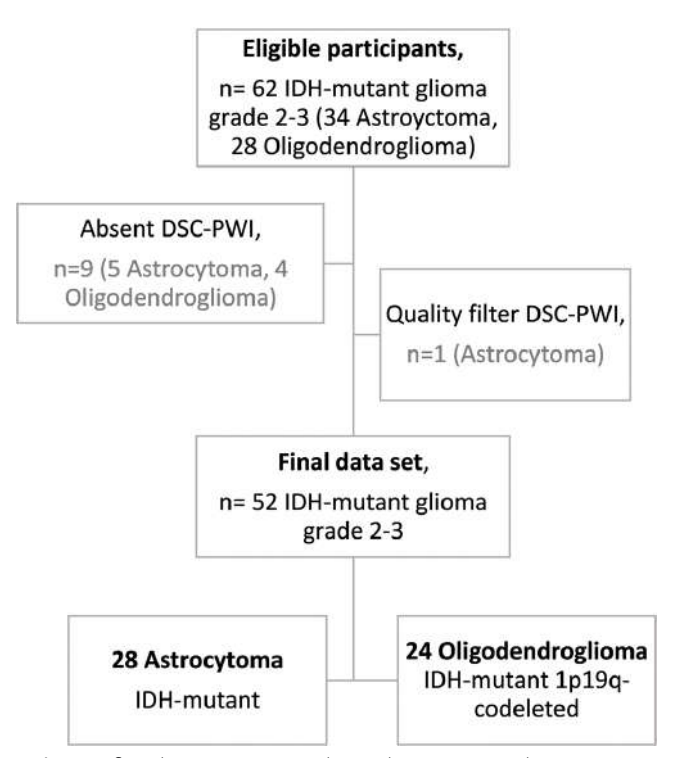
Combination of DSC-PWI metrics percentile values

In order to estimate the potential for classification by jointly considering nrCBV and PSR, we investigated a classifier. First, the correlation between nrCBV and PSR data was analyzed with a Spearman test. Then, the variables were narrowed down by selecting the nrCBV and PSR values with AUC-ROC > 0.8 [28] and p-value < 0.005 [29]. To further refine the number of variables included in the model and avoid overfitting, we limited to five features. The number five was chosen as the optimal according to our sample size [30]. Specifically, the final 5 variables were selected by applying recursive feature elimination choosing the variables that maximized accuracy in an iterative procedure until we were left with the top 5 most important features. Ultimately, we developed a straightforward gradient boosting classifier using a tenfold stratified cross-validation (find the details in Supplemental Materials 2 and 3). Gradient Boosting was chosen due to its ability to automatically capture complex interactions among features, robustness to outliers, and adaptability to avoid overfitting [31]. Lastly, we calculated its AUC-ROC to gauge its classification potential. All statistical computations were performed making combined use of Python version 3.10.5, R version 4.1.3, and IBM SPSS Statistics version 25.

Results

Patients

Sixty-two candidates were initially identified for this study. Nine patients were excluded due to lack of DSC-PWI, and one was because of poor quality of DSC-PWI. The final participant count was 52, consisting of 28 astrocytomas and 24 oligodendrogliomas. Figure 1 provides a summary of the participant flowchart. The descriptive details, including age, sex, and grade, are compiled in Table 1, including statistical comparisons. The mean age for the entire dataset was 45 ± 13 years. Twenty-eight



participants were men and 31 had grade 3 tumors. There were no significant differences between astrocytomas and oligodendrogliomas for the demographic variables.

Description and comparison of DSC-PWI metrics

Oligodendrogliomas exhibited higher nrCBV and lower PSR than astrocytomas across all metrics (e.g., mean nrCBV = 2.05 and 1.55, PSR = 0.68 and 0.81 respectively). The mean, minimum, maximum, and the best percentile values are shown in Table 2, along with their corresponding AUC-ROC and Mann-Whitney U p values. The highest AUC-ROCs derived from PSR percentile p70 (AUC-ROC = 0.84, p value = 0.0005) and nrCBV percentile p75 (AUC-ROC = 0.80, p value = 0.0006). The specificities for these two percentiles were 0.93 and 0.72, sensitivities of 0.65 and 0.80, and accuracies of 0.79 and 0.76, considering the optimal thresholds of 0.71 and 2.02, respectively. The AUC-ROCs for mean nrCBV (0.74) and PSR (0.73) were lower than that of several percentiles. The lowest results were observed for minimum and maximum values (AUC-ROCs from 0.64 to 0.69). A Z-test demonstrated statistically significant differences in AUC-ROCs of PSRp70 and nrCBVp75 above the minimum, maximum, and mean values (p < 0.035). The whole range of results, AUC-ROCs' confidence intervals, and p values before and after the Bonferroni correction are available in Supplemental Material 4. It is also noteworthy that the

Table 1 This table presents the demographic and clinical characteristics of the participants, including age, sex, and tumor grade. Statistical comparisons were made using the Mann-Whitney *U* test for age, and the chi-square test for both sex and tumor grade. *SD* standard deviation

	Oligodendroglioma	Astrocytoma	Whole dataset	<i>p</i> value
Age in years (mean ± SD)	49 ± 14	43 ± 13	45 ± 13	0.17
Sex, men: women	15:09	13:15	28:24	0.38
Grade, 2:3	10:14	11:17	21:31	0.85
Total	24	28	52	

best percentile values exhibited lower standard deviations and narrower confidence intervals, which further suggests an increased level of robustness in comparison to mean, minimum, and maximum. The distributions of all the values for each metric and group are depicted in box-plots in Figs. 2 and 3. These graphics clearly visualize the varying segregation potential, accentuated for percentile values.

Of note, no significant differences in the Mann-Whitney *U* test were found for the nrCBV nor PSR values between grades 2 and 3 (Supplemental Material 5). Ultimately, 7 out of the 28 astrocytomas and 5 out of the 24 oligodendrogliomas were assessed using a 3.0-T scanner. The chi-square test verified that there were no significant differences in the distribution of 3.0-T studies between the two groups (Supplemental Material 6). Furthermore, when comparing DSC-PWI metrics between 1.5 T and 3 T within each tumor type, we found no significant differences attributable to the field strength employed.

Combination of DSC-PWI metrics percentile values

The Spearman correlation analysis revealed a general lack of significant correlation between the nrCBV and

Table 2 Summary of mean \pm standard deviation values for nrCBV and PSR variables for each tumor subtype. These values correspond to the most common preselected mean, minimum, and maximum variables, and the best discriminating percentiles.

PSR values (see the details in Supplemental Material 7). The nrCBV or PSR percentiles with AUC-ROC > 0.8 [28] and p value < 0.005 [29] were nrCBV percentiles p70 and p75 and PSR from p40 to p75. AUC-ROC values ranged from 0.80 to 0.84 and p values from 0.0002 to 0.0007. Of note, all these variables remain significant after Bonferroni correction (Supplemental Material 4). Following the recursive feature elimination, the five definitive variables selected for classification, in order of feature importance (specified in brackets), were PSR_p65 (0.366), CBV_p70 (0.236), PSR_p60 (0.202), CBV_p75 (0.119), and PSR_ p40 (0.078). The mean AUC-ROC for the gradient boosting classifier was 0.87, with a standard deviation of 0.16 and 95% confidence intervals ranging from 0.84 to 0.91 outperforming all the previous single-metric and singlevalue performances (Z-test, p < 0.05). Finally, the best cross-validation fold produced an AUC-ROC of 0.91.

As a final addition to the main analysis, the best differentiating metrics of the study were evaluated by categorizing astrocytomas with or without T2-FLAIR mismatch. This sign, evaluated visually by two experienced neuroradiologists, was only present in 10 out of the 28 astrocytomas (36%). In the T2-FLAIR mismatch

The corresponding AUC-ROC and Mann-Whitney Up values are also included. * indicates statistical significance according to classic criteria (p < 0.05), and ** according to recently suggested more restrictive and robust criteria (p < 0.005)

<u>Mean</u>	nrCBV	PSR	<u>Minimum</u>	nrCBV	PSR
Oligo	2.05 ± 0.58	0.68 ± 0.21	Oligo	0.13 ± 0.13	0.19 ± 0.09
Astro	1.55 ± 0.58	0.81 ± 0.19	Astro	0.09 ± 0.14	0.27 ± 0.12
AUC-ROC	0.74	0.73	AUC-ROC	0.67	0.67
Mann- <i>U, p</i>	0.001**	0.005*	Mann- <i>U, p</i>	0.13	0.01*
<u>Maximum</u>	nrCBV	PSR	<u>Percentiles</u>	nrCBV p75	PSR p70
Oligo	5.91 ± 1.82	1.17 ± 0.60	Oligo	2.53 ± 0.98	0.69 ± 0.11
Astro	4.72 ± 1.75	1.33 ± 0.43	Astro	1.86 ± 0.78	0.81 ± 0.12
AUC-ROC	0.69	0.64	AUC-ROC	0.80	0.84
Mann- <i>U, p</i>	0.01*	0.01*	Mann- <i>U, p</i>	0.0006**	0.0005**

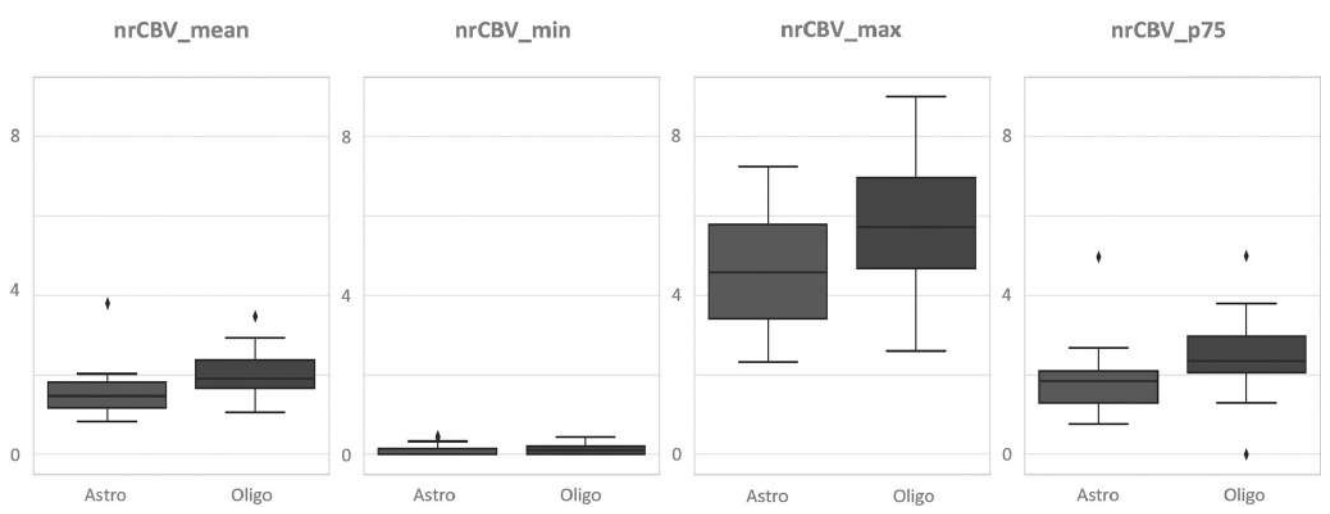


Fig. 2 Whisker plots illustrate the distribution of all nrCBV values for each tumor subtype's mean, minimum, maximum, and best percentile

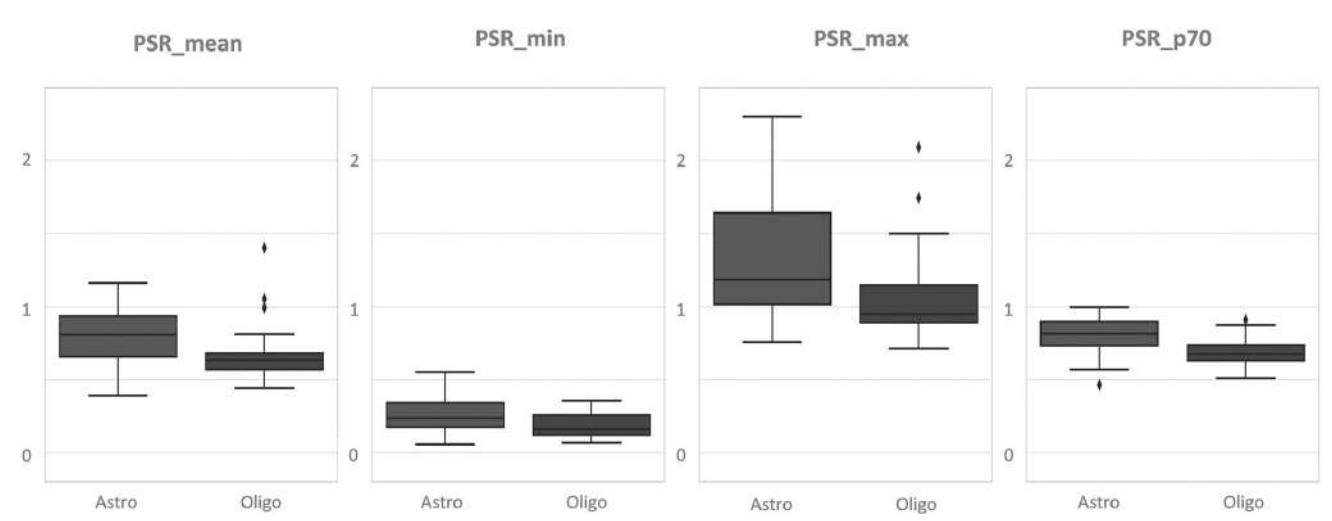


Fig. 3 Whisker plots illustrate the distribution of all PSR values for each tumor subtype's mean, minimum, maximum, and best percentile

absent group, the AUCs of CBVp75, PSRp70, and the classifier were 0.78, 0.82, and 0.85 retaining a good to excellent performance.

Discussion

In this study, we delved into the distinctive features of DSC-PWI in distinguishing astrocytomas and oligodendrogliomas. Firstly, we have pioneered the exploration of the PSR as a potential discriminator between these tumor types. Our data indicates a lower PSR in oligodendrogliomas. Regarding nrCBV, our findings align with previous studies that observed higher nrCBV in this tumor type [32–36]. Furthermore, we have augmented the efficacy of PSR and nrCBV analysis by introducing an unsupervised method to identify the most discriminative voxel-wise

percentiles (AUC-ROC PSRp70 = 0.84 and nrCBVp75 = 0.80), which exceeds the conventional approach of solely relying on single preselected values such as the mean or maximum. Notably, the combined use of nrCBV and PSR does not result in exclusivity, but rather in an additive effect, thereby forming a powerful basis for robust classification. An illustrative example of the applicability of our methodology to classify future presurgical patients is presented in Figs. 4 and 5.

The most common approach for nrCBV calculations involves focusing on the mean values of 2D ROIs manually depicted, or whole-tumor 3D VOIs. However, if a specific ROI is manually selected, operator dependency resurfaces, complicating reproducibility, and only a portion of the whole tumor is evaluated. Also, if only preselected

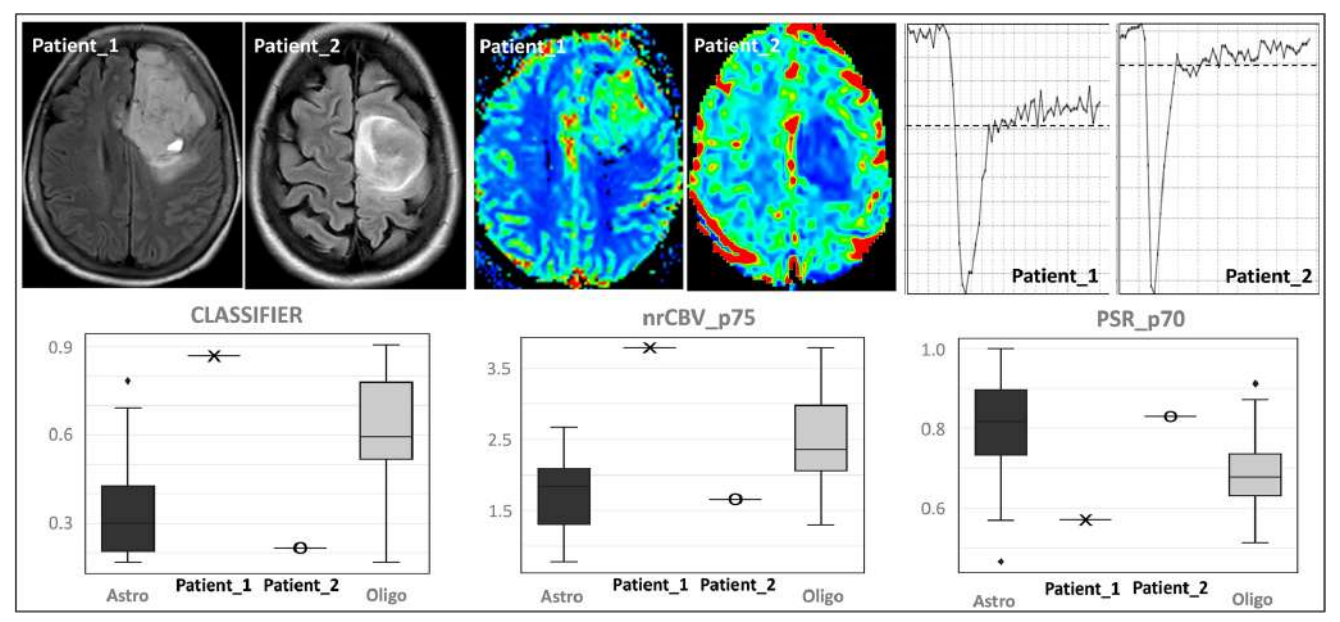


Fig. 4 An illustrative example of the applicability of our proposed methodology for classifying new cases. Patient_1, a 64-year-old female, and Patient_2, a 34-year-old female, both studied using 1.5-T MR scan. Two FLAIR sequences of the patients show two frontal infiltrative tumors along with the rCBV maps and representative time-intensity curves. The classifier probability, nrCBVp75, and PSRp70 values of each case are overlaid onto the corresponding values of all astrocytomas and oligodendrogliomas in whisker plots. The display allows for a visual evaluation of the results, which suggests that Patient_1 would be more likely to be an oligodendroglioma and Patient_2 an astrocytoma. Both cases were histopathology confirmed. The histological grade was 3 in both cases

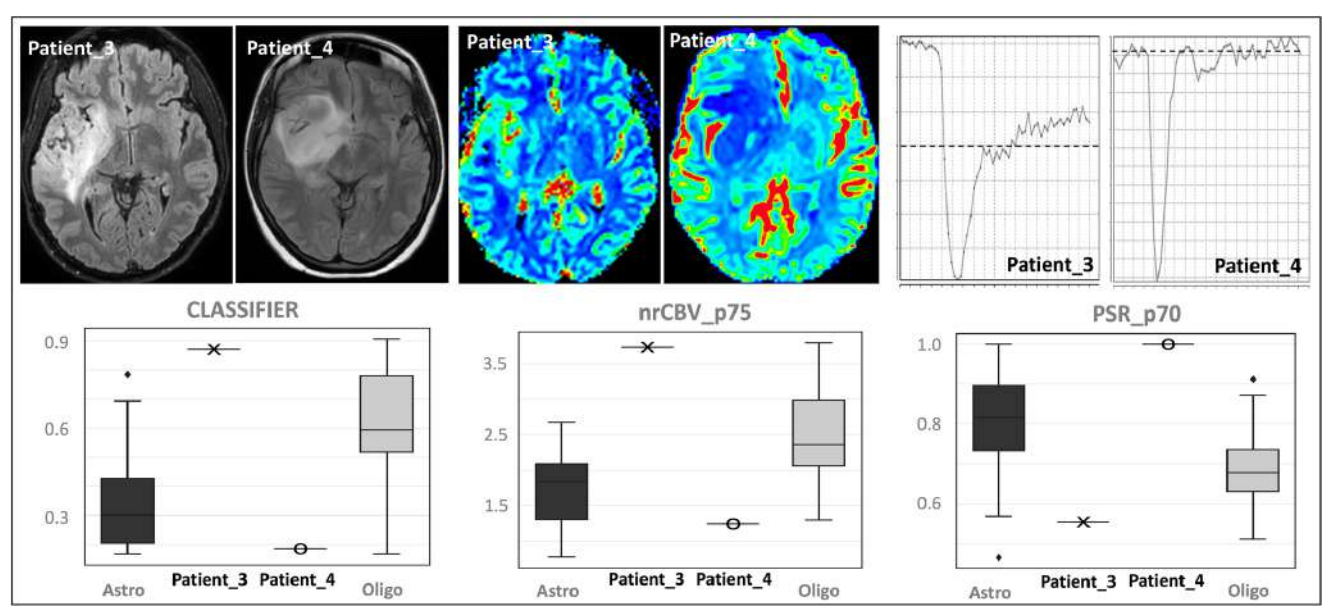


Fig. 5 An illustrative example of the applicability of our proposed methodology for classifying new cases. Patient_3, a 42-year-old male, and Patient_4, a 25-year-old female, both studied using 3-T MR scan. Two FLAIR sequences of the patients show two fronto-insulo-temporal infiltrative tumors along with the rCBV maps and representative time-intensity curves. The classifier probability, nrCBVp75, and PSRp70 values of each case are overlaid onto the corresponding values of all astrocytomas and oligodendrogliomas in whisker plots. The display allows for a visual evaluation of the results, which suggests that Patient_3 would be more likely to be an oligodendroglioma and Patient_4 an astrocytoma. Both cases were histopathology confirmed. The histological grade was 2 in both cases

values of the entire 3D tumor are used, the heterogeneity of the tumors (especially of oligodendrogliomas in the current differential) is overlooked. Indeed, relying on preselected values often assumes that they will capture the most significant differences, an assumption that may lack a robust foundation [12]. Therefore, these methods fail to consider that differences may exist anywhere across the full spectrum of voxel-wise values [22]. In this work, we propose an objective, unsupervised, voxel-level percentile evaluation of 3D segmentations of the whole tumor. This offers more reproducible, robust, and improved information that better captures tumor heterogeneity while avoiding weak assumptions in the preselection of optimal values to differentiate between entities.

In terms of novel insights about the PSR, to our knowledge, only two prior studies involved PSR evaluations in tumors with oligodendrocytic component. However, these studies were conducted prior to the establishment of the current 2021 WHO classification criteria and treated oligodendrocytic tumors as mixed with other low- and highgrade glial tumors [37, 38]. Therefore, their results are not applicable to the current classification system and are not comparable with ours. PSR uniquely provides indirect measures of the interplay between T1 and T2* effects. In general terms, lower PSR values indicate predominant T2* effects, while higher values suggest predominant T1 effects. Based on our current understanding of leakage effects, it is known that PSR is shaped by a complex interplay of BBB disruption, variations in cell size and density, and the size and tortuosity of vessels. This theory mainly applies to brain tumors with extensive BBB disruptions. These disruptions enable a portion of the GBCA to leak through the vessels and interact with the extravascular extracellular space (EES) molecules and adjacent cellularity, while another portion remains within the vessels, reflecting vascular features [39-41]. However, when dealing with brain tumors with a more preserved BBB, such as the entities under investigation, the GBCA does not so significantly leak, thus minimizing the influence of BBB permeability and cellularity on the PSR. Consequently, it is plausible that the PSR in these tumors, such as grade 2–3 gliomas, primarily offers insight into the vascular architecture [42]. In simplified terms for clarity, in such cases, increased vessel disorganization and tortuosity could partially retain intravascular gadolinium. This incomplete wash-out could prevent the signal intensity curve from fully recovering, leading to a lower PSR. It is noteworthy that PSR calculation is not universally standardized. However, this specific vascular characteristic may be enhanced when the metric is calculated early towards the end of the first vascular pass of contrast, as done in this study. At this point, any potential GBCA leakage due to eventual foci of partial BBB disruptions is expected to be minimized.

This theory is further supported by previous observations in CNS tumors that lack a BBB and exhibit prominent tortuous vasculature, such as hypervascular metastases, meningiomas, or hemangioblastomas. These tumors are well-known for presenting with low PSR, attributable to their distinctive vascular features. Despite the different underlying explanation, these tumors share one commonality with the tumors currently under investigation: the absence, for one reason or another, of BBB leakage [22, 23, 26]. At this point, in the case of astrocytomas and oligodendrogliomas, it is crucial to point out that the histological vascular characteristics of oligodendrogliomas are marked by a network of irregular and tortuous vessels, frequently described as a chicken-wire capillary pattern [43-45]. This vascular pattern diverges significantly from that found in astrocytomas which while also altered generally retains a greater similarity to normal brain tissue [46]. This knowledge, especially about the unique microvascular architecture of oligodendrogliomas, aligns with our observations.

On the other hand, when nrCBV and PSR are evaluated, they are generally treated separately and their performances are compared as if one must choose between them. However, the reality is that they offer distinct information that characterizes tumor vascular features from different perspectives. In fact, and especially if correction methods are applied to nrCBV, PSR should not influence nrCBV values and vice versa, as also evidenced by our correlation analysis. Given these considerations, nrCBV and PSR could be combined, providing additive rather than mutually exclusive information [12, 23]. Additionally, by considering both metrics, we are considering the tumors' vascular-microvascular habitats from a broader perspective than what single variables allow. Specifically, our combined nrCBV and PSR classifier demonstrates promising potential, with an estimated AUC-ROC of 0.87, an excellent result which still requires further validation. Beyond improved classification results, the simultaneous consideration of multiple DSC-PWI variables offers a more comprehensive perspective of the tumor's vascular characteristics than traditional single metrics do. Therefore, this approach is likely to be more robust, mitigating single metric variabilities and providing a more holistic assessment of the vascular characteristics of the tumors.

Additionally, our T2-FLAIR mismatch subanalysis suggests that our method retains good to excellent performance in those tumors where the T2-FLAIR mismatch is absent or uncertain (such as in scenarios involving inexperienced radiologists). These preliminary results, out of the main scope of the present study, show promise and deserve dedicated further studies.

The generalizability of our results may be influenced by the technique employed and various post-processing steps, which can significantly impact CBV and PSR values. Current efforts towards standardization, as suggested by Boxerman et al [11] in 2020, recommend using either full-dose preloaded 60° flip-angle or 30° without preload sequences. However, considering the recent introduction of these recommendations and the advancements in genetic classification as per the WHO 2021 guidelines, there is currently scarce comprehensive data. This scarcity impedes the comparison of our results with others obtained using the agreed-upon consensus sequences for our specific purpose. Speculatively, using these preloaded or low FA techniques could result in higher CBV and lower PSR values, by minimizing the T1 leakage effects to optimize nrCBV measures [11], provided other post-processing steps remain consistent[12]. However, the expected differences in the studied tumors should be minor than those seen in tumors with extensive BBB disruption, and ultimately, we also applied post-processing leakage correction [47]. Additionally, nonpreloaded intermediate-high flip-angle sequences (such as used in this study) have proven useful and may be the preferred choice for some authors and clinicians, specifically for pre-surgical diagnosis [13, 16, 17, 48]. Lastly, our methodology should be adaptable to different DSC-PWI pulse-sequence parameters by simply adjusting the thresholds [14]. Regardless, further multicentric validations are needed.

On another hand, our study design grouping grades 2 and 3 is a common approach in radiological papers (usually under the term "lower grade gliomas") [36] and it is supported by the absence of any significant difference between grades in this work, which is also aligned with other radiological studies [49, 50]. Furthermore, several clinical papers also suggest that the precise genetic classification of tumors has reduced the impact of histological grading on biological behaviors [51-54]. All these facts ensure the study objectives and results are the most clinically relevant according to current neuro-oncological diagnostic trends. Also, this design was chosen to strictly adhere to the current WHO classification molecular criteria and, lastly, to avoid excessive dataset fragmentation. At any rate, separated data for each tumor grade is provided as supplemental material for increased clarity and transparency of results.

Some alternative investigations leveraged radiomic features derived from DSC-PWI, yielding promising results with innovative methodology [55]. In contrast, our study concentrates on the specific differentiation between astrocytoma and oligodendroglioma, and employs well-established and clinically accessible metrics, which facilitates ease of understanding and practical application while forges a direct connection with the foundational histological and biological processes, potentially opening new research avenues.

This study has some limitations that must be considered. First, it is a single-site, retrospective study. However, this ensures data homogeneity, which is important for pilot and exploratory studies such as ours. Also, other DSC-PWI metrics such as mean transit time and cerebral blood flow may have a role, yet their implementation requires arterial input function determination, leading to increased complexity in calculations. In contrast, our study boasts notable strengths that deserve mention. First, all tumors are classified according to the most recent 2021 WHO Classification criteria. Our findings offer valuable clinically relevant and applicable insights from various perspectives. For instance, our study reinforces the necessity of semiautomatic and unsupervised assessment of the entire tumor percentile values, instead of assuming that mean or maximum values are the best options, a common practice in clinical settings. Notably, this observation could serve as a suggestion for software vendors to consider including these options in their packages. Additionally, we provide new insights into oligodendrogliomas' vascular and microvascular features using a widely available clinical sequence. Moreover, our findings may be applied to other clinical questions, potentially opening new research avenues. In this regard, we acknowledge emerging DSC sequences and metrics that may offer improved information regarding permeability or vascular architecture. Nevertheless, these sequences have not yet been widely adopted in clinical practice. Ultimately, the foundational knowledge uniquely presented in this work paves the ground for their further implementation.

In conclusion, oligodendrogliomas demonstrate a higher nrCBV and lower PSR than astrocytomas, characteristics that are accentuated when voxel-wise percentile values are considered. We hypothesize that the lower PSR might reflect higher microvascular tortuosity and aligns with the well-established histological substrate of oligodendrogliomas, known as the chicken-wire capillary pattern. Lastly, the combination of nrCBV and PSR percentiles augments the value of standard single-metric and single-value evaluations, yielding promising classification results.

Abbreviations

BBB Blood-brain barrier
CBV Cerebral blood volume

DSC-PWI Dynamic susceptibility contrast perfusion-weighted imaging

EES Extravascular extracellular space
GBCA Gadolinium-based contrast agent
IDH Isocitrate dehydrogenase
PSR Percentage of signal recovery
WHO World Health Organization

Supplementary Information

The online version contains supplementary material available at https://doi.org/10.1007/s00330-024-10611-z.

Below is the link to the electronic supplementary material. Supplementary file1 (PDF 755 KB)

Acknowledgements

Albert Pons-Escoda and Carles Majos acknowledge support from the Instituto de Salud Carlos III (Proyectos de Investigación en Salud,Pl20/00360). The authors thank CERCA Programme/Generalitat de Catalunya for institutional support.

Funding

Open Access funding provided thanks to the CRUE-CSIC agreement with Springer Nature. The authors state that this study did not receive any funding.

Declarations

Guarantor

The scientific guarantor of this publication is Albert Pons-Escoda.

Conflict of interest

Marion Smits declares consultancy fees from Bracco and Speaker fees from GE Healthcare, AuntMinnie and Fondazione Internazionale Menarini (all paid to institution).

Albert Pons-Escoda is a member of the European Radiology Editorial Board. They have not taken part in the review or selection process of this article. The other authors of this manuscript declare no relationships with any companies, whose products or services may be related to the subject matter of the article.

Statistics and biometry

Several authors have significant statistical expertise: Albert Pons-Escoda, Alonso Garcia-Ruiz, Pablo Naval-Baudin, and Ignacio Martinez-Zalacain.

Informed consent

Written informed consent was waived by the Institutional Review Board.

Ethical approval

Institutional Review Board approval was obtained.

Study subjects or cohorts overlap

Some study subjects have been previously reported in Proton MR spectroscopy shows improved performance to segregate high-grade astrocytoma subgroups when defined with the new 2021 World Health Organization classification of central nervous system tumors, European Radiology 2023, in-press.

Methodology

- retrospective
- diagnostic study
- performed at one institution

Author details

¹Radiology Department, Feixa Llarga SN, Hospital Universitari de Bellvitge, 08907 Barcelona, Spain. ²Neuro-oncology Unit, Feixa Llarga SN, Institut d'Investigació Biomèdica de Bellvitge- IDIBELL, 08907 Barcelona, Spain. ³Facultat de Medicina i Ciències de La Salut, Universitat de Barcelona (UB), Carrer de Casanova 143, 08036 Barcelona, Spain. ⁴Diagnostic Imaging and Nuclear Medicine Research Group, Institut d'Investigació Biomèdica de Bellvitge- IDIBELL, Feixa Llarga SN, 08907 Barcelona, Spain. ⁵Radiomics Group, Vall d'Hebron Institut d'Oncologia- VHIO, Carrer de Natzaret, 115-117, 08035 Barcelona, Spain. ⁶Pathology Department, Feixa Llarga SN, Hospital Universitari de Bellvitge, 08907 Barcelona, Spain. ⁷Radiology Department, Hospital Clinic de Barcelona, Villarroel 170, 08036 Barcelona, Spain. ⁸Department of Radiology & Nuclear Medicine, Erasmus MC, Molewaterplein 40, 3015 GD Rotterdam, The

Netherlands. ⁹Erasmus MC Cancer Institute, Erasmus MC, Molewaterplein 40, 3015 GD Rotterdam, The Netherlands. ¹⁰Medical Delta, Delft, The Netherlands.

Received: 31 October 2023 Revised: 13 December 2023 Accepted: 1 January 2024 Published online: 29 January 2024

References

- Mitchell D, Shireman JM, Dey M (2022) Surgical neuro-oncology. Neurol Clin 40:437–453. https://doi.org/10.1016/j.ncl.2021.11.003
- Balana C, Castañer S, Carrato C et al (2022) Preoperative diagnosis and molecular characterization of gliomas with liquid biopsy and radiogenomics. Front Neurol 13:865171. https://doi.org/10.3389/fneur.2022.865171
- Vagvala S, Guenette JP, Jaimes C, Huang RY (2022) Imaging diagnosis and treatment selection for brain tumors in the era of molecular therapeutics. Cancer Imaging 22:19. https://doi.org/10.1186/s40644-022-00455-5
- Blobner J, Dengler L, Blobner S, et al (2023) Significance of molecular diagnostics for therapeutic decision-making in recurrent glioma. Neuro-Oncology Adv 5:vdad060. https://doi.org/10.1093/noajnl/vdad060
- Patel SH, Batchala PP, Mrachek EKS et al (2020) MRI and CT identify isocitrate dehydrogenase (IDH) -mutant lower-grade gliomas misclassified to 1p/19q codeletion status with fluorescence in situ hybridization. Radiology 294:160–167. https://doi.org/10.1148/radiol.2019191140
- Hirschler L, Sollmann N, Schmitz-Abecassis B et al (2023) Advanced MR techniques for preoperative glioma characterization: part 1. J Magn Reson Imaging 57:1655–1675. https://doi.org/10.1002/jmri.28662
- Jain R, Johnson DR, Patel SH et al (2020) "Real world" use of a highly reliable imaging sign: "T2-FLAIR mismatch" for identification of IDH mutant astrocytomas. Neuro Oncol 22:936–943. https://doi.org/10.1093/neuonc/noaa041
- Zhou M, Scott J, Chaudhury B et al (2018) Radiomics in brain tumor: image assessment, quantitative feature descriptors, and machine-learning approaches. AJNR Am J Neuroradiol 39:208–216. https://doi.org/10.3174/ajnr.A5391
- Kaufmann TJ, Smits M, Boxerman J et al (2020) Consensus recommendations for a standardized brain tumor imaging protocol for clinical trials in brain metastases. Neuro Oncol 22:757–772. https://doi.org/10.1093/neuonc/noaa030
- Barajas RF, Politi LS, Anzalone N et al (2021) Consensus recommendations for MRI and PET imaging of primary central nervous system lymphoma: guideline statement from the International Primary CNS Lymphoma Collaborative Group (IPCG). Neuro Oncol 23:1056–1071. https://doi.org/10. 1093/neuonc/noab020
- Boxerman JL, Quarles CC, Hu LS et al (2020) Consensus recommendations for a dynamic susceptibility contrast MRI protocol for use in high-grade gliomas. Neuro Oncol 22:1262–1275. https://doi.org/10.1093/neuonc/noaa141
- Pons-Escoda A, Smits M (2023) Dynamic-susceptibility-contrast perfusion-weighted-imaging (DSC-PWI) in brain tumors: a brief up-todate overview for clinical neuroradiologists. Eur Radiol. https://doi.org/10. 1007/s00330-023-09729-3
- 13. Mangla R, Kolar B, Zhu T et al (2011) Percentage signal recovery derived from MR dynamic susceptibility contrast imaging is useful to differentiate common enhancing malignant lesions of the brain. AJNR Am J Neuroradiol 32:1004–1010. https://doi.org/10.3174/ajnr.A2441
- Lee MD, Baird GL, Bell LC et al (2019) Utility of percentage signal recovery and baseline signal in DSC-MRI optimized for relative CBV measurement for differentiating glioblastoma, lymphoma, metastasis, and meningioma. AJNR Am J Neuroradiol 40:1145–1450. https://doi.org/10.3174/ajnr.A6153
- Pons-Escoda A, Garcia-Ruiz A, Naval-Baudin P et al (2020) Presurgical identification of primary central nervous system lymphoma with normalized time-intensity curve: a pilot study of a new method to analyze DSC-PWI. AJNR Am J Neuroradiol 41:1816–1824. https://doi.org/10.3174/ajnr.A6761
- Cindil E, Sendur HN, Cerit MN et al (2021) Validation of combined use of DWI and percentage signal recovery-optimized protocol of DSC-MRI in differentiation of high-grade glioma, metastasis, and lymphoma. Neuroradiology 63:331–342. https://doi.org/10.1007/s00234-020-02522-9
- Wang F, Zhou X, Chen R et al (2023) Improved performance of non-preloaded and high flip-angle dynamic susceptibility contrast perfusion-weighted imaging sequences in the presurgical differentiation of brain lymphoma and glioblastoma. Eur Radiol. https://doi.org/10.1007/s00330-023-09917-1
- 18. Pons-Escoda A, García-Ruíz A, Naval-Baudin P et al (2022) Diffuse large B-cell epstein-barr virus-positive primary CNS lymphoma in non-AIDS

- patients: high diagnostic accuracy of DSC perfusion metrics. AJNR Am J Neuroradiol 43:1567–1574. https://doi.org/10.3174/ajnr.A7668
- Nakajima S, Okada T, Yamamoto A et al (2015) Primary central nervous system lymphoma and glioblastoma: differentiation using dynamic susceptibility-contrast perfusion-weighted imaging, diffusion-weighted imaging, and 18F-fluorodeoxyglucose positron emission tomography. Clin Imaging 39:390–395. https://doi.org/10.1016/j.clinimag.2014.12.002
- Nakajima S, Okada T, Yamamoto A et al (2015) Differentiation between primary central nervous system lymphoma and glioblastoma: a comparative study of parameters derived from dynamic susceptibility contrastenhanced perfusion-weighted MRI. Clin Radiol 70:1393–1399. https://doi. org/10.1016/j.crad.2015.08.004
- Bhowmik A, Khan R, Ghosh MK (2015) Blood brain barrier: a challenge for effectual therapy of brain tumors. Biomed Res Int 2015:1–20. https://doi. org/10.1155/2015/320941
- 22. Pons-Escoda A, Garcia-Ruiz A, Naval-Baudin P et al (2022) Voxel-level analysis of normalized DSC-PWI time-intensity curves: a potential generalizable approach and its proof of concept in discriminating glioblastoma and metastasis. Eur Radiol. https://doi.org/10.1007/s00330-021-08498-1
- Pons-Escoda A, Garcia-Ruiz A, Garcia-Hidalgo C et al (2023) MR dynamicsusceptibility-contrast perfusion metrics in the presurgical discrimination of adult solitary intra-axial cerebellar tumors. Eur Radiol. https://doi.org/ 10.1007/s00330-023-09892-7
- 24. WHO Classification of Tumours Editorial Board Central nervous system tumours [Internet]. Lyon (France): International Agency for Research on Cancer; 2021 [cited 2023 Jul 13]. (WHO classification of tumours series, 5th ed.). Available from: https://tumourclassification.iarc.who.int/chapters/45
- Cho NS, Hagiwara A, Sanvito F, Ellingson BM (2023) A multi-reader comparison of normal-appearing white matter normalization techniques for perfusion and diffusion MRI in brain tumors. Neuroradiology 65:559–568. https://doi.org/10.1007/s00234-022-03072-v
- Cha S, Lupo JM, Chen M-H et al (2007) Differentiation of glioblastoma multiforme and single brain metastasis by peak height and percentage of signal intensity recovery derived from dynamic susceptibility-weighted contrast-enhanced perfusion MR imaging. AJNR Am J Neuroradiol 28:1078–1084. https://doi.org/10.3174/ajnr.A0484
- 27. Airola A, Pahikkala T, Waegeman W et al (2011) An experimental comparison of cross-validation techniques for estimating the area under the ROC curve. Comput Stat Data Anal 55:1828–1844. https://doi.org/10.1016/j.csda.2010.11.018
- Mandrekar JN (2010) Receiver operating characteristic curve in diagnostic test assessment. J Thorac Oncol 5:1315–1316. https://doi.org/10.1097/ JTO.0b013e3181ec173d
- 29. Benjamin DJ, Berger JO, Johannesson M et al (2017) Redefine statistical significance. Nat Hum Behav 2:6–10. https://doi.org/10.1038/s41562-017-0189-z
- Hair JF, Hult GTM, Ringle CM et al (2021) An introduction to structural equation modeling. Partial Least Squares Structural Equation Modeling (PLS-SEM)
 Using R: A Workbook. Springer International Publishing. Cham. pp 1–29
- 31. Natekin A, Knoll A (2013) Gradient boosting machines, a tutorial. Front Neurorobot 7:21. https://doi.org/10.3389/fnbot.2013.00021
- Latysheva A, Emblem KE, Brandal P et al (2019) Dynamic susceptibility contrast and diffusion MR imaging identify oligodendroglioma as defined by the 2016 WHO classification for brain tumors: histogram analysis approach. Neuroradiology 61:545–555. https://doi.org/10.1007/s00234-019-02173-5
- Song S, Wang L, Yang H et al (2021) Static (18)F-FET PET and DSC-PWI based on hybrid PET/MR for the prediction of gliomas defined by IDH and 1p/19q status. Eur Radiol 31:4087–4096. https://doi.org/10.1007/s00330-020-07470-9
- 34. Yang X, Lin Y, Xing Z et al (2021) Predicting 1p/19q codeletion status using diffusion-, susceptibility-, perfusion-weighted, and conventional MRI in IDH-mutant lower-grade gliomas. Acta Radiol 62:1657–1665. https://doi.org/10.1177/0284185120973624
- Siakallis L, Topriceanu C-C, Panovska-Griffiths J, Bisdas S (2023) The role of DSC MR perfusion in predicting IDH mutation and 1p19q codeletion status in gliomas: meta-analysis and technical considerations. Neuroradiology 65:1111–1126. https://doi.org/10.1007/s00234-023-03154-5
- Lee MK, Park JE, Jo Y et al (2020) Advanced imaging parameters improve the prediction of diffuse lower-grade gliomas subtype, IDH mutant with no 1p19q codeletion: added value to the T2/FLAIR mismatch sign. Eur Radiol 30:844–854. https://doi.org/10.1007/s00330-019-06395-2
- Smitha KA, Gupta AK, Jayasree RS (2015) Relative percentage signal intensity recovery of perfusion metrics—an efficient tool for differentiating grades of glioma. Br J Radiol 88:20140784. https://doi.org/10.1259/bjr.20140784

- Aprile I, Giovannelli G, Fiaschini P et al (2015) High- and low-grade glioma differentiation: the role of percentage signal recovery evaluation in MR dynamic susceptibility contrast imaging. Radiol Med 120:967–974. https://doi.org/10.1007/s11547-015-0511-7
- Quarles CC, Gochberg DF, Gore JC, Yankeelov TE (2009) A theoretical framework to model DSC-MRI data acquired in the presence of contrast agent extravasation. Phys Med Biol 54:5749–5766. https://doi.org/10. 1088/0031-9155/54/19/006
- 40. Sanvito F, Raymond C, Cho NS et al (2023) Simultaneous quantification of perfusion, permeability, and leakage effects in brain gliomas using dynamic spin-and-gradient-echo echoplanar imaging MRI. Eur Radiol. https://doi.org/10.1007/s00330-023-10215-z
- Pons-Escoda A (2023) "Everything everywhere all at once": unraveling perfusion, permeability, and leakage effects in neurooncology with a single-dose, single-acquisition dual-echo DSC. Eur Radiol. https://doi.org/ 10.1007/s00330-023-10277-z
- 42. Lupo JM, Cha S, Chang SM, Nelson SJ (2005) Dynamic susceptibilityweighted perfusion imaging of high-grade gliomas: characterization of spatial heterogeneity. AJNR Am J Neuroradiol 26:1446–1454
- Wesseling P, van den Bent M, Perry A (2015) Oligodendroglioma: pathology, molecular mechanisms and markers. Acta Neuropathol 129:809–827. https://doi.org/10.1007/s00401-015-1424-1
- Smits M (2016) Imaging of oligodendroglioma. Br J Radiol 89:20150857. https://doi.org/10.1259/bjr.20150857
- Arzanforoosh F, van der Voort SR, Incekara F, et al (2023) Microvasculature features derived from hybrid EPI MRI in non-enhancing adult-type diffuse glioma subtypes. Cancers (Basel) 15. https://doi.org/10.3390/cancers15072135
- Cha S, Tihan T, Crawford F et al (2005) Differentiation of low-grade oligodendrogliomas from low-grade astrocytomas by using quantitative blood-volume measurements derived from dynamic susceptibility contrast-enhanced MR imaging. AJNR Am J Neuroradiol 26:266–73
- Paulson ES, Schmainda KM (2008) Comparison of dynamic susceptibilityweighted contrast-enhanced MR methods: recommendations for measuring relative cerebral blood volume in brain tumors. Radiology 249:601–613. https://doi.org/10.1148/radiol.2492071659
- Cindil E, Sendur HN, Cerit MN et al (2022) Prediction of IDH mutation status in high-grade gliomas using DWI and high T1-weight DSC-MRI. Acad Radiol 29:S52–S62. https://doi.org/10.1016/j.acra.2021.02.002
- Yang X, Xing Z, She D et al (2022) Grading of IDH-mutant astrocytoma using diffusion, susceptibility and perfusion-weighted imaging. BMC Med Imaging 22:105. https://doi.org/10.1186/s12880-022-00832-3
- Khalid L, Carone M, Dumrongpisutikul N et al (2012) Imaging characteristics of oligodendrogliomas that predict grade. AJNR Am J Neuroradiol 33:852–857. https://doi.org/10.3174/ajnr.A2895
- Brat DJ, Verhaak RGW, Aldape KD et al (2015) Comprehensive, integrative genomic analysis of diffuse lower-grade gliomas. N Engl J Med 372:2481–2498. https://doi.org/10.1056/NEJMoa1402121
- Reuss DE, Mamatjan Y, Schrimpf D et al (2015) IDH mutant diffuse and anaplastic astrocytomas have similar age at presentation and little difference in survival: a grading problem for WHO. Acta Neuropathol 129:867–873. https://doi.org/10.1007/s00401-015-1438-8
- Carstam L, Corell A, Smits A et al (2022) WHO grade loses its prognostic value in molecularly defined diffuse lower-grade gliomas. Front Oncol 11:803975. https://doi.org/10.3389/fonc.2021.803975
- Aoki K, Nakamura H, Suzuki H et al (2018) Prognostic relevance of genetic alterations in diffuse lower-grade gliomas. Neuro Oncol 20:66–77. https:// doi.org/10.1093/neuonc/nox132
- Pei D, Guan F, Hong X et al (2023) Radiomic features from dynamic susceptibility contrast perfusion-weighted imaging improve the three-class prediction of molecular subtypes in patients with adult diffuse gliomas. Eur Radiol 33:3455–3466. https://doi.org/10.1007/s00330-023-09459-6

Publisher's Note

Springer Nature remains neutral with regard to jurisdictional claims in published maps and institutional affiliations.

DIAGNOSTIC NEURORADIOLOGY



DSC-PWI presurgical differentiation of grade 4 astrocytoma and glioblastoma in young adults: rCBV percentile analysis across enhancing and non-enhancing regions

Albert Pons-Escoda^{1,2,3} • Pablo Naval-Baudin^{1,3,4} • Mildred Viveros¹ • Susanie Flores-Casaperalta¹ • Ignacio Martinez-Zalacaín^{1,4} • Gerard Plans^{2,5} • Noemi Vidal^{2,6} • Monica Cos¹ • Carles Majos^{1,2}

Received: 14 December 2023 / Accepted: 29 May 2024 / Published online: 5 June 2024 © The Author(s) 2024

Abstract

Purpose The presurgical discrimination of IDH-mutant astrocytoma grade 4 from IDH-wildtype glioblastoma is crucial for patient management, especially in younger adults, aiding in prognostic assessment, guiding molecular diagnostics and surgical planning, and identifying candidates for IDH-targeted trials. Despite its potential, the full capabilities of DSC-PWI remain underexplored. This research evaluates the differentiation ability of relative-cerebral-blood-volume (rCBV) percentile values for the enhancing and non-enhancing tumor regions compared to the more commonly used mean or maximum preselected rCBV values.

Methods This retrospective study, spanning 2016–2023, included patients under 55 years (age threshold based on World Health Organization recommendations) with grade 4 astrocytic tumors and known IDH status, who underwent presurgical MR with DSC-PWI. Enhancing and non-enhancing regions were 3D-segmented to calculate voxel-level rCBV, deriving mean, maximum, and percentile values. Statistical analyses were conducted using the Mann-Whitney U test and AUC-ROC. **Results** The cohort consisted of 59 patients (mean age 46; 34 male): 11 astrocytoma-4 and 48 glioblastoma. While glioblastoma showed higher rCBV in enhancing regions, the differences were not significant. However, non-enhancing astrocytoma-4 regions displayed notably higher rCBV, particularly in lower percentiles. The 30th rCBV percentile for non-enhancing regions was 0.705 in astrocytoma-4, compared to 0.458 in glioblastoma (p=0.001, AUC-ROC=0.811), outperforming standard mean and maximum values.

Conclusion Employing an automated percentile-based approach for rCBV selection enhances differentiation capabilities, with non-enhancing regions providing more insightful data. Elevated rCBV in lower percentiles of non-enhancing astrocytoma-4 is the most distinguishable characteristic and may indicate lowly vascularized infiltrated edema, contrasting with glioblastoma's pure edema.

Keywords Brain neoplasms · Astrocytoma · Glioblastoma · Perfusion imaging · Magnetic resonance imaging



Albert Pons-Escoda albert.pons@bellvitgehospital.cat

Radiology Department, Hospital Universitari de Bellvitge, Barcelona, Spain

Neuro-oncology Unit, Institut d'Investigació Biomèdica de Bellvitge- IDIBELL, Barcelona, Spain

Facultat de Medicina i Ciències de La Salut, Universitat de Barcelona (UB), Barcelona, Spain

Diagnostic Imaging and Nuclear Medicine Research Group, Institut d'Investigació Biomèdica de Bellvitge- IDIBELL, Barcelona. Spain

Neurosurgery Department, Hospital Universitari de Bellvitge, Barcelona, Spain

Pathology Department, Hospital Universitari de Bellvitge, Barcelona, Spain

Abbreviations

DSC-PWI Dynamic-Susceptibility-Contrast

Perfusion-Weighted-Imaging

rCBV Relative Cerebral Blood Volume

IDH Isocitrate Dehydrogenase WHO World Health Organization

ROI Region Of Interest

AUC-ROC Area Under the Receiver Operating Charac-

teristic Curve

Introduction

According to the latest World Health Organization (WHO) classification of CNS tumors, Isocitrate Dehydrogenase (IDH)-mutant astrocytoma grade 4 is no longer referred to as Glioblastoma. This term is now reserved exclusively for IDH-wildtype grade 4 astrocytic tumors [1]. A noninvasive differentiation of these grade 4 astrocytic tumors could have significant implications for patient management [2–7]. Astrocytoma grade 4 has been less extensively studied compared to its grade 2-3 counterparts, remaining a major radiological challenge. While lower-grade IDHmutant astrocytomas typically appear as non-enhancing and non-necrotic on morphological images, grade 4 astrocytomas can mimic the imaging characteristics of glioblastomas. Both often exhibit enhancement and necrosis, contrasting starkly with their grade 2-3 IDH-mutant counterparts [7–13]. This overlap in morphological features between IDH-mutant and IDH-wildtype grade 4 tumors highlights the need for advanced quantitative MR techniques, such as Dynamic-Susceptibility-Contrast Perfusion-Weighted-Imaging (DSC-PWI).

DSC-PWI provides insights into the tumors' vascular and microvascular environments [14], particularly relevant because microvascular proliferation is a defining feature of grade 4 according to the 2021 WHO classification [1]. As a result, predictably, both of these tumors, regardless of IDH status, should exhibit elevated relative cerebral-blood-volume (rCBV), which can be considered a radiological manifestation of microvascular proliferation. Thus, the question arises: Does high rCBV predict IDH-mutation status or merely denote a grade 4 tumor? Traditionally, rCBV calculations have focused on either mean or extreme values (maximum or "hot-spots") derived from manually delineated regions-of-interest (ROIs) or entire tumor volumetric segmentations. The practice of using preselected single rCBV values, particularly when focused solely on specific ROIs, tends to overlook tumor heterogeneity, potentially overlooking significant differences across the entire tumor and spectrum of rCBV values [15, 16]. Furthermore, in these grade 4 tumors, both enhancing and non-enhancing components often coexist, which represent different tumor environments, and their separate evaluation could offer diverse perspectives [17].

Differentiating astrocytoma grade 4 and glioblastoma is especially crucial in patients under 55-year-old. According to WHO guidelines, DNA sequencing to confirm IDH mutation status in grade 4 astrocytic tumors is mandatory for patients under 55 years of age, while negative immunohistochemistry suffices for those above this age, given the rarity of IDH mutations beyond this threshold. Yet, for those under 55, IDH mutations are more balanced, emphasizing the need for accurate differentiation in this age group [1, 7, 18, 19]. Given the heavily correlated factors of age, grade, and IDH-mutation status, studies must approach these entities with care to ensure accurate representation of data and interpretation. Thus, focused studies are crucial for a deeper understanding.

Based on these rationales, we believe that the pre-surgical differentiation between IDH-mutant astrocytoma grade 4 and IDH-Wildtype Glioblastoma deserves specific attention [13]. The primary objective of this work is to study the potential of rCBV in distinguishing the IDH-mutation status of grade 4 astrocytic tumors in an age-adjusted cohort, in accordance with WHO recommendations regarding IDH-mutations [1, 18, 19]. We aim to asses both the enhancing and non-enhancing components in a comprehensive voxel-wise, automated, unsupervised manner (exploratory, without the input of prior knowledge or assumptions) using histogram-derived percentile values, contrasting with conventional methods that rely on preselected rCBV values such as mean or maximum.

Methods

This retrospective study received approval from the Research Ethics Committee of our tertiary hospital.

Patients

Patients diagnosed with IDH-mutant astrocytoma grade 4 and IDH-wildtype glioblastoma were retrospectively retrieved from our centre's database spanning the years 2016–2023. The study's inclusion criteria were as follows: (1) Confirmed tumor diagnosis in accordance with the WHO Classification of CNS Tumors 2021 criteria; (2) Age under 55-year-old at the time of tumor diagnosis, adhering to the WHO recommendations; and (3) Availability of a diagnostic pre-surgical MR imaging examination that includes DSC-PWI, T1WI, T2WI, FLAIR, and contrast-enhanced T1WI (CE-T1WI). The study's exclusion criterion was the absence of any of the sequences or a low quality that



prevented adequate tumor segmentation or DSC-PWI data extraction.

Imaging

The MR imaging examinations included in the study were performed using a 1.5-T scanner (Ingenia, Philips Healthcare). All DSC-PWI sequences were gradient-echo, with the following technical parameters: Echo Time, 40ms; Repetition Time, 1500-1700ms; Flip- Angle, 75°; Pixel size, 1.75 mm; Slice Thickness, 5 mm; Image size, 128×128; Number of Slices, 20-25; Number and duration of Dynamics, 60 and 1.5s. A single dose of 0.1 mmol/kg of intravenous gadolinium-based contrast agent (1 mmol/mL) was injected at a rate of 4-5 mL/s. Baseline was in the order of 10-15 points. The quality of the sequences was assessed by two experienced neuroradiologists: A.P.-E and PN-B with more than 10 and 5 years of experience in neuroradiology. Examinations were labelled as poor quality and thus excluded from the study if: (1) motion artifacts prevented the segmentation or coregistration, or (2) an obvious low signal-to-noise ratio was visually assessable in the mean raw time-intensity curves.

Post-processing and DSC-PWI data extraction

After following the standard recommended preprocessing steps, the HD-GLIO pipeline was utilized to segment both enhancing and non-enhancing regions of the whole brain tumor-related abnormality, considering axial T1WI, T2WI, FLAIR, and CE-T1WI [20, 21]. Necrosis was excluded. Subsequently, the FAST tool within FSL was employed to acquire the segmentation for normal-appearing white matter for normalization purposes [22]. Finally, the segmentations were co-registered with the DSC-PWI using the 3D Slicer BRAINSFit module (http://www.slicer.org). The segmentations were reviewed and verified by two experienced neuroradiologists: A.P-E. and PN-B. For each voxel within the tumor segmentations, normalized and leakage corrected rCBV was calculated as described by Boxerman et al. [14]. For each patient's tumor segmentations, the mean and maximum values of all the voxels as well as percentile values in increments of five were calculated.

Description and comparison of DSC-PWI metrics

Statistical comparisons were conducted for Grade 4 Astrocytoma and Glioblastoma rCBV mean, maximum and percentile values via a Mann-Whitney U test. Simultaneously, we calculated the area under the receiver operating characteristic curve (AUC-ROC) for all rCBV values. Finally,

box-plots were constructed to visually assess the segregation potential of the different rCBV value.

As an addition, just to reinforce our observations that these two tumors display similar characteristics on morphological imaging, we referred to the most recent research [8–13]. According to these studies, the primary imaging markers for IDH-mutation status on morphological MRI might include nodular enhancement, necrosis, and T2-FLAIR mismatch. These markers were assessed dichotomously (for enhanced clarity, reproducibility and robustness) by two experienced radiologists (AP-E and PN-B), who determined the presence or absence of such signs.

Results

Patients

The initial cohort consisted of 63 grade 4 astrocytic tumors in patients under 55-year-old. This group was made up of 12 Astrocytoma grade 4 (Astrocytoma 4) and 51 Glioblastoma. Four tumors (1 Astrocytoma 4, and 3 Glioblastomas) were excluded due to the absence of DSC-PWI or the presence of motion artifacts that precluded accurate tumor segmentation or DSC-PWI data extraction. Consequently, the resulting dataset comprised 59 tumors: 11 Astrocytoma 4, and 48 Glioblastoma. A flowchart detailing the patient selection process is provided in Fig. 1.

Demographic details, including age and sex, are presented in Table 1. This table also highlights statistical comparisons between the two groups. The mean age across the dataset was 46-year-old, with 34 of the 59 participants being male. Despite the age-centric nature of the study, a significant age difference (p=0.009) emerged between the entities, with Glioblastoma patients being slightly older, which aligns with prior knowledge [1]. Additionally, warranting particular mention and fully consistent with established knowledge, our reference centre's brain tumor database did not include any Astrocytoma 4 in patients over 55-year-old.

Regarding morphological imaging evaluation (detailed in Table 2), the T2-FLAIR mismatch was the only visual feature showing significant differences associated with IDH-mutation status, boasting perfect specificity. However, it was observed in just 27% of the cases. No significant differences were observed in the presence or absence of nodular enhancement or necrosis, present in vast majority of cases for both entities as shown in Fig. 2.

Description and comparison of DSC-PWI metrics

Tables 3 and 4 present the results for rCBV comparisons using the U-Mann Whitney p-values and AUC-ROCs for



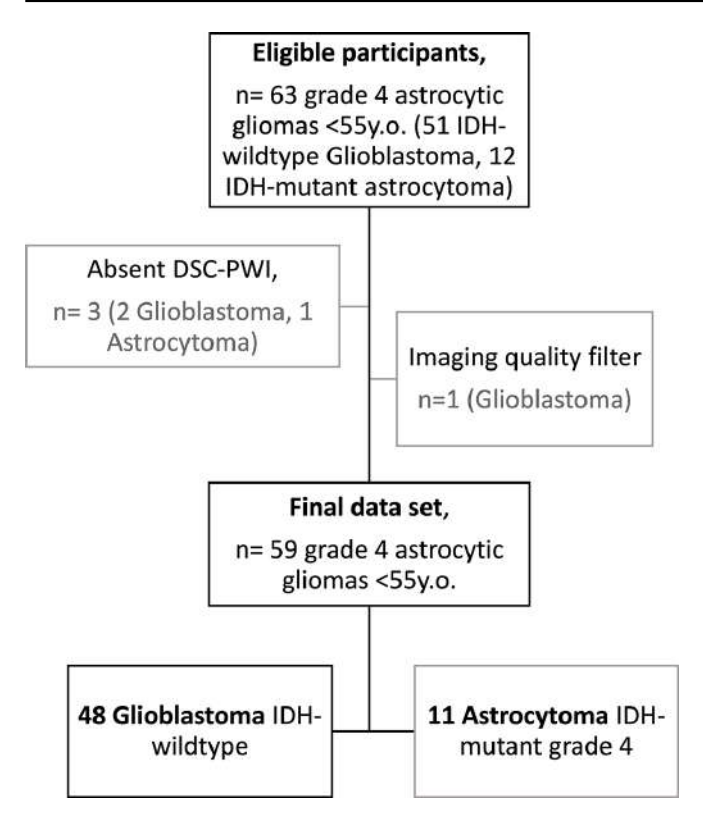


Fig. 1 A flowchart that summarizes the study participant selection process

enhancing and non-enhancing regions respectively. In the context of the enhancing tumor (Table 3), IDH-wildtype displayed higher values overall, but no significant differences emerged between the two tumor types. Interestingly, the lower percentiles (those between p5 and p35) in enhancing regions showed higher rCBV values in IDH-mutant, also no significant. For the non-enhancing regions (Table 4), all rCBV percentile values exhibited significant differences between both entities, using the conventional p-value threshold of 0.05. Overall rCBV in non-enhancing regions

were higher in Astrocytomas 4. Applying the more stringent threshold of p < 0.005, recently proposed as more robust [23], the mean rCBV (Astrocytoma = 1.48 vs. Glioblastoma = 1.14) and percentile rCBV values between p10 and p60 (Astrocytoma=0.35-1.32 vs. Glioblastoma=0.21-0.96) remain significant. In AUC-ROC analysis, excellent discriminatory power considered as above 0.8 [24], was demonstrated by the percentiles between p15 and p30. Whisker-plots for the mean and maximum rCBV of enhancing region are shown in Fig. 3. The plots for non-enhancing region mean, maximum, and the best percentile (p30) rCBV values are shown in Fig. 4. These figures allow for a visual assessment of the different discriminative capabilities and values dispersion. The sensitivity and specificity of rCBVp30, the best percentile, were 0.82 and 0.71, respectively, for a threshold of 0.56.

To clarify, for example, p5 corresponds to the rCBV value below which 5% of voxels within the segmented volume-of-interest fall, meaning 95% are above it, while p10 is the value below which 10% of voxels fall, meaning 90% are above it, and so forth. Therefore, for instance the range from p5 to p35 represents the lower range of rCBV values within the segmented volume-of-interest, from the 5th percentile to the 35th percentile, with values above the lowest 5% and below the highest 65%. For clarity and transparency, we provide the full list of results for all percentiles in both tumor regions. This approach offers an exploratory alternative without relying on prior knowledge or assumptions, and studying all percentiles ensures full data availability and the robustness of the provided information.

Two additional subanalyses were conducted to reinforce the main findings: one involved a class-balanced 5-fold internal cross-validation to address potential class imbalance (11 Astrocytoma: 48 Glioblastoma) biases, and the other applied Bonferroni corrections to p-values. These are detailed in Supplementary Materials 1 and 2, respectively.

Table 1 This table presents the demographic and clinical characteristics of the participants, including age, sex, and tumor grade

	Grade 4 astrocytoma IDH-Mutant	Glioblastoma IDH-wildtype	Whole data-set	<i>p</i> -value
Age (years), Mean +/-SD	41 +/-8	47 +/- 6	46 +/- 7	0.009*
Sex,	6: 5	28: 20	34: 25	1
Men: Women				
Total	11	48	59	

Statistical comparisons were made using the U-Mann Whitney Test for age, and the Chi-Square test for sex. SD denotes Standard Deviation. (*) indicates statistical significance, p < 0.05.

Table 2 Distribution of presence of Nodular enhancement, necrosis and T2-FLAIR mismatch among tumor groups

Tumor type/ imaging features	Grade 4 astrocytoma IDH-Mutant	Glioblastoma IDH-wildtype	<i>p</i> -value
Nodular enhancement	9/11 (82%)	47/48 (98%)	0.16
Necrosis	9/11 (82%)	44/48 (92%)	0.52
T2-FLAIR mismatch	3/11 (27%)	0/48 (0%)	0.03*

Statistical comparisons were made using Chi-Square. (*) indicates statistical significance, p < 0.05.



Fig. 2 Illustrative cases of patients aged between 36 and 51 years diagnosed with Astrocytoma grade 4 (A-C) and Glioblastoma (D-F). These cases demonstrate overlapping imaging characteristics on morphological MR (FLAIR and CE-T1WI) and rCBV color maps. Features such as non-enhancing regions, nodular enhancements, conspicuous signs of necrosis, and high rCBV are common to both tumor types in all shown cases

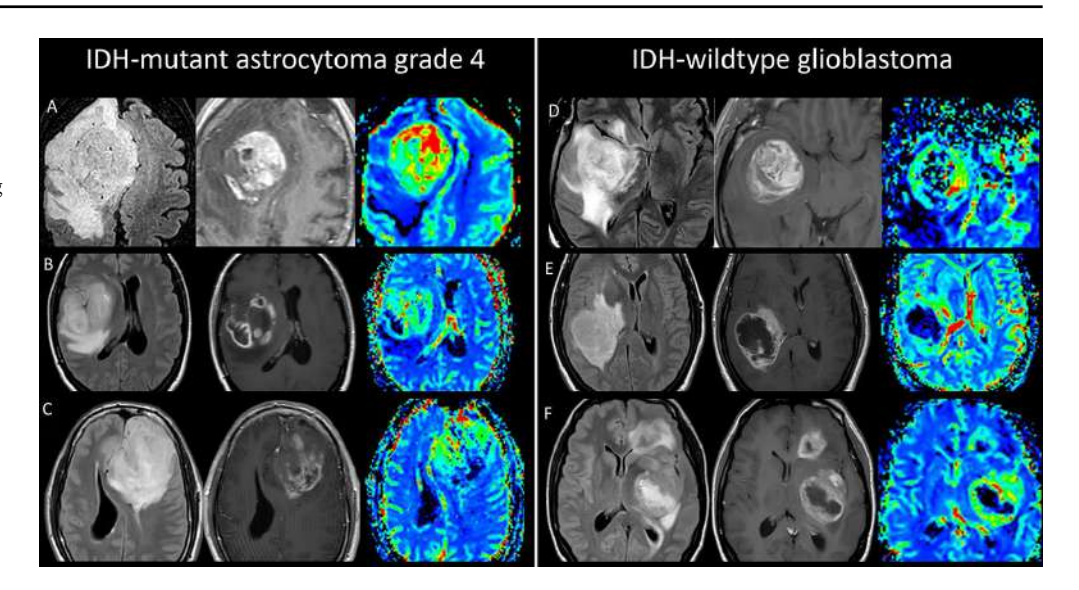


Table 3 Average rCBV values (mean, maximum, and percentiles) for both tumor types in enhancing regions

Enhancing re	egion						
Astro 4	rCBV	Mean	Gb	rCBV	Mean	p	AUC-ROC
	rCBV mean	2.496		rCBV mean	2.784	0.315	0.608
	rCBV p5	0.638		rCBV p5	0.359	0.074	0.690
	rCBV p10	0.901		rCBV p10	0.648	0.103	0.674
	rCBV p15	1.074		rCBV p15	0.894	0.255	0.622
	rCBV p20	1.275		rCBV p20	1.117	0.360	0.598
	rCBV p25	1.454		rCBV p25	1.321	0.475	0.577
	rCBV p30	1.577		rCBV p30	1.513	0.672	0.546
	rCBV p35	1.715		rCBV p35	1.707	0.947	0.508
	rCBV p40	1.860		rCBV p40	1.902	1.000	0.501
	rCBV p45	2.009		rCBV p45	2.106	0.841	0.522
	rCBV p50	2.157		rCBV p50	2.322	0.672	0.546
	rCBV p55	2.300		rCBV p55	2.539	0.577	0.560
	rCBV p60	2.471		rCBV p60	2.777	0.422	0.586
	rCBV p65	2.649		rCBV p65	3.045	0.315	0.608
	rCBV p70	2.830		rCBV p70	3.337	0.237	0.626
	rCBV p75	3.043		rCBV p75	3.700	0.160	0.650
	rCBV p80	3.373		rCBV p80	4.122	0.147	0.655
	rCBV p85	3.812		rCBV p85	4.659	0.129	0.662
	rCBV p90	4.617		rCBV p90	5.417	0.141	0.657
	rCBV max	5.772		rCBV max	6.763	0.090	0.681

Statistical comparisons were conducted using the U-Mann Whitney Test and AUC-ROC. (*) indicates statistical significance, p < 0.05 and/or AUC-ROC> 0.8. (**) indicates statistical significance, p < 0.005.

In these analyses, the lower percentiles of non-enhancing regions remained significant and exhibited stable AUC-ROC values under very stringent conditions, whereas the mean and maximum values lost their significance. This confirms our main results, highlighting not only the superior performance of lower percentiles in the non-enhancing regions but also their greater veracity, robustness and stability compared to the mean and maximum values. For additional comparison of the main rCBV variables, an additional figure of dispersion graphics is also provided in Supplementary Material 3.

Discussion

In this study, we assessed the discriminatory potential of rCBV derived from DSC-PWI to non-invasively differentiate between IDH-mutant astrocytoma grade 4 and IDH-wildtype glioblastoma pre-surgically. Our voxel-wise approach, which accounted for volumetric segmentations and all percentile values, revealed that the most discriminative rCBV values lie within the lower percentiles of the non-enhancing regions. Here, though the values are overall low, they are notably higher in IDH-mutant tumors,



Table 4 Average rCBV values (mean, maximum, and percentiles) for both tumor types in non-enhancing regions

Astro 4	rCBV	Mean	Gb	rCBV	Mean	p	AUC-ROC
	rCBV mean	1.484		rCBV mean	1.137	0.004**	0.782
	rCBV p5	0.204		rCBV p5	0.122	0.053	0.689
	rCBV p10	0.353		rCBV p10	0.205	0.003**	0.792
	rCBV p15	0.449		rCBV p15	0.270	0.002**	0.801*
	rCBV p20	0.535		rCBV p20	0.335	0.002**	0.807*
	rCBV p25	0.621		rCBV p25	0.396	0.001**	0.811*
	rCBV p30	0.705		rCBV p30	0.458	0.001**	0.811*
	rCBV p35	0.794		rCBV p35	0.526	0.002**	0.799
	rCBV p40	0.881		rCBV p40	0.590	0.002**	0.797
	rCBV p45	0.979		rCBV p45	0.662	0.003**	0.79
	rCBV p50	1.082		rCBV p50	0.745	0.002**	0.795
	rCBV p55	1.194		rCBV p55	0.846	0.003**	0.792
	rCBV p60	1.321		rCBV p60	0.957	0.004**	0.784
	rCBV p65	1.459		rCBV p65	1.084	0.006*	0.771
	rCBV p70	1.623		rCBV p70	1.236	0.008*	0.759
	rCBV p75	1.832		rCBV p75	1.420	0.008*	0.759
	rCBV p80	2.091		rCBV p80	1.652	0.015*	0.739
	rCBV p85	2.434		rCBV p85	1.972	0.020*	0.727
	rCBV p90	2.985		rCBV p90	2.498	0.022*	0.723
	rCBV max	4.080		rCBV max	3.440	0.025*	0.72

Statistical comparisons were conducted using the U-Mann Whitney Test and AUC-ROC. (*) indicates statistical significance, p < 0.05 and/or AUC-ROC > 0.8. (**) indicates statistical significance, p < 0.005.

Fig. 3 Whisker plots depict the distribution of mean and maximum rCBV values for the enhancing region of each tumor subtype. For clarity, only mean and maximum rCBV values are shown due to their widespread utilization in clinical practice, and also because none of the percentiles yielded significantly improved results

rCBV_mean 14 12 10 8 8 4 Astro4 Glioblastoma Astro4 Glioblastoma

ENHANCING REGION

suggesting the benefit of using an unsupervised rCBV selection approach over the conventional reliance on preselected mean or maximum values.

Furthermore, given the well-known coexistence of tumor infiltration and edema in the non-enhancing regions, we propose that these differential rCBV values may stem from varying degrees of tumor infiltration in these low-vascularized non-enhancing areas. Such regions may represent a greater degree of coexisting very-low vascularized infiltrated tissue in IDH-mutant cases, while in IDH-wildtype

cases, they may more closely align with pure edema. Indeed, this hypothesis aligns well with prior knowledge: Glioblastomas are known to generate more pronounced edema, whereas Astrocytomas manifest a more substantial proportion of non-enhancing tumor tissue in the T2-FLAIR abnormality [25].

The observed elevated rCBV values in enhancing regions in both tumors, with no significant differences between them, would support the hypothesis that microvascular proliferation is a characteristic of grade 4 tumors, rather than



NON- ENHANCING REGION

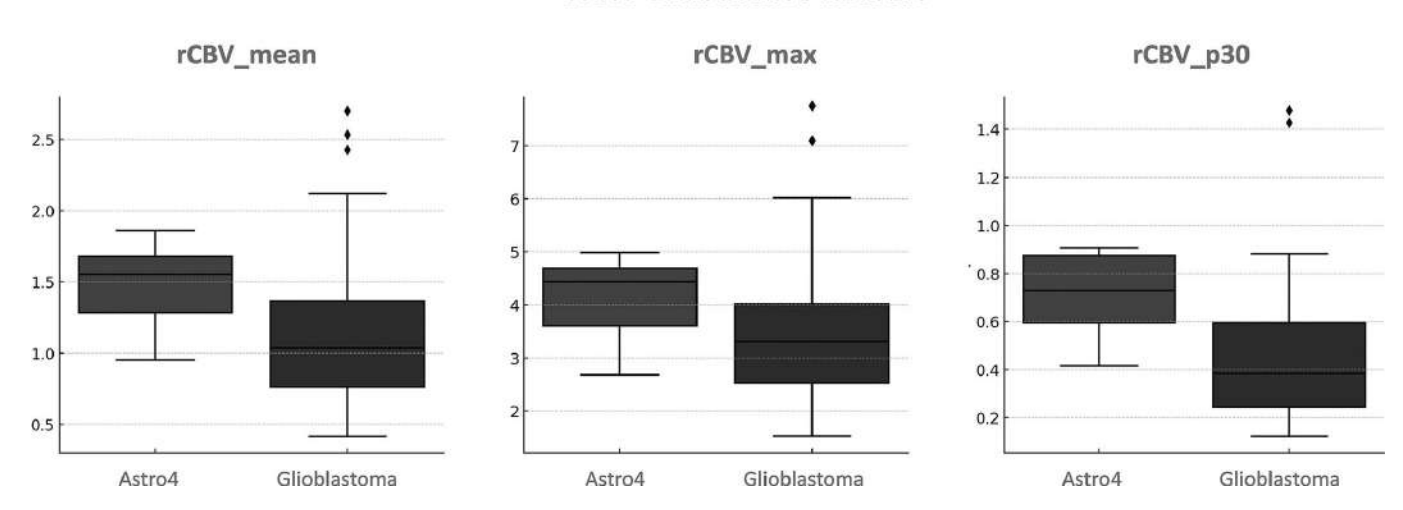


Fig. 4 Whisker plots display the distribution of mean, maximum, and best percentile (p30) rCBV values for the non-enhancing region of each tumor subtype. For clarity, mean and maximum rCBV values are shown for comparison purposes because they are the most standard

measures used in clinical practice. Meanwhile, p30 represents the best percentile result and surpasses those obtained with the standard approaches

a specific attribute of IDH-mutation status. Interestingly, the lower percentile rCBV values for Astrocytoma grade 4 tend to be slightly higher than those for Glioblastoma within these enhancing regions. This trend may suggest a higher homogeneity in Astrocytomas, characterized by a narrower range of rCBV values when compared to Glioblastomas.

Grade 4 Astrocytomas present morphological imaging traits that are distinct from grade 2–3 but are more reminiscent of IDH-wildtype Glioblastoma. The challenge of radiologically distinguishing between these two entities is highlighted by the morphological evaluations in this study, as illustrated in Fig. 2; Table 2, when considering the main markers described for differentiating between IDH-mutant and IDH-wildtype tumors [8–13].

Additionally, this study underscores the clinical significance of this differentiation in patients under 55 years old. In realistic clinical settings, the differentiation becomes crucial in this age group, making our findings especially pertinent. Unlike in those over 55 where the prevalence of the IDH mutation is negligible [1, 18, 19]. This approach mirrors a real-world clinical scenario where such differentiation is genuinely pertinent and impactful. For instance, the noninvasive presurgical differentiation of grade 4 astrocytic tumors is relevant beyond the ultimate histopathological diagnosis and could profoundly impact patient management across different levels. First, in specific scenarios, it could influence surgical decisions, such as whether to opt for function-preserving surgery or a biopsy (in cases of suspected grade 4 astrocytomas) versus total resection (in cases of suspected glioblastomas), particularly in challenging locations. Second, it may guide the sequence of the diagnostic workflow in histopathology and molecular pathology. For instance, by emphasizing and optimizing DNA sequencing utilization (often costly or difficult to access) in the most indicated cases to optimally detect IDH mutations. Ultimately, it offers an early prognosis prediction, which is invaluable, especially for young adults, and their families, enabling informed decisions and setting realistic expectations. Furthermore, such differentiation could be instrumental for the early detection of clinical trial candidates, for instance, for trials on treatments targeting IDH, which are anticipated to increase due to recent positive outcomes [2]. As we move further into the era of personalized and targeted therapies, the insights from our study could play an increasingly important role in shaping treatment strategies. This, in turn, hopefully will positively influence the disease course and enhance the quality of life for patients [3–6]. An illustrative example of potential clinical applicability of results in new patients with unknown diagnosis is shown in Fig. 5. Four additional illustrative cases are provided in Supplementary Material 4, along with the rCBVp30 values for the entire dataset.

Several studies have attempted to identify IDH-mutation status using rCBV while analysing a range of adult diffuse gliomas. Some suggest the feasibility of discerning IDH mutation status, generally reporting higher rCBV values in both enhancing and non-enhancing regions for IDH-wildtype [17, 26, 27]. However, interpreting these findings requires caution, as these studies do not account for potential confounding with age or histological grade which are only reported as descriptive statistics, thereby preventing the optimal discernment of the specific differential in the current study. As an exemplification, considering that the vast majority of grade 4 astrocytic tumors are indeed



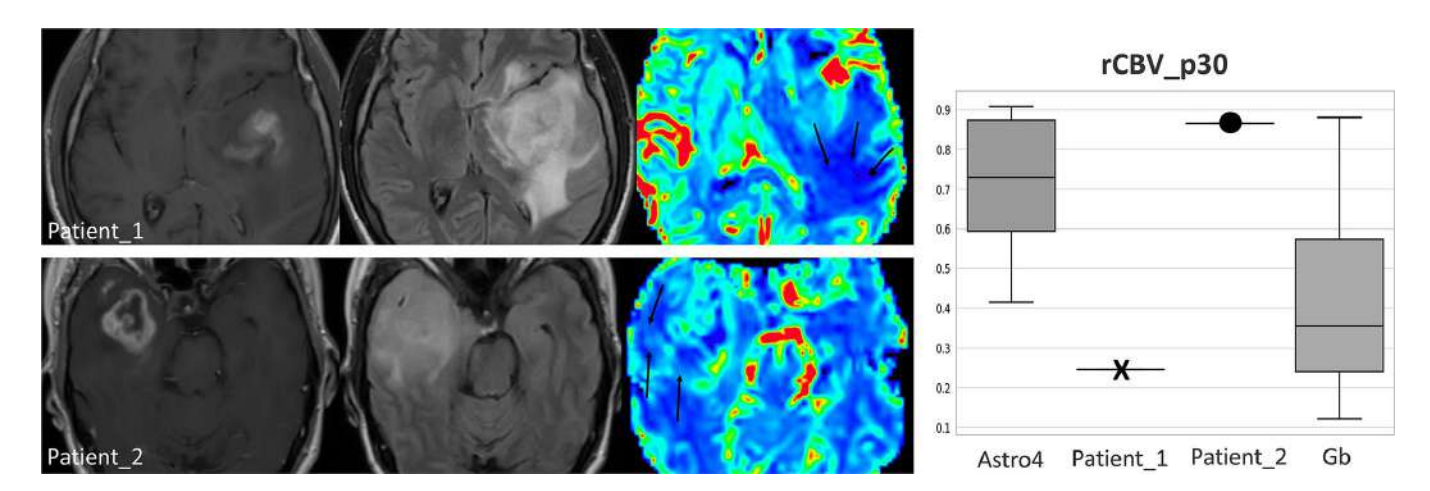


Fig. 5 Illustrative cases of two patients with unknown diagnosis: Patient_1 is 51 years old, and Patient_2 is 49 years old. The images display an extensive non-enhancing component beyond the enhancing tumor margins. This could be attributed to infiltrative tumor, edema, or a coexistence of both. rCBV color maps focused analysis allow the detection of small foci of slightly elevated rCBV (arrows) in the

non-enhancing component of Patient_2, while it depicts clear areas of very low rCBV (arrows) in Patient_1. Quantification of the 30th percentile in non-enhancing areas indicates that Patient_1 has values that fall within the range of Glioblastoma (Gb), while Patient_2 aligns with Astrocytoma grade 4 (Astro 4). The diagnoses for both cases were histopathology confirmed

glioblastomas, and the vast majority of grade 2–3 are IDH-mutant astrocytomas, a study claiming to identify IDH mutation status might actually be reflecting a more familiar differentiation between grade 2–3 and grade 4. Lastly, it is crucial to recognize that astrocytoma grade 4 is often either absent or significantly underrepresented in such studies, which limits the applicability of their results to this specific, smaller subgroup. This subgroup necessitates particular attention, as provided in our study.

Our literature search yielded only two DSC-PWI studies explicitly focused on grade 4 astrocytic tumors [28, 29], which in general terms reported higher rCBV values in IDH-wildtype tumors. However, due to different methodological approaches, direct comparison of results is not feasible. We consider relevant strengths of our methodology to include volumetric segmentations of easily demarcated morphological MR main tumor regions, which provide information on the entire abnormality; and the comprehensive evaluation of voxel-wise rCBV values through percentile analysis, not limited to preselected mean or maximum, which may obscure relevant differences in other parts of the full range of values.

Finally, another advanced MR technique deserving mention in this scenario is MR spectroscopy. It has been proven useful for IDH-mutation identification through specifically edited sequences, achieving high accuracies [30]. Also, more standard MR spectroscopy protocols offer information for glioma classification under the latest WHO guidelines [31]. However, the specific focused performance in grade 4 astrocytic tumors remains less clear because existing research again mixes tumor grades 2, 3, and 4. A potential limitation of this technique is its less extended implementation and use in neuroradiology departments worldwide compared to the

widely extended and accepted DSC-PWI for brain tumor imaging [14, 15, 32, 33]. At any instance, recognizing the challenges, we believe that an ideal approach for the near future would combine comprehensive imaging data, including DSC-PWI and MR spectroscopy, with advanced data analysis techniques, such as AI and radiomics, to enhance presurgical tumor classification.

This study comes with several limitations. This is a single-site retrospective investigation. Nevertheless, this approach ensured data homogeneity, useful in pilot studies. The sample size, though seeming modest, is justified as all tumors were classified based on the stringent 2021 WHO Classification criteria, limiting retrospective patient inclusion. Also, IDH-mutant grade 4 astrocytomas are infrequent tumors, and they are rarely addressed in recent literature as a separate entity from their grade 2-3 counterparts. We recognize that theoretically, preloaded or low Flip-Angle (30°) DSC-PWI sequences might optimize rCBV measures when aligned with histological vascularization evaluations [14]. Yet, the primary differences lie in the non-enhancing region of tumors, where leakage-effects due to blood-brainbarrier disruption should be negligible, thus reducing the impact on rCBV calculations. Moreover, our study's main focus wasn't solely on this alignment. Different techniques have also shown reproducibility and robustness and we applied rigorous leakage correction procedures, mitigating potential leakage impacts [34]. Additionally, it should be highlighted that many clinicians have a preference for non-preloaded intermediate-high Flip-Angle sequences, particularly when it comes to the pre-surgical differential diagnosis [35–41]. This preference aligns with our study's context and has demonstrated to be useful for diffuse gliomas' genetic subtypes presurgical differentiation [42, 43].



However, our methodology can adapt to different DSC-PWI techniques with simple threshold adjustments [44]. Nevertheless, broader multicentric validations remain essential. Lastly, unfortunately, analysing a single case using our proposed methodology currently requires 10–15 min, hindered by the limitations of commercial software in PACS systems that force the use of multiple tools. This situation could impede rapid clinical adoption, but also highlights an opportunity for software enhancement in clinical neuroradiology, especially through improved segmentation tools and presenting CBV values via percentile analysis. With these improvements, post-processing time could potentially be reduced to around 2 min, underscoring the need for software advancements to narrow the gap between clinical practice and research in neuroradiology.

On the other hand, our study's strengths are evident. All tumors were rigorously classified as per the 2021 WHO Classification criteria, ensuring contemporaneity. The tumor groups have been carefully balanced accounting for grade and age. Our insights hold clinical relevance from multiple discussed vantage points. Notably, the automatization of the data-extraction and data-selection ensures reproducibility minimizing operator-dependency. We underscore the importance of an unsupervised evaluation of the tumors' entire percentile values, challenging the common clinical practice of relying on ROIs, mean or maximum values. In essence, our findings could be extrapolated to other clinical scenarios, laying the groundwork for further research.

Conclusion

Using an unsupervised percentile-based approach to select rCBV values from volumetric segmentations provides richer information compared to the use of ROIs and preselected mean and maximum values.

The non-enhancing components of grade 4 astrocytic tumors are potentially more informative than the enhancing region itself.

Although globally low, higher rCBV values in the lower percentiles of the non-enhancing region in IDH-mutant grade 4 astrocytomas rose as the most distinguishing feature from glioblastomas. This suggests that different proportions of infiltrative versus vasogenic edema might be a clue for differentiating these two tumor types.

Supplementary Information The online version contains supplementary material available at https://doi.org/10.1007/s00234-024-03385-0.

Acknowledgements Albert Pons-Escoda and Carles Majos acknowledge support from the Instituto de Salud Carlos III (Proyectos de Investigación en Salud, PI20/00360). The authors thank CERCA Programme/Generalitat de Catalunya for institutional support.

Author contributions Albert Pons-Escoda created the experimental design. Albert Pons-Escoda led the investigation. Albert Pons-Escoda, Noemi Vidal and Carles Majos did the data collection. Albert Pons-Escoda and Pablo Naval-Baudin led the imaging-data processing and extraction. Albert Pons-Escoda, Pablo Naval-Baudin and Ignacio Martinez-Zalacaín performed the statistical data analysis. Albert Pons-Escoda wrote up the manuscript and chose the best tables and figures. Albert Pons-Escoda did the bibliographic research. Pablo Naval-Baudin, Ignacio Martinez-Zalacaín and Carles Majos made important contributions to the final manuscript. Monica Cos and Carles Majos offered relevant logistic support. All the authors played a role in any of the necessary patient data acquisition. All the authors have participated in the review, and correction of the manuscript. All the authors have read and approved its submission to this journal.

Funding No funding was received to assist with the preparation of this manuscript.

Open Access funding provided thanks to the CRUE-CSIC agreement with Springer Nature.

Declarations

Ethical approval and informed consent Institutional Review Board approval was obtained. Written informed consent was waived by the Institutional Review Board.

Conflict of interest The authors declare that we have no conflict of interest to disclose.

Open Access This article is licensed under a Creative Commons Attribution 4.0 International License, which permits use, sharing, adaptation, distribution and reproduction in any medium or format, as long as you give appropriate credit to the original author(s) and the source, provide a link to the Creative Commons licence, and indicate if changes were made. The images or other third party material in this article are included in the article's Creative Commons licence, unless indicated otherwise in a credit line to the material. If material is not included in the article's Creative Commons licence and your intended use is not permitted by statutory regulation or exceeds the permitted use, you will need to obtain permission directly from the copyright holder. To view a copy of this licence, visit http://creativecommons.org/licenses/by/4.0/.

References

- WHO Classification of Tumours Editorial Board Central nervous system tumours [Internet] Lyon (France): International Agency for Research on Cancer; 2021 [cited 2023 Jul 13]. (WHO classification of tumours series, 5th ed.). https://tumourclassification. iarc.who.int/chapters/45
- Mellinghoff IK, van den Bent MJ, Blumenthal DT et al (2023) Vorasidenib in IDH1- or IDH2-Mutant low-Grade Glioma. N Engl J Med. https://doi.org/10.1056/NEJMoa2304194
- Mitchell D, Shireman JM, Dey M (2022) Surgical Neuro-Oncology. Neurol Clin 40:437–453. https://doi.org/10.1016/j. ncl.2021.11.003
- Balana C, Castañer S, Carrato C et al (2022) Preoperative diagnosis and molecular characterization of Gliomas with Liquid Biopsy and Radiogenomics. Front Neurol 13:865171. https://doi.org/10.3389/fneur.2022.865171
- Vagvala S, Guenette JP, Jaimes C, Huang RY (2022) Imaging diagnosis and treatment selection for brain tumors in the era



- of molecular therapeutics. Cancer Imaging 22:19. https://doi.org/10.1186/s40644-022-00455-5
- Blobner J, Dengler L, Blobner S et al (2023) Significance of molecular diagnostics for therapeutic decision-making in recurrent glioma. Neuro-Oncology Adv 5:vdad060. https://doi. org/10.1093/noajnl/vdad060
- Pons-Escoda A, Majos C, Smits M, Oleaga L (2024) Presurgical diagnosis of diffuse gliomas in adults: Post-WHO 2021 practical perspectives from radiologists in neuro-oncology units. Radiol (English Ed). https://doi.org/10.1016/j.rxeng.2024.03.002.
- Kamble AN, Agrawal NK, Koundal S et al (2023) Imaging-based stratification of adult gliomas prognosticates survival and correlates with the 2021 WHO classification. Neuroradiology 65:41– 54. https://doi.org/10.1007/s00234-022-03015-7
- Joyner DA, Garrett J, Batchala PP et al (2023) MRI features predict tumor grade in isocitrate dehydrogenase (IDH)–mutant astrocytoma and oligodendroglioma. Neuroradiology 65:121–129. https://doi.org/10.1007/s00234-022-03038-0
- Lasocki A, Buckland ME, Molinaro T et al (2023) Correlating MRI features with additional genetic markers and patient survival in histological grade 2–3 IDH-mutant astrocytomas. Neuroradiology 65:1215–1223. https://doi.org/10.1007/s00234-023-03175-0
- Lasocki A, Buckland ME, Drummond KJ et al (2022) Conventional MRI features can predict the molecular subtype of adult grade 2–3 intracranial diffuse gliomas. Neuroradiology 64:2295–2305. https://doi.org/10.1007/s00234-022-02975-0
- 12. Park YW, Han K, Ahn SS et al (2018) Prediction of IDH1 -Mutation and 1p/19q-Codeletion status using preoperative MR Imaging Phenotypes in Lower Grade Gliomas. Am J Neuroradiol 39:37–42. https://doi.org/10.3174/ajnr.A5421
- Lee MD, Patel SH, Mohan S et al (2023) Association of partial T2-FLAIR mismatch sign and isocitrate dehydrogenase mutation in WHO grade 4 gliomas: results from the ReSPOND consortium. Neuroradiology 65:1343–1352. https://doi.org/10.1007/ s00234-023-03196-9
- 14. Boxerman JL, Quarles CC, Hu LS et al (2020) Consensus recommendations for a dynamic susceptibility contrast MRI protocol for use in high-grade gliomas. Neuro Oncol 22:1262–1275. https://doi.org/10.1093/neuonc/noaa141
- Pons-Escoda A, Smits M (2023) Dynamic-susceptibility-contrast perfusion-weighted-imaging (DSC-PWI) in brain tumors: a brief up-to-date overview for clinical neuroradiologists. Eur Radiol. https://doi.org/10.1007/s00330-023-09729-3
- Pons-Escoda A, Garcia-Ruiz A, Naval-Baudin P et al (2022) Voxel-level analysis of normalized DSC-PWI time-intensity curves: a potential generalizable approach and its proof of concept in discriminating glioblastoma and metastasis. Eur Radiol. https://doi.org/10.1007/s00330-021-08498-1
- 17. Wu H, Tong H, Du X et al (2020) Vascular habitat analysis based on dynamic susceptibility contrast perfusion MRI predicts IDH mutation status and prognosis in high-grade gliomas. Eur Radiol 30:3254–3265. https://doi.org/10.1007/s00330-020-06702-2
- Barresi V, Eccher A, Simbolo M et al (2020) Diffuse gliomas in patients aged 55 years or over: a suggestion for IDH mutation testing. Neuropathology 40:68–74. https://doi.org/10.1111/ neup.12608
- Robinson C, Kleinschmidt-DeMasters BK (2017) IDH1 -Mutation in diffuse gliomas in persons age 55 years and over. J Neuropathol Exp Neurol 76:nlw112. https://doi.org/10.1093/jnen/nlw112
- Kickingereder P, Isensee F, Tursunova I et al (2019) Automated quantitative tumour response assessment of MRI in neuro-oncology with artificial neural networks: a multicentre, retrospective study. Lancet Oncol 20:728–740. https://doi.org/10.1016/ S1470-2045(19)30098-1

- Isensee F, Jaeger PF, Kohl SAA et al (2021) nnU-Net: a self-configuring method for deep learning-based biomedical image segmentation. Nat Methods 18:203–211. https://doi.org/10.1038/s41592-020-01008-z
- 22. Zhang Y, Brady M, Smith S (2001) Segmentation of brain MR images through a hidden Markov random field model and the expectation-maximization algorithm. IEEE Trans Med Imaging 20:45–57. https://doi.org/10.1109/42.906424
- Benjamin DJ, Berger JO, Johannesson M et al (2017) Redefine statistical significance. Nat Hum Behav 2:6–10. https://doi.org/10.1038/s41562-017-0189-z
- Mandrekar JN (2010) Receiver operating characteristic curve in Diagnostic Test Assessment. J Thorac Oncol 5:1315–1316. https://doi.org/10.1097/JTO.0b013e3181ec173d
- Dubinski D, Won S-Y, Rauch M et al (2021) Association of Isocitrate Dehydrogenase (IDH) Status with Edema to tumor ratio and its correlation with Immune Infiltration in Glioblastoma. Front Immunol 12:627650. https://doi.org/10.3389/ fimmu.2021.627650
- Brendle C, Klose U, Hempel J-M et al (2020) Association of dynamic susceptibility magnetic resonance imaging at initial tumor diagnosis with the prognosis of different molecular glioma subtypes. Neurol Sci off J Ital Neurol Soc Ital Soc Clin Neurophysiol 41:3625–3632. https://doi.org/10.1007/ s10072-020-04474-7
- Hempel J-M, Schittenhelm J, Klose U et al (2019) In vivo molecular profiling of human Glioma: cross-sectional observational study using dynamic susceptibility contrast magnetic resonance perfusion imaging. Clin Neuroradiol 29:479–491. https://doi.org/10.1007/s00062-018-0676-2
- 28. Xing Z, Zhang H, She D et al (2019) IDH genotypes differentiation in glioblastomas using DWI and DSC-PWI in the enhancing and peri-enhancing region. Acta Radiol 60:1663–1672. https://doi.org/10.1177/0284185119842288
- Álvarez-Torres M, del López-Cerdán M, Andreu A Z, et al (2023)
 Vascular differences between IDH- wildtype glioblastoma and astrocytoma IDH -mutant grade 4 at imaging and transcriptomic levels. https://doi.org/10.1002/nbm.5004. NMR Biomed e5004
- Suh CH, Kim HS, Jung SC et al (2018) 2-Hydroxyglutarate MR spectroscopy for prediction of isocitrate dehydrogenase mutant glioma: a systemic review and meta-analysis using individual patient data. Neuro Oncol 20:1573–1583. https://doi.org/10.1093/ neuonc/nov113
- Majós C, Pons-Escoda A, Naval P et al (2023) Proton MR spectroscopy shows improved performance to segregate high-grade astrocytoma subgroups when defined with the new 2021 World Health Organization classification of central nervous system tumors. Eur Radiol 34:2174–2182. https://doi.org/10.1007/s00330-023-10138-9
- 32. Kaufmann TJ, Smits M, Boxerman J et al (2020) Consensus recommendations for a standardized brain tumor imaging protocol for clinical trials in brain metastases. Neuro Oncol 22:757–772. https://doi.org/10.1093/neuonc/noaa030
- Barajas RF, Politi LS, Anzalone N et al (2021) Consensus recommendations for MRI and PET imaging of primary central nervous system lymphoma: guideline statement from the International Primary CNS Lymphoma Collaborative Group (IPCG). Neuro Oncol 23:1056–1071. https://doi.org/10.1093/neuonc/noab020
- Paulson ES, Schmainda KM (2008) Comparison of dynamic susceptibility-weighted contrast-enhanced MR methods: recommendations for measuring relative cerebral blood volume in brain tumors. Radiology 249:601–613. https://doi.org/10.1148/ radiol.2492071659
- 35. Cindil E, Sendur HN, Cerit MN et al (2021) Validation of combined use of DWI and percentage signal recovery-optimized protocol of DSC-MRI in differentiation of high-grade glioma,

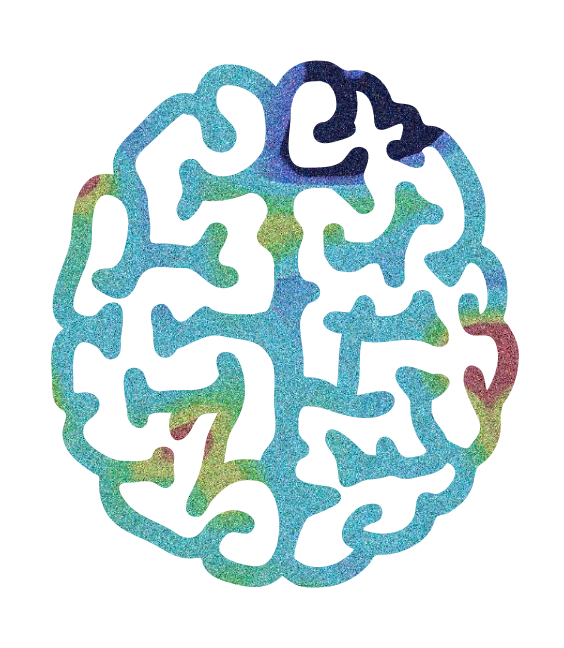


- metastasis, and lymphoma. Neuroradiology 63:331–342. https://doi.org/10.1007/s00234-020-02522-9
- Wang F, Zhou X, Chen R et al (2023) Improved performance of non-preloaded and high flip-angle dynamic susceptibility contrast perfusion-weighted imaging sequences in the presurgical differentiation of brain lymphoma and glioblastoma. Eur Radiol. https://doi.org/10.1007/s00330-023-09917-1
- Mangla R, Kolar B, Zhu T et al (2011) Percentage signal recovery derived from MR dynamic susceptibility contrast imaging is useful to differentiate common enhancing malignant lesions of the brain. Am J Neuroradiol 32:1004–1010. https://doi.org/10.3174/ ajnr.A2441
- Pons-Escoda A, Garcia-Ruiz A, Naval-Baudin P et al (2020) Presurgical identification of primary central nervous system lymphoma with normalized time-intensity curve: a pilot study of a new method to analyze DSC-PWI. Am J Neuroradiol 41:1816–1824. https://doi.org/10.3174/ajnr.A6761
- Pons-Escoda A, Garcia-Ruiz A, Garcia-Hidalgo C et al (2023) MR dynamic-susceptibility-contrast perfusion metrics in the presurgical discrimination of adult solitary intra-axial cerebellar tumors. Eur Radiol. https://doi.org/10.1007/s00330-023-09892-7
- Pons-Escoda A, García-Ruíz A, Naval-Baudin P et al (2022)
 Diffuse large B-Cell Epstein-Barr virus-positive primary CNS lymphoma in Non-AIDS patients: high diagnostic accuracy of

- DSC Perfusion Metrics. AJNR Am J Neuroradiol 43:1567–1574. https://doi.org/10.3174/ajnr.A7668
- 41. Garcia-Ruiz A, Pons-Escoda A, Grussu F et al (2024) An accessible deep learning tool for voxel-wise classification of brain malignancies from perfusion MRI. Cell Rep Med 5:101464. https://doi.org/10.1016/j.xcrm.2024.101464
- Cindil E, Sendur HN, Cerit MN et al (2022) Prediction of IDH Mutation Status in High-grade gliomas using DWI and high T1-weight DSC-MRI. Acad Radiol 29:S52–S62. https://doi. org/10.1016/j.acra.2021.02.002
- Pons-Escoda A, Garcia-Ruiz A, Naval-Baudin P et al (2024) Differentiating IDH-mutant astrocytomas and 1p19q-codeleted oligodendrogliomas using DSC-PWI: high performance through cerebral blood volume and percentage of signal recovery percentiles. Eur Radiol. https://doi.org/10.1007/s00330-024-10611-z
- Lee MD, Baird GL, Bell LC et al (2019) Utility of Percentage Signal Recovery and Baseline Signal in DSC-MRI optimized for relative CBV measurement for differentiating Glioblastoma, Lymphoma, Metastasis, and Meningioma. Am J Neuroradiol 40:1145–1450. https://doi.org/10.3174/ajnr.A6153

Publisher's Note Springer Nature remains neutral with regard to jurisdictional claims in published maps and institutional affiliations.





5. DISCUSSION

5. DISCUSSION

In this thesis, we have demonstrated that DSC-PWI provides significantly more information than merely CBV, which is typically considered a biomarker of overall vascularity. By adopting a curvologic and/or multiparametric approach (including CBV, PSR, and PH), we expanded the scope of biomarkers beyond overall vascularity to encompass BBB integrity, as well as vasculo- and cyto-architecture. This approach yielded remarkable results in classifying various brain tumor types and subtypes, with direct clinical implications for the initial management of patients [49–52].

Of note, in the initial stages of this thesis, we developed a pioneering method for robust visual and quantitative analysis of entire time-intensity curves. For this, we designed an innovative and comprehensible normalization method of the entire curve to NAWM references, enabling curve analysis that transcends patient and specific technical differences. This method ultimately allows for: 1) constructing mean curves for visual analysis (e.g., comparing the curve of an unknown tumor diagnosis with mean curves of different tumor types), 2) performing point-by-point and voxel-wise statistical computations and analysis, and 3) building classifiers [49]. The key advantage of this curvologic approach lies in its unsupervised analysis, which can reveal differences in curve segments that might remain hidden or overlooked when only isolated metrics focusing on specific points of the curve are evaluated [43,45,49,53]. On another hand, we pioneered the analysis of certain metrics in specific tumor groups and subgroups, where their utility was previously unknown, and hypothesized a correlation between these metrics and their specific histological substrates to provide useful biomarkers [51,52].

Furthermore, we employed automatic/semi-automatic data extraction methods that reduce operator dependency and evaluate the entire tumor tissue, utilizing automatic tumor and NAWM segmentations [49-52,54-56]. This contrasts with current clinical standards, which rely on 2D manual ROIs for both tumor and NAWM reference (for normalization). Such traditional approaches can increase operator variability and often fail to capture tumor heterogeneity [1,28-30,33]. To address the latter, several of our studies also demonstrated the superiority of using voxel-wise histogram-derived percentiles over mean or max summarizing values in ROIs or VOIs, particularly in highly heterogeneous tumors [50,52,55,56]. Another important consideration for reducing bias and increasing reproducibility is the use of raw time-intensity curves for curvology, PSR, and PH evaluations. This approach avoids the pre- and post-processing, theories, models, and equations typically required for extracting other metrics, such as CBV, which can introduce biases at each step. Our alternative analysis is based purely on raw data, without prior post-processing, assumptions, or modeling. Indeed, directly related to the last two paragraphs, we have demonstrated that our approaches tend to generalize better when applied to test and validation cohorts compared to standard methods [49,55]. All these findings may pave the way for the ideal creation of optimal, standardized, vendorneutral pipelines for DSC-PWI data extraction, which would be of significant importance for enhancing generalizability [1].

Additionally, our methods enhance the data derived from DSC-PWI, enabling more extensive data mining and making complex analytical techniques (machine learning, deeplearning, artificial intelligence) more applicable than in standards single-metric and single-value approaches [51,52,55].

However, beyond all these more technically profiled considerations for optimal DSC-PWI data extraction and analysis, our investigations maintain a strong clinical focus. Our ultimate goal is to construct clinically useful and relevant pre-surgical tumor classifiers that combine advanced data analysis, classical statistics, and visually accessible displays, avoiding black-box results to enhance usability and clinical applicability [49–52,54–56]. As clinical radiologist, the author of this thesis believes that all findings must be credible, explainable, and grounded in clinical, biological, and pathophysiological basis. Additionally, the results should be visually intuitive, allowing for easy interpretation by radiologists—ideally integrated into PACS systems. Unexplainable black-box results are not easily adopted in clinical practice, where physicians seek to understand both the successes and failures of their decisions in order to learn from them. Moreover, we have hypothesized and provided logical biological explanations for each of our findings, aiming to construct comprehensible biomarkers that could expand their use, open new research avenues, and inspire clinicians to think of novel applications.

In addition, our investigations have expanded and reinforced the clinical understanding of how DSC-PWI technical parameters impact results [2,12,34,48,57]. For instance, the metrics performance vary depending on the technical pulse-parameters of the sequence used. DSC-PWI more highly T1-weighted sequences (e.g., intermediate to high FA without prebolus) enhance the detection of leakage effects and improve PSR performance, whereas highly T2-weighted or preloaded sequences either avoid detecting or directly prevent leakage events respectively, theoretically enhancing CBV performance. In this regard, our studies were conducted using highly T1-weighted and non-preloaded sequences. We believe these subtype of sequences are often preferred by clinicians, partic-

ularly for pre-surgical differential diagnosis, due to the additional information provided by leakage effects, which is lost with the other sequence subtypes. Additionally, we believe the loss in CBV performance with this high T1-weighted technique is less significant than the loss of PSR with highly T2-weighted techniques [31,32,35-37]. Moreover, the specific impact on the entire curve morphology is not fully understood, but we hypothesize that in challenging, heterogeneous technical scenarios, evaluating the full curve may mitigate the performance loss in single metrics like CBV and PSR, thereby offering better generalization even under unfavorable challenging technically heterogenous cohorts. Furthermore, with appropriate re-training and threshold adjustments, all our results can be optimally applied across different technical homogeneous settings. Ultimately, our research lays the groundwork for the future optimization of DSC-PWI protocols, alternative acquisition techniques, and pulse sequence parameters, paving the way for advancements that enable robust, generalizable extraction and interpretation of all metrics and derived biomarkers, without the need to choose one over the other. This will support a more holistic DSC-PWI interpretation and its consequent clinical application.

In the following sections, we will explore these various perspectives and discuss specific results from our primary research, focusing also on their clinical impact.

5.1. DSC-PWI Curves Normalization Method and Its Application for Pre-Surgical Identification of CNS Lymphoma

In the first work of this thesis [49], we present our innovative method to normalize DSC-PWI time-intensity curves, which theoretically overcomes some of the variability caused by differences in patient physiology and acquisition techniques. This approach allows for the creation of mean curves for visual analysis, point-by-point statistical comparisons, and the development of accurate diagnostic classifiers. In this primary work, we applied this method in pre-surgical identification of PCNSL, achieving satisfactory accuracy levels crucial for guiding treatment, as PCNSL requires distinct management strategies compared to other brain tumors (mainly, early stereotactic biopsy before corticosteroid administration is mandatory when PCNSL is suspected from imaging, which differs from the approach in many other brain tumors, where corticosteroids are administered, and direct surgical removal is often pursued) [9,49,50,58,59]. Our findings demonstrate that this method consistently outperforms conventional metrics like CBV and PSR, reaching accuracies between 71% and 96% in distinguishing PCNSL from glioblastoma, anaplastic astrocytoma, metastasis, and meningioma in pairwise comparisons. Beyond traditional measures, our technique integrates key curve points, including previously hidden values, allowing a more comprehensive analysis. With its user-friendly representation, this method supports radiologists by narrowing down likely diagnoses through an interactive classifier, enhancing diagnostic accuracy and opening new possibilities for DSC-PWI evaluation in clinical practice.

A subsequent study [54] expanded the clinical utility of our methods in the pre-surgical diagnosis of lymphoma by applying them specifically to a very rare subtype associated with immunodeficiency: Epstein-Barr virus- positive lymphoma. This subtype poses a unique diagnostic challenge, as its imaging characteristics often contrast with typical lymphoma and closely resemble glioblastoma and metastasis, making pre-surgical diagnosis nearly impossible using conventional imaging [9,21,60–63]. In this study, standard

DSC-PWI metrics like PSR and CBV performed well in differentiating Diffuse Large B-Cell Epstein-Barr Virus-Positive CNS lymphoma from glioblastoma and metastasis. However, TIC analysis yielded even better diagnostic performance. By applying our existing PC-NSL classifier algorithms [50] and developing a dedicated classifier for PCNSL versus glioblastoma/metastasis, we achieved excellent results (accuracies between 82% and 93%).

In both studies, the curve normalization process enabled the overlay of averaged timeintensity curves, providing radiologists with an intuitive and accessible visual tool for diagnostic comparison. For example, the curve of a new case can be directly compared with characteristic curves of different tumor types, facilitating diagnosis.

Also, both promote a high-sensitivity framework that effectively heightens suspicion for CNS lymphoma, thereby helping to prevent pre-biopsy corticosteroid use and unnecessary tumor resections. It is worth noting that all the knowledge gained during these studies focused on lymphoma enabled the author of the thesis and their team to write a highly influential review on CNS lymphomas, which has achieved significant impact at both national and international levels [9].

5.2. The Challenging Differentiation of Glioblastoma and Solitary Brain Metastasis

In another research [50], we applied the normalized TIC methodology to analyze DSC-PWI data of glioblastomas and metastases, adapting it to address the high histological and vascular heterogeneity of these tumors. Our approach, combined point-by-point,

voxel-level histogram-derived percentile analysis of TICs, and generated classifiers based on optimal time points and voxel intensities within the entire tumor extension. This method achieved an accuracy of 81% in distinguishing glioblastoma from metastasis, emphasizing its potential in pre-surgical diagnosis.

This clinical question is especially relevant because glioblastomas and metastases require different management strategies. Misclassification may lead to inappropriate interventions, as glioblastomas typically undergo maximal resection, whereas metastasis patients often need systemic staging before considering other local or systemic therapies. Importantly, brain lesions suspected of being metastases are frequently diagnosed based solely on imaging and clinical context in patients with known primary cancers, without histological confirmation. High diagnostic specificity is essential in these cases to avoid mistreatment, as lesions thought to be metastases may actually be other primary tumors or non-tumoral lesions [17,18,64–67].

Compared to previous approaches that relied solely on metrics like CBV and PSR, our TIC-based method considers the full TIC curve, minimizing variability due to technical factors and enhancing discrimination by incorporating more comprehensive data. DSC-PWI parameters such as CBV, PSR or PH alone sometimes yield inconsistent results in differentiating glioblastoma from metastasis due to tumor heterogeneity and technical variability. By performing a full-TIC our method addresses these limitations, adapting to diverse acquisition setups typical in clinical environments. Our approach further considers intra-tumoral heterogeneity, a key characteristic of both glioblastomas and metastases. Standard methods often overlook the variability within the tumor by focusing only on mean, maximum, or minimum values of specific parameters, while our voxel-

level evaluation incorporates a broader spectrum of tumor values, identifying the most discriminative points in TICs for improved diagnostic performance. This method thus represents a promising, robust alternative for centers with variable imaging protocols, potentially increasing diagnostic precision in real-world clinical settings.

5.3. A fully Automatic Tool for Main Brain Malignancies Pre-surgical Differentiation in Adults

In another multicentric study of this thesis [55], we present an advanced voxel-wise method for analyzing perfusion scans using deep-learning by means of convolutional neural networks, representing a culmination of insights gained from our prior studies on lymphoma, glioblastoma, and metastasis. This comprehensive work has enabled the development of an automatic classifier (DISCERN) openly available on the internet, which leverages prior knowledge on DSC time-intensity curves normalization and delivers significant improvements in brain cancer diagnosis. The classifier integrates point-by-point curve patterns, the temporo-spatial distribution of time-point intensities, and confidence levels for tumor-type classification at the voxel level. It generates probability color maps that visually predict the most probable tumor type, assess spatial tumor heterogeneity, and estimate diagnostic confidence.

By applying this novel method, we achieved a diagnostic performance that surpasses previous models for the noninvasive differential diagnosis of the most common malignant brain tumors — namely, Glioblastoma, metastasis, and primary central nervous system lymphoma — which together account for up to 70% of all malignant brain tumors [68]. Demonstrating superiority over CBV and Percentage of Signal Recovery (PSR), the

classifier achieved accuracies of 80–95% in three-way classification across training and test sets. In technically heterogeneous external validation cohorts from multicentric origin hospitals in Spain and the United States, it maintained robust three-way accuracy (75–80%), outperforming CBV and PSR in generalizability.

This achievement is particularly critical for guiding optimal treatment approaches, as accurate differential diagnosis is essential in clinical decision-making. Key clinical added values include enhancing diagnostic accuracy in less-experienced neuroradiologists (from $\approx\!40\%$ to 80%) and increasing diagnostic confidence in experienced neuroradiologists when faced with challenging differentials (up to 55% of cases in high-complexity units). Thus the DISCERN tool offers substantial promise for assisting radiologists in interpreting brain MRI data, amplifying the diagnostic proficiency of expert neuroradiologists while also providing less experienced radiologists with the support needed to reach a higher level of diagnostic accuracy. This advancement represents a significant step forward in enhancing both the efficiency and accuracy of brain tumor diagnostics in daily clinical practice, as well as a notable progression toward the still distant but envisioned goal of the virtual biopsy.

5.4. Intraaxial Cerebellar Tumors in Adults: Rarer, Yet Also Important

Our research on this subject [51] investigates the use of multiparametric DSC-PWI for the pre-surgical classification of adult solitary intra-axial cerebellar tumors. Leveraging metrics such as normalized TICs, relative CBV, PSR, and PH, the research combines advanced imaging data with a deep-learningbased classifier to achieve robust diagnostic accuracy in a multicentric setting.

The study highlights that individual tumor types exhibit distinctive DSC-PWI patterns, and combining these parameters within a machine-learning framework significantly enhances classification accuracy, achieving 85% in independent test sets from different hospitals. This approach addresses the limitations of single-metric or pairwise comparisons by introducing a multiclass classifier capable of discriminating metastases, medulloblastomas, hemangioblastomas, and pilocytic astrocytomas.

A key contribution is the development of a radiologist-friendly tool that visualizes results through intuitive interfaces. This display integrates physiological insights, clinical expertise, and machine learning outputs, bridging the gap between automated analytics and practical application. By maintaining explainability and avoiding the black-box issue, the interface supports clinical decision-making and ensures the model's trustworthiness.

Ultimately, this work not only demonstrates the utility of DSC-PWI in improving pre-surgical diagnoses but also proposes a comprehensive methodology for integrating multiparametric imaging with advanced statistical and deep-learning techniques. This innovation promotes tailored, patient-centric treatment strategies while enhancing the accessibility of complex data through clinician-friendly tools.

5.5. Opening the Door to the Perfugenomics of Adult Diffuse Gliomas According to the last 2021 World Health Organization Classification of CNS Tumors

The first study in this section [52] addresses the challenge of pre-surgically differentiating IDH-mutant astrocytomas from 1p19q-codeleted oligodendrogliomas, two tumor

types with distinct treatment and prognostic implications [69–71]. Using advanced DSC-PWI metrics, we evaluated cerebral blood volume (CBV) and percentage of signal recovery (PSR) percentile values derived from voxel-level analyses of entire tumor volumes. Unlike traditional approaches relying on mean or extreme values, this method highlights the importance of tumor heterogeneity and nuanced vascular characteristics, significantly improving diagnostic precision.

Oligodendrogliomas demonstrated higher CBV and lower PSR than astrocytomas, with the best performance metrics observed at specific percentiles. By combining the five most discriminative percentiles, a gradient-boosting classifier achieved an AUC-ROC of 0.87, offering robust diagnostic accuracy. This novel classifier integrates CBV and PSR voxel-wise metrics to provide complementary insights into vascular and microvascular tumor habitats, delivering additive value over individual parameters.

A key innovation lies in shifting from standard mean or maximum value approaches to voxel-wise analysis, leveraging percentile metrics to capture tumor heterogeneity more accurately. By combining voxel-level CBV and PSR data, the study achieves superior diagnostic accuracy compared to single-metric, single-value methods.

The study also proposed a clinical-friendly visualization tool that combines the classifier's probabilistic outputs with percentile distributions, ensuring interpretability and alignment with radiological knowledge. This innovation fosters an intuitive understanding of complex multiparametric data.

On the other hand, this study pioneers the use of percentage signal recovery (PSR) in nonenhancing tumors, a context where its application has been scarce. Highlighting its potential as a novel biomarker, the research links lower PSR values in oligodendrogliomas to the characteristic "chicken-wire" capillary pattern, reflecting increased microvascular tortuosity and irregularity.

Of note, this work merited an editorial comment in the renowned European Radiology journal [72].

In a second research work within this section (and the final one included in this thesis) [56], we focused on the pre-surgical differentiation between IDH-mutant grade 4 astrocytomas and IDH-wildtype glioblastomas, addressing a critical understudied challenge in neuro-oncology, particularly for young adult patients, with implications for guiding surgical and treatment decisions [69–71,73]. In this study we analyzed CBV across both enhancing and non-enhancing tumor regions. Unlike traditional methods that rely on mean or maximum preselected values—often based on unsound assumptions—we employed a percentile-based approach to capture the tumor's most distinguishing characteristics in an unsupervised manner.

The results revealed no significant differences in CBV within the enhancing regions, consistent with the fact that both tumor types are histological grade 4 and exhibit similar microvascular proliferation [14]. However, significant distinctions were identified in the non-enhancing regions. Specifically, IDH-mutant astrocytomas showed elevated CBV values in the lower percentiles of non-enhancing areas compared to glioblastomas. This suggests a higher degree of lowly vascularized infiltrated edema, contrasting with glioblastoma's purer edema in this specific tumor regions. Notably, the 30th percentile of CBV in non-enhancing regions emerged as the most robust discriminator, achieving

an AUC-ROC of 0.811 and outperforming conventional metrics such as mean and maximum CBV values, as well as metrics derived from the enhancing region.

Importantly, all the knowledge gathered during these studies also resulted in a narrative review [14], which can be found in the introduction appendix.

5.6. Specific Brain Tumor DSC-PWI Signatures and Hypothetical Pathophysiological Correlates

From our studies, we can identify several key signatures specific to different types of brain tumors and hypothesize about their underlying pathophysiology. These signatures represent one of the most clinically relevant aspects of this thesis, as they provide radiologists with a deeper understanding of novel DSC-PWI parameters. This knowledge has the potential to facilitate reliable pre-surgical diagnoses in routine clinical practice. The following part of this section provides a summary of the key findings, clearly disentangled for better understanding and practical application.

Regarding brain lymphoma, the most salient finding is a prominent T1-leakage effect, which translates into a high PSR. The curve shows a flatter descent compared to glioblastoma, metastasis, or meningioma, a lower peak height, and a sharper, earlier recovery. The AUC (CBV) values are relatively low in comparison. This pattern is explained by the predominant contribution of BBB disruption relative to the more limited vascularity, vessel heterogeneity, and tortuosity. Interestingly, the rapid recovery of the curve might seem paradoxical at first but can be attributed to the rapid onset of leakage. Rather than being driven by vascular washout, this recovery may be primarily related to the

quick efflux of contrast across the disrupted BBB, underscoring the role of BBB dynamics over vascular characteristics in this specific type of brain tumor [49]. Importantly, EBV-positive (immunodeficiency-associated) lymphomas retain the characteristic curve pattern and perfusion parameters typical of lymphomas. While this may initially seem redundant, it holds significant clinical value because this lymphoma subtype often mimics glioblastomas or metastases on morphological imaging. This underscores the critical role of this sequence, which may be the first—and potentially the only—tool to raise suspicion of lymphoma, thereby leading to a radical change in patient management [54]. A take-home message could be: "If you encounter a necrotic tumor suggestive of glioblastoma or metastasis, examine the perfusion parameters closely. If the DSC-PWI pattern aligns more with that of a lymphoma, consider the possibility of an immunodeficiency-associated lymphoma".

Regarding glioblastoma and metastases, glioblastomas exhibit a more balanced interplay between vascular tortuosity, hypercellularity, and BBB leakage, resulting in more equilibrated PSR values than lymphomas. In contrast, metastases are characterized by a predominance of vascular tortuosity and hypercellularity rather than leakage, with T2* effects being more dominant. This also explains the slower curve descent and recovery seen in metastases, potentially reflecting prolonged contrast retention within the denser, heterogeneous and more tortuous vascular network, alongside relatively less BBB disruption. Of note, this does not mean that glioblastomas lack vascular heterogeneity and tortuosity. However, the resultant curve differs due to the coexistence of relevant BBB disruption, which leads to earlier recovery and posterior higher PSR. Ultimately, the entire curve morphology reflects the equilibrium between gross vascularity, vascular dy-

namics, BBB integrity, and cyto- and vasculo-architecture phenomena, all of which are intriguing to disentangle. At any instance, to simplify, glioblastomas tend to show higher PSR values than metastases. While the CBV values are quite similar between glioblastomas and metastases, the curve morphology is distinctly different. Glioblastomas display sharper slopes curves with higher peak heights, whereas metastases show slower, less pronounced slopes and peaks. I.e., these curve differences are not reflected in the CBV values: glioblastomas have a thin, tall curve, while metastases exhibit a wide, short curve. However, the AUC for both remains similar. In a simile, it is like being thin and tall or short and wide—you can still weigh the same despite the difference in shape. On another hand, in differentiating between these entities, incorporating perfusion parameters from non-enhancing tumor regions has been considered particularly valuable. Edema in metastases contrasts with the combined edema and tumor infiltration in glioblastomas. The key distinction here lies in the AUC values: glioblastomas exhibit higher CBV in nonenhancing regions, a difference that becomes more pronounced when focusing on high percentiles. This finding is logical, as the higher percentiles of edema regions represent areas more infiltrated by tumor cells, while lower percentiles correspond to pure edema, similar to what is observed in metastases [50].

Meningioma curve morphology can be described as an "exaggeration" of that seen in metastases. It displays even slower (flattened) entry and exit slopes, with a predominance of early T2* effects and a deeper peak (greater than that of both metastases and glioblastomas). Continuing with the previous simile, if glioblastoma is taller and thinner and metastases are shorter and wider, meningioma would be the tallest and the widest. The recuperation is initially low, while the CBV is significantly higher. This pattern aligns

with its underlying pathophysiology, characterized by high vascularity, tortuous and heterogeneous vessels, and an absent BBB disruption [49]. The gradual increase in the recuperation part of the curve (PSR) observed during the later dynamic phases is potentially related to specific tissue characteristics, possibly linked to the EES and/or cytoarchitectural features of this tumor type. While the authors have a preliminary understanding of this phenomenon, a complete comprehension of its underlying mechanisms remains, for the moment, beyond their total grasp.

Regarding the specific DSC-PWI signatures of adult cerebellar tumors, notable differences emerge in the perfusion curvology across tumor types, with minimal overlap observed, except for the partial similarity in the signal recovery phase of the curve between medulloblastoma and pilocytic astrocytoma. Hemangioblastoma and metastasis exhibit pronounced and rapid T2*-dominant dynamic signal decay, which is more pronounced in hemangioblastoma. Both recover more slowly, with metastasis remaining below the baseline throughout the curve, while hemangioblastoma only reaches the baseline during the final time points. Conversely, medulloblastoma and pilocytic astrocytoma show less pronounced and slower signal decay, with medulloblastoma exhibiting slightly more pronounced changes. Both recover well above the baseline. Metastasis and hemangioblastoma are characterized by high CBV and PH values, along with low PSR. On the other hand, medulloblastoma and pilocytic astrocytoma are associated with low CBV and PH, coupled with high PSR values. Among these, hemangioblastoma demonstrates the highest CBV and PH, while pilocytic astrocytoma has the highest PSR. These DSC-PWI characteristics align well with the underlying pathophysiology of these tumors: hemangioblastoma and metastasis exhibit greater heterogeneous and tortuous

vascularity, while pilocytic astrocytoma and medulloblastoma demonstrate a higher degree of BBB disruption. Among these, medulloblastoma shows slightly more vascularity, whereas pilocytic astrocytoma is characterized by extremely low vascularity (which reminds us that in adults, pilocytic astrocytomas can even present with spontaneous involutional changes and consequent minimal vascularization). The authors highlight two key take-home messages. First, if you encounter a posterior fossa tumor with very low CBV and significant T1-leakage (high PSR), pilocytic astrocytoma should be considered as a likely diagnosis, and in cases where the tumor is asymptomatic or located in a region unsuitable for surgery or biopsy, MR follow-up could be considered as a management option. And second, If you observe a posterior fossa tumor with very high CBV and low initial PSR that recovers during later dynamics (a pattern similar to meningiomas), hemangioblastoma should be strongly suspected, and in such cases, preoperative embolization may be discussed during tumor board meetings to minimize the risk of intraoperative complications [51].

Regarding the differentiation between molecularly defined oligodendrogliomas and astrocytomas, the presence of high CBV values in a non- or scarcely-enhancing (lower-grade appearing) tumor should raise the suspicion of oligodendroglioma. Additionally, a lower early PSR would further support this suspicion, particularly when analyzing higher percentiles, such as 70–75, for both metrics. Notably, no significant differences in DSC-PWI metrics are observed between grade 2 and grade 3 tumors, which may seem contradictory to earlier references, particularly for astrocytomas, where DSC-PWI was previously assumed to differentiate between these grades. The authors hypothesize that this lack of difference may result from the 2021 molecular classification creating more

robust tumor groupings, suggesting that previously reported differences between grade 2 and grade 3 tumors in earlier studies might have been influenced by misclassification based on the current classification standards. The absence of differences in DSC-PWI metrics aligns with the understanding that grade 2 and grade 3 astrocytomas differ primarily in cellular rather than vascular properties, making it plausible for DSC-PWI metrics to remain similar across these grades. An interesting hypothesis emerging from this work is the potential role of early PSR as a cyto-architectural biomarker in tumors without enhancement (i.e., lacking BBB disruption). In this specific context, PSR may serve as a biomarker of the characteristic chicken-wire capillarity of oligodendrogliomas [52].

Finally, when dealing with a primary brain tumor presenting with enhancement, necrosis, and high CBV in older patients (as per the WHO 2021 criteria, above 55 years of age), the most plausible diagnosis is glioblastoma IDH-wildtype. However, in patients below this age threshold, tumors with grade 4 features on imaging (necrosis and/or microvascular proliferation) could represent IDH-mutant astrocytomas, classified as grade 4. This distinction is crucial, especially in younger patients, as IDH-mutant astrocytomas have significant differences in both management and prognosis compared to glioblastoma IDH-wildtype. As previously hypothesized, CBV, an indirect measure of vascular proliferation, does not differ between these tumors in their enhancing components. However, differences arise in the non-enhancing tumor regions (T2-FLAIR abnormality), where the lower percentiles of CBV in grade 4 astrocytomas are higher than in glioblastoma. This likely reflects a higher degree of tumor infiltration in astrocytomas, in contrast to pure edema in these lower percentiles in glioblastoma. Additionally, in glioblastoma, higher CBV values are observed in the higher percentiles of non-enhancing tumor re-

gions, which theoretically correspond to more aggressive tumor areas. This aligns with the inherent heterogeneity of glioblastoma, where regions of high CBV coexist with areas of pure edema (characterized by low CBV) reflected in the lower percentiles. In contrast, grade 4 astrocytomas demonstrate a more homogeneous CBV distribution. As a result, when focusing on lower CBV percentiles, grade 4 astrocytomas exhibit higher values. However, somewhat paradoxically, this does not suggest greater overall aggressiveness compared to glioblastoma, but rather the contrary. Parallelly, no significant differences were observed regarding the presence or absence of necrosis between these entities. And finally an additional morphological imaging take-home message is that the presence of a T2-FLAIR mismatch in solid, non-enhancing parts of the tumor, coexisting with foci of high CBV or necrosis, is almost pathognomonic of grade 4 IDH-mutant astrocytomas. To the authors' knowledge, this was the first work to report this specific diagnostic clue [56].

5.7. Strengths and Limitations

The strengths of the research works in this thesis are evident from the preceding sections. It emphasizes unsupervised, automatic, volumetric, voxel-wise, and multi-parametric analysis of DSC-PWI, which enhances the robustness, reproducibility, and generalizability of the results, paving the way for reliable and impactful integration into clinical workflows. Furthermore, it not only improves performance in current clinical applications but also uncovers new clinical approaches and applications, while fostering the development of clinician-friendly tools.

However, the author also acknowledges some common limitations of the studies presented in this thesis. The primary challenges revolve around the retrospective nature of the research and the use of DSC-PWI predominantly with intermediate-to-high flip-angles and without preload (favoring leakage effects), which may limit the applicability of the results in scenarios where low flip-angles or preloaded sequences are employed (minimizing leakage effects). Nevertheless, prospective studies validating our classifiers and results in technically comparable scenarios, as well as adapting them to different technical settings, are feasible and already underway. Of note, the author indicates that if he had to choose, he would prefer high flip-angle, non-preloaded sequences in current clinical practice, particularly for pre-surgical differential diagnosis settings. This approach enhances information regarding leakage effects while maintaining accurate and robust CBV evaluations [32,37]. In contrast, preloaded or low flip-angle sequences are designed to minimize the impact of leakage effects and focus exclusively on CBV information [2].

Additionally, while some studies are single-center, which may raise concerns about generalizability to other institutions, this limitation is mitigated by the inclusion of two multicenter studies. These multicenter studies not only demonstrate consistency with the results observed in single-center studies but also strengthen the robustness and potential applicability of the findings across diverse clinical settings.

5.8. Future Perspectives and Directions

First, it is important to emphasize that this entire research line is currently active and far from being concluded. In fact, several projects are ongoing. For instance, one focuses on the potential of DSC-PWI to provide accurate prognostic stratification in glioblastoma

patients, the most devastating brain tumor. This could enable concentrating efforts on patients with better prognoses while preserving the best quality of life for those with very poor prognoses, for example.

Another line of investigation revolves around proposing the optimal pulse-sequence parameters for (single-echo) DSC-PWI in the differential diagnosis of tumors. Specifically, we study tumors using various pulse-sequence parameters and compare which provides the best diagnostic performance, taking into account all metrics—not just CBV, as is the case with current consensus protocols.

Finally, we are also testing the feasibility of new tools to quantify tumor burden during the follow-up of treated tumors (both gliomas and metastases). These tools aim to help distinguish progression from treatment-related effects, a current and frequent challenge in neuro-oncology committees. This could enable earlier decisions to continue, discontinue, or adjust treatments, ultimately optimizing the management of these patients.

However, on another line, one of the main limitations of this thesis and our current approaches lies in the inherent nature of the DSC-PWI sequence, which is highly dependent on technical pulse-sequence parameters. Nevertheless, this dependence may also be seen as an opportunity, opening the door to exploring alternative approaches aimed at optimizing and standardizing data acquisition while mitigating these limitations and obtaining the richest information possible from the sequence.

Currently available real-world clinical strategies would involve acquiring two consecutive DSC sequences to obtain complementary information. For instance, the first sequence could use a high flip-angle without preload, favoring the analysis of leakage effects, while

the second sequence could employ an intermediate flip-angle with preload, better suited for precise CBV evaluation. However, this approach requires a double dose of contrast agent, patient safety, costs, and environmental impact [37].

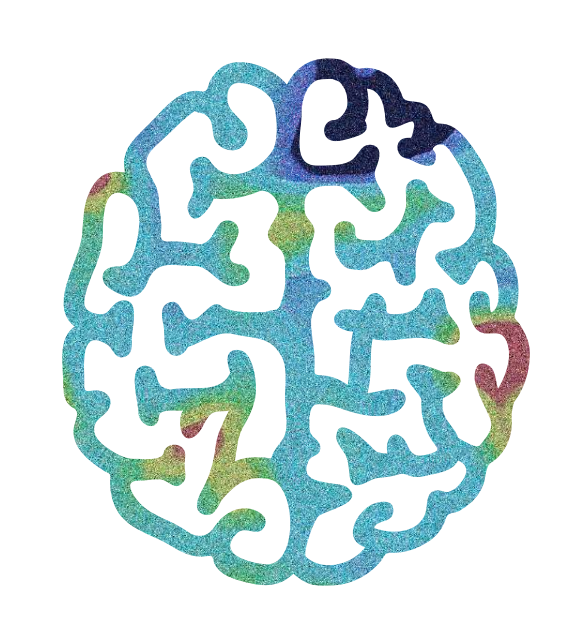
An innovative solution to this challenge lies in dual-echo DSC methods, as highlighted in recent studies. These techniques enable the acquisition of two different echo times within a single-dose, single-acquisition sequence. Then, by disentangling T1 and T2* contributions, dual-echo DSC enables a robust quantification of vascularity (CBV), permeability (Ktrans), while also introducing new biomarkers such as the transverse relaxivity at tracer equilibrium (TRATE), which reflects leakage effects more robustly than traditional metrics like PSR [39,40]. This approach would significantly reduce the need for multiple acquisitions and high doses of gadolinium, addressing key concerns in current clinical practice.

Additionally, synthetic DSC techniques have emerged as a promising development. These methods utilize dual-echo data to simulate synthetic acquisition parameters, enabling post-hoc optimization of protocols. By generating parameter-matched datasets, synthetic DSC would facilitate cross-institutional comparisons and harmonization, thereby enhancing the reproducibility and generalizability of results. Furthermore, this technique supports the generation of CBV-optimized and PSR-optimized maps within a single acquisition, enhancing the robustness and generalizability of these metrics, while also improving workflow efficiency and reducing contrast agent usage [37].

These cutting-edge approaches provide robust, quantifiable metrics while addressing key limitations of traditional DSC methods, making them well-suited for both clinical and

research applications. These innovations align with the goals of this thesis by advancing the field toward more reproducible, generalizable, and richer data extraction, as well as clinically relevant and integrated solutions.

In conclusion, dual-echo and synthetic DSC techniques represent significant advance-ments in perfusion imaging. The author anticipates their increased clinical adoption and integration into neuro-oncology imaging protocols in the coming years. This progression is essential for addressing the current limitations that hinder the full integration of these techniques into both clinical practice and clinical trials, ensuring their continued relevance and utility. Ultimately, our group is also already exploring this type of sequences and methods and initiating clinical projects to test its feasibility, practicality, and clinical relevance.



6. CONCLUSIONS

6. CONCLUSIONS

Our innovative methodologies and developed classifiers have significantly improved the diagnostic accuracy of DSC-PWI for the presurgical diagnosis of brain tumors, providing a more reliable and nuanced understanding of tumor vascular and microvascular characteristics.

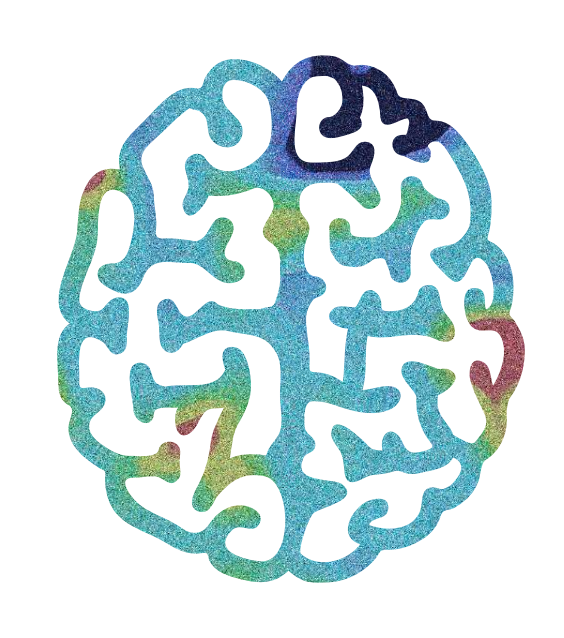
Through our methods, DSC-PWI can reliably differentiate, presurgically and noninvasively, between various tumor types and subtypes in adults, including:

- The most common brain malignancies: lymphoma, glioblastoma, and metastasis.
- The most common intra-axial cerebellar tumors: pilocytic astrocytoma, hemangioblastoma, medulloblastoma, and metastasis.
- Clinically relevant molecularly defined subtypes of adult-type diffuse gliomas as per the 2021 World Health Organization Classification: oligodendroglioma and astrocytoma (grades 2–3), astrocytoma grade 4, and glioblastoma.

Comprehensive visual and quantitative analysis of DSC-PWI time-intensity curves is feasible through our pioneering normalization method, which has enabled consistent and clinically relevant insights from DSC-PWI data.

Semi-automatic methods for volume-of-interest delineation and normalization of DSC-PWI data have proven to be both robust and feasible, minimizing operator dependency and ensuring reproducibility across different clinical settings. The incorporation of additional DSC-PWI metrics—such as time-intensity curves, PSR, and PH—alongside CBV in a voxel-wise, semi-automatic, and unsupervised manner captures the full heterogeneity of brain tumors and has enhanced the diagnostic power of DSC-PWI sequences, supporting the development of clinically useful classifiers for presurgical brain tumor diagnosis.

Ultimately, all these advances have a twofold impact. First, they directly influence current clinical practice: DSC-PWI analysis enables more precise and informative presurgical diagnostics, with significant implications for improved patient management and personalized treatment planning. Second, and importantly, they lay the groundwork for ongoing research and development, fostering future innovations, investigations, and advancements in the field.



7. REFERENCES

7. REFERENCES

- [1] Pons-Escoda A, Smits M. Dynamic-susceptibility-contrast perfusion-weighted imaging (DSC-PWI) in brain tumors: a brief up-to-date overview for clinical neuroradiologists. Eur Radiol. 2023;33:8026-8030. https://doi.org/10.1007/s00330-023-09729-3.
- [2] Boxerman JL, Quarles CC, Hu LS, Erickson BJ, Gerstner ER, Smits M, et al. Consensus recommendations for a dynamic susceptibility contrast MRI protocol for use in high-grade gliomas. Neuro Oncol. 2020;22:1262–75. https://doi.org/10.1093/neuonc/noaa141.
- [3] Kaufmann TJ, Smits M, Boxerman J, Huang R, Barboriak DP, Weller M, et al. Consensus recommendations for a standardized brain tumor imaging protocol for clinical trials in brain metastases. Neuro Oncol. 2020;22:757–72. https://doi.org/10.1093/neuonc/noaa030.
- [4] Barajas RF, Politi LS, Anzalone N, Schöder H, Fox CP, Boxerman JL, et al. Consensus recommendations for MRI and PET imaging of primary central nervous system lymphoma: guideline statement from the International Primary CNS Lymphoma Collaborative Group (IPCG). Neuro Oncol. 2021;23:1056–71. https://doi.org/10.1093/neuonc/noab020.
- [5] Rosen BR, Belliveau JW, Vevea JM, Brady TJ. Perfusion imaging with NMR contrast agents. Magn Reson Med. 1990;14:249-65. https://doi.org/10.1002/mrm.1910140211.

- [6] Quarles CC, Gochberg DF, Gore JC, Yankeelov TE. A theoretical framework to model DSC-MRI data acquired in the presence of contrast agent extravasation. Phys Med Biol. 2009;54:5749–66. https://doi.org/10.1088/0031-9155/54/19/006.
- [7] Boxerman JL, Hamberg LM, Rosen BR, Weisskoff RM. *Mr contrast due to intravascular magnetic susceptibility perturbations. Magn Reson Med.* 1995;34:555–66. https://doi.org/10.1002/mrm.1910340412.
- [8] Sawlani V, Patel MD, Davies N, Flintham R, Wesolowski R, Ughratdar I, et al. *Multi-* parametric MRI: practical approach and pictorial review of a useful tool in the evaluation of brain tumours and tumour-like lesions. *Insights Imaging*. 2020;11:84. https://doi.org/10.1186/s13244-020-00888-1.
- [9] Pons-Escoda A, Naval-Baudin P, Velasco R, Vidal N, Majós C. Imaging of Lymphomas Involving the CNS: An Update-Review of the Full Spectrum of Disease with an Emphasis on the World Health Organization Classifications of CNS Tumors 2021 and Hematolymphoid Tumors 2022. AJNR Am J Neuroradiol. 2023;44:358–66. https://doi.org/10.3174/ajnr.A7795.
- [10] Cha S, Lupo JM, Chen M-H, Lamborn KR, McDermott MW, Berger MS, et al. Differentiation of Glioblastoma Multiforme and Single Brain Metastasis by Peak Height and Percentage of Signal Intensity Recovery Derived from Dynamic Susceptibility-Weighted Contrast-Enhanced Perfusion MR Imaging. Am J Neuroradiol. 2007;28:1078–84. https://doi.org/10.3174/ajnr.A0484.

- [11] Hirschler L, Sollmann N, Schmitz-Abecassis B, Pinto J, Arzanforoosh F, Barkhof F, et al. Advanced MR Techniques for Preoperative Glioma Characterization: Part 1. J Magn Reson Imaging. 2023;57:1655–75. https://doi.org/10.1002/jmri.28662.
- [12] Boxerman JL, Schmainda KM, Weisskoff RM. Relative cerebral blood volume maps corrected for contrast agent extravasation significantly correlate with glioma tumor grade, whereas uncorrected maps do not. AJNR Am J Neuroradiol. 2006;27:859–67.
- [13] Jabehdar Maralani P, Melhem ER, Wang S, Herskovits EH, Voluck MR, Kim SJ, et al. Association of dynamic susceptibility contrast enhanced MR Perfusion parameters with prognosis in elderly patients with glioblastomas. Eur Radiol. 2015;25:2738–44. https://doi.org/10.1007/s00330-015-3640-4.
- [14] Pons-Escoda A, Majos C, Smits M, Oleaga L. Presurgical diagnosis of diffuse gliomas in adults: Post-WHO 2021 practical perspectives from radiologists in neuro-oncology units. Radiol. English Ed. 2024;66:260-277. https://doi.org/10.1016/j.rxeng.2024.03.002.
- [15] Fu R, Szidonya L, Barajas RFJ, Ambady P, Varallyay C, Neuwelt EA. *Diagnostic performance of DSC perfusion MRI to distinguish tumor progression and treatment-related changes: a systematic review and meta-analysis.* Neuro-Oncology Adv. 2022;4:vdac027. https://doi.org/10.1093/noajnl/vdac027.

- [16] Chiavazza C, Pellerino A, Ferrio F, Cistaro A, Soffietti R, Rudà R. *Primary CNS Lymphomas: Challenges in Diagnosis and Monitoring. Biomed Res Int.* 2018;2018:3606970. https://doi.org/10.1155/2018/3606970.
- [17] Altwairgi AK, Raja S, Manzoor M, Aldandan S, Alsaeed E, Balbaid A, et al. *Management and treatment recommendations for World Health Organization Grade*III and IV gliomas. Int J Health Sci (Qassim). 2017;11:54–62.
- [18] Enrique G-V, Irving S-R, Ricardo B-I, Jesus F-L, Alan R-M, Inigo VAA, et al. *Diagnosis and management of brain metastases: an updated review from a radiation oncology perspective. J Cancer Metastasis Treat.* 2019;5. https://doi.org/10.20517/2394-4722.2019.20.
- [19] van Santwijk L, Kouwenberg V, Meijer F, Smits M, Henssen D. A systematic review and meta-analysis on the differentiation of glioma grade and mutational status by use of perfusion-based magnetic resonance imaging. Insights Imaging. 2022;13:102. https://doi.org/10.1186/s13244-022-01230-7.
- [20] Haldorsen IS, Espeland A, Larsson E-M. Central Nervous System Lymphoma: Characteristic Findings on Traditional and Advanced Imaging. Am J Neuroradiol. 2011;32:984–92. https://doi.org/10.3174/ajnr.A2171.
- [21] Sauter A, Faul C, Bitzer M, Bares R, Kraus S, Fenchel M, et al. *Imaging findings in immunosuppressed patients with epstein barr virus-related B cell malignant lymphoma*. *Am J Roentgenol*. 2010;194:141–9. https://doi.org/10.2214/AJR.09.3264.

- [22] Upadhyay N, Waldman AD. Conventional MRI evaluation of gliomas. Br J Radiol. 2011;84:S107–11. https://doi.org/10.1259/bjr/65711810.
- [23] Fink K, Fink J. Imaging of brain metastases. Surg Neurol Int. 2013;4:209-19. https://doi.org/10.4103/2152-7806.111298.15(6):1085-107.
- [24] Shih RY, Smirniotopoulos JG. Posterior Fossa Tumors in Adult Patients. Neuroimaging Clin N Am. 2016;26:493–510. https://doi.org/10.1016/j.nic.2016.06.003.
- [25] Jain R, Johnson DR, Patel SH, Castillo M, Smits M, van den Bent MJ, et al. "Real world" use of a highly reliable imaging sign: "T2-FLAIR mismatch" for identification of IDH mutant astrocytomas. Neuro Oncol. 2020;22:936–43. https://doi.org/10.1093/neuonc/noaa041.
- [26] Lasocki A, Buckland ME, Drummond KJ, Wei H, Xie J, Christie M, et al. Conventional MRI features can predict the molecular subtype of adult grade 2–3 intracranial diffuse gliomas. Neuroradiology. 2022;64:2295–305. https://doi.org/10.1007/s00234-022-02975-0.
- [27] Lee MD, Patel SH, Mohan S, Akbari H, Bakas S, Nasrallah MP, et al. *Association of partial T2-FLAIR mismatch sign and isocitrate dehydrogenase mutation in WHO grade 4 gliomas: results from the ReSPOND consortium. Neuroradiology.* 2023;65:1343–52. https://doi.org/10.1007/s00234-023-03196-9.
- [28] Herings SDA, van den Elshout R, de Wit R, Mannil M, Ravesloot C, Scheenen TWJ, et al. How to evaluate perfusion imaging in post-treatment glioma: a com-

- parison of three different analysis methods. Neuroradiology. 2024;66:1279–89. https://doi.org/10.1007/s00234-024-03374-3.
- [29] Cho NS, Hagiwara A, Sanvito F, Ellingson BM. A multi-reader comparison of normal-appearing white matter normalization techniques for perfusion and diffusion MRI in brain tumors. Neuroradiology. 2023;65:559–68. https://doi.org/10.1007/s00234-022-03072-y.
- [30] Smits M, Bendszus M, Collette S, Postma LA, Dhermain F, Hagenbeek RE, et al. Repeatability and reproducibility of relative cerebral blood volume measurement of recurrent glioma in a multicentre trial setting. Eur J Cancer. 2019;114:89–96. https://doi.org/10.1016/j.ejca.2019.03.007.
- [31] Cindil E, Sendur HN, Cerit MN, Dag N, Erdogan N, Celebi FE, et al. *Validation of combined use of DWI and percentage signal recovery-optimized protocol of DSC-MRI in differentiation of high-grade glioma, metastasis, and lymphoma.* Neuroradiology. 2021;63:331–42. https://doi.org/10.1007/s00234-020-02522-9.
- [32] Wang F, Zhou X, Chen R, Kang J, Yang X, Lin J, et al. *Improved performance of non-preloaded and high flip-angle dynamic susceptibility contrast perfusionweighted imaging sequences in the presurgical differentiation of brain lymphoma and glioblastoma. Eur Radiol.* 2023;33:8800-8808. https://doi.org/10.1007/s00330-023-09917-1.
- [33] Kouwenberg V, van Santwijk L, Meijer FJA, Henssen D. Reliability of dynamic susceptibility contrast perfusion metrics in pre- and post-treatment

- glioma. Cancer Imaging Off Publ Int Cancer Imaging Soc. 2022;22:28. https://doi.org/10.1186/s40644-022-00466-2.
- [34] Lee MD, Baird GL, Bell LC, Quarles CC, Boxerman JL. Utility of Percentage Signal Recovery and Baseline Signal in DSC-MRI Optimized for Relative CBV Measurement for Differentiating Glioblastoma, Lymphoma, Metastasis, and Meningioma. Am J Neuroradiol. 2019;40:1145–450. https://doi.org/10.3174/ajnr.A6153.
- [35] Cindil E, Sendur HN, Cerit MN, Erdogan N, Celebi F, Dag N, et al. *Prediction of IDH Mutation Status in High-grade Gliomas Using DWI and High T1-weight DSC-MRI.*Acad Radiol. 2022;29:S52–62. https://doi.org/10.1016/j.acra.2021.02.002.
- [36] Mangla R, Kolar B, Zhu T, Zhong J, Almast J, Ekholm S. Percentage signal recovery derived from MR dynamic susceptibility contrast imaging is useful to differentiate common enhancing malignant lesions of the brain. Am J Neuroradiol. 2011;32:1004–10. https://doi.org/10.3174/ajnr.A2441.
- [37] Sanvito F, Yao J, Cho NS, Raymond C, Telesca D, Pope WB, et al. "Synthetic" DSC perfusion MRI with adjustable acquisition parameters in brain tumors using dynamic spin-and-gradient echo echoplanar imaging. Am J Neuroradio. 2025;46:311-320. https://doi.org/10.3174/ajnr.A8475.
- [38] Neska-Matuszewska M, Zimny A, Bladowska J, Czarnecka A, Sąsiadek M. The role of diffusion and perfusion magnetic resonance imaging in differentiation of haemangioblastomas and pilocytic astrocytomas. Polish J Radiol. 2018;83:e197–203. https://doi.org/10.5114/pjr.2018.75870.

- [39] Sanvito F, Raymond C, Cho NS, Yao J, Hagiwara A, Orpilla J, et al. *Simultaneous quantification of perfusion, permeability, and leakage effects in brain gliomas using dynamic spin-and-gradient-echo echoplanar imaging MRI. Eur Radiol.* 2024;34:3087-3101. https://doi.org/10.1007/s00330-023-10215-z.
- [40] Pons-Escoda A. "Everything Everywhere All at Once": Unraveling perfusion, permeability, and leakage effects in neurooncology with a single-dose, single-acquisition dual-echo DSC. Eur Radiol. 2024;34:3084-3086. https://doi.org/10.1007/s00330-023-10277-z.
- [41] Lupo JM, Cha S, Chang SM, Nelson SJ. *Dynamic susceptibility-weighted perfusion imaging of high-grade gliomas: characterization of spatial heterogeneity.*AJNR Am J Neuroradiol. 2005;26:1446–54.
- [42] Chinchure S, Thomas B, Wangju S, Jolappara M, Kesavadas C, Kapilamorthy TR, et al. *Mean intensity curve on dynamic contrast-enhanced susceptibility-weighted perfusion MR imaging review of a new parameter to differentiate intracranial tumors. J Neuroradiol.* 2011;38:199–206. https://doi.org/10.1016/j.neurad.2011.07.002.
- [43] Yun J, Yun S, Park JE, Cheong E-N, Park SY, Kim N, et al. Deep Learning of Time—Signal Intensity Curves from Dynamic Susceptibility Contrast Imaging Enables
 Tissue Labeling and Prediction of Survival in Glioblastoma. Am J Neuroradiol.
 2023;44:543–52. https://doi.org/10.3174/ajnr.A7853.
- [44] Choi KS, Choi SH, Jeong B. Prediction of IDH genotype in gliomas with dynamic susceptibility contrast perfusion MR imaging using an ex-

- plainable recurrent neural network. Neuro Oncol. 2019;21:1197–209. https://doi.org/10.1093/neuonc/noz095.
- [45] Akbari H, Macyszyn L, Da X, Wolf RL, Bilello M, Verma R, et al. *Pattern Analysis of Dynamic Susceptibility Contrast-enhanced MR Imaging Demonstrates Peritumoral Tissue Heterogeneity. Radiology.* 2014;273:502–10. https://doi.org/10.1148/radiol.14132458.
- [46] Bell LC, Hu LS, Stokes AM, McGee SC, Baxter LC, Quarles CC. Characterizing the Influence of Preload Dosing on Percent Signal Recovery (PSR) and Cerebral Blood Volume (CBV) Measurements in a Patient Population With High-Grade Glioma Using Dynamic Susceptibility Contrast MRI. Tomogr (Ann Arbor, Mich). 2017;3:89– 95. https://doi.org/10.18383/j.tom.2017.00004.
- [47] Barajas RF, Chang JS, Sneed PK, Segal MR, McDermott MW, Cha S. Distinguishing recurrent intra-axial metastatic tumor from radiation necrosis following gamma knife radiosurgery using dynamic susceptibility-weighted contrastenhanced perfusion MR imaging. AJNR Am J Neuroradiol. 2009;30:367–72. https://doi.org/10.3174/ajnr.A1362.
- [48] Boxerman JL, Paulson ES, Prah MA, Schmainda KM. The effect of pulse sequence parameters and contrast agent dose on percentage signal recovery in DSC-MRI: Implications for clinical applications. Am J Neuroradiol. 2013;34:1364–9. https://doi.org/10.3174/ajnr.A3477.
- [49] Pons-Escoda A, Garcia-Ruiz A, Naval-Baudin P, Cos M, Vidal N, Plans G, et al.

 Presurgical identification of primary central nervous system lymphoma with nor-

- malized time-intensity curve: A pilot study of a new method to analyze DSC-PWI.

 Am J Neuroradiol. 2020;41:1816–24. https://doi.org/10.3174/ajnr.A6761.
- [50] Pons-Escoda A, Garcia-Ruiz A, Naval-Baudin P, Grussu F, Fernandez JJS, Simo AC, et al. *Voxel-level analysis of normalized DSC-PWI time-intensity curves: a potential generalizable approach and its proof of concept in discriminating glioblastoma and metastasis. Eur Radiol.* 2022;32:3705-3715. https://doi.org/10.1007/s00330-021-08498-1.
- [51] Pons-Escoda A, Garcia-Ruiz A, Garcia-Hidalgo C, Gil-Solsona R, Naval-Baudin P, Martin-Noguerol T, et al. MR dynamic-susceptibility-contrast perfusion metrics in the presurgical discrimination of adult solitary intra-axial cerebellar tumors. Eur Radiol. 2023;33:9120-9129. https://doi.org/10.1007/s00330-023-09892-7.
- [52] Pons-Escoda A, Garcia-Ruiz A, Naval-Baudin P, Martinez-Zalacain I, Castell J, Camins A, et al. Differentiating IDH-mutant astrocytomas and 1p19q-codeleted oligodendrogliomas using DSC-PWI: high performance through cerebral blood volume and percentage of signal recovery percentiles. Eur Radiol. 2024;34:5320-5330. https://doi.org/10.1007/s00330-024-10611-z.
- [53] Park YW, Han K, Ahn SS, Bae S, Choi YS, Chang JH, et al. *Prediction of IDH1 -Mutation and 1p/19q-Codeletion Status Using Preoperative MR Imaging Phenotypes in Lower Grade Gliomas. Am J Neuroradiol.* 2018;39:37–42. https://doi.org/10.3174/ajnr.A5421.
- [54] Pons-Escoda A, García-Ruíz A, Naval-Baudin P, Grussu F, Viveros M, Vidal N, et al. Diffuse Large B-Cell Epstein-Barr Virus-Positive Primary CNS Lymphoma in

Non-AIDS Patients: High Diagnostic Accuracy of DSC Perfusion Metrics. AJNR Am J Neuroradiol. 2022;43:1567–74. https://doi.org/10.3174/ajnr.A7668.

- [55] Garcia-Ruiz A, Pons-Escoda A, Grussu F, Naval-Baudin P, Monreal-Aguero C, Hermann G, et al. An accessible deep learning tool for voxel-wise classification of brain malignancies from perfusion MRI. Cell Reports Med. 2024;5:101464. https://doi.org/10.1016/j.xcrm.2024.101464.
- [56] Pons-Escoda A, Naval-Baudin P, Viveros M, Flores-Casaperalta S, Martinez-Zalacaín I, Plans G, et al. *DSC-PWI presurgical differentiation of grade 4 astrocytoma and glioblastoma in young adults: rCBV percentile analysis across enhancing and non-enhancing regions.* Neuroradiology. 2024;66:1267–77. https://doi.org/10.1007/s00234-024-03385-0.
- [57] Leu K, Boxerman JL, Ellingson BM. Effects of MRI protocol parameters, preload injection dose, fractionation strategies, and leakage correction algorithms on the fidelity of dynamic susceptibility contrast MRI estimates of relative cerebral blood volume in gliomas. Am J Neuroradiol. 2017;38:478-484. https://doi.org/10.3174/ajnr.A5027.
- [58] Velasco R, Mercadal S, Vidal N, Alañá M, Barceló MI, Ibáñez-Juliá MJ, et al. *Diagnostic delay and outcome in immunocompetent patients with primary central nervous system lymphoma in Spain: a multicentric study. J Neurooncol.* 2020;148:545–54. https://doi.org/10.1007/s11060-020-03547-z.

- [59] Deckert M, Brunn A, Montesinos-Rongen M, Terreni MR, Ponzoni M. *Primary lym-phoma of the central nervous system--a diagnostic challenge. Hematol Oncol.* 2014;32:57–67. https://doi.org/10.1002/hon.2087.
- [60] Lee HY, Kim HS, Park JW, Baek HJ, Kim SJ, Choi CG. Atypical imaging features of epstein-barr virus-positive primary central nervous system lymphomas in patients without AIDS. Am J Neuroradiol. 2013;34:1562–7. https://doi.org/10.3174/ajnr.A3429.
- [61] Jiménez de la Peña M del M, Vicente LG, Alonso RC, Cabero SF, Suárez AM, de Vega VM. The Multiple Faces of Nervous System Lymphoma. Atypical Magnetic Resonance Imaging Features and Contribution of the Advanced Imaging. Curr Probl Diagn Radiol. 2017;46:136–45. https://doi.org/10.1067/j.cpradiol.2016.04.004.
- [62] Lin X, Khan IRA, Seet YHC, Lee HY, Yu WY. Atypical radiological findings of primary central nervous system lymphoma. Neuroradiology. 2020;62:669–76. https://doi.org/10.1007/s00234-020-02377-0.
- [63] Suh CH, Kim HS, Lee SS, Kim N, Yoon HM, Choi C-G, et al. Atypical Imaging Features of Primary Central Nervous System Lymphoma That Mimics Glioblastoma: Utility of Intravoxel Incoherent Motion MR Imaging. Radiology. 2014;272:504–13. https://doi.org/10.1148/radiol.14131895.
- [64] Ostrom QT, Cioffi G, Gittleman H, Patil N, Waite K, Kruchko C, et al. *CBTRUS*Statistical Report: Primary Brain and Other Central Nervous System Tumors Di-

- agnosed in the United States in 2012–2016. Neuro Oncol. 2019;21:v1–100. https://doi.org/10.1093/neuonc/noz150.
- [65] Morton LM, Onel K, Curtis RE, Hungate EA, Armstrong GT. The Rising Incidence of Second Cancers: Patterns of Occurrence and Identification of Risk Factors for Children and Adults. Am Soc Clin Oncol Educ B. 2014:e57–67. https://doi.org/10.14694/edbook_am.2014.34.e57.
- [66] Donin N, Filson C, Drakaki A, Tan H-J, Castillo A, Kwan L, et al. *Risk of second primary malignancies among cancer survivors in the United States,* 1992 through 2008. Cancer. 2016;122:3075–86. https://doi.org/10.1002/cncr.30164.
- [67] Fuentes-Raspall R, Vilardell L, Perez-Bueno F, Joly C, Garcia-Gil M, Garcia-Velasco A, et al. *Population-based incidence and survival of central ner-vous system (CNS) malignancies in Girona (Spain)* 1994-2005. *J Neurooncol*. 2011;101:117–23. https://doi.org/10.1007/s11060-010-0240-7.
- [68] Miller KD, Ostrom QT, Kruchko C, Patil N, Tihan T, Cioffi G, et al. Brain and other central nervous system tumor statistics, 2021. CA Cancer J Clin. 2021;71:381– 406. https://doi.org/10.3322/caac.21693.
- [69] Vagvala S, Guenette JP, Jaimes C, Huang RY. *Imaging diagnosis and treatment selection for brain tumors in the era of molecular therapeutics. Cancer Imaging.* 2022;22:19. https://doi.org/10.1186/s40644-022-00455-5.
- [70] Blobner J, Dengler L, Blobner S, Eberle C, Weller J, Teske N, et al. Significance of molecular diagnostics for therapeutic decision-

- making in recurrent glioma. Neuro-Oncology Adv. 2023;5:vdad060. https://doi.org/10.1093/noajnl/vdad060.
- [71] Balana C, Castañer S, Carrato C, Moran T, Lopez-Paradís A, Domenech M, et al. Preoperative Diagnosis and Molecular Characterization of Gliomas With Liquid Biopsy and Radiogenomics. Front Neurol. 2022;13:865171. https://doi.org/10.3389/fneur.2022.865171.
- [72] Lui E. Perfusion percentage signal recovery and a mundane chicken wire: what could they have to do in oligodendrogliomas? Eur Radiol. 2024;34:5317–9. https://doi.org/10.1007/s00330-024-10711-w.
- [73] Mellinghoff IK, van den Bent MJ, Blumenthal DT, Touat M, Peters KB, Clarke J, et al. *Vorasidenib in IDH1- or IDH2-Mutant Low-Grade Glioma. N Engl J Med.* 2023;389(7):589-601. https://doi.org/10.1056/NEJMoa2304194.

